

ACTIVE CR FILTER STRUCTURES USING MULTIPLE FEEDBACK

DAVID JOHN PERRY

November 1985

A thesis submitted for the degree of Doctor of  
Philosophy of the University of London and for  
the Diploma of Imperial College.

Imperial College of Science and Technology, London SW7

---

**ABSTRACT**

---

A study is made of multiple feedback filters, which are defined to be an interconnection of unilateral, active, CR sections, forming a structure which has at least one forward path through the filter and a multiplicity of feedback loops. Particular attention is paid to structure, which is taken to be the configuration of feedback loops and forward paths.

The analysis of multiple feedback filters is described. Both a matrix method related to the block diagram representation, and a topological method related to the signal flow graph representation are given. Sensitivity performance is of special interest, and explicit expressions are given for both differential and finite difference sensitivities of the transfer function with respect to changes in the block diagram parameters. A new summed sensitivity invariant is given, applicable to the branches of a 'cut' of the signal flow graph. The dynamic range of a multiple feedback filter is discussed, and is related to the imperfections of the constituent sections by the use of 'noise transfer functions' and 'intermediate transfer functions'.

Methods of transforming a multiple feedback filter are described in some detail. These may be used to obtain new structures or to obtain some improvement in performance. Some transformations presented here have the interesting property of altering the structure without affecting the block diagram sensitivities.

Multiple feedback filters are classified in this thesis firstly by the arrangement of feedback loops which are introduced to reduce the sensitivity of the filter, and secondly by the three methods of realizing transfer function zeros. This classification gives insight into the function of structure in multiple feedback filters, and it also reveals some new structures, for which simple design methods are proposed.

Finally the new structures presented in this thesis, together with a representative selection of known structures, are compared by means of a computational study of sensitivity. This study verifies some theoretical results given in earlier chapters, and it increases our understanding of filter sensitivity.

---

STATEMENT OF ORIGINALITY

---

My aim in this thesis is to advance the study of multiple feedback active CR filters, by giving new insight into the mechanisms by which the structure of a filter influences certain performance characteristics. During the course of this dissertation I give several results which to the best of my knowledge and belief are new, and are my original work. Most of these results I have published in references [45], [77], [84] and [88], which by their nature give supporting evidence of originality.

The principal contributions are some new facts concerning the analysis and transformation of multiple feedback filters in general, a new classification of multiple feedback filters as an aid to insight, and the development of several new multiple feedback structures.

In respect of the analysis and transformation of multiple feedback filters, I have given a scaling transformation which is new in its generality of application. I have shown that sensitivity is invariant for this transformation, and I have discussed the use of scaling to maximize dynamic range. Related to this scaling transformation, but derived independently, is a new summed sensitivity invariant, applicable to the branches of a cutset of the signal flow graph of the multiple feedback filter. I have also pointed out the previously unrecognized sensitivity invariance of flow graph reversal, and the sensitivity invariance of interchanging cascaded subnetworks.

The new classification presented in this thesis is a refinement of the one I published in Ref [84]. I have classified multiple feedback filters in terms of two aspects of their structure. Firstly by the arrangement of the feedback loops which are introduced to reduce the sensitivity of the filter, and secondly by the method of realizing transfer function zeros. I identify three fundamental methods of producing these zeros, namely series zero producing sections, parallel forward paths, and the method which I call complex



feedback. This classification gives insight into the function of structure in multiple feedback filters, and it also reveals the existence of new structures.

I have given several new multiple feedback filters. The one which has aroused the most interest has come to be known in the literature as the Inverse Follow the Leader Feedback filter. I have shown that other new structures may be obtained from known structures by the use of flow graph reversal, and I also demonstrate the existence of certain intermediate structures which are based on little used analogue computing networks. Yet another new structure results from a continued fraction expansion of a lowpass prototype transfer function.

I have undertaken a computational study of the sensitivity of various multiple feedback filters. For several of these structures the sensitivity performance has not previously been investigated. This study shows that the worst case deviation of transmission zeros is lower if series notch sections are used as opposed to parallel forward paths. The analysis also reveals a common pattern to the sensitivity of structures having nested feedback loops.

---

**CONTENTS**

---

	Abstract	2
	Statement of originality	4
1	Introduction	8
	1.1 Active CR filters derived from LCR filters	10
	1.2 Sensitivity	20
	1.3 Gain and dynamic range	26
	1.4 Multiple feedback filters	27
	1.5 Objectives of this thesis	42
2	The concept of multiple feedback	43
	2.1 Definition of multiple feedback	44
	2.2 Analysis of multiple feedback filters	54
	2.2.1 Transfer function	55
	2.2.2 Sensitivity of the transfer function	59
	2.2.3 A summed sensitivity invariant	64
	2.2.4 Dynamic range	77
	2.3 Summary	83
3	Transformation of multiple feedback filters	84
	3.1 Equivalent signal flow graphs	85
	3.2 Interchange of cascade sub-networks	91
	3.3 Flow graph reversal	94
	3.4 Scaling of signal levels	98
	3.5 Similarity transformation	106
	3.6 Summary	108
4	Classification of multiple feedback structures	109
	4.1 The basis of the classification	109
	4.2 Multiple feedback loops for reducing passband sensitivity	113
	4.3 Method of producing transmission zeros	117
	4.4 New structures indicated by the classification	122
	4.5 Low sensitivity structures	125
	4.6 Summary	126

5	Computational study of multiple feedback filters	127
	5.1 Details of the sensitivity computation	128
	5.2 The three canonic expansions of a transfer function	132
	5.2.1 Cascade or factored structure	132
	5.2.2 Partial fraction structure	136
	5.2.3 Continued fraction structure	139
	5.2.4 Sensitivity relations	139
	5.3 Structures with leapfrog feedback	144
	5.3.1 Node-voltage simulation	144
	5.3.2 Coupled-biquad structure	151
	5.3.3 Ford's structure	160
	5.3.4 Leapfrog feedback with complex feedback	168
	5.4 Structures having nested feedback loops	172
	5.4.1 Follow the leader feedback and its transpose	172
	5.4.2 Shifted companion form and intermediate structures	178
	5.4.3 Choice of pre-distortion constant	185
	5.5 Structures having all feedback loops	193
	5.5.1 An adaptation of the Crab's Eye filter	193
	5.6 Summary	197
6	Conclusions	199
	References	203

---

## INTRODUCTION

---

Electric wave filters are widely used in electronic systems to alter the energy content of electrical signals. For instance, if a filter is considered in the frequency domain, it may be required to pass energy in a certain band of frequencies (the passband) and to block the transmission of energy at other frequencies (the stopbands). The first filters comprised an interconnection of inductors, capacitors, and resistors (LCR filters). Subsequently many other electronic components have been used in filters, and of considerable practical interest are filters composed of capacitors, resistors, and active devices which are usually monolithic integrated circuit amplifiers. These are called active CR filters [138].

Such filters avoid the use of inductors, and therefore offer the potential advantages of fabrication as a microelectronic integrated circuit, and of having response characteristics which are not degraded by the imperfections associated with inductors. However in active CR filters the imperfections of integrated circuit amplifiers can have a considerable effect on the response characteristics, and in some cases can cause the filter to oscillate. Such parasitic effects, combined with a high sensitivity to component tolerances, limited the initial application of active CR filters to low frequencies and low orders of complexity.

The construction of more complicated active CR filters became possible when techniques were developed for deriving active CR filters from LCR filter designs, in a way which gives the active CR filters some of the desirable low sensitivity properties of certain LCR filters. Some of these techniques will be described briefly in this introduction.

Firstly we will describe the method of inductor replacement, whereby active CR 1-port sub-networks are used to realize inductance

in place of each magnetic inductor in the LCR filter. Secondly the method of applying complex impedance scaling to an LCR filter, which results in a network of capacitors, resistors, and active CR 2-port impedance converters. Thirdly we will see that an analogue simulation of the LCR filter results in an interconnection of active CR sub-networks, which are unilateral, and are of a type commonly used in the tandem or cascade connection to form simple filters.

In the filter produced by simulation, the unilateral sub-networks (called sections) are interconnected by a forward path and several feedback loops. It is the presence of these feedback loops which gives the simulation filter a low passband sensitivity when compared with more simple active CR filters. There are several ways of arranging feedback loops around unilateral sub-networks in order to reduce the passband sensitivity, and three of them will be described in this introductory Chapter. The first arrangement occurs in the network which simulates an LCR ladder filter, and it is called 'leapfrog feedback'<sup>[15]</sup>. The other two arrangements result from a method of designing the filter directly from the required transfer function, and in the literature they are called 'follow the leader feedback'<sup>[30]</sup> and 'inverse follow the leader feedback'.

Some types of filter responses require transmission zeros, and in this introduction we will describe the three ways in which the unilateral sub-networks or sections may be interconnected to produce transmission zeros. The first is the use of notch sections in the forward path of the filter; the second method is by the cancellation of signals from a number of parallel forward paths; and the third method is to use feedback loops in a particular way, called in this thesis 'complex feedback'.

Many patterns of forward paths and feedback loops are possible and the examples to be described are just some members of a class of networks which comprise an interconnection of active CR sections. It is this class of networks which forms the subject matter of this thesis.

### 1.1 Active CR filters derived from LCR filters

Orchard[1] was the first to suggest that high-order insensitive active CR filters could be made by first designing a low-sensitivity LCR filter, that is one having maximum power transfer in the passband, and then replacing each inductor with an active CR network exhibiting inductance at a pair of terminals. It is possible to design such inductance networks, and moreover they can often be made with a higher Q-factor than the corresponding magnetic inductor, and can have a smaller temperature coefficient. The result is an active CR filter with a performance superior to that of the corresponding LCR filter[2].

It is important to base the design on a low sensitivity LCR filter. To obtain low sensitivity at passband frequencies it is desirable to use an LC 2-port to couple a resistive source to a resistive load, and to arrange that maximum power transfer occurs at the frequencies of minimum loss in the passband. It is this feature which has been found in practice to make the passband response insensitive to variations in the value of inductance and capacitance. This was explained by Orchard[1] in the following way. At a frequency at which maximum power transfer occurs, a change in the value of any inductance or capacitance can only reduce the transfer of power. Thus if the amplitude response is considered as a function of an element value, the response will have a maximum at the nominal element value, and the first derivative will be zero. Hence a variation of an element value from its nominal will cause less change in the response at this frequency than it would if the filter were not designed for maximum power transfer. Furthermore it is argued that at other passband frequencies there will be almost maximum power transfer, and the sensitivity will not be degraded by very much. This explanation and subsequent elaborations[3,4,5] are qualitative rather than quantitative, since only the first derivative is considered. In practice the second and higher derivatives are usually acceptably low.

To obtain low stopband sensitivity it is usual to choose the LC 2-port to have a ladder structure. The transfer function zeros may then occur at the zeros of series admittances, and at the zeros of shunt impedances.

As a simple example of the method of inductor replacement consider the 6-th degree bandpass filter shown in Fig 1.1(a). An active CR filter is obtained when the two grounded inductances,  $L_1$  and  $L_3$ , are realized by active CR grounded inductance networks, and the

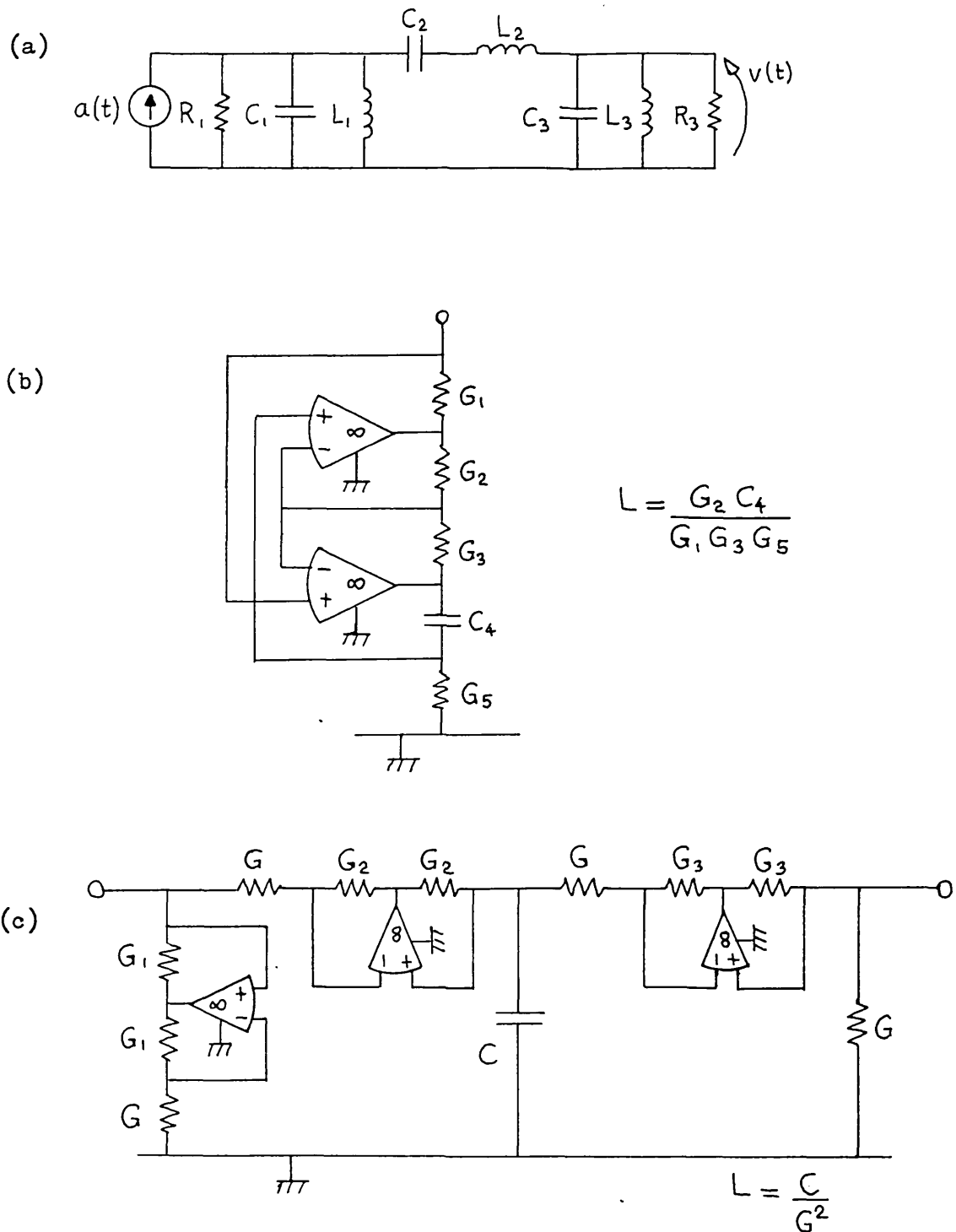


Fig 1.1 Filter produced by inductor replacement

- (a) LCR filter
- (b) Active CR circuit realizing grounded inductance [6]
- (c) Active CR circuit realizing floating inductance [7]

floating inductance  $L_2$  is realized by an active CR floating inductance network. Examples of active CR realizations of grounded and floating inductance are shown respectively in Fig 1.1(b) and Fig 1.1(c). Although the technique of inductor replacement was known earlier [8], Orchard's paper [1] is widely regarded as a turning point in the design of high complexity, precision, active CR filters.

The main difficulty with inductor replacement concerns floating inductance, e.g.  $L_2$  in Fig 1.1. Although floating inductance can be produced in several different ways [9], the ensuing networks are all in some way inferior to those which are used to produce grounded inductance. Complex impedance scaling was introduced as a means of avoiding the need for floating inductance networks. It is a development of the ideas of Gorski-Popiel [10] and Bruton [11], in which impedance scaling is applied to various parts of the LCR filter, and where the scale factor is not a constant but is some multiple of the complex frequency variable  $s$ , or its reciprocal. The method is described most fully in Ref [12], and one way of proceeding, called full impedance scaling, is illustrated in Fig 1.2. The first step is to use Norton equivalent networks [13] to change the LCR filter into a network having all its capacitors grounded, or a network with all its inductors grounded, or a tandem connection of the two as shown in Fig 1.2(b). Equivalent networks may also be used to reduce the range of element values to within practically realizable limits. The second step is to scale the impedance of the capacitor subnetwork by  $s$ , and to scale the impedance of the resistor-inductor subnetwork by  $1/s$ . Impedance converters are then inserted between the two scaled sub-networks, as shown in Fig 1.2(c) and (d). The forward transfer voltage ratio  $F(s) \triangleq v(s)/e(s)$  is unaltered by impedance scaling. Furthermore the active CR filter (Fig 1.2(c)) retains the structure of the LCR filter (Fig 1.2(b)), and each resistor in Fig 1.2(c) corresponds to a capacitor or an inductor in Fig 1.2(b). Consequently a change in the value of one of these resistors has the same effect on  $F(\cdot)$  as a change in the value of the corresponding inductor or capacitor, and the desirable low sensitivity property of the LCR filter is retained. The impedance converters have no counterpart in the LCR filter, but the effect of a change in a conversion ratio is the same as a change in the value of one or more components of the LCR filter. In addition to having a low sensitivity, the active CR filter is particularly suitable for fabrication as a microelectronic unit. The resistors may be accurate and easily adjustable thick-film



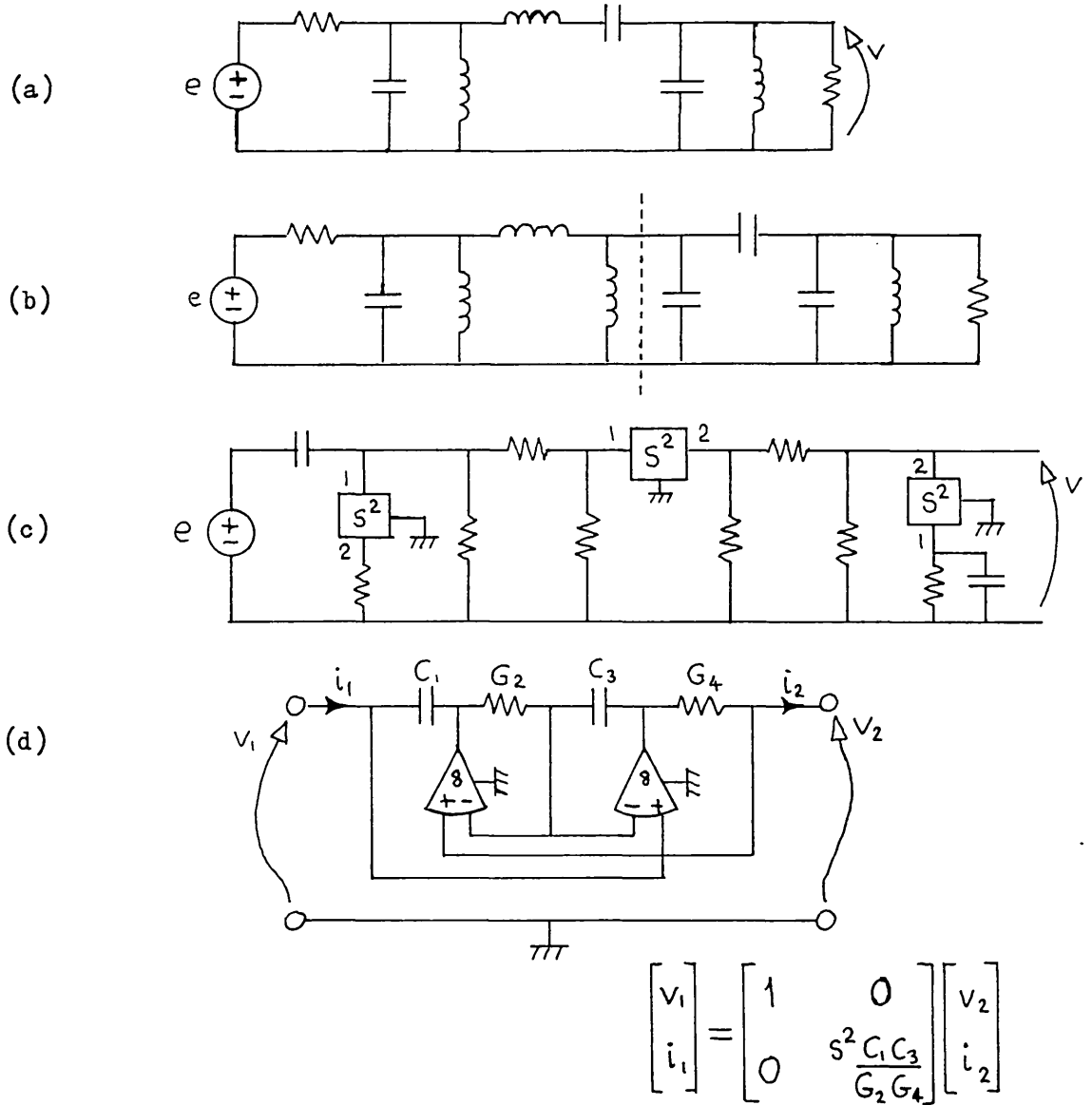


Fig 1.2 Filter produced by complex impedance scaling

- (a) LCR filter
- (b) LCR filter after Norton transformations
- (c) Active CR filter
- (d) Circuit of the  $1:s^2$  impedance converter used in (c) [6]

devices, and the impedance converters may be adjusted individually in a way which takes into account all their component tolerances and amplifier imperfections (at a given frequency). The capacitors may then have wide selection tolerances, and be all of the same nominal value. Another method of complex impedance scaling, called partial impedance scaling [12], can have certain advantages in the more demanding filter applications.

Simulation is another method of designing an active CR filter by derivation from an LCR filter. It is closely related to methods of simulating networks on analogue computers [14], in which equations describing the constitutive constraints, and equations describing the topological constraints are represented or 'simulated' by an interconnection of summing amplifiers, coefficient potentiometers and summing integrators. Voltages in the analogue computer simulation are proportional to, and represent, voltages and currents in the network being simulated. The technique of designing filters by simulation was originated by Girling and Good in 1955 [15], but was not popularized until later [16], when integrated circuit operational amplifiers were readily available. The essence of simulation is to arrange circuits to represent equations of the LCR network. It is convenient for our purposes to represent these equations by a block diagram. Simulation then proceeds in two stages: first the derivation of a block diagram from the LCR filter, and then the creation of an active CR circuit realization of the block diagram. There are many active CR circuits that can simulate a given LCR ladder network, and the use of a block diagram will allow us to investigate properties common to all realizations of a given set of equations. The process of obtaining a block diagram from a ladder network is illustrated in Fig 1.3. Fig 1.3(a) shows an impedance  $Z$  and a corresponding block diagram representation\* of the equation  $v = Zi$ . Dually, the representation of admittance is shown in Fig 1.3(b). Kirchhoff's current law equations and Kirchhoff's voltage law equations are represented in the block diagram by a symbol which we shall call an adder, as shown in Fig 1.3(c) and (d). One other block diagram symbol will be used, this is an open arrow as used in the two feedback paths in Fig 1.3(f), and it indicates multiplication by the associated constant; in this case  $-1$ . It should now be possible

---

\* Such a representation is often called a "Black box". This is in honour of the network theorist H. S Black, who first used the symbol in 1934 in connection with stabilized feedback amplifiers.

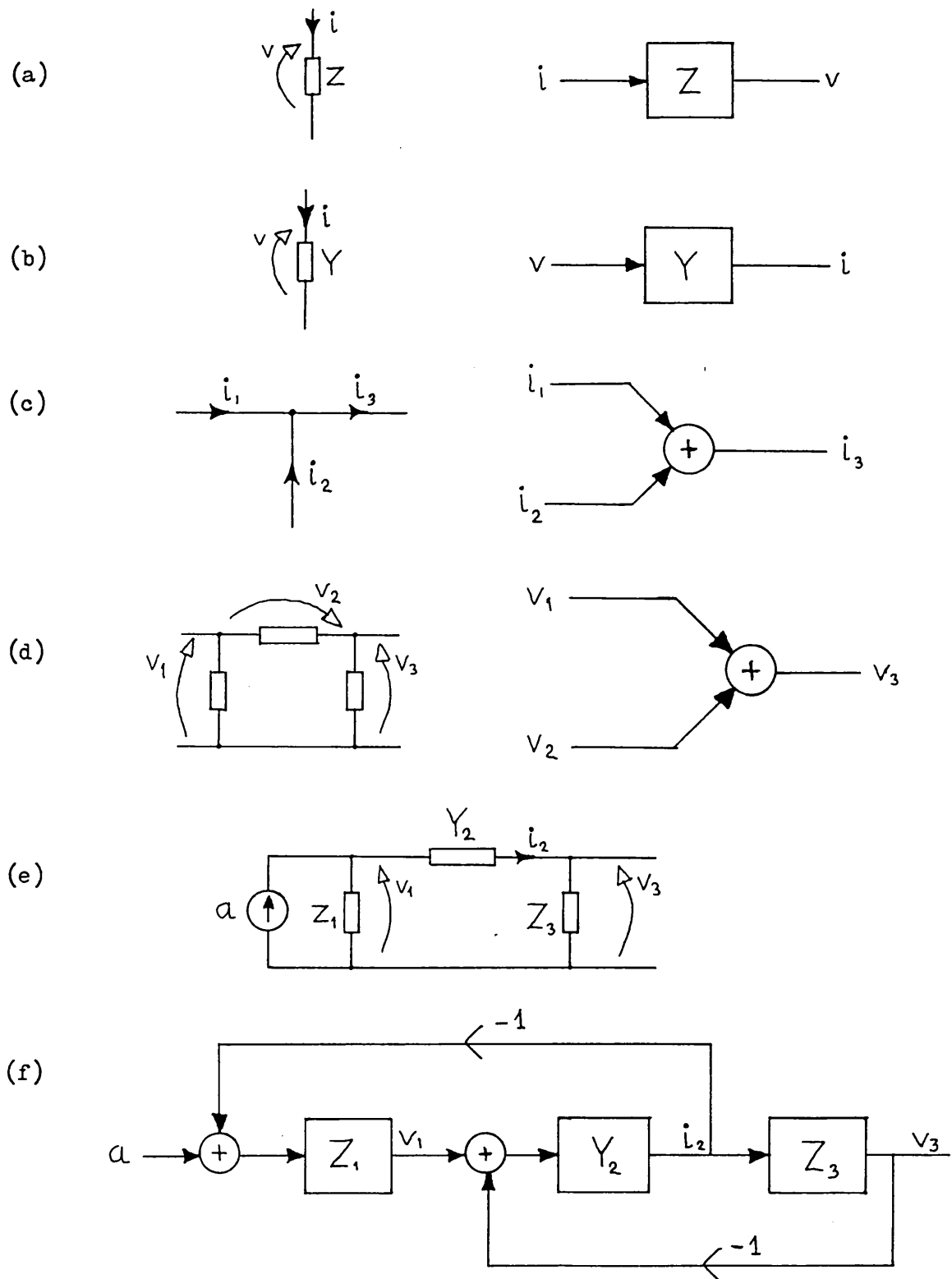


Fig 1.3 Block diagram of a ladder network

- (a) Representation of impedance
- (b) Representation of admittance
- (c) Representation of Kirchhoff's current law
- (d) Representation of Kirchhoff's voltage law
- (e) Ladder network
- (f) Block diagram derived from the ladder network in (e)

for the reader to trace the way in which the block diagram in Fig 1.3(f) represents the ladder network shown in Fig 1.3(e).

Several different block diagrams can be obtained from a given ladder network, depending on which set of Kirchhoff equations is used, and depending on the choice of impedance representation or admittance representation for each branch of the ladder. Not all block diagrams are useful, and the one shown in Fig 1.3(f) was chosen as an example because in at least two cases it leads to practical filter realizations, using the required type of active CR circuits.

Firstly, if the ladder network is a lowpass filter as shown in Fig 1.4(a), then the block diagram (shown in Fig 1.4(b)) may be realized by an interconnection of summing integrators, summing lossey integrators, and inverting amplifiers. A simple manipulation of the block diagram, involving sign changes only, enables us to use inverting integrators and just one inverting amplifier, as shown in Fig 1.4(c). This is the 'leapfrog feedback' filter introduced by Girling and Good [16].

Secondly, if the ladder network is a bandpass filter as shown in Fig 1.5(a), then the blocks will be quadratic functions as shown in Fig 1.5(b), and the block diagram may be realized by an interconnection of active CR quadratic circuits [17,18,19]. Such unilateral quadratic circuits\* have been studied at great length for use in simple active CR filters, and the types shown in Fig 1.5(c) and (d) were given respectively by Haigh† and Fliege [20]. We have avoided the use of inverting amplifiers by using an inverting quadratic circuit to realize the block  $Y_2$ , and the adders have been realized as an integral part of the quadratic circuits [22].

Complex impedance scaling and simulation, as represented respectively in Fig 1.2 and Fig 1.5, are widely used methods of designing high order active CR filters. Comparison of the performance of the two configurations is difficult; depending for instance on the type of impedance converter used in impedance scaling, and on the type of quadratic circuit used in simulation. One contribution [23] compares a filter using the circuit in Fig 1.2(c) and (d), with a filter of the type shown in Fig 1.5 but using quadratic circuits

---

\* Variously called blocks, sections, building blocks, resonators, biquads, cells, filter modules (filterbausteine) or standard selective functional blocks.

† This unpublished circuit was described to the writer on 3 March 1980 by Dr D G Haigh, who designed it from the Fliege circuit by the method of terminal interchange [21].

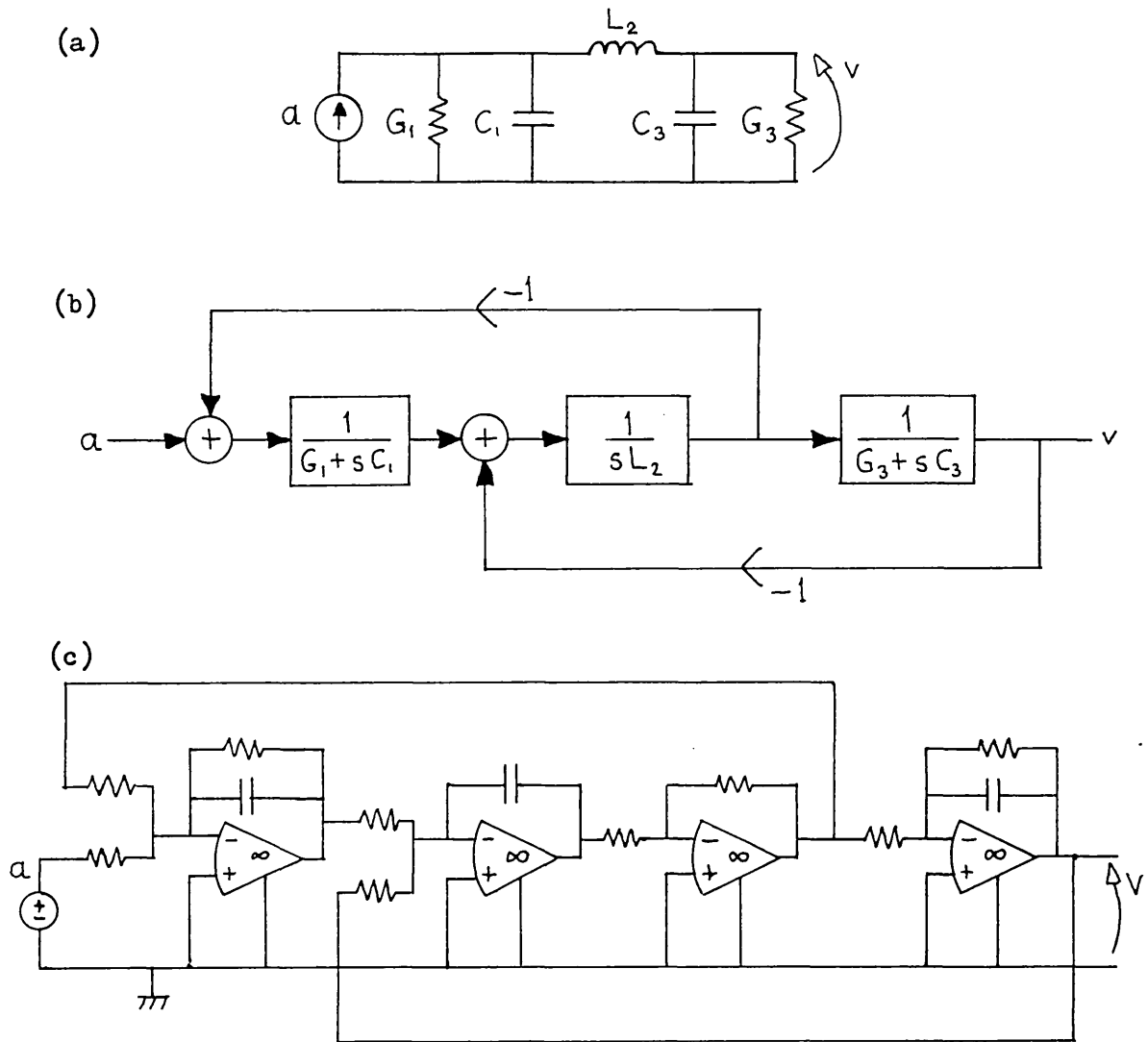


Fig 1.4 Lowpass leapfrog feedback filter

- (a) LCR ladder
- (b) Block diagram of simulation
- (c) Active CR realization

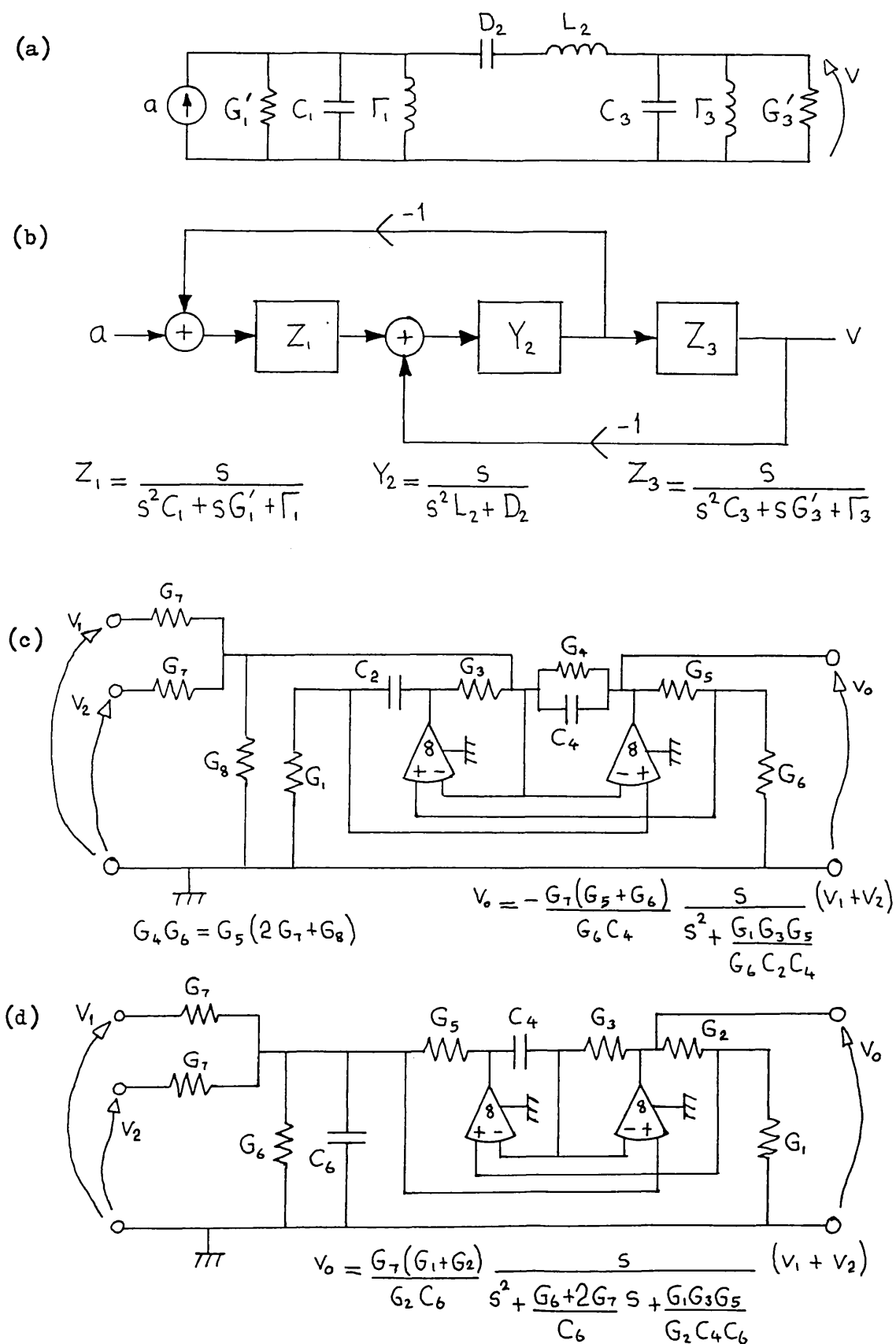


Fig 1.5 Filter produced by simulation

- (a) LCR filter
- (b) Block diagram of simulation
- (c) Circuit realizing block  $Y_2$  and its associated adder<sup>†</sup>
- (d) Circuit realizing block  $Z_1$  and its associated adder [20].  
Block  $Z_3$  is similar.

having one amplifier and three capacitors each. The authors indicate that the two methods give roughly comparable sensitivity performance, with the leapfrog feedback\* filter slightly inferior in the variation of frequency independent gain. It must be noted however that the single amplifier quadratic circuits they use are probably inferior to the two-amplifier circuits suggested in Fig 1.5. Whilst there remains some doubt about the detailed comparison, it is certain that both configurations have good sensitivity performance in the passband (compared with the simple cascade filter) as a result of being derived from a low sensitivity LCR filter.

The methods of complex impedance scaling and simulation are examples of the two major trends in high order active CR filter synthesis, one based on the use of impedance converters, and the other based on the use of unilateral subnetworks. Both methods are capable of extension beyond the scope indicated by the simple examples given here, but in this thesis we shall consider only filters based on the use of unilateral subnetworks.

We will be concerned with various aspects of the performance of such filters, the most important being sensitivity and dynamic range. Our treatment of these will be introduced in the next two sections, using the simulating filter as an example.

---

\* The nomenclature used in Ref 23 is different to that adopted in this thesis. In Ref 23 the filter produced by complex impedance scaling is referred to as a Simulating Circuit, and the filter produced by simulation is called a Leapfrog Circuit.

## 1.2 Sensitivity

In the previous section we have seen that in the case of complex impedance scaling there is a correspondence between the resistors in the active CR realization and the inductors and capacitors in the LCR realization. It follows that the sensitivity of the transfer function to changes in the values of these components is the same for both realizations. Such is not the case for the filter designed by simulation, since for example in Fig 1.5(a) and (b) the components  $G'_1$ ,  $C_1$ , and  $\Gamma_1$  are all simulated by the first block  $Z_1$ . This block would normally be characterized by its resonance frequency  $\omega_0 = \sqrt{\Gamma_1/C_1}$ , its quality factor  $Q = \sqrt{\Gamma_1 C_1} / G'_1$ , and its gain constant  $K = 1/C_1$ , so that:

$$Z_1 = K \frac{s}{s^2 + \frac{\omega_0}{Q} s + \omega_0^2} \quad (1.2.1)$$

These intermediate variables are functions of the constituent elements of the block, and the functions depend on the type of quadratic circuit being used to realize the block. We will in Chapter 5 be studying sensitivity in terms of these intermediate variables in order to obtain results which are independent of the particular way in which the blocks are realized. In this section we will show that it is the presence of feedback loops which gives the simulating filter its low passband sensitivity, and in doing so we will introduce the formal definitions of sensitivity.

Accordingly consider first the structure of the simple cascade filter shown in Fig 1.6(a). If the blocks represent quadratic circuits then this structure would realize a 6-th degree response. Evidently we have:

$$F(s) \triangleq \frac{v(s)}{e(s)} = G_1 G_2 G_3 \quad (1.2.2)$$

For purposes of design it is usually desirable to know how, in the sinusoidal steady state, the amplitude response  $|F(i\omega)|$  deviates from its nominal value due to component tolerances and parasitic effects. This information can be obtained by a statistical analysis<sup>[25]</sup> or a worst-case analysis<sup>[24]</sup> of the complete filter network. Our purpose however is to acquire an understanding of network behaviour in the hope that new insight will enable us to design better filters. We therefore consider separately the effect of changes in each element of the block diagram. So in (1.2.2) we give, for instance, in



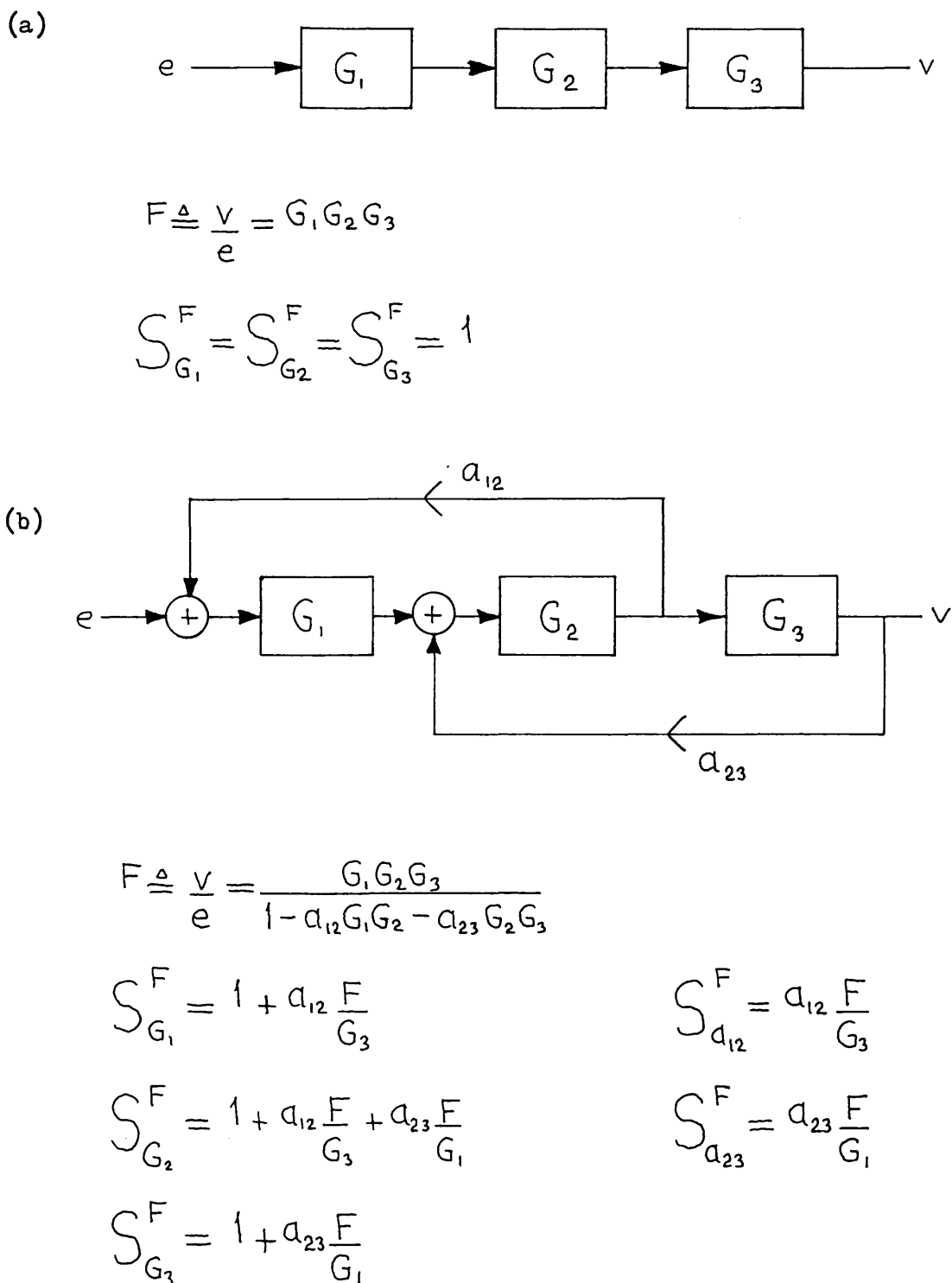


Fig 1.6 Two structures and their differential sensitivities

- (a) Cascade structure of simple active CR filters  
 (b) Leapfrog feedback structure of the analogue simulation filter

$G_3$ , an increment  $\Delta G_3$  which causes an increment  $\Delta F = F(s; G_3 + \Delta G_3) - F(s; G_3)$ . One measure of sensitivity would be the divided difference  $\Delta F / \Delta G$ , but it is usual to take the dimensionless ratio of the fractional change in the transfer function  $F(s)$  to the fractional change in an element  $w$ , and to define this as the finite difference sensitivity, thus:

$$\mathcal{S}_w^F = \frac{w}{F(s; w)} \frac{F(s; w + \Delta w) - F(s; w)}{\Delta w} \quad (1.2.3)$$

whence from (1.2.2) the finite difference sensitivity of  $F(s)$  to change in  $G_3$  is found to be:

$$\mathcal{S}_{G_3}^F = 1 \quad (1.2.4)$$

Similarly for the other block diagram elements.

It is often useful, and easier, to use the differential sensitivity, defined as :

$$S_w^F \triangleq \lim_{\Delta w \rightarrow 0} \mathcal{S}_w^F = \frac{w}{F(s)} \frac{\partial F(s)}{\partial w} \quad (1.2.5)$$

For example from (1.2.4) we have:

$$S_{G_3}^F = 1 \quad (1.2.6)$$

This known result is in fact a very simple special case of a summed sensitivity invariant, which has been found by the writer and is described fully in Chapter 2.

Using a known result of the sensitivity calculus, it follows from (1.2.6) that:

$$S_{G_3}^{|F|} = \operatorname{Re} S_{G_3}^F = 1 \quad (1.2.7)$$

and similarly for the blocks  $G_1$  and  $G_2$ . Such modulus sensitivities give us the information we require to study the way in which the deviation of the amplitude response  $|F(i\omega)|$  is influenced by each element in the block diagram. In addition to providing insight into network behaviour, these sensitivities may be combined to give an estimate of the worst case variation [24] or the statistical variation [25] of the amplitude response.

Now consider the structure of the filter designed by simulation, shown in Fig 1.6(b). When feedback paths occur around adjacent pairs of blocks, the structure is said to have 'leapfrog feedback'. The transfer function may be found by analysis (described in Chapter 2) to be:

$$F(s) \triangleq \frac{v(s)}{e(s)} = \frac{G_1 G_2 G_3}{1 - a_{12} G_1 G_2 - a_{23} G_2 G_3} \quad (1.2.8)$$

The differential sensitivities of this structure may be found by direct application of the definition (1.2.5) to the transfer function (1.2.8), or by one of the many other methods, including the one described in Chapter 2. This gives, for example, for the third block:

$$\sum_{G_3(s)}^{F(s)} = 1 + a_{23} \frac{F(s)}{G_1(s)} \quad (1.2.9)$$

from which we see, by comparison with (1.2.6) for the cascade structure, that the presence of the feedback path  $a_{23}$  has altered the sensitivity of the third block.

Expressions for the sensitivities to the other block diagram elements have been found, and are shown in Fig 1.6(b). Notice that we have, for example:

$$\sum_{G_3}^F - \sum_{a_{23}}^F = 1 \quad (1.2.10)$$

This again is a special case of the summed sensitivity invariant, to be described in Chapter 2.

For the leapfrog feedback structure the sensitivities are evidently frequency dependent. To investigate these further we identify the leapfrog feedback structure shown in Fig 1.6(b), with the filter designed by simulation, shown in Fig 1.5(a) and (b). We will assume that this filter has been designed from a lowpass prototype having equal valued terminating resistances (for low sensitivity), and that the usual transformation has been used to give a bandpass response which is geometrically symmetrical about a centre frequency of  $\omega_0$ . It follows that:

$$\omega_0^2 = \frac{\Gamma_1}{C_1} = \frac{D_2}{L_2} = \frac{\Gamma_3}{C_3} \quad (1.2.11)$$

and at the center frequency, when  $s = i\omega_0$ , we have:

$$F = \frac{1}{G_1' + G_3'} \quad , \quad Z_1 = \frac{1}{G_1'} \quad , \quad Z_3 = \frac{1}{G_3'} \quad (1.2.12)$$

so that, referring to Fig 1.6(b), the frequency dependent terms which appear in the sensitivities have the values:

$$a_{12} \frac{F(i\omega_0)}{G_3(i\omega_0)} = a_{23} \frac{F(i\omega_0)}{G_1(i\omega_0)} = -\frac{1}{2} \quad (1.2.13)$$

whereupon the modulus sensitivities for the three blocks become:

$$\int_{G_1(i\omega_0)} |F(i\omega_0)| = \int_{G_3(i\omega_0)} |F(i\omega_0)| = \frac{1}{2}$$

$$\int_{G_2(i\omega_0)} |F(i\omega_0)| = 0 \quad (1.2.14)$$

compared with unity for all three blocks in the cascade structure.

We also have:

$$\int_{a_{12}} |F(i\omega_0)| = \int_{a_{23}} |F(i\omega_0)| = -\frac{1}{2} \quad (1.2.15)$$

At frequencies in the upper stopband of the filter we have in Fig 1.5(b):

$$Z_1 \doteq \frac{1}{sC_1}, \quad Y_2 \doteq \frac{1}{sL_2}, \quad Z_3 \doteq \frac{1}{sC_3} \quad (1.2.16)$$

so that, for  $s=i\omega_1$ ,  $\omega_1 \gg \omega_0$ , referring to Fig 1.6(b), we have:

$$a_{12} \frac{F(i\omega_1)}{G_3(i\omega_1)} \doteq \frac{1}{\omega_1^2 C_1 L_2} \quad (1.2.17)$$

For flat passband filters the factor  $C_1 L_2$  has the approximate value:

$$C_1 L_2 \doteq \frac{2q^2}{\omega_0^2} \quad (1.2.18)$$

where  $q$  is the geometric centre frequency  $\omega_0$  divided by the width of the passband. Whence for upper stopband frequencies:

$$\begin{aligned} a_{12} \frac{F(i\omega_1)}{G_3(i\omega_1)} &\doteq \frac{\omega_0^2}{\omega_1^2} \frac{1}{2q^2} \\ &\ll 1 \end{aligned} \quad (1.2.19)$$

Similarly for  $a_{22} F(i\omega_1)/G_1(i\omega_1)$ . Hence for the upper stopband the modulus sensitivities become:

$$\int_{G_1(i\omega_1)} |F(i\omega_1)| \doteq \int_{G_2(i\omega_1)} |F(i\omega_1)| \doteq \int_{G_3(i\omega_1)} |F(i\omega_1)| \doteq 1 \quad (1.2.20)$$

as in the cascade structure, and

$$\int_{a_{12}} |F(i\omega_1)| \doteq \int_{a_{23}} |F(i\omega_1)| \ll 1 \quad (1.2.21)$$

A similar argument shows that (1.2.20) and (1.2.21) are also valid for the lower stopband.

In this section we have compared the structure of the filter designed by simulation with the structure of the simple cascade filter, as an illustration of how the presence of feedback loops

affects the sensitivities with respect to the blocks. At a frequency in the centre of the passband the sensitivities are reduced by feedback, and at stopband frequencies, where the feedback loops become inoperative, the sensitivities of the two structures are approximately the same.

The reduced sensitivities at the frequency  $\omega_0$  are not a complete indication of superior performance, because we are also interested in the sensitivity at other passband frequencies. When studying the sensitivity of filters in Chapter 5, we will compute the sinusoidal steady state amplitude response  $|F(i\omega)|$  of the filter and will plot this as a function of frequency. Superimposed on this will be a plot of the amplitude frequency response which results from one of the block diagram elements being changed by a finite non-zero amount, or from one or more of the intermediate variables ( $\omega_0$ ,  $Q$  etc.) of a block being changed by a finite non-zero amount. A collection of such plots for changes in all block diagram elements of a given filter will give a very good indication of the sensitivity performance of the filter, and will allow us to compare structures in a way which is independent of the particular circuits used to realize the sections of the filter.

### 1.3 Gain and dynamic range

The gain of the filter designed by simulation is determined by the gain of the LC filter which it simulates. The gain can usually be adjusted. For instance in Fig 1.5(c) and (d) the potential dividers at the input of the sections can be changed to alter the gain of the sections, without any alteration to the main part of the circuit, and hence their sensitivity performance as isolated quadratic circuits is not changed.

In terms of the block diagram elements in Fig 1.6(b), if, for the first block,  $G_1$  is multiplied by a constant  $\lambda$ , and if the feedback constant  $Q_{1,2}$  is divided by  $\lambda$ , then the transfer function of the filter (hence the gain) will be multiplied by a factor  $\lambda$ . However the block diagram will no longer simulate the ladder network, because, for example, the first adder will no longer represent a Kirchhoff equation. This raises the question of whether the sensitivity performance of the complete filter will be affected. The answer is no, as will be proved in Chapter 3, where a much more general scaling transformation will be presented, together with an account of its affect on sensitivity.

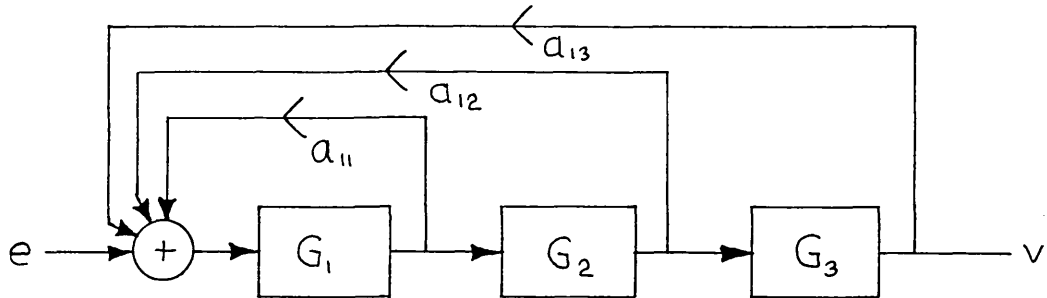
In addition to adjusting the overall gain of the filter, the scaling transformation may be used to adjust independently the signal levels at the outputs of each internal section of the filter. By this means the maximum signal levels at the outputs of all sections can be made equal to each other, thus maximizing dynamic range without impairing the sensitivity performance. A fuller discussion of dynamic range, and the use of the scaling transformation to maximize dynamic range, is given in Chapters 2 and 3.

#### 1.4 Multiple feedback filters

In section 1.2 we illustrated how the low passband sensitivity of the filter designed by simulation was made possible by the presence of the feedback paths. It is possible to obtain comparably low sensitivity with several other arrangements of feedback paths, and one such structure called 'follow the leader feedback' is shown in Fig 1.7, for the case where the filter has three blocks. This structure is related to a method of simulating transfer functions on an analogue computer [26] by an interconnection of integrators, coefficient potentiometers, and summing amplifiers. It was first used to realize high order filters by Hurtig III [27] in his 'primary resonator block' filter. Hurtig's design proceeds directly from the required transfer function, and it is not in any way related to an LCR filter. All the blocks are identical to each other, and for a bandpass filter could for example be realized by the type of section shown in Fig 1.5(d). The quality factor  $Q$  of the sections is predetermined in Hurtig's design by the fact that he sets the first feedback path  $Q_{11}$  equal to zero. The primary resonator block filter is capable of a sensitivity performance similar to that of a filter designed by simulation [28].

The same structure was used later but independently by Laker [29] in his 'follow the leader feedback' filter. Laker did not restrict all blocks to have the same value of  $Q$ , and he used this additional flexibility to minimize a measure of sensitivity, in a computer optimization procedure. This procedure used a multiparameter sensitivity measure that was integrated over a wide band of frequencies. The integrated sensitivity measure of the optimized follow the leader feedback filter was lower than that of a filter having a leapfrog feedback structure. At a frequency in the center of the passband however the leapfrog feedback filter had a lower sensitivity measure. In subsequent work, Laker showed that the sensitivity measure of the follow the leader feedback filter had a broad minimum [30], thus allowing some flexibility in the choice of  $Q$  values without serious degradation of sensitivity. He also showed that the sensitivity measure of the primary resonator block filter was not far short of the minimum [31]. Schaumann and others [32] have shown how Laker's follow the leader feedback filter may be designed to have maximum dynamic range.

We have so far considered polynomial filters, that is filters which have their transfer function zeros all either at the origin of



$$F \triangleq \frac{v}{e} = \frac{G_1 G_2 G_3}{1 - a_{11} G_1 - a_{12} G_1 G_2 - a_{13} G_1 G_2 G_3}$$

$$S_{G_1}^F = 1 + a_{11} \frac{F}{G_2 G_3} + a_{12} \frac{F}{G_3} + a_{13} F$$

$$S_{a_{11}}^F = a_{11} \frac{F}{G_2 G_3}$$

$$S_{G_2}^F = 1 + a_{12} \frac{F}{G_3} + a_{13} F$$

$$S_{a_{12}}^F = a_{12} \frac{F}{G_3}$$

$$S_{G_3}^F = 1 + a_{13} F$$

$$S_{a_{13}}^F = a_{13} F$$

Fig 1.7 Follow the leader feedback structure



the  $s$ -plane or at infinity. It is often desirable to realize transfer functions which have zeros in complex conjugate pairs on the imaginary axis of the  $s$ -plane. These give transmission zeros at finite non-zero frequencies, and would be used for example in Causer type filters.

There are three methods of introducing such transmission zeros, the most common of which is the method used in the simple cascade filter. Referring to Fig 1.6(a), if one of the blocks has the factor  $s^2 + \omega_n^2$  in the numerator polynomial of its transfer function, then by (1.2.2) this will also be a factor in the numerator of  $F(s)$  and the filter will have a transmission zero at  $\omega_n$  rad/s. The case where such a factor is cancelled by the same factor being introduced to the denominator of  $F(s)$  by one of the other blocks is always avoided in practice. A section having a factor  $s^2 + \omega_n^2$  in the numerator of its transfer function is called a 'notch section', and when such a section occurs in the forward path of a structure we say that a transmission zero is produced by a 'series notch section'.

Consider now the leapfrog feedback structure shown together with its transfer function in Fig 1.6(b). One can see that again a quadratic factor in the numerator polynomial of one of the blocks will also appear in the numerator of the transfer function. Szentirmai [33], Dubois & Neiryneck [34,104] and Müller [35] have given methods of designing leapfrog feedback structures which incorporate series notch sections. Series notch sections may also be used with the 'follow the leader' feedback structure, shown in Fig 1.7, and suitable design methods have been given by Biernacki & Mulawka [36], Dubois & Neiryneck [37], Tow [38,39], Gensel [40,41], and Padukone, Mulawka & Ghausi [42]. These design methods allow transmission zeros to be placed at any required frequency, and the resulting structures are therefore often called 'generalized'.

Whilst series notch sections allow arbitrary placing of transmission zeros, the next method to be described leads to a very simple realization for geometrically symmetrical bandpass filters. It consists of adding together signals from a number of forward paths, and the transmission zeros occur at frequencies at which these signals sum to zero. Many structures use this method, and because of its importance in the study of structure it will be illustrated here by describing in detail one particular structure which uses the technique.

The method is applicable to any bandpass filter that can be obtained from a lowpass prototype by the usual lowpass to bandpass transformation. The lowpass prototype transfer function is synthesized by a well known analogue computing circuit, using integrators as active components, and the required bandpass network is obtained by lowpass to bandpass transformation. This changes the integrators into bandpass quadratic sections having an infinite Q-factor. We prefer to use sections having a finite Q-factor, and this is achieved by predistortion [138].

To describe the method in detail, let the transfer function of the lowpass prototype be:

$$\Phi(s) = \frac{\nu_0 + \nu_1 s + \dots + \nu_n s^n}{\delta_0 + \delta_1 s + \dots + \delta_n s^n}, \quad \delta_n = 1 \quad (1.4.1)$$

This is predistorted by the transformation  $s \longmapsto s - \alpha_1$ , giving:

$$\Phi(s - \alpha_1) = \frac{\nu_0 + \nu_1 (s - \alpha_1) + \dots + \nu_n (s - \alpha_1)^n}{\delta_0 + \delta_1 (s - \alpha_1) + \dots + \delta_n (s - \alpha_1)^n}, \quad \delta_n = 1 \quad (1.4.2)$$

which, using the binomial theorem, can be written as:

$$\Phi(s - \alpha_1) = \frac{\sum_{j=0}^n \nu_j \sum_{\ell=0}^j \binom{j}{\ell} (-\alpha_1)^\ell s^{j-\ell}}{\sum_{j=0}^n \delta_j \sum_{\ell=0}^j \binom{j}{\ell} (-\alpha_1)^\ell s^{j-\ell}}, \quad \delta_n = 1 \quad (1.4.3)$$

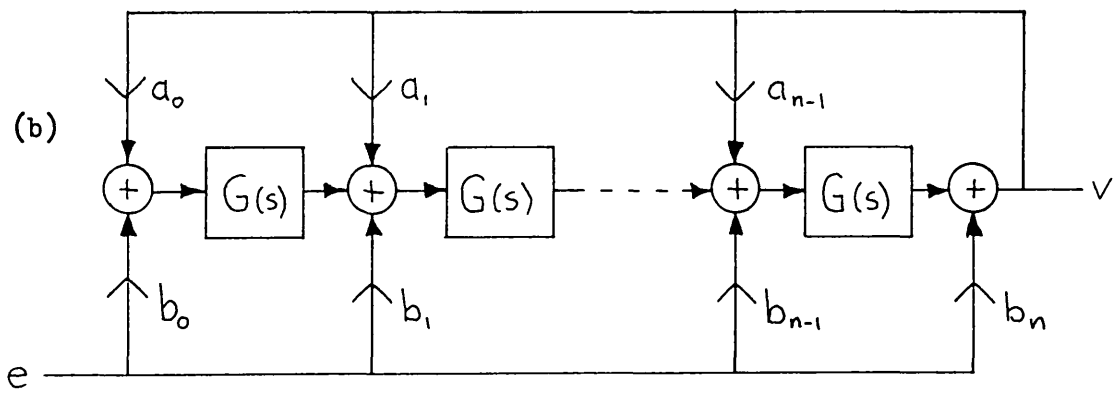
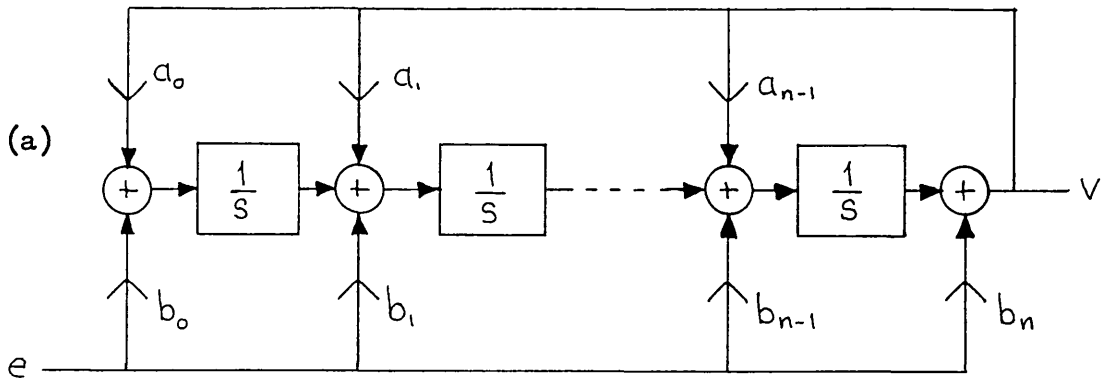
As an intermediate step, we synthesize  $\Phi(s - \alpha_1)$ , using the 'successive-integration' method of simulating transfer functions on analogue computers [43,44]. The computer network (using positive-gain integrators) is shown in Fig 1.8(a), and its transfer function is:

$$F(s) = \frac{v(s)}{e(s)} = \frac{b_0 + b_1 s + \dots + b_n s^n}{-a_0 - a_1 s - \dots - a_{n-1} s^{n-1} + s^n} \quad (1.4.4)$$

Now  $\Phi(s - \alpha_1)$  can be written in this form by interchanging the order of summation in (1.4.3) and introducing the index  $k = j - \ell$ , so that the coefficients of the powers of  $s$  are stated explicitly:

$$\Phi(s - \alpha_1) = \frac{\sum_{k=0}^n \sum_{j=k}^n \nu_j \binom{j}{k} (-\alpha_1)^{j-k} s^k}{\sum_{k=0}^n \sum_{j=k}^n \delta_j \binom{j}{k} (-\alpha_1)^{j-k} s^k}, \quad \delta_n = 1 \quad (1.4.5)$$

Comparing (1.4.4) and (1.4.5), we have the design equations for the analogue computer network:



For lowpass prototype response

$$G(s) = \frac{1}{s + \alpha_i}$$

For required bandpass response

$$G(s) = \frac{1}{q} \frac{s}{s^2 + \frac{\alpha_i}{q}s + 1}$$

Fig 1.8 Multiple feedback structure with parallel forward paths

- (a) Analogue computer network
- (b) Multiple feedback structure

$$b_k = \sum_{j=k}^n v_j \binom{j}{k} (-\alpha_1)^{j-k} \quad k = 0, 1, \dots, n \quad (1.4.6)$$

$$a_k = -\sum_{j=k}^n \delta_j \binom{j}{k} (-\alpha_1)^{j-k} \quad k = 0, 1, \dots, n-1 \quad (1.4.7)$$

The effect of predistortion is now removed by applying the inverse transformation  $s \longrightarrow s + \alpha_1$  to the computer network. This affects only the integrator blocks, which become  $G(s) = 1/(s + \alpha_1)$ , and the result is a block diagram, shown in Fig 1.8(b), which realizes the lowpass prototype transfer function  $\bar{\Phi}(s)$ .

It should be noted that in the conventional use of predistortion,  $\bar{\Phi}(s - \alpha_1)$  would be synthesized as a passive network and would therefore need to be stable, thus limiting the possible values of  $\alpha_1$ . Such is not the case here and  $\alpha_1$  is not limited.

The required bandpass response can now be obtained by applying the lowpass to bandpass transformation [140]:

$$s \longrightarrow q \left( s + \frac{1}{s} \right) \quad (1.4.8)$$

where  $q$  is the geometric center frequency divided by the width of the passband. This affects only the blocks  $G(s)$ , which will now have the transfer function:

$$G(s) = \frac{1}{q} \frac{s}{s^2 + \frac{\alpha_1}{q} s + 1} \quad (1.4.9)$$

as shown in Fig 1.8(b). The resulting bandpass structure consists of an interconnection of identical bandpass quadratic blocks, which, due to predistortion, have a finite quality factor  $Q = q/\alpha_1$ . Evidently, if the filter is to use sections having a positive  $Q$ -factor, then  $\alpha_1$  must be positive. The feedback and feedforward constants are given by (1.4.7) and (1.4.6) as for the lowpass prototype. They may be positive or negative, and their signs will vary, depending on the value chosen for  $\alpha_1$ . The consequent need for inverting amplifiers can sometimes be avoided by the use of inverting and non-inverting quadratic sections, as will be shown by an example.

As an illustration of the design method, a 6-th degree, elliptic function, bandpass filter has been designed and is shown in Fig 1.9. The lowpass prototype response has a passband ripple of 1.25dB, a minimum stopband attenuation of 40.5dB, and a transition band of

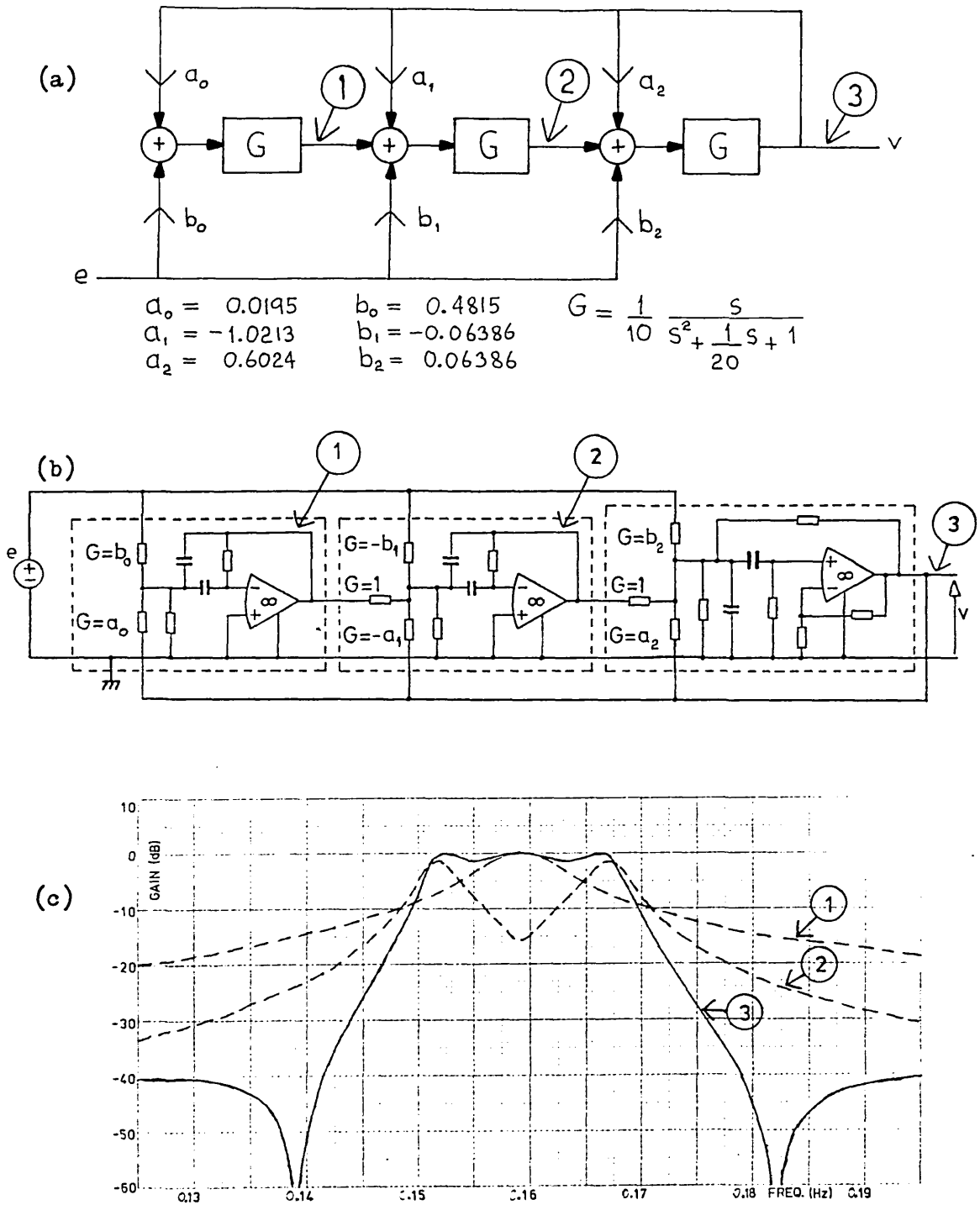


Fig 1.9 6-th degree elliptic-function bandpass filter

- (a) Block diagram
- (b) Active CR realization
- (c) Computed frequency response

1: 2.3662. The lowpass prototype transfer function is:

$$\bar{\Phi}(s) = \frac{0.06386 s^2 + 0.4655}{s^3 + 0.8975 s^2 + 1.1688 s + 0.4655} \quad (1.4.10)$$

For the required bandpass response  $q = 10$ . The value of the predistortion constant  $\alpha_1$  was chosen to be 0.5, whence from (1.4.6), (1.4.7) and (1.4.10):

$$\begin{aligned} b_0 &= 0.4815 \\ b_1 &= -0.06386 \\ b_2 &= 0.06386 \\ b_3 &= 0 \\ a_0 &= 0.0195 \\ a_1 &= -1.0213 \\ a_2 &= 0.6024 \end{aligned} \quad (1.4.11)$$

The transfer function of the blocks  $G$  is given by (1.4.9) with  $q = 10$  and  $\alpha_1 = 0.5$ , thus giving a quality factor  $Q = 20$ , as shown in Fig 1.9(a). The two negative constants  $a_1$  and  $b_1$  were accommodated by changing the signs of these constants and also changing the signs of the first two blocks. This is a simple application of the scaling transformation which will be described in Chapter 3. The resulting network, shown in Fig 1.9(b), uses two inverting bandpass quadratic sections and one non-inverting bandpass quadratic section, thus avoiding the need for inverting amplifiers. Each of the three sections, shown encompassed by dashed lines in Fig 1.9(b), realizes a block together with its preceding adder and associated constant multipliers.

The multiple feedback structure described above was first published by the writer in Ref. [45], where it was presented as having an advantage over existing structures in some cases by virtue of using fewer operational amplifiers. It is described here to illustrate how transmission zeros may be realized by adding together signals from a number of forward paths. In the example shown in Fig 1.9(a) there are three forward paths which come together at the third adder, and it is at the output of this adder that the two pairs of complex conjugate zeros of the bandpass transfer function first appear. These zeros are not present at the outputs of the first two sections, as can be seen from the frequency responses at these two points, which have been superimposed on a plot of the frequency response of the filter in Fig 1.9(c). We say that these transmission zeros are produced by 'parallel forward paths'. The third block has one zero at the origin of the  $s$ -plane and another zero at infinity, and, since

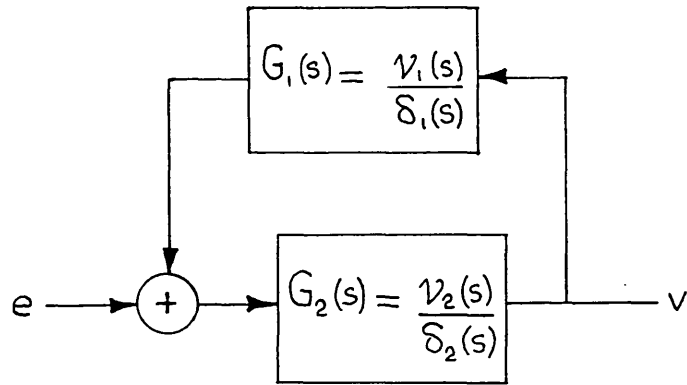
all three forward paths pass through the third block, these zeros form the two transmission zeros of the bandpass response at extreme frequencies.

It is worth noting that although no attempt was made to minimise sensitivity in the example, the structure can have a low sensitivity at passband frequencies, due to the presence of the three feedback loops. The sensitivity does depend on the choice of the predistortion constant  $\alpha$ , and this will be discussed further in Chapter 5. The three feedback loops are nested in a manner similar to the follow-the-leader feedback, and in the literature this structure has been called 'inverse follow the leader feedback'[76]. It will be seen in Chapter 3 that this arrangement of feedback paths may preferably be described as 'flow graph reversed follow the leader feedback' or 'transpose follow the leader feedback'.

It should also be noted that the design method can be applied with minor modification to other analogue computer networks [46], thus leading to other multiple feedback structures. For example Tow's 'Shifted companion form' network in Ref. [47] can be obtained by using the computer network in section 3.20 of Ref. [46]. Conversely Tow's design method can be adapted to yield the structure described above.

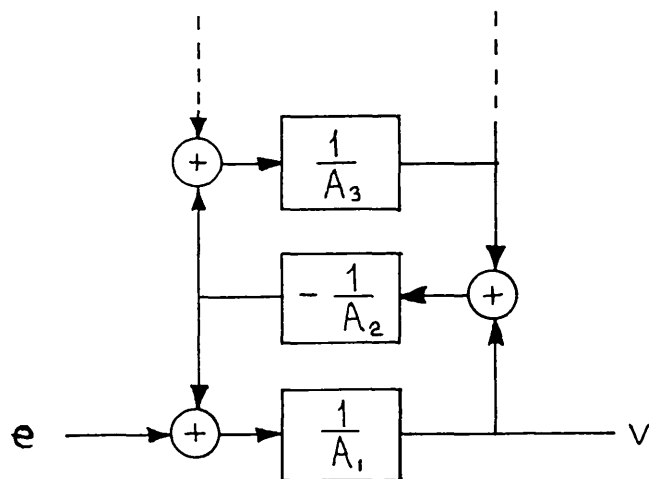
Tow's shifted companion form network [47,28] uses a structure which combines parallel forward paths with follow the leader feedback. Other design methods for this combination have been given by Laker & Ghausi [48], and Gensel [40,41]. Parallel forward paths may also be combined with leapfrog feedback, and suitable design methods for some structures which use this combination have been given by Tow & Kuo [49]; Wetenkamp & Van Valkenberg [50]; Ford (see section 3.1); Krüger [51]; Jacobs, Allstot, Brodersen & Gray [52]; Müller [53]; and Davis [143].

We will now consider the third method of producing transmission zeros. Although the concept is very simple, and despite the fact that it can be identified in published circuits, this remaining method of realizing transmission zeros in multiple feedback filters was not recognized as such in the literature until it was pointed out by the writer in Ref. [88]. The method may be illustrated by considering the simple feedback network shown in Fig 1.10. If the block  $G_1(s)$  has a numerator polynomial  $v_1(s)$  and a denominator polynomial  $\delta_1(s)$  which are relatively prime, and if  $v_2(s)$  and  $\delta_2(s)$  are also relatively prime, then the transfer function



$$F(s) \triangleq \frac{v(s)}{e(s)} = \frac{\delta_1 v_2}{\delta_1 \delta_2 - v_1 v_2}$$

Fig 1.10 Simple network illustrating 'complex feedback'



$$F(s) \triangleq \frac{v}{e} = \frac{1}{A_1} + \frac{1}{A_2} + \frac{1}{A_3} + \dots$$

Fig 1.11 Continued fraction structure



of this network may be written as:

$$F(s) \triangleq \frac{V}{E} = \frac{\delta_1 \nu_2}{\delta_1 \delta_2 - \nu_1 \nu_2} \quad (1.4.12)$$

and we may make two observations. Firstly if  $\nu_2(s)$  has a factor  $s^2 + \omega_n^2$  then this will also be a factor in the numerator of  $F(s)$  and the network will have a transmission zero at  $\omega_n$  rad/s. This would be a transmission zero produced by a series notch section as previously defined. Secondly if  $\delta_1(s)$  has a factor  $s^2 + \omega_o^2$  then this will also be a factor of the numerator of  $F(s)$ , and the network will have a transmission zero at  $\omega_o$  rad/s. This process whereby the complex conjugate poles of a block  $G_i(s)$  become complex conjugate zeros of  $F(s)$  is the third method of realizing transmission zeros, and in this thesis we will refer to it as producing transmission zeros by 'complex feedback'.

The use of complex feedback will be illustrated by describing the continued fraction structure, which was first published by the writer in Ref. [84]. A lowpass prototype transfer function  $\Phi(s)$  is expanded into a continued fraction of the form:

$$\Phi(s) = \frac{1}{A_1 + \frac{1}{A_2 + \frac{1}{A_3 + \dots}}} \quad (1.4.13)$$

where the partial remainders are of the form:

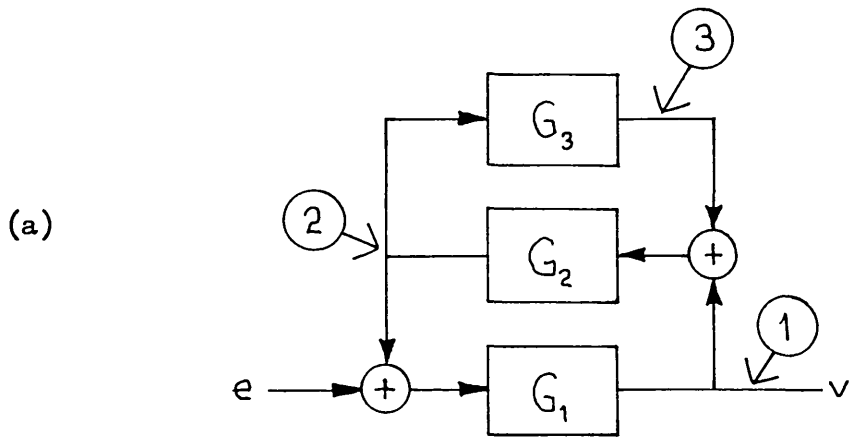
$$A_j = a_j s + b_j \quad a_j, b_j \text{ real, constant} \quad (1.4.14)$$

If the continued fraction exists, the partial remainders  $A_j$  may be identified with the denominators of the blocks in the continued fraction structure, as shown in Fig 1.11. Application of the lowpass to bandpass transformation will then give a realization of the required bandpass transfer function as an interconnection of bandpass quadratic sections. All transmission zeros at finite non-zero frequencies are realized in this structure by complex feedback.

For example the lowpass prototype transfer function  $\Phi(s)$  given in (1.4.10) may be expanded into a continued fraction of the form (1.4.13) with partial remainders:

$$\begin{aligned} A_1 &= 15.658 \quad s + 14.053 \\ A_2 &= -0.010436s + 0.01036 \\ A_3 &= -11.581 \quad s - 11.498 \end{aligned} \quad (1.4.15)$$

Identifying these with the denominators of the blocks, and performing the lowpass to bandpass transformation (1.4.8) with  $q = 10$  gives the bandpass network shown in Fig 1.12. This example has a structure comprising one forward path and two feedback loops. The feedback



$$G_1 = \frac{0.006386 s}{s^2 + 0.08975 s + 1} \quad Q = 11.14$$

$$G_2 = \frac{9.583 s}{s^2 - 0.09928 s + 1} \quad Q = -10.07$$

$$G_3 = - \frac{0.008634 s}{s^2 + 0.09928 s + 1} \quad Q = 10.07$$

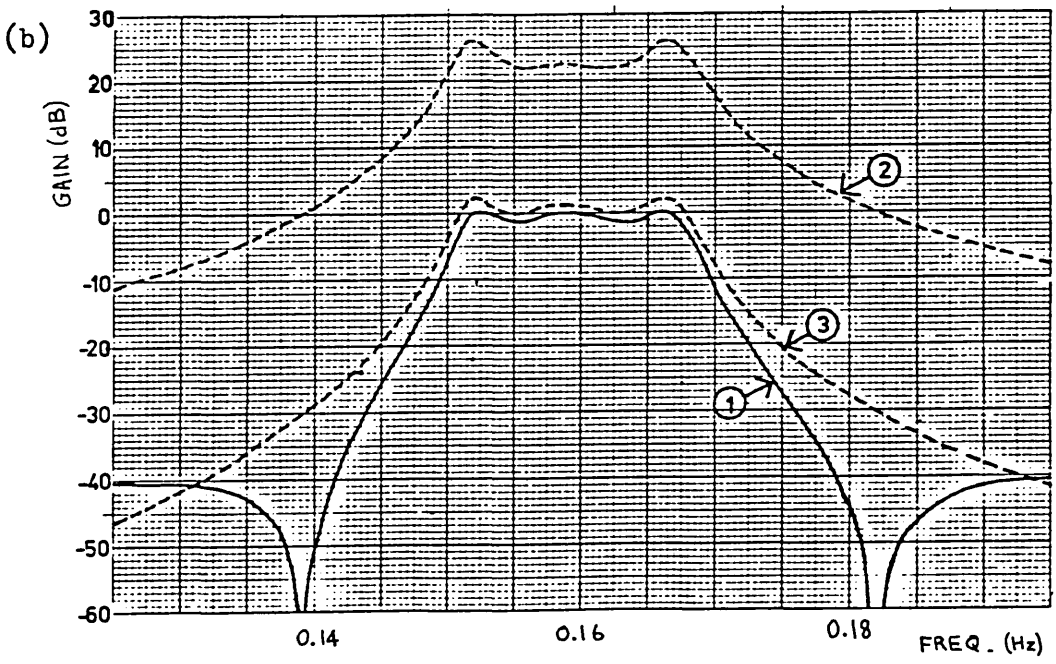


Fig 1.12 6-th degree elliptic-function bandpass filter

- (a) Block diagram
- (b) Computed frequency response

loops exist to provide transmission zeros by complex feedback, and are not in this case introduced to reduce sensitivity. Indeed it will be shown in Chapter 5 that this filter has a very large sensitivity at passband frequencies.

From Fig 1.12(b) it will be seen that at passband frequencies the signal level at the output of block-2 is about twelve times the signal level at the outputs of the other two blocks. This disparity can be reduced considerably by using the scaling transformation which will be described in Chapter 3.

Note that the block  $G_2$  in Fig 1.12(a) has a negative  $Q$ -factor on account of  $a_2$  and  $b_2$  having different signs in (1.4.15). If it is necessary to avoid the use of sections having a negative  $Q$ -factor then this may be achieved by using a slightly different continued fraction expansion. This is of the form (1.4.13) but has partial remainders of the form (1.4.14) alternating with partial remainders of the form:

$$A_j = \frac{a_j s + b_j}{s} \quad (1.4.16)$$

and is such that for each partial remainder  $A_j$ , the constants  $a_j$  and  $b_j$  have the same sign. According to a theorem given by Gorski-Popiel & Drew [54] such an expansion always exists. Whilst this ensures that all blocks have a positive  $Q$ -factor, a partial remainder of the form (1.4.16) produces a notch section in the bandpass filter if the constants  $a_j, b_j$  are both non-zero. Continued fractions have been used in a similar way for digital filters, but the expansion (1.4.13) (1.4.14), when bilinearly transformed, will not in general be realizable as a digital filter due to the occurrence of delay free loops [55].

The first use of complex feedback was by Scott [56], who connected a parallel-T notch circuit in the feedback path of an amplifier to give a tuned amplifier response, for use as a wave-form analyser. Scott's circuit has the structure shown in Fig 1.10 with  $G_2 = K$  and  $G_1 = (s^2 + \omega_o^2) / (s^2 + 4\omega_o s + \omega_o^2)$ , so that by (1.4.12) the transfer function is:

$$F(s) \triangleq \frac{v}{e} = \frac{K}{1-K} \frac{s^2 + 4\omega_o s + \omega_o^2}{s^2 + \frac{4\omega_o}{1-K} s + \omega_o^2} \quad (1.4.17)$$

The complex conjugate zeros of  $F(s)$  are the complex conjugate poles of  $G_1(s)$ , and we may say that these zeros are produced by complex

feedback, even though the zeros are not on the imaginary axis as would usually be the case for  $\lambda$ <sup>notch</sup> filters.

In the context of multiple feedback filters it is possible to identify the use of complex feedback in at least two structures, in addition to the continued fraction structure just described. The first is the signal flow graph simulation of LC ladder filters as described by Brackett & Sedra [57,58,59]. Wherever the LC ladder filter has a resonant circuit for realizing a transmission zero, and when this resonant circuit is associated with either a loopset of capacitors or a cutset of inductors, then the simulation will have in its forward path a subnetwork with the structure shown in Fig 1.10. In this subnetwork, the block  $G_2$  will be an infinite-gain operational amplifier, and the block  $G_1$  will be a two-integrator loop forming an inverting bandpass quadratic section having an infinite Q-factor. The transmission zero is thus produced by complex feedback. The operational amplifier occurring in the forward path of such subnetworks is called a 'reciprocator' by Brackett & Sedra, on account of the fact that it simulates that part of the reactance extraction procedure of ladder synthesis where one takes the reciprocal of an immittance function [57]. Our observation that the simulating network employs complex feedback is an alternative interpretation of how the reciprocators contribute to the production of transmission zeros.

The other published structure which may be interpreted as having complex feedback is Adams' 'coupled band-elimination filter' [60]. Whereas for bandpass filters it is usually important to have low sensitivity at passband frequencies, for bandstop filters it is also important to have low sensitivity at stopband frequencies. For many filters the sensitivity at stopband frequencies is determined by the sensitivity of the transmission zeros, or equivalently the sensitivity of the transfer function zeros; and the sensitivity at passband frequencies is determined by the sensitivity of the transfer function poles. Adams derived his network by simulating a low sensitivity LC ladder network, and then using some signal flow graph transformations to arrive at a structure in which both the passband sensitivity and the stopband sensitivity are lower than that of the simple cascade structure. Adams gives an example of a 6-th degree bandstop filter designed using his method. It may be thought of as having the simple feedback structure shown in Fig 1.10, with the block  $G_2$  representing a constant multiplier, and the block  $G_1$

representing a complex subnetwork. This subnetwork  $G_1$  comprises three infinite- $Q$  bandpass quadratic blocks interconnected by leapfrog feedback and a multiplicity of forward paths. The leapfrog feedback ensures that the poles of  $G_1$  have a low sensitivity at mid-band frequencies, and by complex feedback, in association with  $G_2$ , these low-sensitivity poles become the zeros of the transfer function of the filter. The concept of complex feedback thus explains why Adams' structure has a low stopband sensitivity.

By describing some carefully chosen examples in this Chapter, we have introduced the main topics of interest in this thesis; which concerns multiple feedback filters formed by an interconnection of unilateral subnetworks. We are primarily interested in obtaining low sensitivity and maximum dynamic range from such filters, and we are interested in understanding how the structure or pattern of interconnection affects these performance criteria. We have so far encountered three feedback structures which may be used to reduce sensitivity at passband frequencies: namely leapfrog feedback, follow the leader feedback and transpose follow the leader feedback. We have also identified three properties of structure which are used to produce transmission zeros: namely series notch sections, parallel forward paths, and complex feedback. We have also seen that low sensitivity multiple feedback filters may be designed by simulating a low sensitivity LCR filter, or they may be designed directly from the required transfer function. The reader is now sufficiently acquainted with the subject to be able to appreciate the objectives of this thesis, which are described in the next section.

In the course of this introductory chapter, some material has been presented which is the original work of the writer. Firstly the multiple feedback structure with parallel forward paths shown in Fig 1.8, together with the derivation of explicit design equations (1.4.1) to (1.4.9). Secondly the introduction of the concept of complex feedback for the realization of transmission zeros, as illustrated in Fig 1.10. Thirdly the continued fraction structure, shown in Fig 1.11. These contributions were first published by the writer in references [45], [88], and [84] respectively.

## 1.5 Objectives of this thesis

Many multiple feedback filters have been proposed in the literature, for instance in respect of bandpass filters there are currently more than fifty design methods, using between them more than twenty five different structures of interconnection. We will in this thesis attempt to form the beginnings of a unified treatment by giving some analytical results which apply to all multiple feedback filters. It is hoped that this general approach will give some new insight into the mechanisms which produce the good performance shown by some multiple feedback filters, and in particular we wish to determine how the structure of the filter contributes to this good performance.

In order to study the structure it will be useful to use the language and notation of graph theory, in addition to the block diagrams used so far. This is done in Chapter 2 which deals with the definition and analysis of multiple feedback filters, and in Chapter 3 which describes the transformation of multiple feedback filters.

Some of the general results to be presented in Chapters 2 and 3 have already been mentioned in this introduction. For instance the summed sensitivity invariant has as a special case the equation (1.2.10) which was used to demonstrate how leapfrog feedback reduced the passband sensitivity in the simple analogue simulation filter. Also the general scaling transformation has been mentioned in section 1.3 in connection with adjusting the gain of the analogue simulation filter, and it has been used to eliminate unnecessary inverting amplifiers in the 6-th degree bandpass filter example shown in Fig 1.9.

It will be shown in Chapter 4 that a particular classification of existing structures for multiple feedback filters reveals the possibility of new structures. The basis for this classification has already been established in this introduction. It is in terms of the feedback loops used to reduce passband sensitivity, and the way in which transmission zeros are produced.

In Chapter 5 we will study the sensitivity of some specific filters with a view to understanding how best to choose a structure for low sensitivity. It will be demonstrated that the use of a particular structure is not enough to guarantee low sensitivity. The insight obtained in this study will lead to some guidelines for choosing suitable structures for low sensitivity multiple feedback filters.

---

THE CONCEPT OF MULTIPLE FEEDBACK

---

The reader will already have a concept of multiple feedback. This will be as a result of reading the introductory chapter, and as a result of recalling the many other instances in electrical engineering where the term occurs. The concept being the sum total of the ideas brought to mind by the use of the term multiple feedback. Although in a sense this chapter can only add to the concept, the real purpose is to both expand it by the presentation of some analytic results of a general nature, and to delimit it by a definition of terms as used in this thesis. This should convey the writer's concept of multiple feedback in the specific context of this thesis.

Accordingly in this chapter we will discuss our use of the term to refer to the interconnection of a number of active CR sections to form a multiple feedback filter. We will describe the properties required of the active CR sections, and will give a more detailed account of how a multiple feedback filter can be represented by a block diagram or a signal flow graph.

A general form of multiple feedback filter will be analysed to find its transfer function. The finite difference sensitivities and differential sensitivities of the transfer function to changes in the block diagram parameters will also be found, and in the context of analysis a new summed sensitivity invariant will be given. The mechanisms which limit dynamic range will be discussed, and a method of analysing the dynamic range of any given multiple feedback filter will be given.

## 2.1 Definition of multiple feedback

In this section we will define multiple feedback, and as a starting point we will consider the individual active CR circuits which are to be interconnected. Such circuits have been studied in great detail in connection with cascade active CR filters, particularly in respect of their sensitivity. Two examples have already been given in Fig.1.5, and another is shown in Fig 2.1(a) [61]. This is commonly called a multiple feedback circuit on account of the three feedback paths from the output of the operational amplifier. To avoid confusion of ideas, we do not call it a multiple feedback circuit, we call this and all similar circuits an active CR section, or just section for brevity. The properties required of a section are that it can be characterised by a single equation, and that this equation is not affected by the interconnections. For the example in Fig 2.1(a) the characteristic of interest is the forward transfer voltage ratio  $G_{21}(s) \triangleq v_2(s)/v_1(s)$ . Since the voltage  $v_2$  is the output of an operational amplifier,  $G_{21}$  will (within limits set by the performance of the operational amplifier) be independent of the output port termination, and  $v_2$  can form the input to another section without mutual interaction. A section will usually contain capacitors whence  $G_{21}$  will be a rational function of the complex frequency variable  $s$ . The degree of the denominator is seldom greater than two, and this fact allows us to characterize the transfer function by a small number of constants. In the case of the bandpass quadratic section shown in Fig 2.1(a), the transfer function is of the form:

$$G_{21}(s) \triangleq \frac{v_2(s)}{v_1(s)} = K \frac{s}{s^2 + \frac{\omega_0}{Q} s + \omega_0^2} \quad (2.1.1)$$

fully characterized by the values of the resonance frequency  $\omega_0$ , the quality factor  $Q$ , and the constant multiplier  $K$ . In this thesis we will consider the performance of sections in terms of such constants, and we will not be concerned with the particular realization of sections. In order to interconnect the sections we will have to accommodate several inputs, and we will have to control the constant multiplier  $K$ . This can usually be done by having a potential divider network at the input of the section [22] as illustrated in Fig 2.1(b).

More generally, a section will be an unbalanced\*  $(n+1)$ -port

---

\* An unbalanced N-port is one in which all ports have a common terminal, usually called the ground or datum terminal.



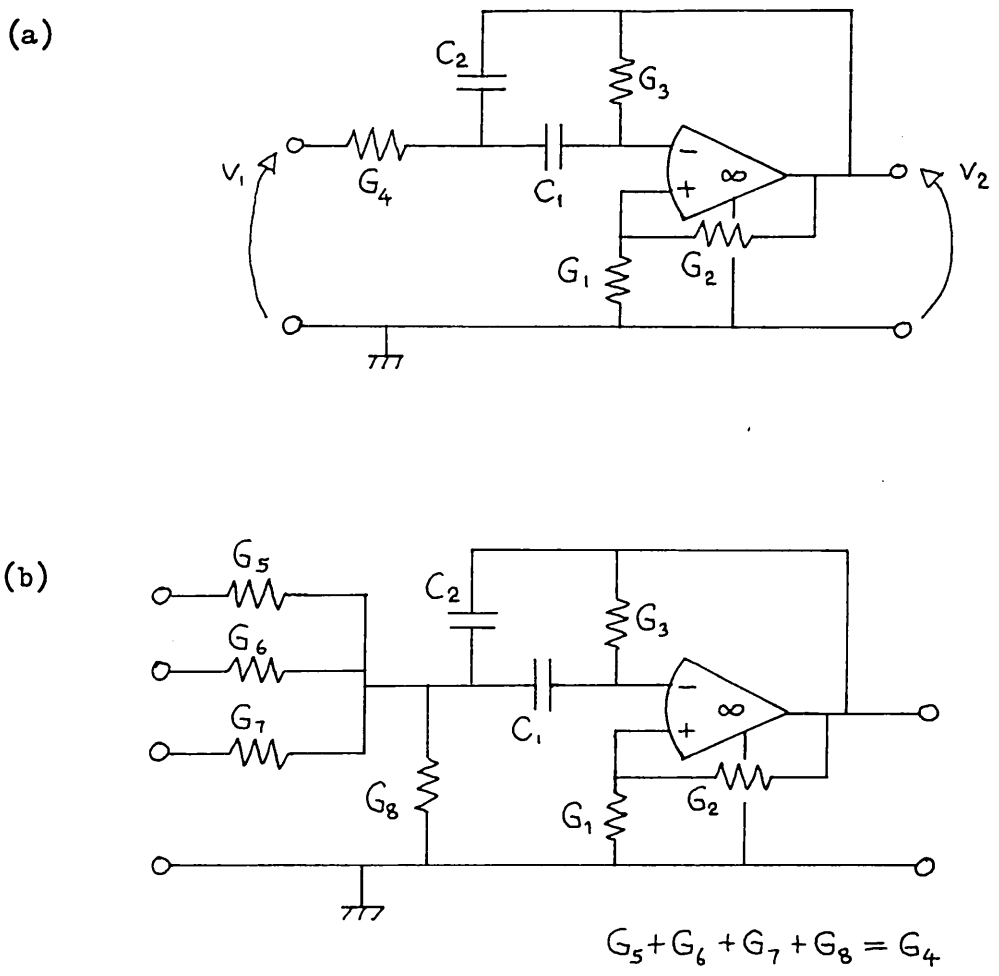


Fig 2.1 Example of an active CR section  
 (a) as used in simple filters  
 (b) as used in multiple feedback filters

network, with  $n$  input ports and one output port, as shown in Fig 2.2. It will have a hybrid matrix description of the form:

$$\begin{bmatrix} i_1 \\ \cdot \\ \cdot \\ \cdot \\ i_n \\ v_o \end{bmatrix} = \begin{bmatrix} Y_{n1} & \cdot & \cdot & \cdot & Y_{nn} & 0 \\ \cdot & \cdot & \cdot & \cdot & \cdot & \cdot \\ \cdot & \cdot & \cdot & \cdot & \cdot & \cdot \\ \cdot & \cdot & \cdot & \cdot & \cdot & \cdot \\ Y_{n1} & \cdot & \cdot & \cdot & Y_{nn} & 0 \\ G_{o1} & \cdot & \cdot & \cdot & G_{on} & 0 \end{bmatrix} \begin{bmatrix} v_1 \\ \cdot \\ \cdot \\ \cdot \\ v_n \\ i_o \end{bmatrix} \quad (2.1.2)$$

where the zero elements are a consequence of an (ideal) amplifier output being connected to the output port. A multiple feedback filter comprises an interconnection of a number of such sections. The rules of interconnection are obvious and are as follows:

- (i) because the sections are unbalanced, all interconnections are made by connecting ports in parallel,
- (ii) no two output ports can be connected together on account of each having zero source impedance,
- (iii) an input port is always connected to an output port or the input to the filter,
- (iv) the input to the filter is an independent voltage source, and it is connected to one or more input ports,
- (v) the output from the filter is taken to be the output port voltage of one of its sections.

In multiple feedback filters, the port voltages and relations between the port voltages are our main concern. It would of course be possible to consider multiple feedback filters on a current basis, or even on a mixed voltage/current basis, but with present circuit techniques using operational voltage amplifiers, there seems to be no practical advantage in doing so.

From (2.1.2) the  $(n+1)$ -port section is characterized by the equation:

$$v_o = G_{o1} v_1 + \dots + G_{on} v_n \quad (2.1.3)$$

which has a block diagram representation shown in Fig 2.3(a). If, as is usually the case, the functions  $G_{oj}$  are equal to constant multiples of a function  $G(s)$ , then the equation will have the representation shown in Fig 2.3(b). Most sections are of this form, but there are a few exceptions [62,63,64,101,145,155], for instance Bach's circuit [62] in Fig 2.4(a) uses sections of the type shown in Fig 2.4(b), for which the representation in Fig 2.3(a) is necessary. With Bach's circuit we have:

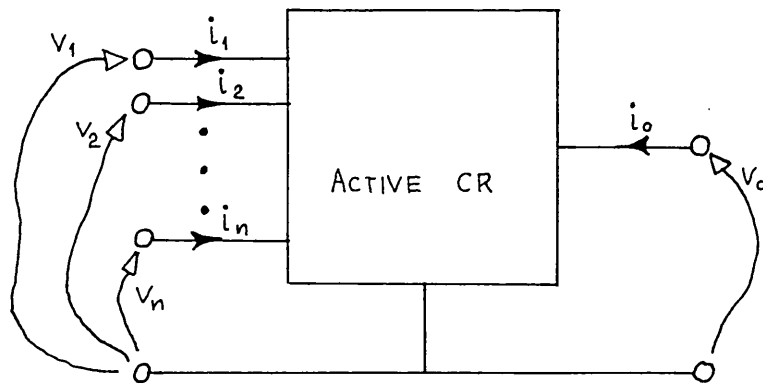


Fig 2.2 (n+1)-port representation of a section

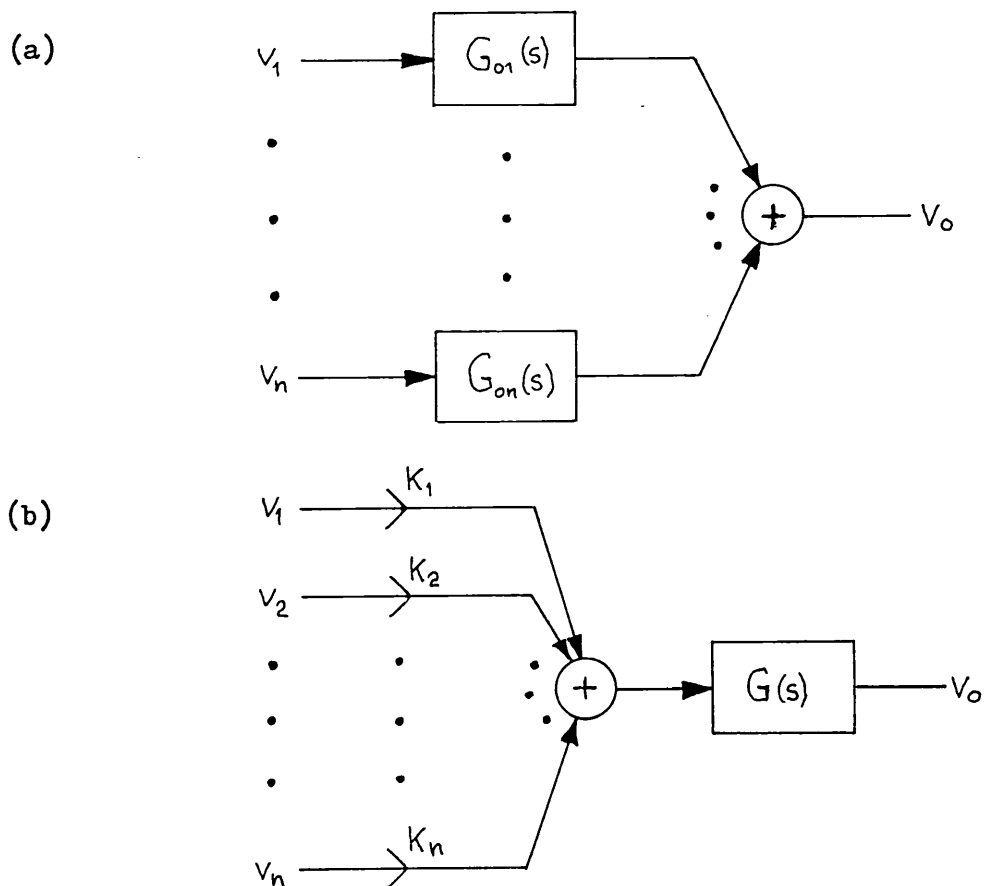


Fig 2.3 Block diagram representations of the equation characterizing a section

- (a) General case  
 (b) Special case of (a) with  $G_{oj}(s) = K_j G(s)$ ,  $j = 1, 2, \dots, n$

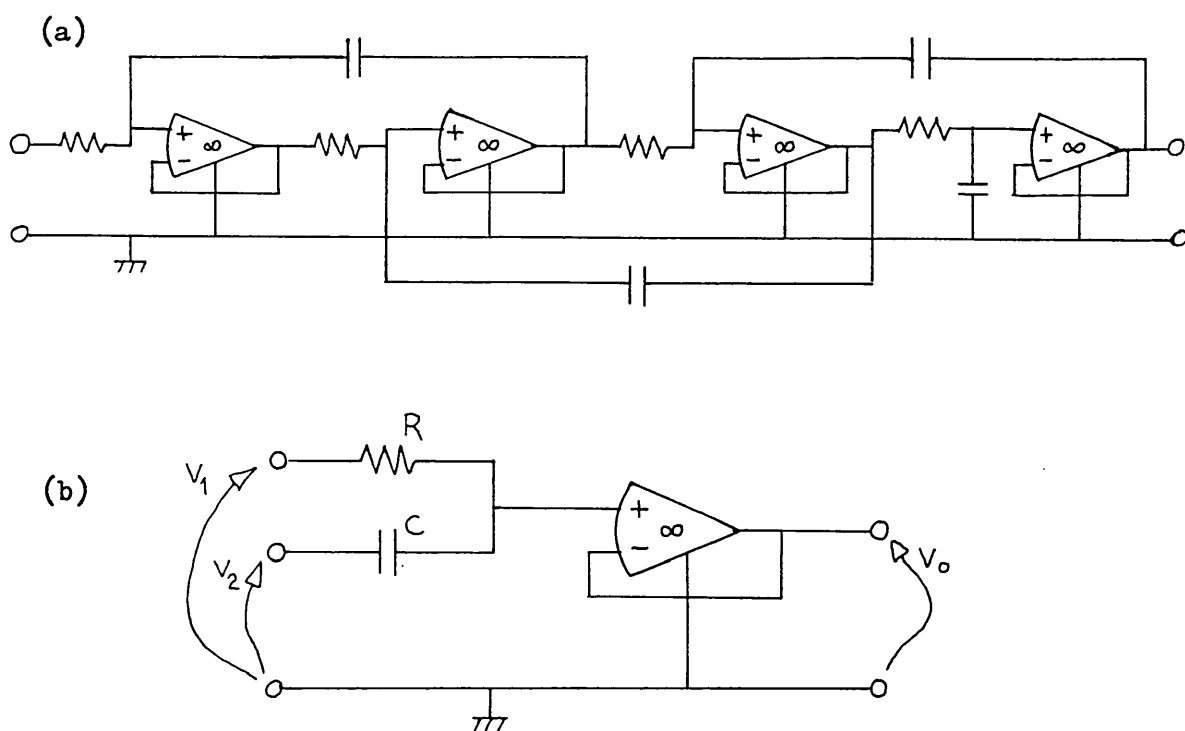


Fig 2.4 Bach's circuit

- (a) Configuration for fourth degree, polynomial, lowpass filter  
 (b) Section used in Bach's circuit

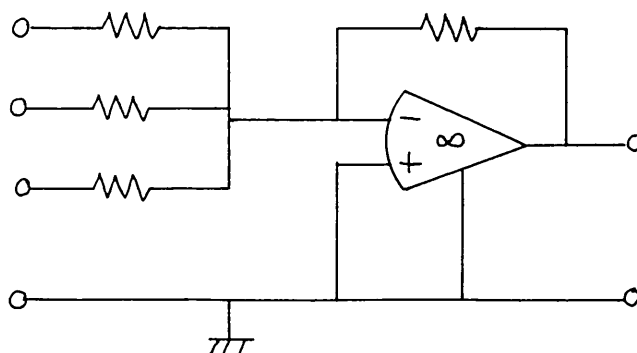


Fig 2.5 Summing amplifier section

$$G_{01} = \frac{1}{1 + sCR} \quad (2.1.4)$$

and:

$$G_{02} = \frac{sCR}{1 + sCR} \quad (2.1.5)$$

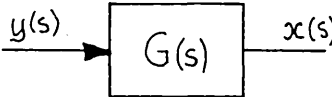

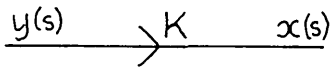

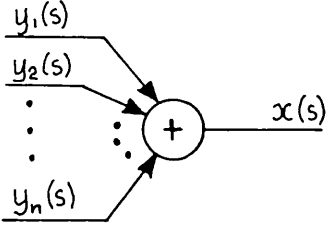
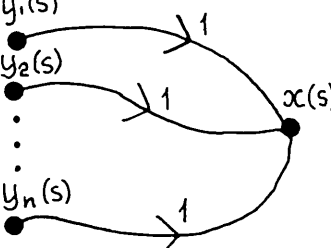
The block diagrams obtained in these few cases, although valid, are somewhat cumbersome for practical analysis, and other approaches may be preferred. Most sections however will, like that in Fig 2.1(b), admit of the representation in Fig 2.3(b). Sometimes we will use a section which does not contain capacitors, such as the summing amplifier in Fig 2.5, in which case we can put  $G(s)=1$  and omit the block from the diagram.

As we have already indicated, a block diagram is simply a way of writing down a set of equations. When a block diagram represents the characterizing equations of a multiple feedback filter, it will be called the block diagram of the filter. Where a multiple feedback filter is designed so that its characterizing equations are those of a given block diagram, it will be called a realization of the block diagram.

Each block diagram symbol represents an equation of a particular type. These equations may also be represented by a Mason signal flow graph [65,66,67]. In Table 2.1 we show the equations, the block diagram representation, and the equivalent signal flow graph (SFG). Evidently for every block diagram representing a multiple feedback filter, there exists an equivalent signal flow graph. As an illustration we show a multiple feedback filter [45] in Fig 2.6, together with its block diagram and an equivalent SFG. This filter has been designed to have a 6-th degree, 1.25dB ripple, Chebychev bandpass characteristic, with a passband width equal to 10% of the center frequency, which is 100 rad/s. The quadratic sections were chosen to have a Q-factor of 30. Each of the three sections, shown encompassed by dashed lines, realizes a block, its associated adder, and a constant multiplier. In a block diagram we distinguish a block from a constant multiplier as an aid to visualization of how the block diagram may be realized. This distinction is lost in the SFG, however, it will be convenient to express certain results in terms of signal flow graphs.

The pattern of feedback loops and forward paths shown by a block diagram or a signal flow graph will be called the structure of the

Table 2.1 Block diagram symbols

Element	Equation	Block Diagram Symbol	Equivalent SFG
Block	$x(s) = G(s)y(s)$		
Constant multiplier	$x(s) = K y(s)$		
Adder	$x(s) = \sum_{j=1}^n y_j(s)$		

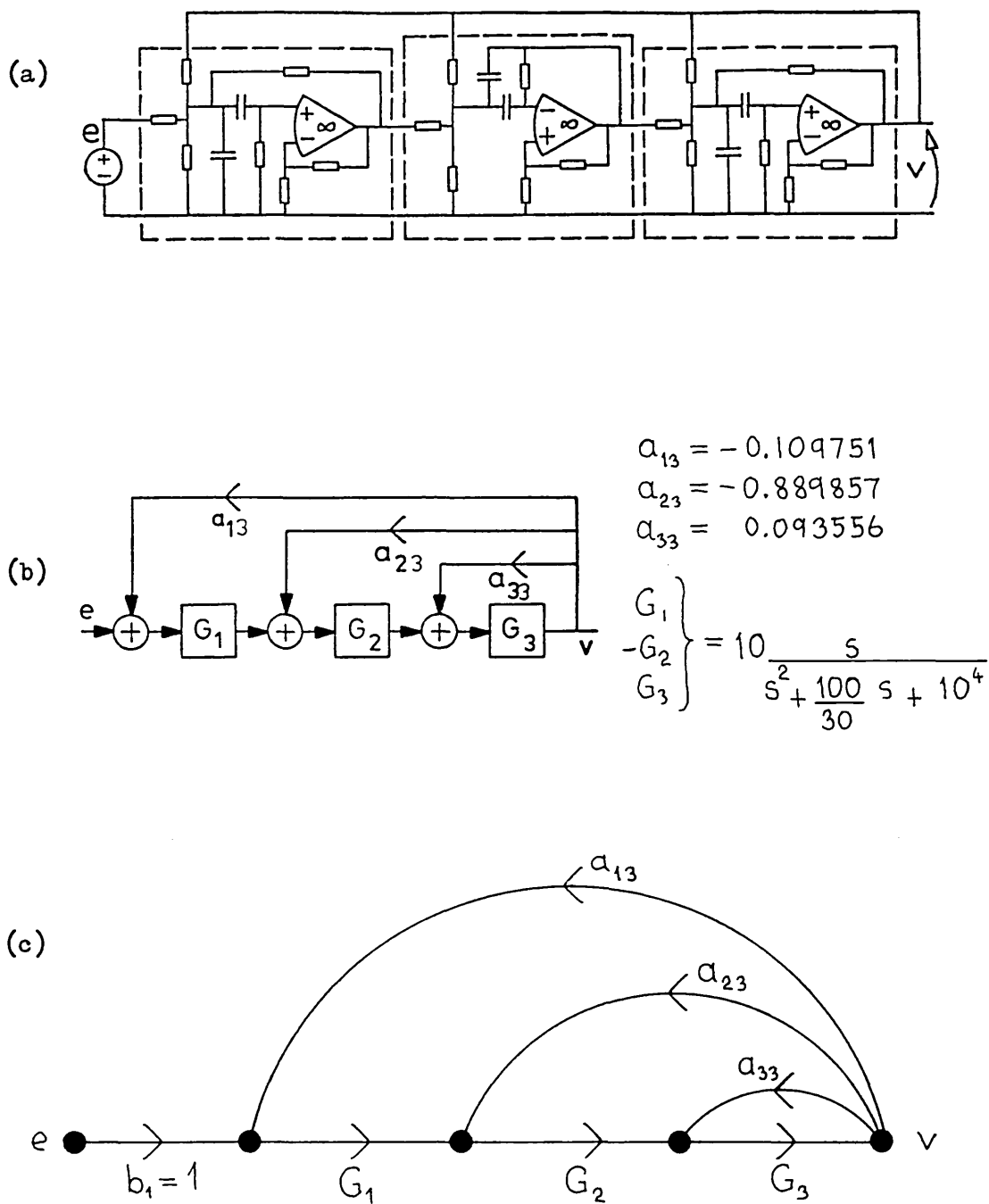


Fig 2.6 Example of a multiple feedback filter and its representation

- (a) Active CR filter
- (b) Block diagram of filter
- (c) Signal flow graph equivalent to (b)

filter. Various aspects of structure can be defined in terms of signal flow graphs, and will be of use later.

- (i) A cutset is a minimal set of branches the removal of which will separate the graph into exactly two pieces. For example  $\{G_1, a_{13}\}$  and  $\{G_1, a_{23}, a_{33}, G_3\}$  are cutsets\* in Fig 2.6(c).
- (ii) A loopset is the set of branches of a connected subgraph such that every node is common to exactly two branches. For example  $\{G_1, a_{13}, a_{23}\}$  and  $\{G_2, G_3, a_{23}\}$  are loopsets.
- (iii) A forward path is the set of branches of a connected subgraph such that the nodes and branches form a sequence, starting from node e (the filter input) and terminating at node v (the filter output), in which all nodes and branches occur once only, and where the direction of the branches determines the sequence. For example the SFG in Fig 2.6(c) has only one forward path:  $\{b_1, G_1, G_2, G_3\}$ .
- (iv) A feedback loop is a loopset in which all branches have the same direction. For example the loopset  $\{G_2, G_3, a_{23}\}$  is a feedback loop, but the loopset  $\{G_1, a_{13}, a_{23}\}$  is not.
- (v) In an m-node graph, any connected m-node, (m-1)-branch subgraph is called a tree and its branches are called tree branches. For any tree, the complementary sub-graph is called its co-tree. In Fig 2.6(c) for example one of the trees has tree branches  $b_1, a_{13}, a_{23}, G_2$ , and its co-tree has branches  $G_1, a_{33}, G_3$ .
- (vi) For any tree, each tree branch forms a cutset in association with one and only one set of co-tree branches. These are called basic cutsets. For example  $\{b_1\}, \{a_{13}, G_1\}, \{G_1, a_{23}, a_{33}, G_3\}, \{G_2, a_{33}, G_3\}$  is the set of basic cutsets for the tree given in (v).

Associated with every forward path is a forward path gain P, given by the product of the weights of the branches in the forward path. Similarly, associated with every feedback loop is a feedback loop gain (or loop gain for brevity) T, given by the product of the weights of the branches in the feedback loop.

Multiple feedback is defined to be a plurality of feedback loops. A multiple feedback filter thus has a structure comprising at least one forward path (to provide signal transmission through the filter) and two or more feedback loops. This definition does not include certain simple structures which we shall consider, for instance the

---

\* We identify a branch of a graph by its associated weight



cascade structure which has no feedback loops, but our analysis will accommodate all structures allowed by the rules given on page 46. Our main concern however is with structures having multiple feedback, because of their potential for improved performance.

## 2.2 Analysis of multiple feedback filters

Having defined multiple feedback we now show how a multiple feedback filter may be analysed. Our main interest is in the transfer function, from which the frequency domain or the time domain response of the filter may be found as required. In section 2.2.1 we give both an algebraic method and Mason's topological method of finding the transfer function.

Also of interest is the effect on the transfer function of variations in the constituent parts of the filter. This is a complicated subject and in a later chapter we will resort to computation to investigate the sensitivity of filters. However a certain amount can be done analytically as was discussed in section 1.2, and in section 2.2.2 we derive some expressions for various sensitivities. We also introduce a new summed sensitivity invariant which is of use in the calculation of sensitivity.

The dynamic range of a filter is often important, and as a contribution to the study of dynamic range we show in section 2.2.4 how multiple feedback determines the way in which the dynamic range of a filter is related to the imperfections of its constituent sections.

### 2.2.1 Transfer function

In this section an analysis of a filter having a general structure will be given. Most structures are particular cases of this general structure, and those which are not can be made so by simple manipulation. The filter we shall consider is composed of  $n + 1$  sections, each section having a block diagram of the type shown in Fig 2.3(b). The first  $n$  sections are fully interconnected, with constant multipliers  $a_{jk}$ , as shown in Fig 2.7. The (single) filter input  $e$  is applied to all  $n$  sections, with constant multipliers  $b_j$ . The  $n$  section outputs are added together with weights  $c_j$  by a summing amplifier section, and the (single) filter output  $v$  is taken to be the output of this section. There is also a direct connection of the filter input  $e$  to the summing amplifier section, with a constant multiplier  $d$ . We define the following matrices:

$$\mathcal{A} \triangleq \begin{bmatrix} a_{11} & \cdot & \cdot & \cdot & a_{1n} \\ \cdot & & & & \cdot \\ \cdot & & & & \cdot \\ \cdot & & & & \cdot \\ a_{n1} & \cdot & \cdot & \cdot & a_{nn} \end{bmatrix} \quad \mathcal{G} = \mathcal{G}(s) \triangleq \begin{bmatrix} G_1(s) \\ G_2(s) \\ \cdot \\ \cdot \\ G_n(s) \end{bmatrix}$$

$$\underline{b} \triangleq \begin{bmatrix} b_1 \\ b_2 \\ \cdot \\ \cdot \\ b_n \end{bmatrix} \quad \underline{c} \triangleq \begin{bmatrix} c_1 \\ c_2 \\ \cdot \\ \cdot \\ c_n \end{bmatrix} \quad \underline{x} \triangleq \begin{bmatrix} x_1 \\ x_2 \\ \cdot \\ \cdot \\ x_n \end{bmatrix} \quad \underline{y} \triangleq \begin{bmatrix} y_1 \\ y_2 \\ \cdot \\ \cdot \\ y_n \end{bmatrix} \quad (2.2.1)$$

whence, for the  $n$  blocks we may write:

$$\underline{x} = \mathcal{G} \underline{y} \quad (2.2.2)$$

The equations of the associated adders may be written as:

$$\underline{y} = \mathcal{A} \underline{x} + \underline{b} e \quad (2.2.3)$$

and the equation of the output adder is:

$$v = \underline{c}_t \underline{x} + d e \quad (2.2.4)$$

Eliminating  $\underline{y}$  from (2.2.2) and (2.2.3), and substituting in (2.2.4) gives the transfer function of the filter  $F(s)$ :

$$F(s) \triangleq \frac{v(s)}{e(s)} = \underline{c}_t (\mathcal{G}(s)^{-1} - \mathcal{A})^{-1} \underline{b} + d \quad (2.2.5)$$

This is similar to expressions used in state variable theory and

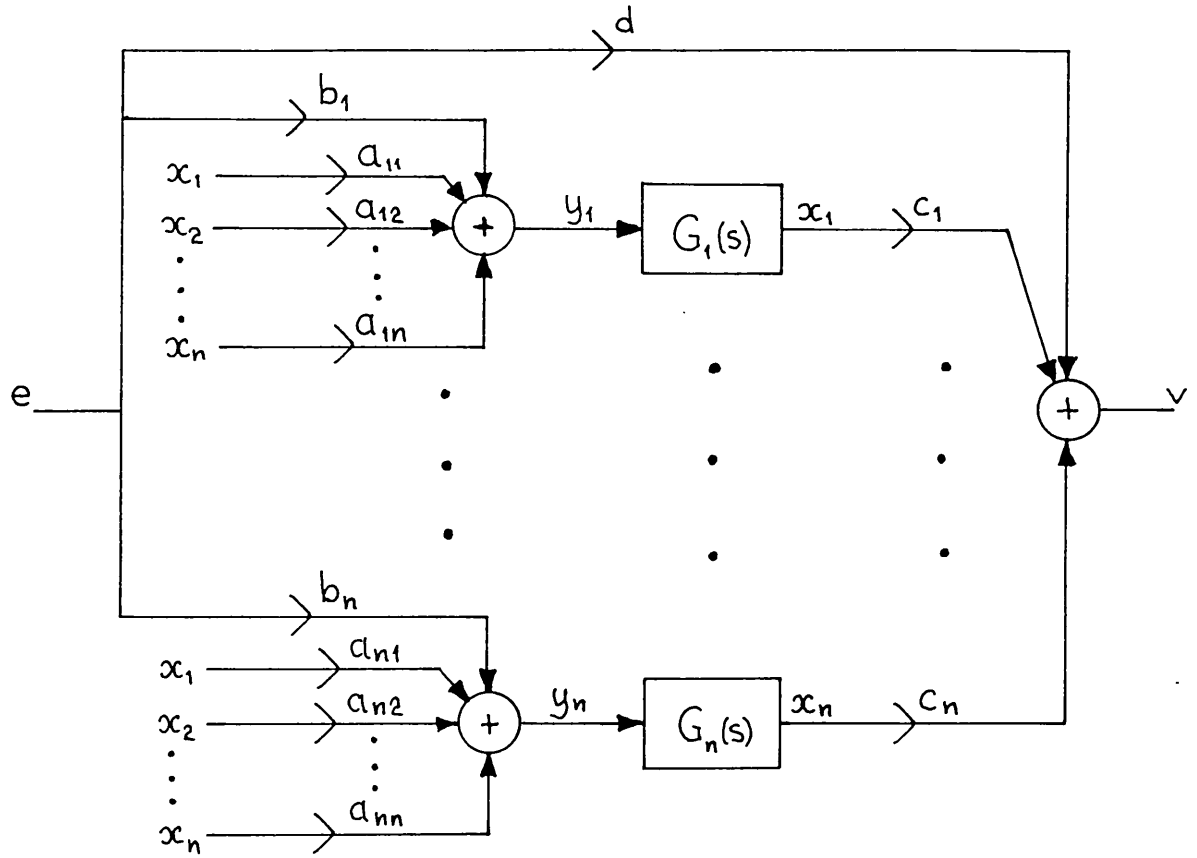


Fig 2.7 Multiple feedback filter having  $n$  fully interconnected sections.

feedback theory. When used in state variable theory, the matrix  $ly(s)$  would represent differentiation thus  $ly(s)^{-1} = \frac{1}{s} U$  [69]. In Sandberg's multi-loop feedback theory [68], the matrix  $ly$  would represent the constants associated with dependent sources. As an example of its application to multiple feedback filters, consider the filter shown in Fig 2.6. From the block diagram we construct the matrices:

$$A = \begin{bmatrix} 0 & 0 & a_{13} \\ 1 & 0 & a_{23} \\ 0 & 1 & a_{33} \end{bmatrix} \quad ly = \begin{bmatrix} G_1 & & \\ & G_2 & \\ & & G_3 \end{bmatrix} \quad (2.2.6)$$

$$\underline{b} = \begin{bmatrix} 1 \\ 0 \\ 0 \end{bmatrix} \quad \underline{c} = \begin{bmatrix} 0 \\ 0 \\ 1 \end{bmatrix} \quad d = 0$$

and using (2.2.5) we obtain the transfer function of the filter:

$$F(s) = \frac{v}{e} = [0 \ 0 \ 1] \begin{bmatrix} G_1^{-1} & 0 & -a_{13} \\ -1 & G_2^{-1} & -a_{23} \\ 0 & -1 & G_3^{-1} - a_{33} \end{bmatrix}^{-1} \begin{bmatrix} 1 \\ 0 \\ 0 \end{bmatrix}$$

$$F(s) = \frac{1}{G_1^{-1} G_2^{-1} G_3^{-1} - a_{33} G_1^{-1} G_2^{-1} - a_{23} G_1^{-1} - a_{13}}$$

$$F(s) = \frac{G_1 G_2 G_3}{1 - a_{33} G_3 - a_{23} G_2 G_3 - a_{13} G_1 G_2 G_3} \quad (2.2.7)$$

Alternatively the filter may be analysed by taking the equivalent signal flow graph and using Mason's topological rule for the analysis of SFG's [66, 67]. Mason's Rule has the form:

$$F(s) = \frac{\sum_f P_f \left[ 1 - \sum_a T_j + \sum_b T_j T_k - \dots \right]}{1 - \sum_p T_j + \sum_q T_j T_k - \sum_r T_j T_k T_l + \dots} \quad (2.2.8)$$

in which the transfer function  $F(s)$  is expressed in terms of loop gains  $T$  and forward path gains  $P$  only. The summation  $p$  is over all feedback loops. The summations  $q, r, \dots$  are over all products of 'non-touching' feedback loops. Two feedback loops  $L_1$  and  $L_2$  do not 'touch' if for all branches  $w_1 \in L_1$  and for all branches  $w_2 \in L_2$  there is no pair of branches  $w_1, w_2$  incident at a common node. The summation  $f$  is over all forward paths, and for each forward path the

summations  $a, b, \dots$  are over all products of feedback loops which do not touch each other or the forward path.

As an example consider again the filter in Fig 2.6. The SFG has one forward path  $\{b, G_1, G_2, G_3\}$  and three feedback loops  $\{G_3, a_{33}\}$ ,  $\{G_2, G_3, a_{23}\}$  and  $\{G_1, G_2, G_3, a_{13}\}$ . The corresponding forward path gain is  $P_1 = b, G_1 G_2 G_3 = G_1 G_2 G_3$ , and the corresponding loop gains are  $T_1 = G_3 a_{33}$ ,  $T_2 = G_2 G_3 a_{23}$  and  $T_3 = G_1 G_2 G_3 a_{13}$ . All feedback loops touch each other, and all touch the forward path. Thus (2.2.8) becomes:

$$F(s) = \frac{P_1}{1 - (T_1 + T_2 + T_3)}$$

$$F(s) = \frac{G_1 G_2 G_3}{1 - G_3 a_{33} - G_2 G_3 a_{23} - G_1 G_2 G_3 a_{13}} \quad (2.2.9)$$

which agrees with (2.2.7).

### 2.2.2 Sensitivity of the transfer function

Having obtained an expression for the transfer function of a multiple feedback filter, we are now able to investigate the sensitivity of the transfer function to changes in the block diagram parameters  $a_{jk}$ ,  $b_j$ ,  $c_j$ ,  $d$  and  $G_j(s)$ . Some authors give expressions for differential sensitivity [69,70,134], but the expressions for finite difference sensitivity given in this section have not yet appeared in the literature.

Using the definition of finite difference sensitivity (1.2.3), and the expression for the transfer function in (2.2.5), we can obtain the sensitivities to  $b_j$ ,  $c_j$  and  $d$  directly. If  $\underline{u}_j$  represents the  $j$ -th column of the unit matrix, then as

$b_j \longmapsto b_j + \Delta b_j$  we obtain:

$$\mathcal{S}_{b_j}^{F(s)} = \frac{b_j}{F(s)} \underline{c}_t \left( \underline{y}(s)^{-1} - \mathcal{A} \right)^{-1} \underline{u}_j \quad (2.2.10)$$

Similarly as  $c_j \longmapsto c_j + \Delta c_j$  we obtain:

$$\mathcal{S}_{c_j}^{F(s)} = \frac{c_j}{F(s)} \underline{u}_{jt} \left( \underline{y}(s)^{-1} - \mathcal{A} \right)^{-1} \underline{b} \quad (2.2.11)$$

and as  $d \longmapsto d + \Delta d$  we obtain:

$$\mathcal{S}_d^{F(s)} = \frac{d}{F(s)} \quad (2.2.12)$$

Notice that the sensitivities in (2.2.10), (2.2.11) and (2.2.12) are all independent of the increment. Therefore in each case the finite difference sensitivity is equal to the differential sensitivity. This is not true of the remaining sensitivities. To find these we use the following expression for the inverse of a matrix in which one component  $m_{jk}$  is given an increment  $m_{jk} \longmapsto m_{jk} + \Delta m_{jk}$

$$\left( \mathcal{M} + \Delta m_{jk} \underline{u}_j \underline{u}_{kt} \right)^{-1} = \mathcal{M}^{-1} - \frac{\Delta m_{jk}}{1 + \Delta m_{jk} \frac{\text{cof } m_{jk}}{\det \mathcal{M}}} \mathcal{M}^{-1} \underline{u}_j \underline{u}_{kt} \mathcal{M}^{-1} \quad (2.2.13)$$

This expression may be verified by multiplying the incremented matrix  $(\mathcal{M} + \Delta m_{jk} \underline{u}_j \underline{u}_{kt})$  by its inverse as given in (2.2.13), to obtain the unit matrix.

Now as  $a_{jk} \longmapsto a_{jk} + \Delta a_{jk}$  we have from (1.2.3) and (2.2.5):

$$\mathcal{S}_{a_{jk}}^{F(s)} = \frac{a_{jk}}{F(s) \Delta a_{jk}} \left( \underline{c}_t \left( \underline{y}(s)^{-1} - \mathcal{A} - \Delta a_{jk} \underline{u}_j \underline{u}_{kt} \right)^{-1} \underline{b} - \underline{c}_t \left( \underline{y}(s)^{-1} - \mathcal{A} \right)^{-1} \underline{b} \right) \quad (2.2.14)$$

using (2.2.13):

$$\mathcal{S}_{a_{jk}}^{F(s)} = \frac{a_{jk}}{F(s) \Delta a_{jk}} \frac{\Delta a_{jk}}{1 - \Delta a_{jk} \frac{\text{cof } e_{jk}}{\det(\mathcal{L}_y(s)^{-1} \mathcal{A})}} \underline{c}_t (\mathcal{L}_y(s)^{-1} \mathcal{A})^{-1} \underline{u}_j \underline{u}_{kt} (\mathcal{L}_y(s)^{-1} \mathcal{A})^{-1} \underline{b} \quad (2.2.15)$$

where  $\text{cof } e_{jk}$  is the cofactor of the element  $e_{jk}$  in the matrix  $\mathcal{E} \triangleq \mathcal{L}_y(s)^{-1} \mathcal{A}$ . Simplifying (2.2.15) gives the finite difference sensitivity as a function of the fractional change  $\Delta a_{jk}/a_{jk}$ :

$$\mathcal{S}_{a_{jk}}^{F(s)} = \frac{1}{F(s)} \frac{1}{\frac{1}{a_{jk}} - \frac{\Delta a_{jk}}{a_{jk}} \frac{\text{cof } e_{jk}}{\det(\mathcal{L}_y(s)^{-1} \mathcal{A})}} \underline{c}_t (\mathcal{L}_y(s)^{-1} \mathcal{A})^{-1} \underline{u}_j \underline{u}_{kt} (\mathcal{L}_y(s)^{-1} \mathcal{A})^{-1} \underline{b} \quad (2.2.16)$$

From (2.2.16) and (1.2.5) we may also obtain the differential sensitivity:

$$\mathcal{S}_{a_{jk}}^{F(s)} = \frac{a_{jk}}{F(s)} \underline{c}_t (\mathcal{L}_y(s)^{-1} \mathcal{A})^{-1} \underline{u}_j \underline{u}_{kt} (\mathcal{L}_y(s)^{-1} \mathcal{A})^{-1} \underline{b} \quad (2.2.17)$$

Similarly as  $G_j \longmapsto G_j + \Delta G_j$  we have:

$$G_j^{-1} \longmapsto (G_j + \Delta G_j)^{-1} = G_j^{-1} - \frac{\Delta G_j}{G_j (G_j + \Delta G_j)} \quad (2.2.18)$$

so that from (1.2.3) and (2.2.5):

$$\mathcal{S}_{G_j(s)}^{F(s)} = \frac{G_j}{F(s) \Delta G_j} \left( \underline{c}_t \left( \mathcal{L}_y(s)^{-1} \mathcal{A} - \frac{\Delta G_j}{G_j (G_j + \Delta G_j)} \underline{u}_j \underline{u}_{jt} \right)^{-1} \underline{b} - \underline{c}_t (\mathcal{L}_y(s)^{-1} \mathcal{A})^{-1} \underline{b} \right) \quad (2.2.19)$$

using (2.2.13):

$$\mathcal{S}_{G_j(s)}^{F(s)} = \frac{G_j}{F(s) \Delta G_j} \frac{\frac{\Delta G_j}{G_j (G_j + \Delta G_j)}}{1 - \frac{\Delta G_j}{G_j (G_j + \Delta G_j)} \frac{\text{cof } e_{jj}}{\det(\mathcal{L}_y(s)^{-1} \mathcal{A})}} \underline{c}_t (\mathcal{L}_y(s)^{-1} \mathcal{A})^{-1} \underline{u}_j \underline{u}_{jt} (\mathcal{L}_y(s)^{-1} \mathcal{A})^{-1} \underline{b} \quad (2.2.20)$$

$$\mathcal{S}_{G_j(s)}^{F(s)} = \frac{1}{F(s)} \frac{1}{G_j + \frac{\Delta G_j}{G_j} \left( G_j - \frac{\text{cof } e_{jj}}{\det(\mathcal{L}_y(s)^{-1} \mathcal{A})} \right)} \underline{c}_t (\mathcal{L}_y(s)^{-1} \mathcal{A})^{-1} \underline{u}_j \underline{u}_{jt} (\mathcal{L}_y(s)^{-1} \mathcal{A})^{-1} \underline{b} \quad (2.2.21)$$

From this we may also obtain:

$$\mathcal{S}_{G_j(s)}^{F(s)} = \frac{1}{F(s)} \frac{1}{G_j} \underline{c}_t (\mathcal{L}_y(s)^{-1} \mathcal{A})^{-1} \underline{u}_j \underline{u}_{jt} (\mathcal{L}_y(s)^{-1} \mathcal{A})^{-1} \underline{b} \quad (2.2.22)$$

The differential sensitivities (2.2.22) and (2.2.17) may also be obtained directly from (2.2.5) by differentiation.



We have now found both the finite difference sensitivity and the differential sensitivity of the transfer function  $F(s)$  to changes in each of the parameters in the block diagram in Fig 2.7.

As an example we use these expressions to find some of the sensitivities of the multiple feedback filter shown in Fig 2.6. Using (2.2.21) and the matrices in (2.2.6) we obtain:

$$\begin{aligned} \mathcal{S}_{G_1}^{F(s)} &= \frac{1}{F(s)} \frac{1}{G_1 + \frac{\Delta G_1}{G_1} \left( G_1 - \frac{G_2^{-1} G_3^{-1} - a_{33} G_2^{-1} - a_{23}}{G_1^{-1} G_2^{-1} G_3^{-1} - a_{33} G_1^{-1} G_2^{-1} - a_{23} G_1^{-1} - a_{13}} \right)} \times \\ &\quad \begin{bmatrix} 0 & 0 & 1 \end{bmatrix} \begin{bmatrix} G_1^{-1} & 0 & -a_{13} \\ -1 & G_2^{-1} & -a_{23} \\ 0 & -1 & G_3^{-1} - a_{33} \end{bmatrix}^{-1} \begin{bmatrix} 1 \\ 0 \\ 0 \end{bmatrix} \begin{bmatrix} 1 & 0 & 0 \end{bmatrix} \begin{bmatrix} G_1^{-1} & 0 & -a_{13} \\ -1 & G_2^{-1} & -a_{23} \\ 0 & -1 & G_3^{-1} - a_{33} \end{bmatrix}^{-1} \begin{bmatrix} 1 \\ 0 \\ 0 \end{bmatrix} \\ \mathcal{S}_{G_1}^{F(s)} &= \frac{1}{F(s)} \frac{1}{G_1 + \frac{\Delta G_1}{G_1} \left( G_1 - \frac{G_2^{-1} G_3^{-1} - a_{33} G_2^{-1} - a_{23}}{G_1^{-1} G_2^{-1} G_3^{-1} - a_{33} G_1^{-1} G_2^{-1} - a_{23} G_1^{-1} - a_{13}} \right)} \frac{\text{cof } e_{13}}{\det(\mathcal{L}_y^{-1} \mathcal{A})} \frac{\text{cof } e_{11}}{\det(\mathcal{L}_y^{-1} \mathcal{A})} \\ \mathcal{S}_{G_1}^{F(s)} &= \frac{\frac{G_2^{-1} G_3^{-1} - a_{33} G_2^{-1} - a_{23}}{G_1^{-1} G_2^{-1} G_3^{-1} - a_{33} G_1^{-1} G_2^{-1} - a_{23} G_1^{-1} - a_{13}}}{G_1 + \frac{\Delta G_1}{G_1} \left( G_1 - \frac{G_2^{-1} G_3^{-1} - a_{33} G_2^{-1} - a_{23}}{G_1^{-1} G_2^{-1} G_3^{-1} - a_{33} G_1^{-1} G_2^{-1} - a_{23} G_1^{-1} - a_{13}} \right)} \\ \mathcal{S}_{G_1}^{F(s)} &= \frac{\frac{G_1 - a_{33} G_1 G_3 - a_{23} G_1 G_2 G_3}{1 - a_{33} G_3 - a_{23} G_2 G_3 - a_{13} G_1 G_2 G_3}}{G_1 + \frac{\Delta G_1}{G_1} \left( G_1 - \frac{G_1 - a_{33} G_1 G_3 - a_{23} G_1 G_2 G_3}{1 - a_{33} G_3 - a_{23} G_2 G_3 - a_{13} G_1 G_2 G_3} \right)} \quad (2.2.23) \end{aligned}$$

Similarly using (2.2.16) and (2.2.6) we obtain

$$\begin{aligned} \mathcal{S}_{a_{23}}^{F(s)} &= \frac{1}{F(s)} \frac{1}{\frac{1}{a_{23}} - \frac{\Delta a_{23}}{a_{23}} \frac{G_1^{-1}}{G_1^{-1} G_2^{-1} G_3^{-1} - a_{33} G_1^{-1} G_2^{-1} - a_{23} G_1^{-1} - a_{13}}} \times \\ &\quad \begin{bmatrix} 0 & 0 & 1 \end{bmatrix} \begin{bmatrix} G_1^{-1} & 0 & -a_{13} \\ -1 & G_2^{-1} & -a_{23} \\ 0 & -1 & G_3^{-1} - a_{33} \end{bmatrix}^{-1} \begin{bmatrix} 0 \\ 1 \\ 0 \end{bmatrix} \begin{bmatrix} 0 & 0 & 1 \end{bmatrix} \begin{bmatrix} G_1^{-1} & 0 & -a_{13} \\ -1 & G_2^{-1} & -a_{23} \\ 0 & -1 & G_3^{-1} - a_{33} \end{bmatrix}^{-1} \begin{bmatrix} 1 \\ 0 \\ 0 \end{bmatrix} \end{aligned}$$

$$\mathcal{S}_{a_{23}}^{F(s)} = \frac{1}{F(s)} \frac{1}{\frac{1}{a_{23}} - \frac{\Delta a_{23}}{a_{23} G_1^{-1} G_2^{-1} G_3^{-1} - a_{33} G_1^{-1} G_2^{-1} - a_{23} G_1^{-1} - a_{13}}} \frac{\text{cof } e_{23}}{\det(\mathcal{L}_y^{-1} \mathcal{A})} \frac{\text{cof } e_{13}}{\det(\mathcal{L}_y^{-1} \mathcal{A})}$$

$$\mathcal{S}_{a_{23}}^{F(s)} = \frac{\frac{G_2 G_3}{1 - a_{33} G_3 - a_{23} G_2 G_3 - a_{13} G_1 G_2 G_3}}{\frac{1}{a_{23}} - \frac{\Delta a_{23}}{a_{23} (1 - a_{33} G_3 - a_{23} G_2 G_3 - a_{13} G_1 G_2 G_3)}} \quad (2.2.24)$$

Using (2.2.17) and (2.2.6) we obtain:

$$\mathcal{S}_{a_{33}}^{F(s)} = \frac{a_{33}}{F(s)} [0 \ 0 \ 1] \begin{bmatrix} G_1^{-1} & 0 & -a_{13} \\ -1 & G_2^{-1} & -a_{23} \\ 0 & -1 & G_3^{-1} - a_{33} \end{bmatrix}^{-1} \begin{bmatrix} 0 \\ 0 \\ 1 \end{bmatrix} [0 \ 0 \ 1] \begin{bmatrix} G_1^{-1} & 0 & -a_{13} \\ -1 & G_2^{-1} & -a_{23} \\ 0 & -1 & G_3^{-1} - a_{33} \end{bmatrix}^{-1} \begin{bmatrix} 1 \\ 0 \\ 0 \end{bmatrix}$$

$$\mathcal{S}_{a_{33}}^{F(s)} = \frac{a_{33}}{F(s)} \frac{\text{cof } e_{33}}{\det(\mathcal{L}_y^{-1} \mathcal{A})} \frac{\text{cof } e_{13}}{\det(\mathcal{L}_y^{-1} \mathcal{A})}$$

$$\mathcal{S}_{a_{33}}^{F(s)} = \frac{a_{33} G_1^{-1} G_2^{-1}}{G_1^{-1} G_2^{-1} G_3^{-1} - a_{33} G_1^{-1} G_2^{-1} - a_{23} G_1^{-1} - a_{13}} = \frac{a_{33} G_3}{1 - a_{33} G_3 - a_{23} G_2 G_3 - a_{13} G_1 G_2 G_3} \quad (2.2.25)$$

Using (2.2.22) and (2.2.6) we obtain:

$$\mathcal{S}_{G_3}^{F(s)} = \frac{G_3^{-1}}{F(s)} [0 \ 0 \ 1] \begin{bmatrix} G_1^{-1} & 0 & -a_{13} \\ -1 & G_2^{-1} & -a_{23} \\ 0 & -1 & G_3^{-1} - a_{33} \end{bmatrix}^{-1} \begin{bmatrix} 0 \\ 0 \\ 1 \end{bmatrix} [0 \ 0 \ 1] \begin{bmatrix} G_1^{-1} & 0 & -a_{13} \\ -1 & G_2^{-1} & -a_{23} \\ 0 & -1 & G_3^{-1} - a_{33} \end{bmatrix}^{-1} \begin{bmatrix} 1 \\ 0 \\ 0 \end{bmatrix}$$

$$\mathcal{S}_{G_3}^{F(s)} = \frac{G_1^{-1} G_2^{-1} G_3^{-1}}{G_1^{-1} G_2^{-1} G_3^{-1} - a_{33} G_1^{-1} G_2^{-1} - a_{23} G_1^{-1} - a_{13}} = \frac{1}{1 - a_{33} G_3 - a_{23} G_2 G_3 - a_{13} G_1 G_2 G_3} \quad (2.2.26)$$

From (2.2.23) and (2.2.24) we can write the corresponding differential sensitivities, which, together with (2.2.25) and (2.2.26), will be used to illustrate the summed sensitivity invariant described in the next section:

$$\mathcal{S}_{G_1}^{F(s)} = \frac{1 - a_{33} G_3 - a_{23} G_2 G_3}{1 - a_{33} G_3 - a_{23} G_2 G_3 - a_{13} G_1 G_2 G_3} \quad (2.2.27)$$

$$\mathcal{S}_{a_{23}}^{F(s)} = \frac{a_{23} G_2 G_3}{1 - a_{33} G_3 - a_{23} G_2 G_3 - a_{13} G_1 G_2 G_3} \quad (2.2.28)$$

The expressions (2.2.10), (2.2.11), (2.2.12), (2.2.17) and

(2.2.22) could form the basis of an efficient computer programme for the analysis of differential sensitivities. Assuming that the matrix method (2.2.5) is used to determine the nominal response  $F(s)$ , the matrix  $(\underline{y}(s)^{-1} - \mathcal{A})^{-1}$  would be available. From this the matrices  $\underline{\xi}_t (\underline{y}(s)^{-1} - \mathcal{A})^{-1}$  and  $(\underline{y}(s)^{-1} - \mathcal{A})^{-1} \underline{b}$  are readily obtained, and need be determined once only at each frequency. From these two matrices, all the differential sensitivities follow with very little extra computation. It will be seen in Section 2.2.4 that  $(\underline{y}(s)^{-1} - \mathcal{A})^{-1} \underline{b}$  is a column matrix of intermediate transfer functions, and that  $\underline{\xi}_t (\underline{y}(s)^{-1} - \mathcal{A})^{-1}$  is a row matrix of noise transfer functions, which are used in the analysis of dynamic range.

Both finite difference sensitivity and differential sensitivity may also be found from a signal flow graph by using Mason's rule and flow graph reversal (commonly called the adjoint approach when used in network analysis) [71]. The concept of flow graph reversal will be described in section 3.3.

### 2.2.3 A summed sensitivity invariant

For LCR and active CR networks, various summed sensitivity invariants have been derived from Euler's relation for homogeneous functions. They are of theoretical interest in that they provide bounds [72] to some sensitivity norms [73]\*, and they have a practical use as an aid to the computation of sensitivities.

In this section we present a new summed sensitivity invariant, which is novel in several respects. It is not here derived from Euler's relation, but is found from a consideration of the SFG of a multiple feedback filter, and the associated sensitivities as given in the previous section. The invariant applies to the branches of a cut of the SFG. A cut is similar to a cutset but is slightly more general. We will derive the summed sensitivity invariant for certain specific cuts, and will then combine these results in such a way that enables us to write a summed sensitivity invariant for any given cut.

First we define a cut. If the  $m$  nodes of an  $m$ -node graph are divided into two non-null sets  $N_a$  and  $N_b$ , then any set of branches each of which has one node in  $N_a$  and the other node in  $N_b$ , is called a cut (or seg [74]) of the graph. A cut is either a cutset or a disjoint union of cutsets. If  $N_a$  or  $N_b$  contains only one node, the corresponding cut is the set of branches incident at that node, and it is called a nodal cut or node cut. It follows that every node of the graph defines a node cut.

Now consider the block diagram of the general multiple feedback filter shown in Fig 2.7. This has an equivalent SFG shown in Fig 2.8. A cut  $C$  of the SFG will divide the nodes of the SFG into two sets  $N_a$  and  $N_b$ , and without loss of generality we take  $N_a$  to be the set containing the node  $e$ . If the  $p$  branches of the cut  $C$  are represented by their associated branch weights  $w_1, w_2, \dots, w_p$  then we may represent the cut:

$$C = \{w_1, w_2, \dots, w_p\} \quad (2.2.29)$$

We define the sensitivity sum  $\sigma$  associated with the cut  $C$  to be:

$$\sigma \triangleq \sum_{j=1}^p \left( \text{sgn } w_j \ S_{w_j}^F \right) \quad (2.2.30)$$

where  $S_{w_j}^F$  is the differential sensitivity of the transfer function  $F$  with respect to  $w_j$ , as found in the preceding section; and  $\text{sgn } w_j$  is

---

\* A sensitivity norm is sometimes taken to be a measure of multiparameter sensitivity, and in the mathematical sense that is just what it is. Most sensitivity norms however do not assign relative importance to different sensitivities, and none so far proposed give any indication of the deviation  $\Delta F$  or  $\Delta|F|$ .

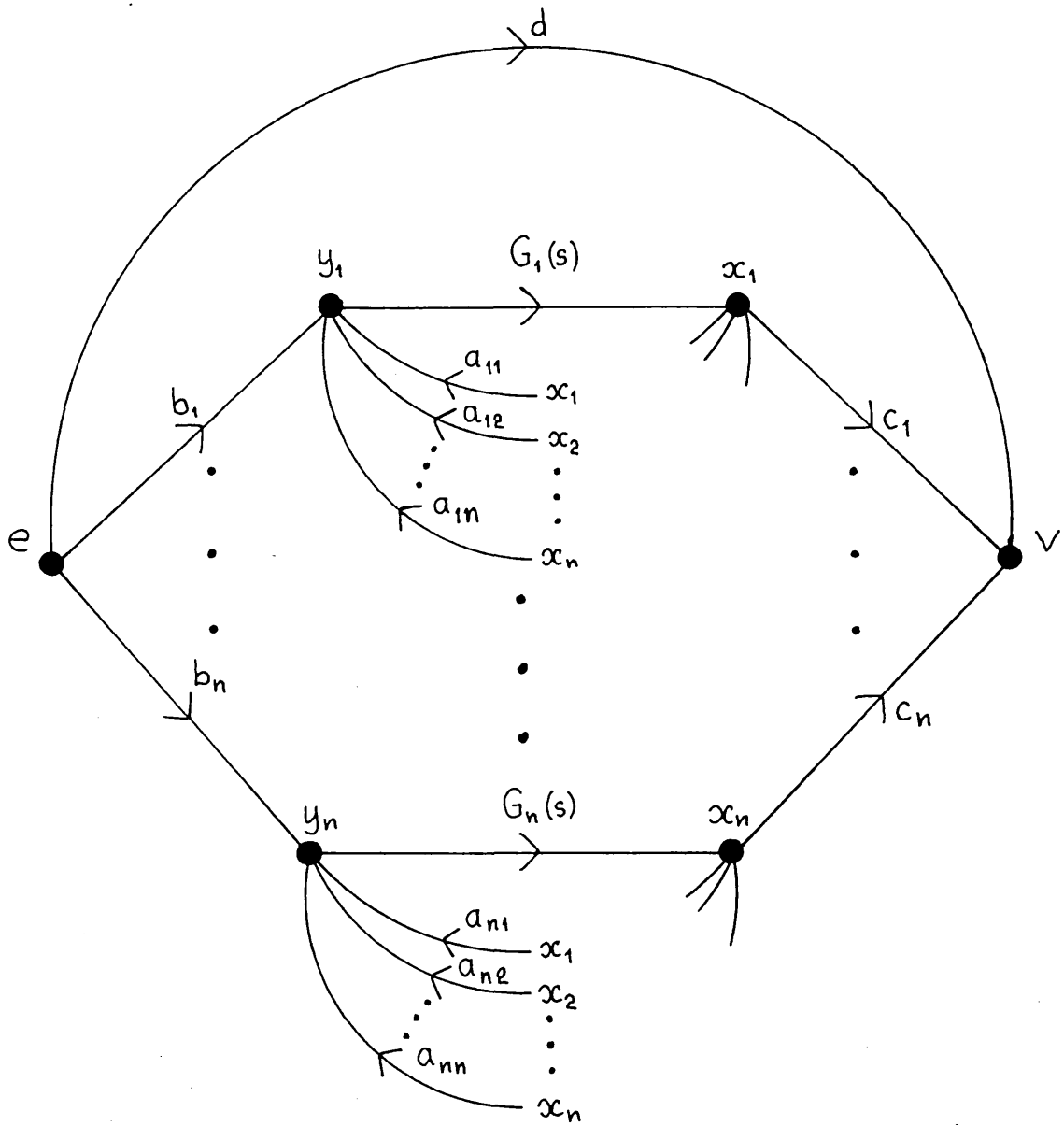


Fig 2.8 Signal flow graph of general multiple feedback filter

+1 or -1 depending respectively on whether the branch  $w_j$  is directed away from or towards the set  $N_a$  (which contains the filter input node  $e$ ).

We will now determine the sensitivity sum  $\sigma$  for each of three node cuts of the SFG in Fig 2.8. Firstly, the  $k$ -th output node  $x_k$  which defines a node cut  $C_{x_k}$ :

$$C_{x_k} = \{G_k, c_k, a_{1k}, a_{2k}, \dots, a_{nk}\} \quad (2.2.31)$$

for which the set  $N_b$  contains only one node, namely  $x_k$ . Since  $G_k$  is the only branch of  $C_{x_k}$  directed away from the set  $N_a$ , the sensitivity sum  $\sigma_{x_k}$  associated with the cut  $C_{x_k}$  is:

$$\sigma_{x_k} = \sum_{G_k}^F - \sum_{c_k}^F - \sum_{j=1}^n \sum_{a_{jk}}^F \quad (2.2.32)$$

This may be evaluated using (2.2.22), (2.2.11) and (2.2.17):

$$\begin{aligned} \sigma_{x_k} &= \frac{1}{F} \frac{1}{G_k} \underline{c}_t (\underline{I}_y^{-1} - \underline{A})^{-1} \underline{u}_k \underline{u}_{kt} (\underline{I}_y^{-1} - \underline{A})^{-1} \underline{b} - \frac{c_k}{F} \underline{u}_{kt} (\underline{I}_y^{-1} - \underline{A})^{-1} \underline{b} \\ &\quad - \sum_{j=1}^n \frac{a_{jk}}{F} \underline{c}_t (\underline{I}_y^{-1} - \underline{A})^{-1} \underline{u}_j \underline{u}_{kt} (\underline{I}_y^{-1} - \underline{A})^{-1} \underline{b} \\ &= \left\{ G_k^{-1} \underline{c}_t (\underline{I}_y^{-1} - \underline{A})^{-1} \underline{u}_k - c_k - \sum_{j=1}^n a_{jk} \underline{c}_t (\underline{I}_y^{-1} - \underline{A})^{-1} \underline{u}_j \right\} \frac{1}{F} \underline{u}_{kt} (\underline{I}_y^{-1} - \underline{A})^{-1} \underline{b} \\ &= \left\{ \underline{c}_t (\underline{I}_y^{-1} - \underline{A})^{-1} \begin{bmatrix} -a_{1k} \\ -a_{2k} \\ \vdots \\ G_k^{-1} - a_{kk} \\ \vdots \\ -a_{nk} \end{bmatrix} - c_k \right\} \frac{1}{F} \underline{u}_{kt} (\underline{I}_y^{-1} - \underline{A})^{-1} \underline{b} \end{aligned} \quad (2.2.33)$$

which, using the matrix  $\underline{E} \triangleq \underline{I}_y^{-1} - \underline{A}$ , may be written as:

$$\sigma_{x_k} = \left\{ \underline{c}_t \underline{E}^{-1} \begin{bmatrix} e_{1k} \\ e_{2k} \\ \vdots \\ e_{nk} \end{bmatrix} - c_k \right\} \frac{1}{F} \underline{u}_{kt} (\underline{I}_y^{-1} - \underline{A})^{-1} \underline{b}$$

$$\sigma_{x_k} = \left\{ \frac{1}{\det \mathcal{E}} \underline{c}_t \begin{bmatrix} \text{cof } e_{11} & \cdots & \text{cof } e_{n1} \\ \vdots & & \vdots \\ \text{cof } e_{1n} & \cdots & \text{cof } e_{nn} \end{bmatrix} \begin{bmatrix} e_{1k} \\ \vdots \\ e_{nk} \end{bmatrix} - c_k \right\} \frac{1}{F} \underline{u}_{kt} (\mathcal{L}_y^{-1} - \mathcal{A})^{-1} \underline{b} \quad (2.2.34)$$

and since:

$$\sum_{j=1}^n e_{jk} \text{cof } e_{je} = \begin{cases} 0 & : l \neq k \\ \det \mathcal{E} & : l = k \end{cases} \quad (2.2.35)$$

we have:

$$\sigma_{x_k} = \{ \underline{c}_t \underline{u}_k - c_k \} \frac{1}{F} \underline{u}_{kt} (\mathcal{L}_y^{-1} - \mathcal{A})^{-1} \underline{b}$$

$$\sigma_{x_k} = 0 \quad (2.2.36)$$

Thus the sensitivity sum  $\sigma_{x_k}$  associated with the node cut  $C_{x_k}$  defined by the  $k$ -th output node  $x_k$  is equal to zero. This is true for each of the  $n$  output nodes  $x_1, x_2, \dots, x_n$ .

Secondly the  $k$ -th input node  $y_k$  defines a node cut  $C_{y_k}$

$$C_{y_k} = \{ G_k, b_k, a_{k1}, a_{k2}, \dots, a_{kn} \} \quad (2.2.37)$$

for which the sensitivity sum  $\sigma_{y_k}$  is:

$$\sigma_{y_k} = -S_{G_k}^F + S_{b_k}^F + \sum_{j=1}^n S_{a_{kj}}^F \quad (2.2.38)$$

which may be evaluated using (2.2.22), (2.2.10) and (2.2.17):

$$\begin{aligned} \sigma_{y_k} = & -\frac{G_k^{-1}}{F} \underline{c}_t (\mathcal{L}_y^{-1} - \mathcal{A})^{-1} \underline{u}_k \underline{u}_{kt} (\mathcal{L}_y^{-1} - \mathcal{A})^{-1} \underline{b} + \frac{b_k}{F} \underline{c}_t (\mathcal{L}_y^{-1} - \mathcal{A})^{-1} \underline{u}_k \\ & + \sum_{j=1}^n \frac{a_{kj}}{F} \underline{c}_t (\mathcal{L}_y^{-1} - \mathcal{A})^{-1} \underline{u}_k \underline{u}_{jt} (\mathcal{L}_y^{-1} - \mathcal{A})^{-1} \underline{b} \end{aligned}$$

$$\sigma_{y_k} = \frac{1}{F} \underline{c}_t (\mathcal{L}_y^{-1} - \mathcal{A})^{-1} \underline{u}_k \left\{ b_k - \begin{bmatrix} -a_{k1} \\ -a_{k2} \\ \vdots \\ G_k^{-1} - a_{kk} \\ \vdots \\ -a_{kn} \end{bmatrix}_t (\mathcal{L}_y^{-1} - \mathcal{A})^{-1} \underline{b} \right\} \quad (2.2.39)$$

In a manner similar to treatment of the output node  $x_k$  we may show that:

$$\sigma_{y_k} = 0 \quad (2.2.40)$$

that is the sensitivity sum  $\sigma_{y_k}$  associated with the cut  $C_{y_k}$  defined by the k-th input node  $y_k$  is equal to zero. This is true for each of the n input nodes  $y_1, y_2, \dots, y_n$ .

Thirdly the filter output node v defines a node cut  $C_v$ :

$$C_v = \{d, c_1, c_2, \dots, c_n\} \quad (2.2.41)$$

for which the sensitivity sum  $\sigma_v$  is:

$$\sigma_v = \int_d^F + \sum_{j=1}^n \int_{c_j}^F \quad (2.2.42)$$

This may be evaluated using (2.2.12) and (2.2.11):

$$\sigma_v = \frac{d}{F} + \sum_{j=1}^n \frac{c_j}{F} \underline{u}_{jt} (\underline{L}_j^{-1} - \mathcal{A})^{-1} \underline{b}$$

$$\sigma_v = \frac{1}{F} \left\{ d + \underline{c}_t (\underline{L}_j^{-1} - \mathcal{A})^{-1} \underline{b} \right\}$$

Using (2.2.5):

$$\sigma_v = 1 \quad (2.2.43)$$

Thus the sensitivity sum  $\sigma_v$  associated with the node cut  $C_v$  defined by the filter output node v is equal to unity.

The three results (2.2.36), (2.2.40) and (2.2.43) together give the sensitivity sum  $\sigma$  for each node cut of the SFG shown in Fig 2.8, except the node cut corresponding to the filter input node e. We have therefore considered all cuts for which the set  $N_b$  contains only one node. Now we describe how these cuts may be combined.

Consider a first cut  $C_1$  dividing the nodes of the SFG into two sets  $N_{a1}$  and  $N_{b1}$  (with node e in  $N_{a1}$ ). This is illustrated in Fig 2.9(a), where the nodes constituting the set  $N_{b1}$  are shown inside the dashed line marked  $N_{b1}$ , and where the branches constituting the cut  $C_1$  are the branches intersected by the dashed line marked  $N_{b1}$ . Similarly consider a second cut  $C_2$  dividing the nodes of the SFG into two sets  $N_{a2}$  and  $N_{b2}$  (with node e in  $N_{a2}$ ), with the condition that  $N_{b1}$  and  $N_{b2}$  are disjoint (that is  $N_{b1}$  and  $N_{b2}$  have no nodes in common). This is also illustrated in Fig 2.9(a). Notice that although  $N_{b1}$  and  $N_{b2}$  are disjoint, the cuts  $C_1$  and  $C_2$  may have branches in common.

Now consider a third cut  $C_3$  dividing the nodes of the SFG into two sets  $N_{a3}$  and  $N_{b3}$ , where  $N_{b3}$  consists of the nodes in  $N_{b1}$



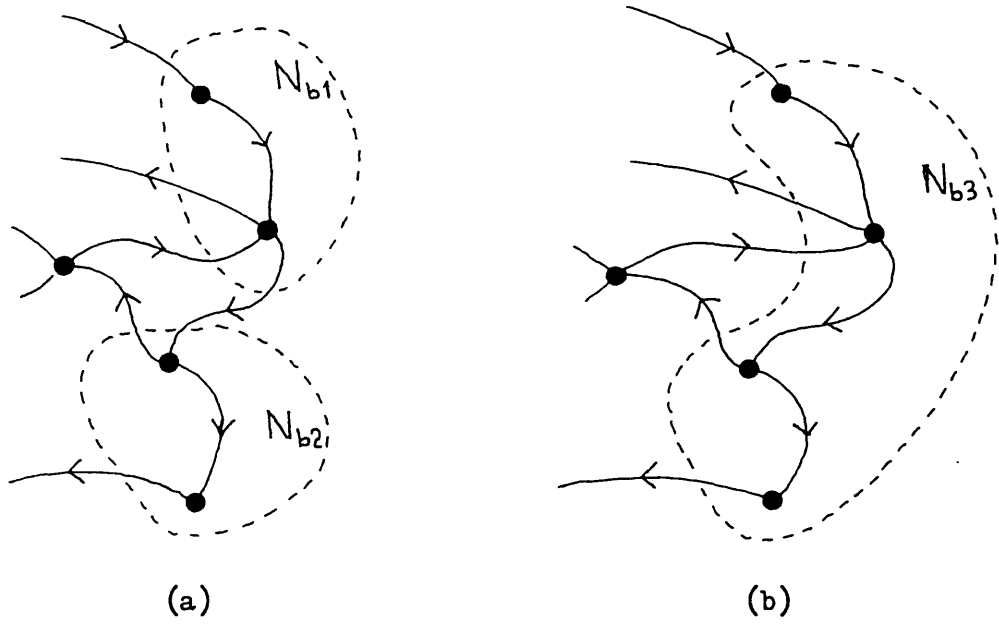


Fig 2.9 Combination of cuts

- (a) Cuts defined by disjoint sets  $N_{b1}$  and  $N_{b2}$
- (b) Cut defined by  $N_{b3} = N_{b1} \cup N_{b2}$

together with the nodes in  $N_{b_2}$  :

$$N_{b_3} = N_{b_1} \cup N_{b_2} \quad (2.2.44)$$

as illustrated in Fig 2.9(b). The branches of the cut  $C_3$  will evidently be the branches in  $C_1$  together with the branches in  $C_2$  but excluding any branches common to  $C_1$  and  $C_2$ . This is known as the symmetrical difference of the two sets  $C_1$  and  $C_2$  and is denoted thus:

$$C_3 = C_1 + C_2 \quad (2.2.45)$$

Let  $\sigma_1$ ,  $\sigma_2$  and  $\sigma_3$  be the sensitivity sums corresponding respectively to the cuts  $C_1$ ,  $C_2$  and  $C_3$ . Then the sum  $\sigma_1 + \sigma_2$  will have one term for each branch in  $C_1$  and one term for each branch in  $C_2$ . Hence for branches common to  $C_1$  and  $C_2$  there will be two terms in  $\sigma_1 + \sigma_2$ . They will be equal in magnitude, but one of them will have a positive sign and the other will have a negative sign, on account of the common branches having one orientation with respect to  $N_{b_1}$  and the opposite orientation with respect to  $N_{b_2}$ . These terms will cancel in  $\sigma_1 + \sigma_2$  leaving only terms corresponding to the non-common branches in  $C_1$  and  $C_2$ . But these non-common branches are identically the branches in  $C_3$ , furthermore the orientation of these branches with respect to  $N_{b_3}$  is the same as their orientation with respect to  $N_{b_1}$  or  $N_{b_2}$  as appropriate. Therefore  $\sigma_1 + \sigma_2$  is the sensitivity sum corresponding to the cut  $C_3$ . So we can say that if a cut  $C_3$  is the symmetrical difference of two cuts  $C_1$  and  $C_2$  :

$$C_3 = C_1 + C_2 \quad (2.2.46)$$

such that:

$$N_{b_3} = N_{b_1} \cup N_{b_2} \quad , \quad N_{b_1} \cap N_{b_2} = \emptyset \quad (2.2.47)$$

then:

$$\sigma_3 = \sigma_1 + \sigma_2 \quad (2.2.48)$$

This result can be used successively to combine any number of node cuts as follows. Consider any cut  $C$  of the SFG shown in Fig 2.8, dividing the nodes of the SFG into two sets  $N_a$  (which contains node  $e$ ) and  $N_b$ . If the set  $N_b$  contains  $q$  nodes then  $N_b$  is the disjoint union of  $q$  sets  $N_{b_1}, \dots, N_{b_q}$  each containing a single node of  $N_b$ :

$$N_b = N_{b_1} \cup N_{b_2} \cup \dots \cup N_{b_q} \quad (2.2.49)$$

Corresponding to each of these  $q$  nodes is a node cut  $C_1, C_2, \dots, C_q$ , and since the symmetrical difference is associative, we may write, using (2.2.44) and (2.2.45):

$$C = C_1 + C_2 + \dots + C_q \quad (2.2.50)$$

and from (2.2.46) and 2.2.48) it follows that:

$$\sigma = \sigma_1 + \sigma_2 + \dots + \sigma_q \quad (2.2.51)$$

But we have already evaluated the sensitivity sums for each possible node cut, and they are all equal to zero, except  $\sigma_v$  which is equal to unity (see(2.2.36), (2.2.40) and (2.2.43)), Whence:

$$\sigma = \begin{cases} 0 & : v \notin N_b \\ 1 & : v \in N_b \end{cases} \quad (2.2.52)$$

which is the required result. Since the value of the sensitivity sum  $\sigma$  is quite independent of the values of any of the branch weights, we call it a summed sensitivity invariant. We summarise our conclusion in the following:

For any cut  $C = \{w_1, w_2, \dots\}$  dividing the nodes of the SFG of a multiple feedback filter into two sets  $N_a$  and  $N_b$ , with  $e \in N_a$ , there exists an invariant sensitivity sum  $\sigma$  given by:

$$\sigma = \sum_{w_j \in C} \left( \text{sgn } w_j S_{w_j}^F \right) = \begin{cases} 0 & : v \notin N_b \\ 1 & : v \in N_b \end{cases} \quad (2.2.53)$$

$$\text{where } \text{sgn } w_j = \begin{cases} +1 & : w_j \text{ directed away from } N_a \\ -1 & : w_j \text{ directed towards } N_a \end{cases}$$

As an example take the multiple feedback filter shown in Fig 2.6, and consider the cut  $C = \{G_1, a_{23}, a_{33}, G_3\}$  as indicated by the dashed line in Fig 2.10. Here extra unity weight branches have been inserted to make this graph a special case of the SFG in Fig 2.8. The branches  $G_1, a_{23}, a_{33}$  are directed away from the set of nodes  $N_a$  containing node  $e$ , hence  $\text{sgn } G_1 = \text{sgn } a_{23} = \text{sgn } a_{33} = 1$ . The branch  $G_3$  has the opposite direction, hence  $\text{sgn } G_3 = -1$ . Furthermore the node  $v$  is not in the set  $N_b$ , so that we have from (2.2.53):

$$\sigma = \sum_{w_j \in C} \left( \text{sgn } w_j S_{w_j}^F \right) = S_{G_1}^F + S_{a_{23}}^F + S_{a_{33}}^F - S_{G_3}^F = 0 \quad (2.2.54)$$

Expressions for the four sensitivities in (2.2.54) were given in the previous section, and one use of the sensitivity invariant is to check the results so obtained. Thus from (2.2.25), (2.2.26), (2.2.27) and (2.2.28):

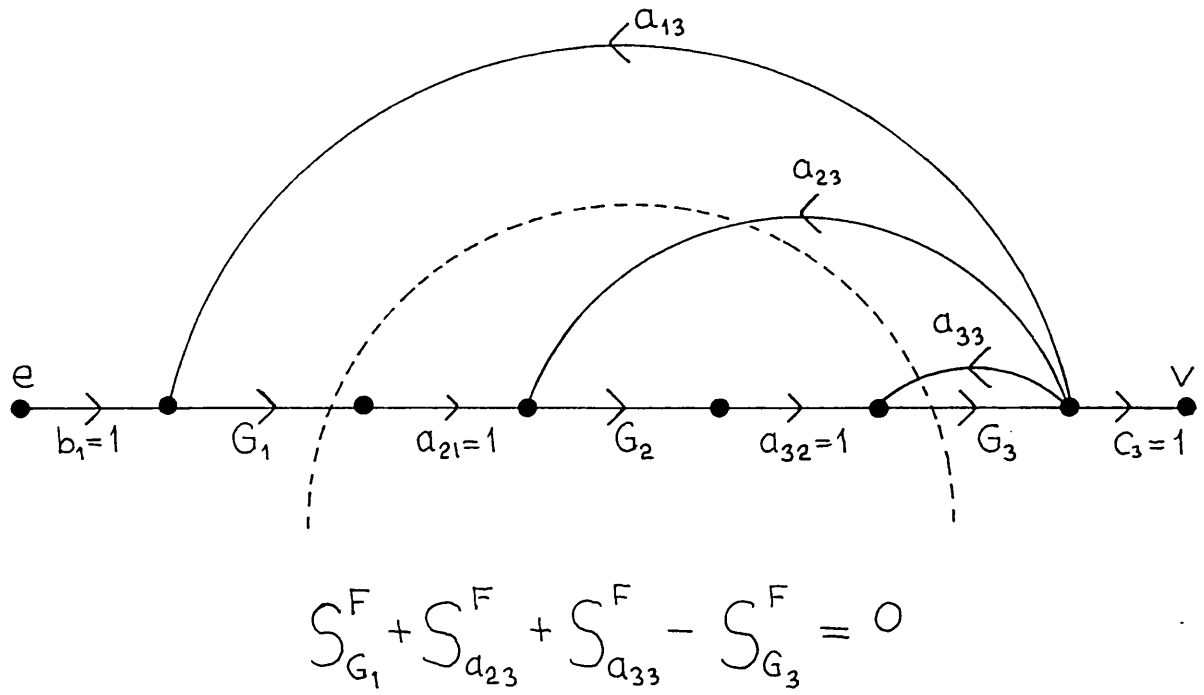


Fig 2.10 Example of the summed sensitivity invariant

$$S_{G_1}^F + S_{a_{23}}^F + S_{a_{33}}^F - S_{G_3}^F = \frac{(1 - a_{33}G_3 - a_{23}G_2G_3) + a_{23}G_2G_3 + a_{33}G_3 - 1}{1 - a_{33}G_3 - a_{23}G_2G_3 - a_{13}G_1G_2G_3} = 0$$

which checks with (2.2.54).

Alternatively the sensitivity invariant may be used to simplify the calculation of sensitivity. For example consider the leapfrog feedback structure shown in Fig 2.11. Using the cut:

$$C = \{a_{k,k+1}, G_{k+1}, G_{k+2}, \dots, G_n\}$$

we can write the sensitivity sum  $\sigma$ :

$$\sigma = -S_{a_{k,k+1}}^F + \sum_{j=1}^{n-k} (-1)^{j+1} S_{G_{k+j}}^F = \begin{cases} 0 & : v \notin N_b \\ 1 & : v \in N_b \end{cases}$$

and, since  $v \in N_b$  when  $n-k$  is odd and  $v \notin N_b$  when  $n-k$  is even, this enables us to express the sensitivity to the feedback path  $a_{k,k+1}$  in terms of the sensitivities to the subsequent blocks as:

$$S_{a_{k,k+1}}^F = \sum_{j=1}^{n-k} (-1)^{j+1} S_{G_{k+j}}^F + \frac{(-1)^{n-k}}{2} - \frac{1}{2} \quad (2.2.55)$$

Thus once the sensitivities to the branches  $G_j$  have been determined, the sensitivities to the branches  $a_{k,k+1}$  may be easily found. It is of interest to note that Szentirmai [33] has given the following expression, based purely on intuitive reasoning:

$$S_{a_{k,k+1}}^F = \sum_{j=1}^{n-k} (-1)^{j+1} S_{G_{k+j}}^F \quad (2.2.56)$$

Comparison with (2.2.55) proves that it is valid for cases where  $n-k$  is even. The reader may construct further examples of the sensitivity invariant from the sensitivity expressions given in Fig 1.6 and Fig 1.7.

The sensitivity invariant (2.2.53) was first reported by the writer as a footnote in Ref.[77]. Subsequently the writer published a proof in Ref.[88], which will be given in Chapter 3 since it is an alternative proof to that given in this chapter. Simultaneously with Ref.[88], but quite independent from it, Acar published very similar results for SFG's in general [137]. His approach is quite different, and it involves the construction of a 'sensitivity graph' to find relationships between dependent and independent sensitivities.

Stimulated by Acar's work, we may say in the context of multiple feedback filters that a set of basic cutsets of the SFG will yield a set of independent relationships between the sensitivities.

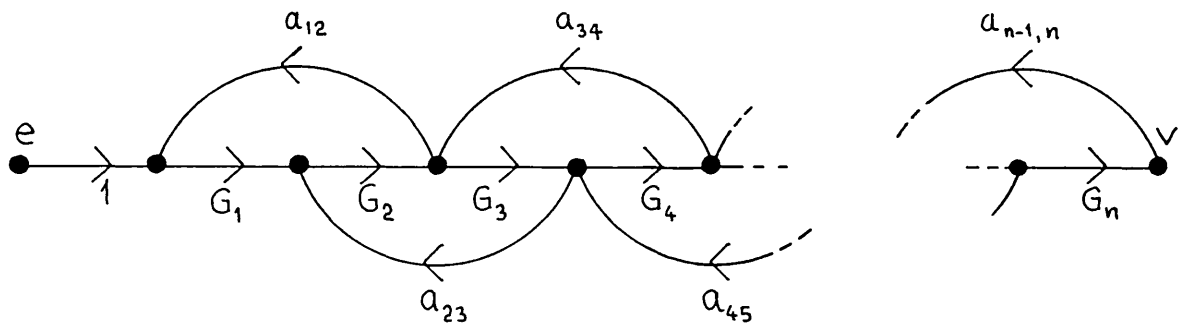


Fig 2.11 Leapfrog feedback structure

If the SFG has  $m$ -nodes, then a tree of the SFG will have  $m-1$  branches. Each tree-branch defines a basic cutset, for which we can write the corresponding summed sensitivity invariant. The set of invariants defined by a given tree will constitute a set of  $m-1$  linearly independent equations relating the SFG sensitivities. We may also say that the sensitivities of the transfer function with respect to the co-tree branch weights will constitute a set of independent sensitivities. Note that the use of the summed sensitivity invariant enables us to arrive at these results without having to construct Acar's Sensitivity Graph.

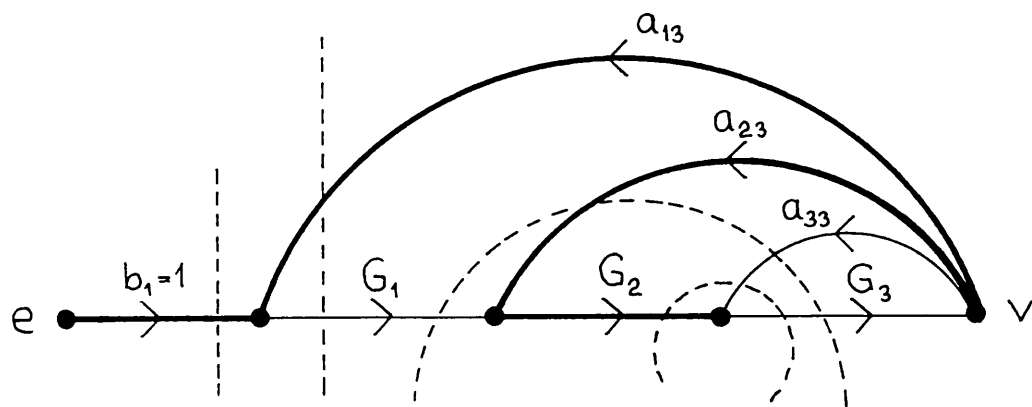
For example, consider again the multiple feedback filter shown in Fig 2.6, and take the particular tree indicated by the heavy line in Fig 2.12. Each of the four tree branches  $b_1, a_{13}, a_{23}, G_2$  defines a basic cutset, and the summed sensitivity invariant for each of these cutsets is shown in the figure. The four equations are linearly independent, and the sensitivities of  $F$  with respect to the co-tree branch weights  $G_1, a_{33}$  and  $G_3$  form a set of independent sensitivities.

In Chapter 5 we will be studying the deviations of the magnitude response  $|F(i\omega)|$ , caused by the weights of the branches in the SFG being changed by small amounts. We note here that taking separately the real part and the imaginary part of (2.2.53) leads to equations relating respectively the magnitude sensitivities and the phase sensitivities:

$$\sum_{w_j \in C} \left( \text{sgn } w_j \sum_{w_j}^{|F|} \right) = \begin{cases} 0 & : v \notin N_b \\ 1 & : v \in N_b \end{cases} \quad (2.2.57)$$

$$\sum_{w_j \in C} \left( \text{sgn } w_j \sum_{w_j}^{\arg F} \right) = 0 \quad (2.2.58)$$

These follow using known results of the sensitivity calculus.



$$\begin{aligned}
 S_{b_1}^F &= 1 \\
 -S_{a_{13}}^F + S_{G_1}^F &= 1 \\
 S_{G_1}^F + S_{a_{23}}^F + S_{a_{33}}^F - S_{G_3}^F &= 0 \\
 S_{G_2}^F + S_{a_{33}}^F - S_{G_3}^F &= 0
 \end{aligned}$$

Fig 2.12 Example of a set of independent sensitivity equations



### 2.2.4 Dynamic range

In the context of filtering, dynamic range is a measure of signal handling capability. It is an indication of the limits imposed by the filter on the range of signal levels over which the filter performance is acceptable. At the upper limit the signal is distorted by the non-linear voltage or slew-rate<sup>[138]</sup> limitations of the operational amplifiers, and at the lower limit the signal is distorted by noise generated within the filter.

Dynamic range is usually considered in the frequency domain, although for pulse filters it would be more appropriate to use the time domain. We will use the frequency domain, and will consider the lower and upper limits to dynamic range separately.

The upper limit to dynamic range is imposed by the voltage limited or slew-rate limited outputs of the operational amplifiers. If the signal level is high enough, these lead to non-linear distortion of the filter output, and in some cases to jump resonance [75]. We assume that to maintain acceptable performance it is necessary that, in the sinusoidal steady state, the operational amplifier output voltages do not exceed a specific value. In single amplifier sections, such as that shown in Fig 2.1(b), the amplifier output is coincident with the output of the section, and we therefore consider the section output voltages  $x_j$  in Fig 2.7. If multiple amplifier sections such as the ones shown in Fig 1.5(c) and (d) are used, then there will be a further problem (not considered here) of relating the output voltages of the additional amplifiers to the section output voltage. The sinusoidal steady state output voltage phasor  $V = |V| e^{i \arg V}$  (where  $v(t) = \text{Re } V e^{i \omega t}$ ) of the filter is determined by the transfer function (2.2.5), and its magnitude is:

$$|V| = |\underline{c}_t (\underline{h}_j(i\omega)^{-1} - \mathcal{A})^{-1} \underline{b} + d| \cdot |E| \quad (2.2.59)$$

and the output voltages  $X_j$  of the internal sections are determined by the intermediate transfer functions  $x_j(s)/e(s)$ , which are obtained from (2.2.2) and (2.2.3) as:

$$G_{j_e}(s) \triangleq \frac{x_j(s)}{e(s)} = \underline{u}_{j_t} (\underline{h}_j(s)^{-1} - \mathcal{A})^{-1} \underline{b} \quad j = 1, 2, \dots, n \quad (2.2.60)$$

thus:

$$|X_j| = |\underline{u}_{j_t} (\underline{h}_j(i\omega)^{-1} - \mathcal{A})^{-1} \underline{b}| \cdot |E| \quad j = 1, 2, \dots, n \quad (2.2.61)$$

The input  $|E|$  must not exceed the value (denoted by  $|\hat{E}|$ ) which causes any one of these voltages to become distorted.

Discussion is aided by plotting these voltages as functions of

frequency. As an example these voltages have been computed for the filter design illustrated in Fig 2.6, and they are plotted in Fig 2.13. The voltages are plotted for an input  $|E| = 1$ , so that the graphs also represent the moduli of the intermediate transfer functions from the filter input to the outputs of the various sections. The output of section 3 is, in this example, also the filter output and it is determined by the specified transfer function of the filter. If, as the input voltage  $|E|$  is increased, it is an internal section which first causes distortion, then the dynamic range of the filter is probably unnecessarily restricted, because, as will be shown in section 3.4, it is in theory always possible to scale the signal levels without affecting sensitivity. Thus the signal level at the output of the offending internal section could be reduced in scale until that section is no longer the prime cause of distortion.

Conversely, if it is the output section which first causes distortion, there may be an internal section at which the signal level is too low, so that the section makes an unnecessarily large contribution to the filter noise. It is usually assumed therefore that the optimum condition is achieved when all amplifiers start to distort at the same value of  $|E|$ . The graphs in Fig 2.13 show that this condition is almost achieved in the example, for the usual case of all amplifiers having identical performance, in that the maxima of the three curves are within about 1dB of each other. The attainment of this optimum condition depends on being able to obtain the required gain from the type of section being used.

In practice the input to the filter is unlikely to be a steady state sinusoid, and the above analysis may not give a good indication of the maximum voltages. However, if the input signal has a Laplace transform, the filter transfer function (2.2.5) and the intermediate transfer functions (2.2.60) can be used to determine the maximum voltages. If the input signal is a random process, then it may or may not be possible to determine the maximum voltages, depending on the nature of the process. If, for instance, all that is known about the input signal is its spectral density, then it is possible to find the mean square voltages, but not the peak voltages. In these circumstances one might assume that the optimum condition for maximum dynamic range is obtained when the mean square voltages at the outputs of all the sections are equal.

It will be noticed in Fig 2.13 that the frequency response at the output of an internal section can have considerable variation over the

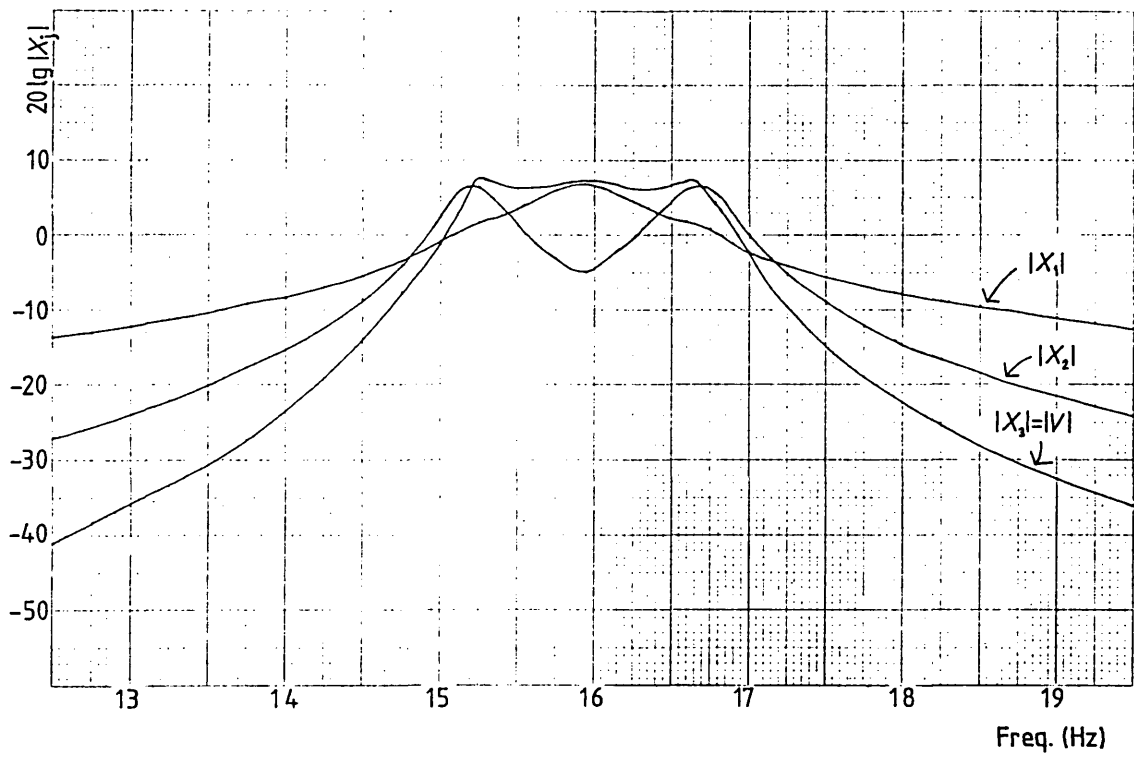


Fig 2.13 Signal levels of the filter shown in Fig 2.6; plotted  
for  $|E|=1$

passband. In the example, the passband response of  $|X_2|$  varies by 11.5dB. Multiple feedback filters differ in the extent of such variation, and at one time it was assumed that the filter with the lowest variation had the best dynamic range [76,77]. The intuitive assumption was that since the signal level was more removed from the noise level, the noise produced by the filter would be lower. More recent work [78,79,80] has questioned this assumption, and it is therefore necessary to investigate the way in which noise is produced by the filter.

In active CR filters, thermal noise is generated in the resistors, and various mechanisms generate noise in the operational amplifiers [81]. With careful design the noise produced by an isolated section can be minimized [82]. When several sections are interconnected to form a multiple feedback filter, each section will contribute to the noise output of the filter, and we are interested in how this noise is affected by multiple feedback. The noise produced by a given section can be modelled by an equivalent noise voltage source connected to the input of that section.

Accordingly we will analyse the general multiple feedback filter in Fig 2.7 with an additional voltage source  $e_j$  at the input of each section, and with the filter input suppressed, such that:

$$\underline{y} = \mathcal{A} \underline{x} + \underline{e} \quad \text{where} \quad \underline{e} \triangleq \begin{bmatrix} e_1 \\ \cdot \\ \cdot \\ \cdot \\ e_n \end{bmatrix} \quad (2.2.62)$$

whence from (2.2.62), (2.2.2) and (2.2.4) with the filter input  $e=0$  we obtain:

$$\begin{aligned} v &= \underline{c}_t (U - \underline{h}_y(s) \mathcal{A})^{-1} \underline{h}_y(s) \underline{e} \\ v &= \underline{c}_t (\underline{h}_y(s)^{-1} - \mathcal{A})^{-1} \underline{e} \end{aligned} \quad (2.2.63)$$

Thus the voltage transfer ratio  $G_{v_j}(s)$  from the voltage source  $e_j$  to the filter output  $v$  is:

$$G_{v_j}(s) \triangleq \frac{v(s)}{e_j(s)} = \underline{c}_t (\underline{h}_y(s)^{-1} - \mathcal{A})^{-1} \underline{u}_j \quad j = 1, 2, \dots, n \quad (2.2.64)$$

We will call these the noise transfer functions. Now when  $e_j(t)$  is taken to be an equivalent noise source it is assumed to be a sample function from an ergodic random process, and it is characterized by its

spectral density  $e_{nj}(\omega)$  with units of volts<sup>2</sup>/Hz.\* The 'power' transfer function†  $|G_{vj}(i\omega)|^2$  is used to find the resulting spectral density  $e'_{nj}(\omega)$  at the output of the filter [83] thus:

$$e'_{nj}(\omega) = |G_{vj}(i\omega)|^2 e_{nj}(\omega) \quad (2.2.65)$$

The mean square noise voltage  $\overline{e'^2_{nj}}$  produced at the output of the filter by the noise generated in the j-th section may be obtained from the spectral density [83] ‡ :

$$\overline{e'^2_{nj}} = \frac{1}{2\pi} \int_{-\infty}^{\infty} e'_{nj}(\omega) d\omega \quad (2.2.66)$$

$$= \frac{1}{2\pi} \int_{-\infty}^{\infty} |G_{vj}(i\omega)|^2 e_{nj}(\omega) d\omega \quad (2.2.67)$$

$$= \frac{1}{2\pi i} \int_{-i\infty}^{i\infty} G_{vj}(s) G_{vj}(-s) e_{nj}\left(\frac{s}{i}\right) ds \quad (2.2.68)$$

Since the noise sources are uncorrelated and have zero mean value, the noise spectral densities  $e'_{nj}(\omega)$  (and hence the mean square noise voltages  $\overline{e'^2_{nj}}$ ) will add together at the output of the filter. Thus the spectral density  $e_{nv}(\omega)$  at the filter output is given by:

$$e_{nv}(\omega) = e_{ns}(\omega) + \sum_{j=1}^n e'_{nj}(\omega) \quad (2.2.69)$$

$$e_{nv}(\omega) = e_{ns}(\omega) + \sum_{j=1}^n \left| \zeta_t (l_j(i\omega)^{-1} - \mathcal{A})^{-1} u_j \right|^2 e_{nj}(\omega)$$

where  $e_{ns}(\omega)$  is the spectral density of the noise produced by the summing amplifier section at the output of the filter (Fig 2.7), and is unaffected by multiple feedback. The mean square noise voltage at the filter output is:

$$\overline{e_{nv}^2} = \frac{1}{2\pi} \int_{-\infty}^{\infty} e_{nv}(\omega) d\omega \quad (2.2.70)$$

Computation of this noise is simplified when one can assume that the spectral densities are constant over the frequency range of interest [80].

\* Many engineers prefer to use the square root of the spectral density, with units of volts/ $\sqrt{\text{Hz}}$ , for which the familiar voltage transfer functions obtain.

† Note that the spectral density of a random voltage is often thought of as a normalized power density, and the squared modulus functions are hence called power transfer functions.

‡ Some authors prefer to use the one-sided spectral density for which the corresponding expression is of the form:  $\overline{e^2} = \int_0^{\infty} e(f) df$ .

The dynamic range  $D$  of a filter is usually defined to be the ratio of the root mean square value of the maximum undistorted sinusoidal steady state output voltage  $|\hat{V}|/\sqrt{2}$ , that is achievable for all passband frequencies, to the root mean square value of the noise voltage  $\sqrt{\overline{e_{nv}^2}}$  at the output of the filter. Thus for multiple feedback filters:

$$D = \frac{|\hat{V}|}{\sqrt{2} \overline{e_{nv}^2}} \quad (2.2.71)$$

where  $|\hat{V}|$  is given by (2.2.59) with  $|\mathcal{E}| = |\hat{\mathcal{E}}|$ , and  $\overline{e_{nv}^2}$  is given by (2.2.69) substituted in (2.2.70).

We have seen that the dynamic range of a multiple feedback filter is related to the imperfections of its constituent sections by the intermediate transfer functions (2.2.60) and the noise transfer functions (2.2.64). In section 3.4 we will show how the scaling transformation can be used to maximise the dynamic range of any given filter, without degrading the sensitivity performance.

### 2.3 Summary

In this chapter we have defined a multiple feedback filter to be an interconnection of active CR sections, forming a structure which has at least one forward path, and a multiplicity of feedback loops. The definition is flexible enough to encompass all structures proposed to date, including Bach's circuit which is not normally thought of in this context. We have seen how a multiple feedback filter may be represented by either a block diagram or a signal flow graph.

We have shown that a multiple feedback filter may be analysed using Sandberg's matrix method, or Mason's topological method. Explicit expressions have been given for the differential sensitivities and the finite difference sensitivities of the transfer function of any given multiple feedback filter with respect to changes in the block diagram parameters. The expressions for finite difference sensitivities are given here for the first time. An indication has been given of how sensitivities may alternatively be found by using Mason's rule and flow graph reversal.

A new summed sensitivity invariant has been given, applicable to the branches of a cut of a SFG. It is valid for SFG's in general, but has been presented here in the specific context of multiple feedback filters. The proof given in this chapter is based on matrix analysis of a general structure. An alternative proof based on the scaling transformation and Euler's relation will be given in Chapter 3. The result was first published by the writer as a footnote in Ref [77], and later in Ref [88] together with the alternative proof.

Dynamic range has been discussed, and it has been shown that, given the noise and limiting properties of the sections, the dynamic range of any given multiple feedback filter may be determined by using the noise transfer functions and the intermediate transfer functions of the structure.

---

TRANSFORMATION OF MULTIPLE FEEDBACK FILTERS

---

There are many methods of synthesising a multiple feedback filter, and they lead to a variety of different structures. Once a particular filter has been obtained as a result of synthesis, it may be manipulated further by an application of the transformations described in this chapter. The transformations may be used to obtain new structures from known structures, or they may be used to improve the performance of the filter in some way. For instance they have been used variously to reduce complexity, to reduce sensitivity, and to increase dynamic range; all without affecting the transfer function.

Most transformations are manipulations of the SFG of a filter, and we start by describing rudimentary SFG equivalents which are useful for simplifying the realization. Some transformations have the interesting property, first pointed out by the writer in [84,77], of altering the SFG without affecting the block diagram sensitivities (block diagram sensitivities were given in section 2.2.2). One of these, namely scaling of signal levels, has already been mentioned in the discussion of dynamic range. The other two are the interchange of cascaded sub-networks, and the reversal of a signal flow graph. These may also affect the dynamic range, and flow graph reversal may sometimes reduce the complexity.

In some cases a similarity transformation of the matrix  $\mathcal{A}$  can be used to alter the structure of a filter without affecting the transfer function. It has been used by some authors [49,69,85,86] in a search for low sensitivity structures.



### 3.1 Equivalent signal flow graphs

Mason [65] has given some equivalent signal flow graphs which can be used to manipulate a SFG in order to obtain new structures or to simplify the realization. These rudimentary equivalents are shown in Fig 3.1.

The use of these equivalents will be illustrated by the derivation of a structure which will be studied in a later chapter. Starting from the LCR filter shown in Fig 3.2(a), we obtain a block diagram by simulation, in the way that was described in section 1.1. This block diagram (Fig 3.2(b)) is not in a form suitable for practical realization because the transfer function of the second block has a pole at infinity. In practice a voltage ratio can never have a pole at infinite frequency, and circuits which give the required response over a limited band of frequencies are usually excessively noisy. The difficulty is overcome by redrawing the block diagram as an SFG (Fig 3.2(c)) and then using the rudimentary SFG equivalents to eliminate the term  $sC_2$  from the transfer function of the second block (Fig 3.2(d) and (e)). The resulting realization would need three integrator sections and two summing amplifier sections. However further use of the SFG equivalents (Fig 3.2(f) and (g)) leads to a structure with a simpler realization.

In the process of drawing the block diagram in Fig 3.2(h) equivalent to the SFG in Fig 3.2(g), we have changed the sign of some branch weights, in a way which does not alter the transfer function but which associates the negative signs with the blocks. Although this is a fairly obvious transformation, it is interesting to note that it is a special case of the scaling transformation which will be described in section 3.4. A realization of this block diagram uses three integrator sections and only one summing amplifier section, and in this form the realization is the circuit attributed to Ford in Ref [17].

It should also be noted that having transformed the network, it is no longer a direct simulation of the LCR filter. The leapfrog feedback structure has been retained, but the term  $sC_2$  in the transfer function of the second block in Fig 3.2(b) has been replaced by extra feedback and feedforward paths in Fig 3.2(h). In the same way that the capacitor  $C_2$  affects mainly the stopband performance of the LCR filter, so these extra paths affect mainly the stopband performance of the multiple feedback filter in Fig 3.2(h), as will be shown in Chapter 5, where we study a bandpass version of this filter.

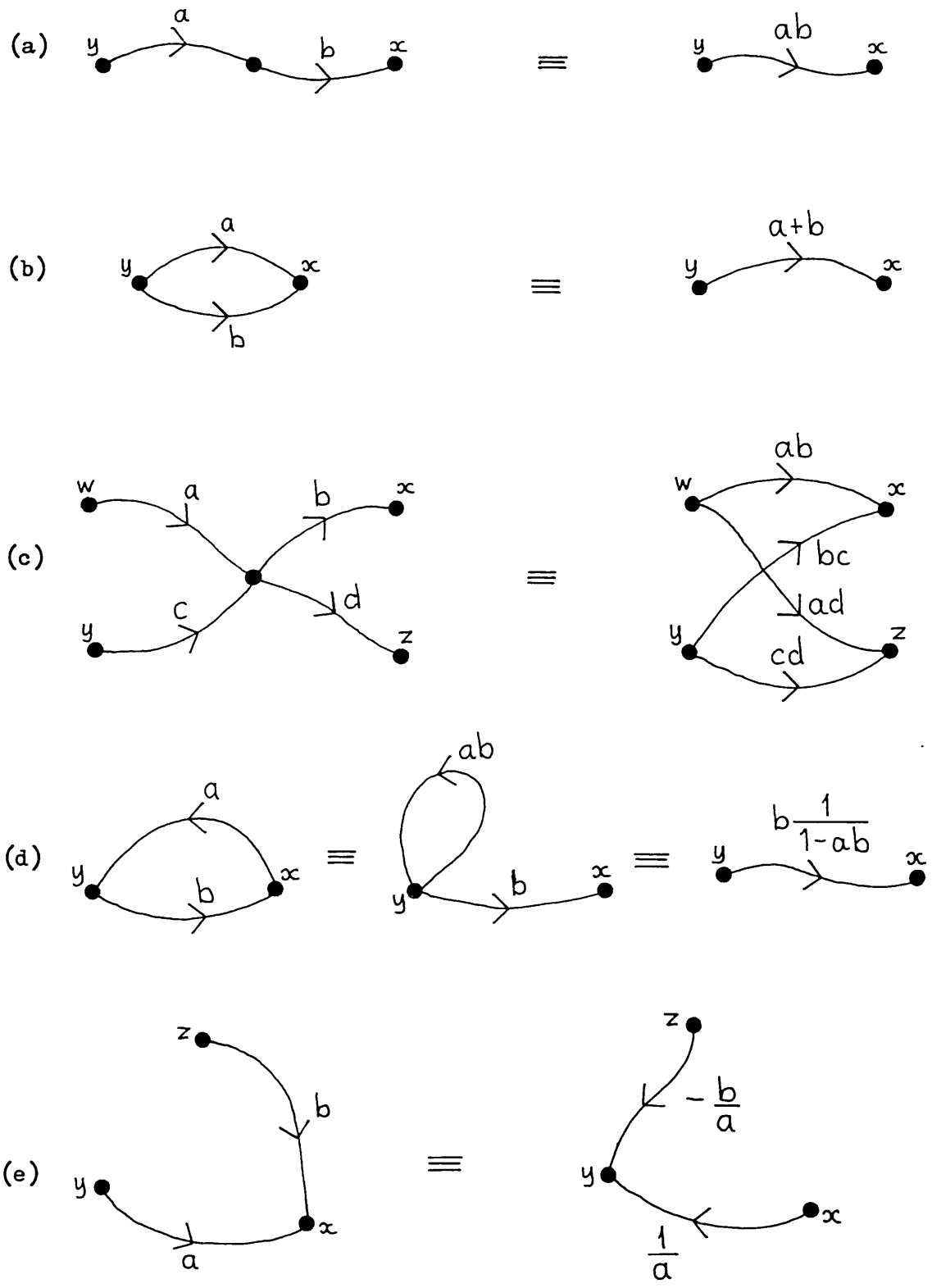


Fig 3.1 Five rudimentary signal flow graph equivalents

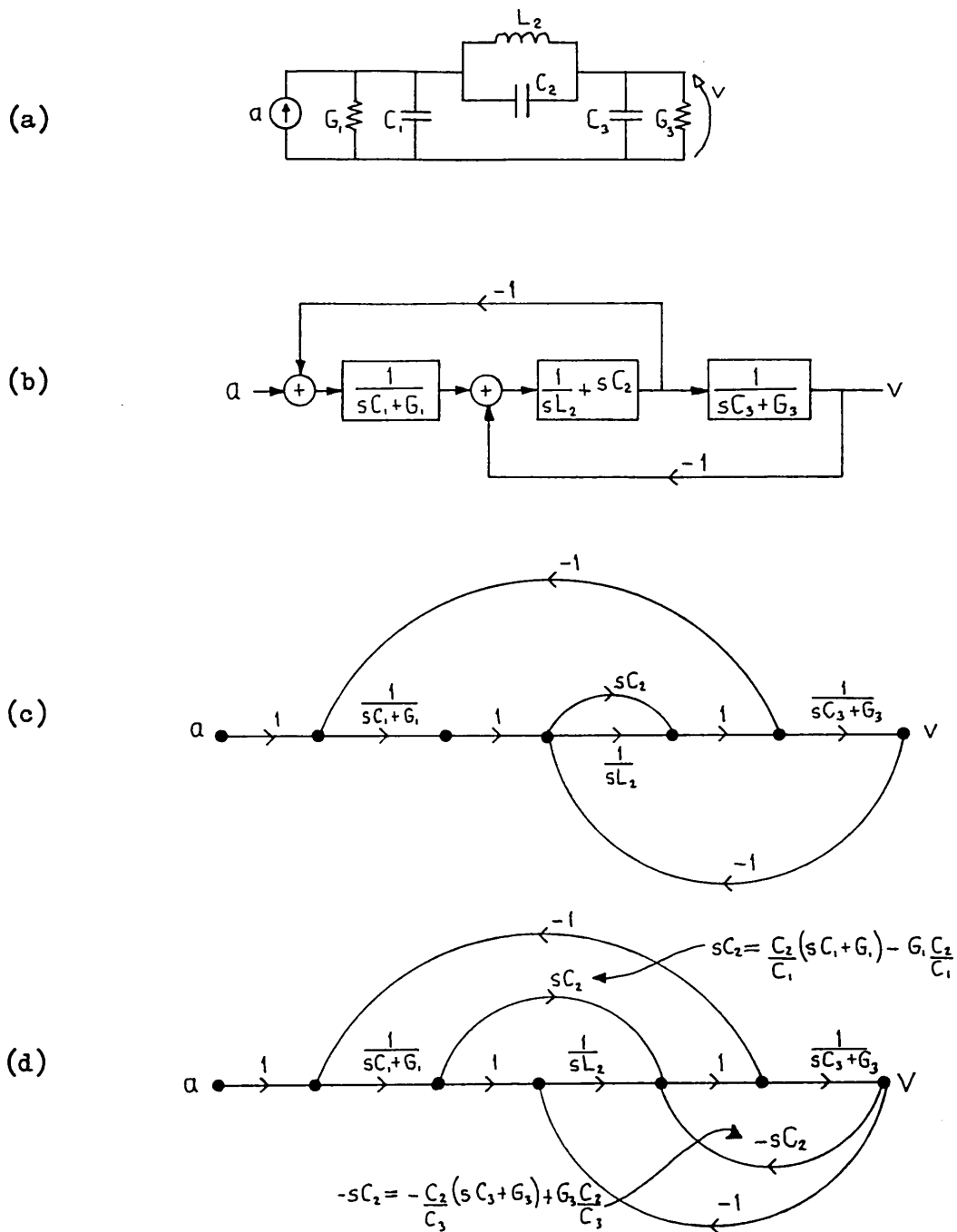


Fig 3.2 Transformation using equivalent signal flow graphs

- (a) LCR lowpass ladder filter
- (b) Block diagram obtained by simulation (see Fig 1.3)
- (c) Signal flow graph equivalent to (b)
- (d) Transformation of the SFG using rudimentary equivalents

continued:

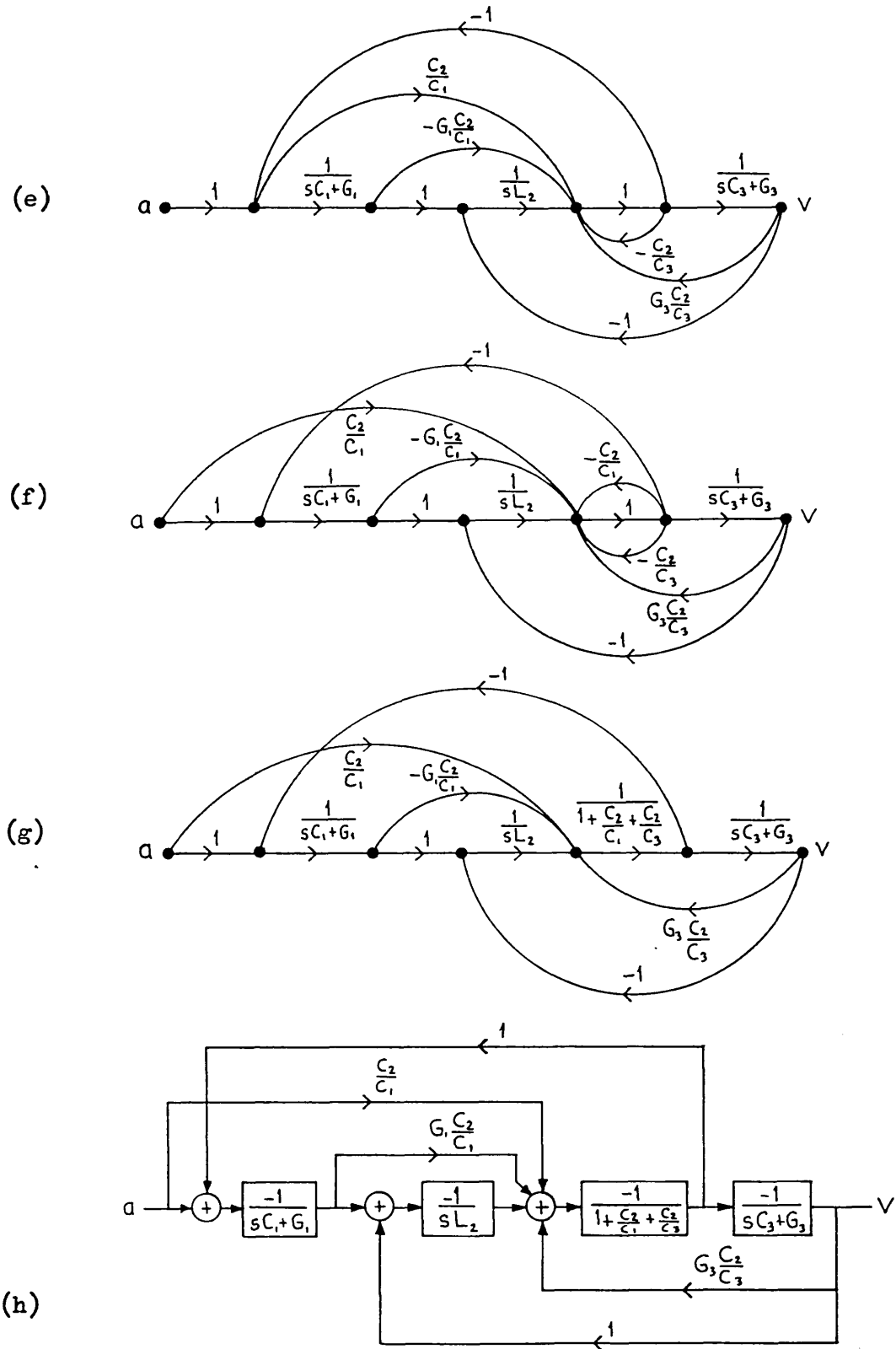


Fig 3.2 continued

- (e) to (g) Successive transformations of the SFG using rudimentary equivalents
- (h) Block diagram equivalent to (g)

In Fig 3.2 the SFG equivalents have been used to obtain a block diagram which may be easily realized by active CR sections. There are other possibilities, for instance SFG equivalents have been applied to the same simulation (Fig 3.2(b)) to obtain a block diagram which is suitable in some circumstances\* for realization by three switched capacitor sections, and the result is shown in Fig 3.3 [52]. A different application of SFG equivalents to the simulation shown in Fig 3.2(b) results in the block diagram given by Doblinger [144], which is suitable for realization by differential-input integrator sections and summing amplifier sections.

---

\* This is suitable when the sampling frequency is much greater than the highest frequency present in the input  $e$ . If this is not the case then the sampled-data nature of switched capacitor filters must be taken into consideration.

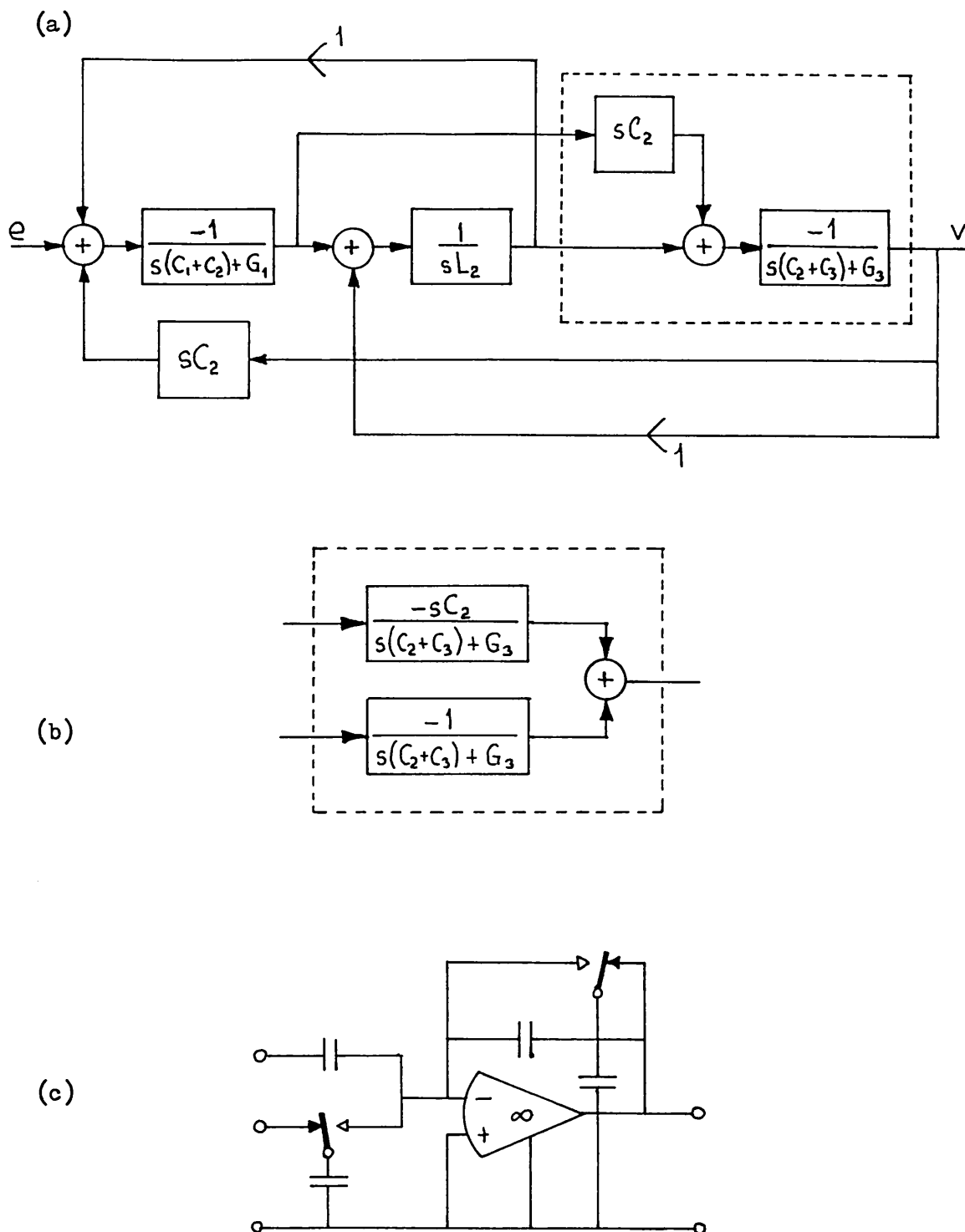


Fig 3.3 Block diagram transformed for switched capacitor realization

- (a) Block diagram
- (b) Block diagram of the third section
- (c) Realization of the third section

### 3.2 Interchange of cascade subnetworks

Certain flexibilities in the cascade structure are often exploited to maximize dynamic range. One can for instance change the order in which the blocks occur. This transformation can sometimes be applied to filters having a more complicated structure, as was first pointed out by the writer in Ref [77].

For example the network in Fig 2.6 has been redrawn in Fig 3.4(a) with dashed lines indicating two subnetworks which are connected in cascade. These two subnetworks may be interchanged without affecting the transfer function; and without affecting the differential sensitivities or the finite difference sensitivities of the transfer function to changes in the block diagram parameters. The result of interchanging the two subnetworks is shown in Fig 3.4(b). In this example the process can be repeated to give other networks, as shown in Fig 3.4(c) and (d). In the case of a multiple feedback filter having  $n$  blocks, one forward path, and  $n$  nested feedback loops, successive interchange of cascaded subnetworks will yield a total of  $2^{n-1}$  different networks, each one having identical block diagram sensitivities.

Although the different networks have the same transfer function, the responses at the internal sections will in general be different. These responses have been computed for the networks shown in Fig 3.4, and are shown in the Figure. They are different for each network.

The two networks in Fig 3.4(a) and (c) have known structures [45,29] and are related to each other by flow graph reversal (which will be described in the next section). Schaumann [78,80] has given examples of eighth degree versions of these two networks, for which he has calculated and also measured the dynamic range. He reports that there is only a small difference between the dynamic ranges of the two networks, despite the fact that one of the networks (FLF structure) has very much greater passband ripple at the internal sections. This disproves by counterexample the intuitive assumption, mentioned in section 2.2.4, that the filter with the lowest variation has the best dynamic range.

Schaumann's results need careful interpretation because the two networks he uses have different realizations of the adders. In the FLF structure the adder is realized by a separate operational summing amplifier section (similar to the one shown in fig 2.5), whereas in the other network the three adders are realized by resistive networks at the input of the associated sections (in the manner illustrated in

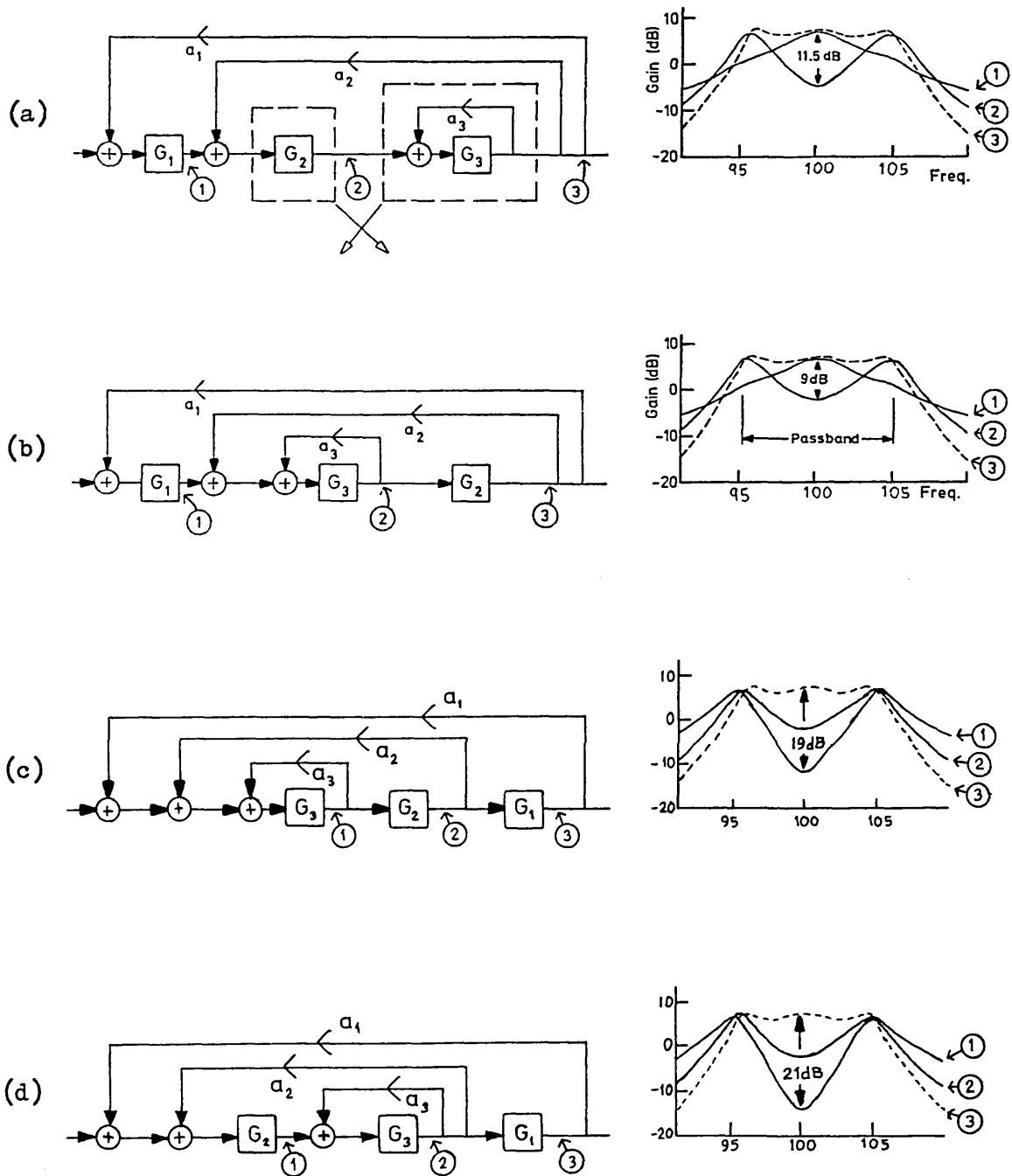


Fig 3.4 Successive interchange of cascade sub-networks

- (a) Block diagram from Fig 2.6
- (b) Intermediate structure -1
- (c) FLF structure
- (d) Intermediate structure -2



Fig 2.1(b)). Only when the filters are designed to have unity gain does the extra amplifier in the FLF filter not substantially affect the dynamic range, and only in that case is there a direct comparison of the two structures which is independent of the realization. When the two filters are designed to have higher than unity gain, Schaumann reports that the FLF filter has better dynamic range. This is entirely due to the extra operational amplifier which is used as an adder and which provides gain in the FLF filter. If a similar amplifier were to be included in the other network then the two filters would again have approximately the same dynamic range.

### 3.3 Flow graph reversal

We now consider the transformation of a multiple feedback filter by reversal of its signal flow graph. To reverse a SFG one simply reverses the direction of all the branches, thus reversing the direction of 'signal flow' through the network. It is known that flow graph reversal (FGR) does not alter the transfer function of the filter [67], and since the branch weights are not changed, it follows that the differential sensitivities and the finite difference sensitivities of the transfer function to changes in the branch weights (or equivalently the block diagram parameters) are not altered either. This was first pointed out by the writer in Ref [84].

As an example consider the block diagram shown in Fig 3.5(a), which is of a 6th-degree elliptic-function bandpass filter, having a 1.25dB passband ripple, 40.5dB stopband attenuation, a passband width equal to 10% of the centre frequency, a transition bandwidth of 1:2.366, and a centre frequency of 100 rad/s. The quadratic sections were chosen to have a Q-factor of 20. The structure has three nested feedback loops, and three parallel forward paths for the realization of transfer function zeros. The equivalent SFG is shown in Fig 3.5(b) together with the frequency responses at the output of each section. Reversal of this graph results in the SFG shown in Fig 3.5(c). In this example the reversed network has smaller variation of passband frequency response at the internal sections. Note also that it does not use a summing amplifier section at the filter output, hence it can be built using fewer components.

If we reverse the SFG of the general multiple feedback filter shown in Fig 2.8, then matrix analysis of its transfer function

$F_{\text{FGR}}(s)$  would give:

$$F_{\text{FGR}}(s) = \underline{b}_t \left( \underline{h}_y(s)^{-1} - \underline{A}_t \right)^{-1} \underline{c} + d \quad (3.3.1)$$

which is simply the transpose of the matrix expression (2.2.5) for the transfer function of the original network. For this reason the flow graph reversed network is most aptly called the transpose network.

We may represent flow graph reversal of the general multiple feedback filter (Fig 2.8) by the mapping:

$$\left\{ \begin{array}{l} \underline{h}_y(s) \longrightarrow \underline{h}_y(s) \\ \underline{A} \longrightarrow \underline{A}_t \\ \underline{b} \longrightarrow \underline{c} \\ \underline{c} \longrightarrow \underline{b} \\ d \longrightarrow d \end{array} \right. \quad (3.3.2)$$

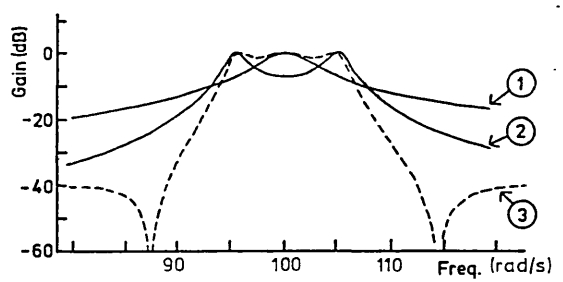
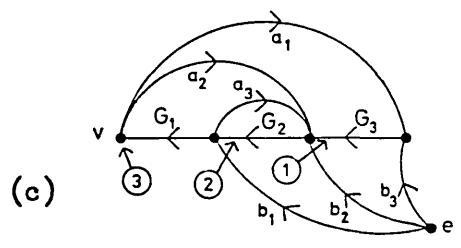
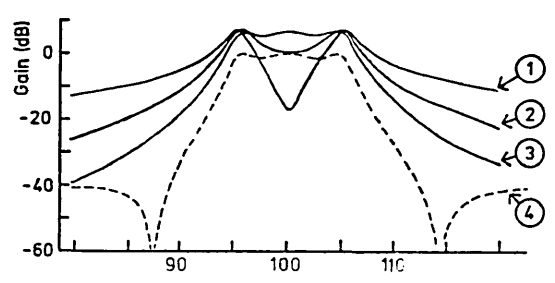
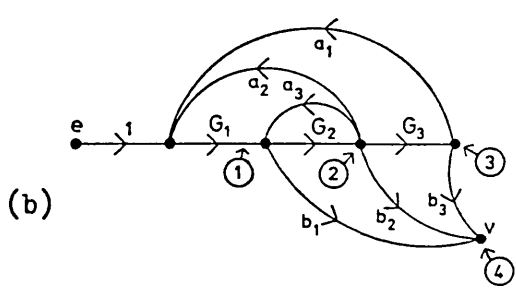
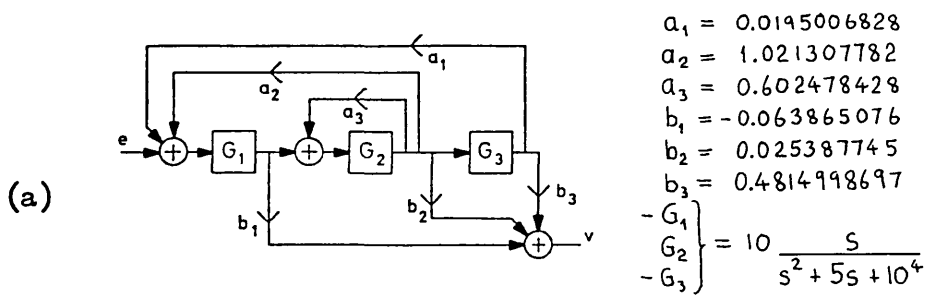


Fig 3.5 Flow graph reversal

- (a) Block diagram
- (b) Equivalent SFG
- (c) Reversed SFG [84]

It is of interest to note that when this mapping is applied to the intermediate transfer functions (2.2.60) we obtain for the reversed network:

$$\frac{x_j}{e} = \underline{u}_{jt} (l_j(s)^{-1} - \mathcal{A}_t)^{-1} \underline{c} \quad j = 1, 2, \dots, n \quad (3.3.3)$$

which may be written as:

$$\frac{x_j}{e} = \underline{c}_t (l_j(s)^{-1} - \mathcal{A})^{-1} \underline{u}_j \quad j = 1, 2, \dots, n \quad (3.3.4)$$

which will be recognized as the noise transfer functions (2.2.64) of the original network. Also if we apply the mapping (3.3.2) to the noise transfer functions (2.2.64), then we obtain for the reversed network:

$$\frac{v}{e_j} = \underline{b}_t (l_j(s)^{-1} - \mathcal{A}_t)^{-1} \underline{u}_j \quad j = 1, 2, \dots, n \quad (3.3.5)$$

$$\frac{v}{e_j} = \underline{u}_{jt} (l_j(s)^{-1} - \mathcal{A})^{-1} \underline{b} \quad j = 1, 2, \dots, n \quad (3.3.6)$$

which will be recognized as the intermediate transfer functions (2.2.60) of the original network. Thus one effect of flow graph reversal is to interchange the intermediate transfer functions and the noise transfer functions.

It is of interest to consider the product of the noise transfer function  $G_{vj}$  and the intermediate transfer function  $G_{je}$  associated with a particular block  $G_j$  :

$$G_{vj} G_{je} = \underline{c}_t (l_j(s)^{-1} - \mathcal{A})^{-1} \underline{u}_j \underline{u}_{jt} (l_j(s)^{-1} - \mathcal{A})^{-1} \underline{b} \quad (3.3.7)$$

The right hand side will be recognized as a factor in the expression for the sensitivity  $\sum_{G_j(s)}^{F(s)}$  given in (2.2.22). From (2.2.22) and (3.3.7) we may write:

$$\frac{\partial F(s)}{\partial G_j(s)} = \frac{G_{vj}}{G_j} \frac{G_{je}}{G_j} \quad (3.3.8)$$

The second factor in (3.3.8) may be identified with the particular transfer function of the SFG in Fig 2.8 from node e to node  $y_j$ . The first factor in (3.3.8) may be identified with a transfer function in the reversed SFG, between the nodes corresponding to nodes v and  $x_j$  in Fig 2.8. Both of these transfer functions may be evaluated by using Mason's rule for SFG's (2.2.8), and in fact equation (3.3.8) illustrates the relationship between the explicit formulation adopted in this chapter, and the so called 'adjoint' method, mentioned at the

end of section 2.2.2, for finding sensitivities by using Mason's rule and FGR. A similar relationship exists between the expression for the finite difference sensitivity  $\Delta_{G_1(s)}^{F(s)}$  in (2.2.21) and the SFG method given in Ref [71]. Equation (3.3.8) and its counterpart for finite differences also provide an alternative proof of the invariance of sensitivity under flow graph reversal.

### 3.4 Scaling of signal levels

We have already mentioned that the signal level at the output of an internal section of a multiple feedback filter may be scaled in order to improve the dynamic range of the filter, without affecting its transfer function. Many authors have used scaling in this simple form, and for some specific structures it has been demonstrated [32,33] that scaling does not affect the differential sensitivity of the transfer function with respect to the block diagram parameters.

Here we present scaling in a novel way by considering it to be an operation on the branches of a cutset of a SFG. It will as a consequence apply to all multiple feedback filters, and furthermore, we will show that not only are differential sensitivities unaffected but that also the finite difference sensitivities are not affected by this scaling transformation.

Consider any cutset of a SFG. The cutset will divide the nodes of the graph into two sets  $N_a$  and  $N_b$ , and without loss of generality we take  $N_a$  to be the set containing the input node  $e$ . The scaling operation consists of multiplying the weight of each branch in the cutset by a factor  $\lambda$  or  $1/\lambda$ . If a branch is directed towards  $N_b$  then its weight is multiplied by  $\lambda$ , and if it is directed away from  $N_b$  its weight is multiplied by  $1/\lambda$ . The result is that the signal level at the nodes in the set  $N_b$  will be scaled by a factor  $\lambda$  relative to the signal level at the input of the filter.

As an example consider again the filter shown in Fig 2.6, and take the cutset  $\{G_1, a_{23}, a_{33}, G_3\}$  as indicated by the dashed line in Fig 3.6. Since the branches  $G_1$ ,  $a_{23}$  and  $a_{33}$  are directed towards the set of nodes  $N_b$  (not containing the input node  $e$ ), their weights are multiplied by  $\lambda$ , and since the branch  $G_3$  is directed away from  $N_b$  its weight is multiplied by  $1/\lambda$ . The result is that the signal levels at the nodes  $x_1$  and  $x_2$  have been scaled by the factor  $\lambda$ .

To show the effect of the scaling transformation on the transfer function in the general case we use Mason's rule (2.2.8), which expresses the transfer function  $F(s)$  as a function of feedback loop gains  $T_j$  and forward path gains  $P_j$  only.

Consider first the feedback loops. There will be an even number (possibly zero) of branches common to both the cutset and any given feedback loop, as illustrated in Fig 3.7(a). Half of these common branches will be directed towards the set of nodes  $N_b$ , and the other half will be directed away from  $N_b$ . Hence the feedback loop

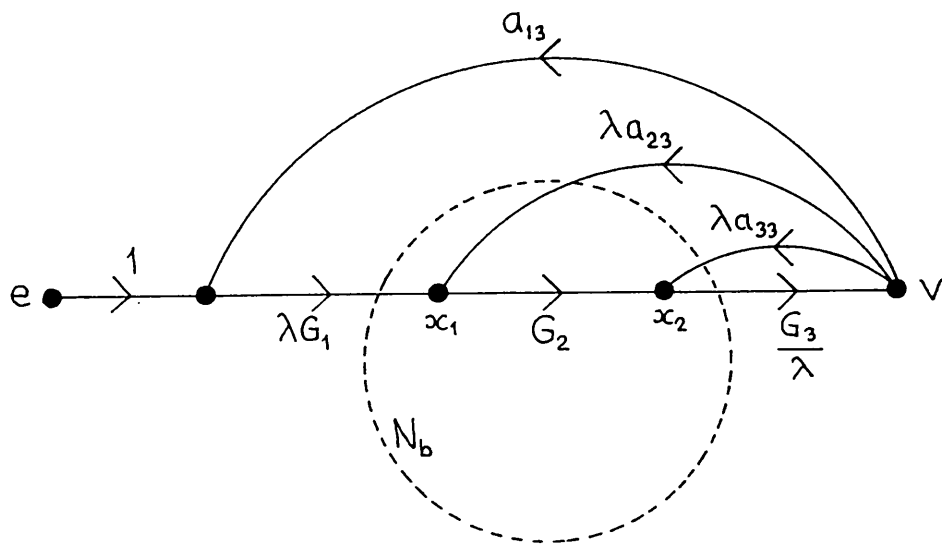


Fig 3.6 Example of the scaling transformation

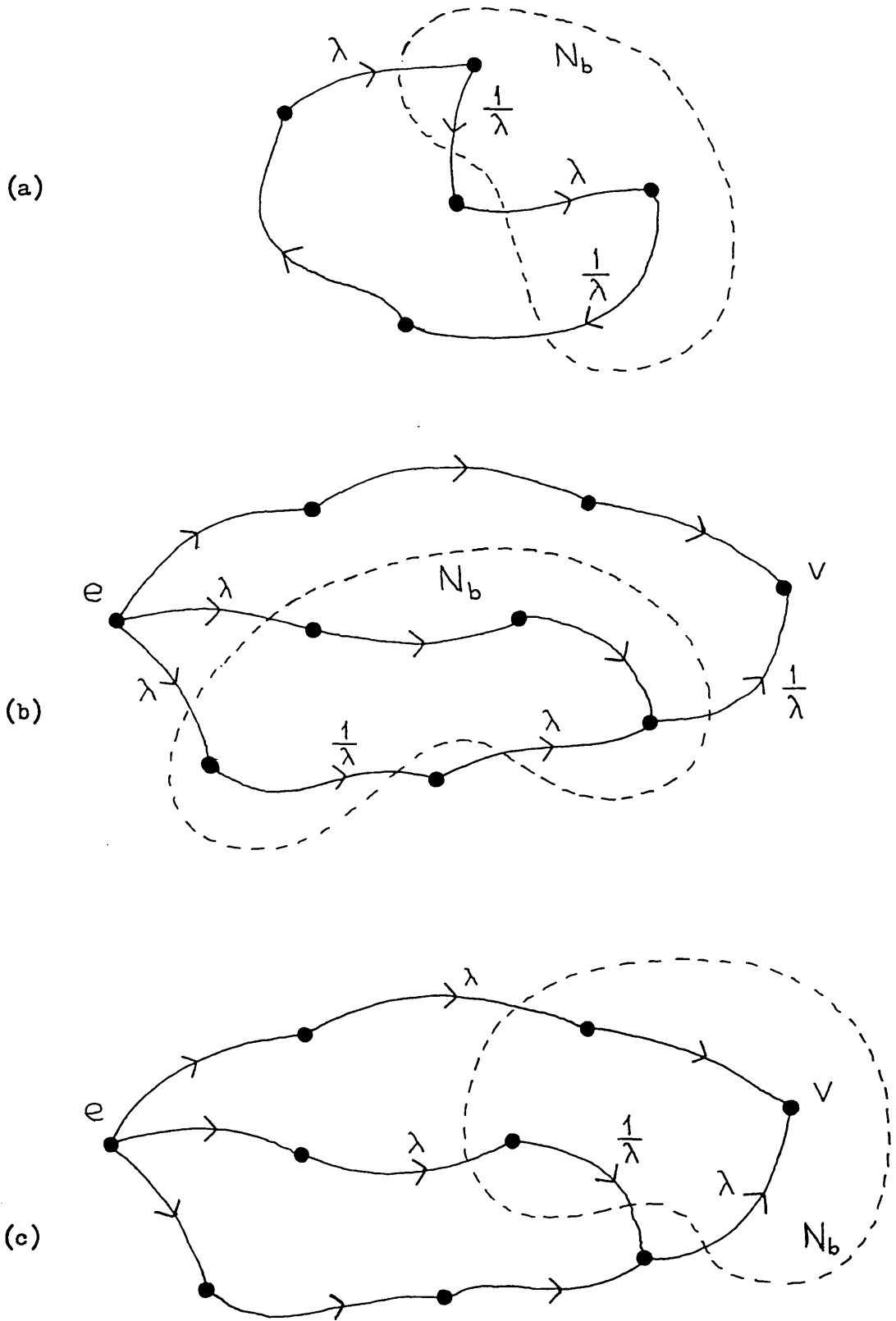


Fig 3.7 Effect of scaling on the transfer function

- (a) Effect on loopgains  $T_j$  - a feedback loop is shown in isolation
- (b) Effect on forward path gains  $P_j$  , case (i) - node  $v$  in set  $N_a$
- (c) Effect on forward path gains  $P_j$  , case (ii) - node  $v$  in set  $N_b$



gain  $T_j$  will be multiplied by the factor  $\lambda$  and multiplied by the factor  $1/\lambda$  an equal number of times. These factors will cancel leaving  $T_j$  unaffected by the scaling transformation.

Now consider the forward paths. There are two cases:

Case (i) where the cutset is such that the output node  $v$  is in the set  $N_a$  (which also contains the input node  $e$ ), as illustrated in Fig 3.7(b). In this case the cutset has an even number (possibly zero) of branches in common with any given forward path, one half of them directed towards  $N_b$  and the other half directed away from  $N_b$ . Hence the forward path gain  $P_j$  will be multiplied by the factor  $\lambda$  and the factor  $1/\lambda$  an equal number of times. These factors will cancel leaving  $P_j$  unaffected by the scaling transformation.

Case (ii) where the cutset is such that the output node  $v$  is in the set  $N_b$ , as illustrated in Fig 3.7(c). In this case the cutset has an odd number of branches in common with any given forward path. This odd number may be thought of as an even number plus one. The factors due to the even part will cancel as before, but the extra common branch will cause each forward path gain  $P_j$  to be multiplied by the factor  $\lambda$ .

From Mason's rule (2.2.8) it follows that scaling does not affect the transfer function  $F(s)$ , unless the cutset separates the input node  $e$  from the output node  $v$  (case (ii) where node  $e$  is in set  $N_a$  and node  $v$  is in set  $N_b$ ), in which case the transfer function  $F(s)$  is multiplied by the factor  $\lambda$ .

The scaling transformation may be applied in turn to any number of different cutsets of a SFG, and it follows that the transformation is also valid for a cut; a cut being either a cutset or a disjoint union of cutsets.

So far we have said nothing about the nature of the factor  $\lambda$ . In general  $\lambda$  may be a function of the complex frequency variable  $s$ , although scaling with  $\lambda = \lambda(s)$  would not normally be used with cutsets (or cuts) for which node  $v \in N_b$  (case (ii)), because the transfer function would then be multiplied by the complex factor  $\lambda(s)$ . In other cases a complex scale factor can be useful. For instance consider the leapfrog feedback network shown in Fig 3.8(a), which may be realized by four bandpass sections and three inverters. Use of the scaling transformation with  $\lambda = 1/s$  will permit the same transfer function to be realized using the same structure, but with two highpass sections and two lowpass sections instead of the four bandpass sections, as shown in Fig 3.8(b). The effect of this particular transformation on sensitivity and dynamic range has not yet been investigated. Note that one would not perform the corresponding transformation on a

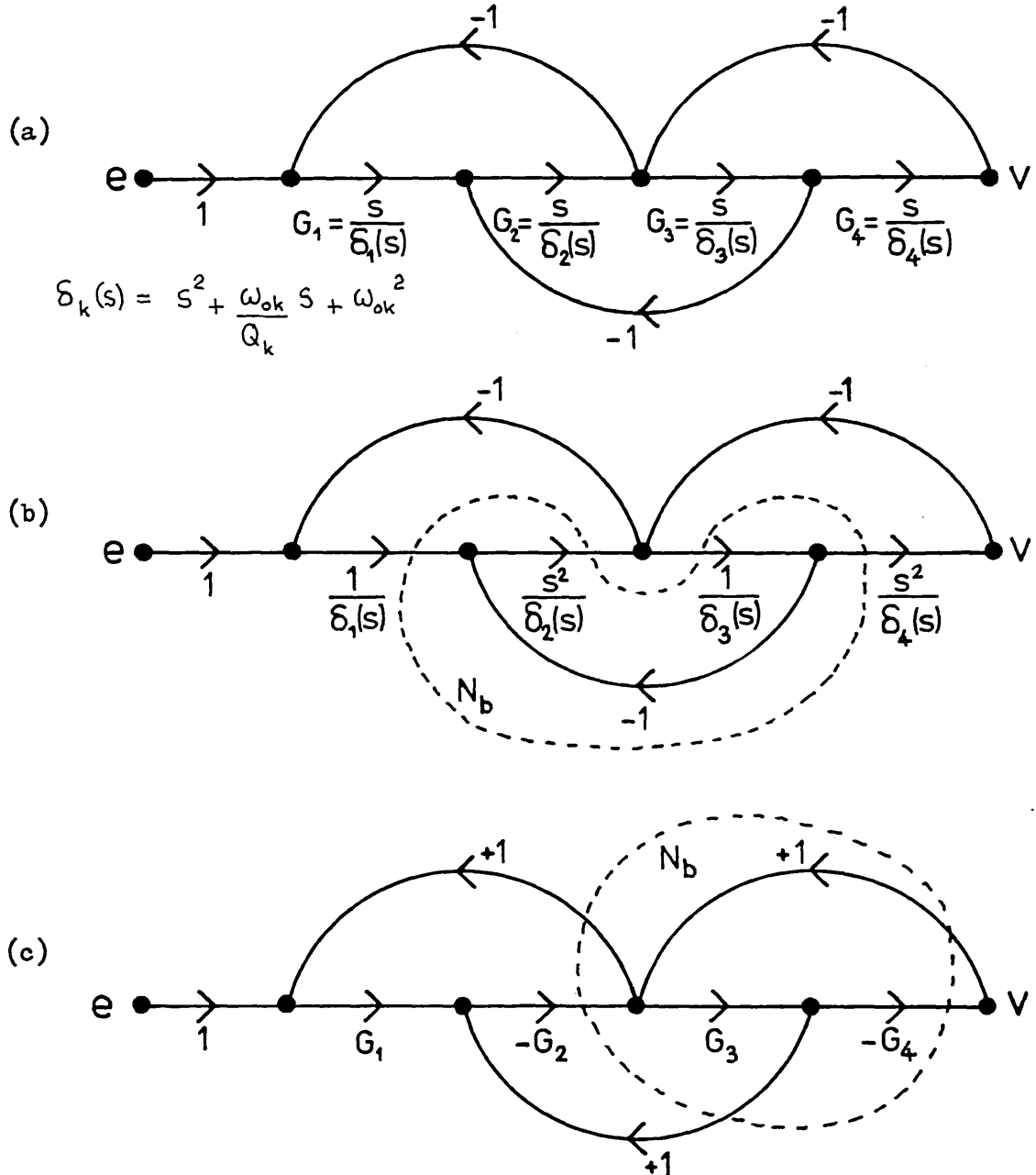


Fig 3.8 Some uses of the scaling transformation

- (a) SFG of a filter using the leapfrog feedback structure
- (b) A transformation of (a) with  $\lambda = 1/s$
- (c) A transformation of (a) with  $\lambda = -1$

leapfrog feedback network having an odd number of sections since the transfer function would in that case be multiplied by  $1/s$ .

For other uses of the scaling transformation the factor  $\lambda$  is restricted to be real and constant. This constant may be negative, and this is often useful for eliminating unnecessary inverting amplifiers. For example a direct realization of the SFG in Fig 3.8(a) would use three inverting amplifier sections corresponding to the three branches with weights equal to  $-1$ . This would be necessary because bandpass sections do not normally accommodate both positive and negative inputs. However, if the scaling transformation is applied with  $\lambda = -1$  to the cut of the SFG shown in Fig 3.8(c), then the resulting SFG may be realized without using any inverting amplifier sections. Note that two of the bandpass sections have become inverting bandpass sections. For most types of section, both inverting and non-inverting versions are known.

Transformations of the type shown in Fig 3.8 are not new, indeed it may be said that they are intuitively obvious. They are mentioned here because they are now seen to be special cases of the more general scaling transformation described in this section. This fact may be useful in that it provides a systematic way of applying the transformations to more complicated networks.

When the scaling transformation is used to alter the gain of a filter, or to maximize its dynamic range, then the factor  $\lambda$  is restricted to be a real positive constant. This is the case which we now consider in respect of sensitivity.

The fact that scaling does not alter the differential sensitivity of the transfer function  $F(s)$  with respect to any branch weight  $w$  follows from a known result of the sensitivity calculus:

$$\int_w^F = \int_{q,w}^{pF} \quad p, q \text{ real, positive, constant} \quad (3.4.1)$$

since the effect of scaling is to multiply  $F(s)$  by a constant  $p$  (which may be  $\lambda$  or  $1$ ), and to multiply  $w$  by a constant  $q$  (which may be  $\lambda$ ,  $1/\lambda$  or  $1$ ). This result can be extended to finite difference sensitivities by using Taylor's theorem as follows. From (1.2.3) we have:

$$\begin{aligned} \mathcal{S}_w^F &\triangleq \frac{w}{F} \frac{\Delta F}{\Delta w} \\ &= \frac{w}{F} \left\{ \frac{dF}{dw} + \frac{1}{2!} \left( \frac{\Delta w}{w} \right) w \frac{d^2 F}{dw^2} + \dots + \frac{1}{n!} \left( \frac{\Delta w}{w} \right)^{n-1} w^{n-1} \frac{d^n F}{dw^n} + R_n \right\} \end{aligned} \quad (3.4.2)$$

and similarly for the scaled network:

$$\begin{aligned} \mathcal{S}_{q_w}^{PF} &\triangleq \frac{q_w}{pF} \frac{\Delta(pF)}{\Delta(q_w)} \\ &= \frac{q_w}{pF} \left\{ \frac{d(pF)}{d(q_w)} + \frac{1}{2!} \left( \frac{\Delta(q_w)}{q_w} \right) q_w \frac{d^2(pF)}{d(q_w)^2} + \dots + \frac{1}{n!} \left( \frac{\Delta(q_w)}{q_w} \right)^{n-1} (q_w)^{n-1} \frac{d^n(pF)}{d(q_w)^n} + R_n' \right\} \end{aligned} \quad (3.4.3)$$

which, since  $\frac{dw}{d(q_w)} = \frac{1}{\frac{d(q_w)}{dw}} = \frac{1}{q}$ , may be written:

$$\mathcal{S}_{q_w}^{PF} = \frac{w}{F} \left\{ \frac{dF}{dw} + \frac{1}{2!} \left( \frac{\Delta(q_w)}{q_w} \right) w \frac{d^2F}{dw^2} + \dots + \frac{1}{n!} \left( \frac{\Delta(q_w)}{q_w} \right)^{n-1} w^{n-1} \frac{d^n F}{dw^n} + \frac{q}{p} R_n' \right\} \quad (3.4.4)$$

If the Taylor series converge\* then from (3.4.2) and (3.4.4) we see that:

$$\mathcal{S}_w^F \left( \frac{\Delta w}{w} \right) = \mathcal{S}_{q_w}^{PF} \left( \frac{\Delta(q_w)}{q_w} \right) \quad (3.4.5)$$

thus the finite difference sensitivity of the transfer function  $F(s)$  to changes in any branch weight  $w$  is in general a function of the fractional change of the branch weight  $\Delta w/w$ , and this function is not altered by scaling.

The summed sensitivity invariant in section 2.2.3, and the scaling transformation in this section have been derived independently. The two results are however related by Euler's relation for homogeneous functions. Every scaling transformation implies a certain homogeneity of the transfer function, and Euler's relation for this homogeneity in turn implies a summed sensitivity invariant. Since Euler's relation is both a necessary and a sufficient condition for homogeneity [87], the converse is true: every summed sensitivity invariant implies a certain homogeneity of the transfer function, which in turn implies a possible scaling transformation.

For example, consider again the scaling transformation illustrated in Fig 3.6. From this transformation we can say that the transfer function  $F(s)$  is homogeneous of degree 0 with respect to the variables  $G_1$ ,  $a_{23}$ ,  $a_{33}$  and  $G_3^{-1}$ , thus:

$$F(s; \lambda G_1, \lambda a_{23}, \lambda a_{33}, \lambda G_3^{-1}) = \lambda^0 F(s; G_1, a_{23}, a_{33}, G_3^{-1}) \quad (3.4.6)$$

from which follows Euler's relation:

---

\* It is possible to derive the result in (3.4.5) by matrix analysis. This alternative proof does not rely on convergence of the Taylor series, but is much longer than that presented here.

$$G_1 F_{G_1} + a_{23} F_{a_{23}} + a_{33} F_{a_{33}} + G_3^{-1} F_{G_3^{-1}} = 0 \quad (3.4.7)$$

whence:

$$S_{G_1}^F + S_{a_{23}}^F + S_{a_{33}}^F + S_{G_3^{-1}}^F = 0 \quad (3.4.8)$$

and since  $S_{G_3^{-1}}^F = -S_{G_3}^F$  we have the summed sensitivity invariant:

$$S_{G_1}^F + S_{a_{23}}^F + S_{a_{33}}^F - S_{G_3}^F = 0 \quad (3.4.9)$$

as was shown in Fig 2.10.

The formulation of the scaling transformation as an operation on a cutset of a SFG so that it applies to all multiple feedback filters, and the demonstration of the invariance of the finite difference sensitivities and differential sensitivities, were first given by the writer in Ref [77].

### 3.5 Similarity transformation

The matrix analysis of multiple feedback filters described in section 2.2.1 provides a means of changing the structure of a filter by the use of a similarity transformation. The similarity transformation  $A \longrightarrow \mathcal{Y}^{-1} A \mathcal{Y}$  will alter the values of the components of  $A$ . In particular it can give a non-zero component where there was previously a zero valued component, thus introducing a new branch into the SFG. Similarly it can give a zero valued component where previously there was a non-zero component, thus suppressing a branch in the SFG. By suppressing and introducing branches, the similarity transformation can be used to alter the structure of the SFG.

If the transfer function  $F(s)$  is to remain unaltered, then the other matrices must be changed in accordance with the following mapping:

$$\left\{ \begin{array}{l} \underline{y}(s) \longrightarrow \mathcal{Y}^{-1} \underline{y}(s) \mathcal{Y} \\ \underline{A} \longrightarrow \mathcal{Y}^{-1} \underline{A} \mathcal{Y} \\ \underline{b} \longrightarrow \mathcal{Y}^{-1} \underline{b} \\ \underline{c} \longrightarrow \mathcal{Y}_t \underline{c} \\ \underline{d} \longrightarrow \underline{d} \end{array} \right. \quad (3.5.1)$$

When this mapping is applied to the transfer function  $F(s)$  in (2.2.5) it gives:

$$\begin{aligned} F(s) &= \underline{c}_t \mathcal{Y} \left( (\mathcal{Y}^{-1} \underline{y}(s) \mathcal{Y})^{-1} - \mathcal{Y}^{-1} \underline{A} \mathcal{Y} \right)^{-1} \mathcal{Y}^{-1} \underline{b} + \underline{d} \\ &= \underline{c}_t \mathcal{Y} \left( \mathcal{Y}^{-1} (\underline{y}(s)^{-1} - \underline{A}) \mathcal{Y} \right)^{-1} \mathcal{Y}^{-1} \underline{b} + \underline{d} \\ &= \underline{c}_t \left( \underline{y}(s)^{-1} - \underline{A} \right)^{-1} \underline{b} + \underline{d} \end{aligned} \quad (3.5.2)$$

which is the same as (2.2.5), hence  $F(s)$  is not altered by the mapping (3.5.1). Thus the mapping may be applied to a known structure, having a given transfer function, in order to derive new structures having the same transfer function. The new structures do not necessarily have the same sensitivity and dynamic range properties as the initial structure, and the mapping (3.5.1) may therefore be used to search for structures with improved performance [49,69,85,86,157]. The algebraic procedure described in Ref [49] is equivalent to using the transformation to change a follow-the-leader feedback structure into a leapfrog feedback structure. In Refs [69,85,86] the final structure is the outcome of a computer optimization procedure.

If the transformed structure is to be a multiple feedback filter as defined in Section 2.1, then the matrix  $\mathcal{Y}^{-1} \mathcal{L}_y(s) \mathcal{Y}$  must be a diagonal matrix, just as the matrix  $\mathcal{L}_y(s)$  must be diagonal. This may be achieved in one of two ways. Either  $\mathcal{L}_y(s)$  is a scalar multiple of the unit matrix,  $\mathcal{L}_y(s) = G(s) \mathcal{U}$ , in which case  $\mathcal{L}_y(s)$  is unchanged by the mapping, irrespective of  $\mathcal{Y}$ , since

$$\mathcal{Y}^{-1} \mathcal{L}_y(s) \mathcal{Y} = G(s) \mathcal{Y}^{-1} \mathcal{U} \mathcal{Y} = G(s) \mathcal{U} \quad (3.5.3)$$

or, if  $\mathcal{L}_y(s)$  is not a scalar multiple of the unit matrix, the transformation matrix  $\mathcal{Y}$  must be chosen such that  $\mathcal{Y}^{-1} \mathcal{L}_y(s) \mathcal{Y}$  is constrained to be diagonal.

In the first case all the blocks  $G_j(s)$  in the block diagram are identical to each other. This case was used in Refs. [49,69,86], and it is related to the method in linear system theory of finding all 'equivalent realizations'. In the second case the blocks  $G_j(s)$  are not necessarily identical. The only use of this case has been in Ref [85], but unfortunately the authors of that paper overlooked the fact that their similarity transformation did not constrain the matrix  $\mathcal{Y}^{-1} \mathcal{L}_y(s) \mathcal{Y}$  to be diagonal. Their method is consequently of little practical value since an extra block must be used for each non-diagonal term introduced by the transformation.

This difficulty does not arise in the method proposed by Mackay & Sedra [86]. In their method, all blocks are identical to each other and are taken to be simple integrators  $G_j(s) = 1/s$ . Constraints are introduced in the optimization procedure to ensure that successive pairs of integrators become connected as two-integrator loops, thus forming quadratic sections. These two-integrator loop quadratic sections need not all be the same.

It is of interest to note that for the case where all blocks are identical to each other, Biswas & Kuh [69] have shown that the sensitivity sum:

$$\sum_{j=1}^n \int_{G_j(s)}^{F(s)} = \frac{1}{F(s)} \frac{1}{G(s)} \zeta_t (\mathcal{L}_y(s)^{-1} - \mathcal{A})^{-2} \underline{b} \quad (3.5.4)$$

is invariant under the similarity transformation. Application of the transformation (3.5.1) to the following expression obtained from (2.2.22)

$$\sum_{j=1}^n \int_{G_j(s)}^{F(s)} = \frac{1}{F(s)} \zeta_t (\mathcal{L}_y(s)^{-1} - \mathcal{A})^{-1} \mathcal{L}_y(s)^{-1} (\mathcal{L}_y(s)^{-1} - \mathcal{A})^{-1} \underline{b} \quad (3.5.5)$$

shows that the sensitivity sum is also invariant for the case where the blocks  $G_j(s)$  are not identical to each other.

### 3.6 Summary

Several ways of transforming a multiple feedback filter have been described. Mason's equivalent signal flow graphs may be used to manipulate the SFG of the filter, and as an example they have been used here to derive a structure which will be studied in Chapter 5. Cascade subnetworks may be interchanged without affecting the transfer function or the sensitivities, as was first pointed out by the writer in Ref [77]. A multiple feedback filter may be transformed by reversing its SFG, again without affecting the sensitivities, as was first pointed out by the writer in Ref [84]. We have shown that one effect of FGR is to interchange the noise transfer functions and the intermediate transfer functions.

We have shown that the signal levels of a multiple feedback filter may be scaled, systematically and with complete generality, by performing the described transformation on the branches of a cut of the SFG. A complex scale factor can sometimes be used to change the types of section used; a negative scale factor can be used to eliminate unnecessary inverting amplifiers, and a real positive constant scale factor is used to alter the gain of the filter and to maximize its dynamic range. We have shown that neither the differential sensitivities nor the finite difference sensitivities are altered by this transformation. These new results were first described by the writer in Ref [77]. The use of the scaling transformation together with Euler's relation for homogeneous functions provides an alternative proof of the summed sensitivity invariant given in Chapter 2. The presentation of both proofs in this thesis is justified in the writer's view because (apart from the fact that he discovered both proofs) the more ways we have available for studying networks, the richer our understanding of the subject becomes, and greater is the stimulus to further investigation.

For completeness, this chapter included a comment on the use of the matrix similarity transformation to alter the structure of a multiple feedback filter.



---

## CLASSIFICATION OF MULTIPLE FEEDBACK STRUCTURES

---

The human propensity to classify can sometimes be of great help in understanding the complexities of nature, provided always that care is taken to avoid stereotyping and the consequent prejudice. Many different multiple feedback filters have been proposed, and in this chapter we will classify those filters which use biquadratic sections. The classification is in terms of structure and it uses concepts introduced in Chapter 1. It is presented in the form of a Table, which shows relationships between existing networks, and which also reveals some new structures. Two methods of determining the block diagram parameters for these new structures will be described. In addition to revealing new structures this classification is related to the sensitivity properties of the various networks, and it provides a framework for the study of sensitivity undertaken in Chapter 5.

### 4.1 The basis of the classification

We have already seen that the ability to construct transfer functions is fundamental to the study of multiple feedback filters, in that it not only allows us to investigate the frequency response of the filter but also enables us to determine sensitivities using the concept of flow graph reversal (3.3.8), and to compute dynamic range using the noise transfer functions (2.2.64) together with the intermediate transfer functions (2.2.60). Mason's rule (2.2.8) for determining a transfer function of a SFG is expressed in terms of forward path gains and feedback loop gains only. It follows that forward paths and feedback loops are the essential elements of structure.

Obviously at least one forward path is necessary to provide signal transmission through the filter, and in Chapter 1 we saw that

a multiplicity of forward paths may be used to produce transmission zeros at finite non-zero frequencies. We also saw that feedback loops may be used to reduce sensitivity, or they may be used to produce transmission zeros by complex feedback.

The classification presented here is based on the arrangement of forward paths and feedback loops, in a way which relates to the sensitivity properties of the various structures. Firstly we consider the patterns of feedback loops which are introduced specifically for the purpose of reducing sensitivity at passband frequencies, e.g. leapfrog feedback, follow the leader feedback etc., and secondly we consider the method used to produce transmission zeros (which will have a dominant effect on sensitivity at stopband frequencies), e.g. series notch sections, parallel forward paths or complex feedback.

The two dimensional classification is presented in Table 4.1, with the types of feedback listed horizontally and the methods of producing transmission zeros listed vertically. Numerical entries in the table are references to the published design methods which utilize the structure indicated by the particular row and column in which the entry occurs. Alphabetical entries occur where the writer's classification has led to the design of new structures.

The majority of published multiple feedback filters are composed of an interconnection of biquadratic sections, and the Table is restricted to such networks. Other filters such as those comprising an interconnection of integrators are not included\*. Most of the entries in the Table refer to bandpass filters, and where other types occur they are indicated as follows: lowpass (LP), bandstop (BS), equalizers (EQ), variable equalizers (VE), multiple notch (MN). A design procedure which has been shown to be applicable to several different types of frequency response (e.g. lowpass, highpass and bandpass) is indicated as (G). Multiple feedback has of course many other uses, for example in the linearization and stabilization of amplifiers [128], in automatic control systems [129], multi-loop feedback oscillators [130], and quadrature phase shift networks [131]. In this thesis however we restrict our attention to multiple feedback filters.

The implementation of multiple feedback filters may take one of several different forms, in that the blocks may be realized not only by active CR sections, but also by active switched C sections [52,156],

---

\* Except inasmuch as a two-integrator loop can be considered to be a quadratic section.

active R sections [105], active C sections [127], active piezoelectric sections [108], voltage or current tunable sections [114,144], or digitally controlled sections [135]. Although we have in this thesis considered mainly active CR sections when discussing specific realizations of block diagrams, we could equally have considered any of the different types of section just mentioned. All that is required of a section for it to realize a block is that it must be unilateral and that its port voltages must be related by the characterising equation of the block, without being affected by the interconnection of blocks. This was described fully in Chapter 2, but is repeated here to indicate the scope of the design methods listed in the Table.

TABLE 4.1 Classification of multiple feedback filters using quadratic sections

		Type of feedback used to reduce passband sensitivity						
		None	Leapfrog	Nested			All paths	Other
				Follow the leader	Intermediate	Transpose follow the leader		
Polynomial filters		89 Sallen, Key 101 Haigh	17 Girling, Good 18 Girling, Good 19 Adams 96 Bruton 97 Bruton, Salama 98 Laker, Ghausi, Kelly 99 Laker, Ghausi, Kelly 100 Constantinides + 52 Jacobs, Allstot ++	27 Hurtig III 29 Laker, Ghausi 105 Laker, Schaumann + 106 Schaumann, Brand + 114 Hurtig III 154 Johnson, Hilburn + 159 Schubert	77 Perry	84 Perry 113 Spudil	115(G) Gorski-Popiel 116 Laker, Ghausi 70 Styblińska 86 Mackay, Sedra 136 Laker, Ghausi	132 Deliyannis + 133 Deliyannis + 146 Fliege 161 Fotopoulos + 162 Mijat, Moschytz
Method of producing finite transmission zeros	Series notch sections	90 Kerwin, Huelsman	33 Szentirmai 102 Szentirmai 103 Tuttle 34 Dubois, Neiryneck 104 Dubois, Neiryneck 35 Müller 63 Yoshihiro ++	36 Biernacki, Mulawka 37 Dubois, Neiryneck 38 Tow 39 Tow 40 Gensel 41 Gensel 42 Padukone, Mulawka +	B	37 Dubois, Neiryneck	117 Cönüleren	38 Tow 39 Tow 120 Biey, Premoli 147(G) Gonuleren 148(G) Krüger 149(LP) Biey
	Parallel forward paths							
	Feedforward to output	91 Pearl 92 Calahan 121(MN) Plotkin	49 Tow, Kuo	48 Laker, Ghausi 107 Laker, Ghausi 28 Tow 40 Gensel 41 Gensel 108 Hrubý, Novotný	D	A		
	Feedforward from input		49 Tow, Kuo 51 Krüger	47 Tow 28 Tow	C	45 Perry 109(G) Biernacki + 110(G) Biernacki + 111(G) Biernacki + 112(G) Biernacki + 145(G) El-Masry		
	Other	93 Russell, Chan 94 Moran 122(EQ) Lüder 118 Hills 119 Gadenz	84 Perry 53 Müller 144 Doblinger				86 Mackay, Sedra	124(BS) Gadenz 125(BS) Gadenz 160 Takagi, Fujii
	Complex feedback	84 Perry	57 Brackett, Sedra 58 Brackett, Sedra 59 Martin, Sedra 60(BS) Adams					
Mixed	95 Urbas 123(VE) Takasaki +++ 126(VE) Takasaki +++							

## 4.2 Multiple feedback loops for reducing passband sensitivity

We now consider the first aspect of the classification, namely the pattern of the feedback loops which are used to reduce sensitivity at passband frequencies. These are listed horizontally in Table 4.1.

The first column is composed of networks which do not have any feedback loops for the purpose of reducing passband sensitivity. These include certain 'canonic' structures which will be described in Section 4.3.

The subsequent five columns contain the common arrangements of feedback loops, most of which have already been encountered in earlier chapters. They are illustrated diagrammatically in Fig 4.1 for the case of filters having three sections. The leapfrog feedback structure in Fig 4.1(a) was described in Chapter 1, and a design using the method of simulation was shown in Fig 1.5. The follow the leader feedback structure in Fig 4.1(b) was shown previously in Fig 1.7, and the transpose or flow graph reversed follow the leader feedback structure in Fig 4.1(d) (proposed by the writer in Ref [84]) has been used as an example in several places throughout earlier chapters. Figure 4.1(c) shows one of the structures which are intermediate between follow the leader feedback and transpose follow the leader feedback, these intermediate structures being obtained by interchange of cascade subnetworks as described by the writer in [77]. They were illustrated earlier in Fig 3.4.

The column headed "All Paths" in Table 4.1 contains structures which have all possible constant multiplier feedback paths around the blocks in some given forward path. In the absence of complex feedback, this arrangement may be defined more precisely in terms of the components of the matrix  $\mathcal{A}$  (2.2.1). If the blocks are numbered in the sequence in which they occur in the given forward path, then the lower diagonal of  $\mathcal{A}$  will contain components corresponding to the forward path, and all components in the upper triangle of  $\mathcal{A}$  corresponding to the feedback paths, will be non-zero, as in (4.2.1). Any non-zero components in the lower triangle (apart from the lower diagonal) would correspond to extra forward paths. If any of these are present then there may be more than one forward path which passes through all the blocks, depending on the components of the column matrices  $\underline{b}$  and  $\underline{c}$ . The Crab's Eye filter [118] is an example of a structure which has all feedback paths and also extra forward paths. It was originally conceived as a channel bank filter but in Chapter 5 we will consider the use of the Crab's Eye structure as a single

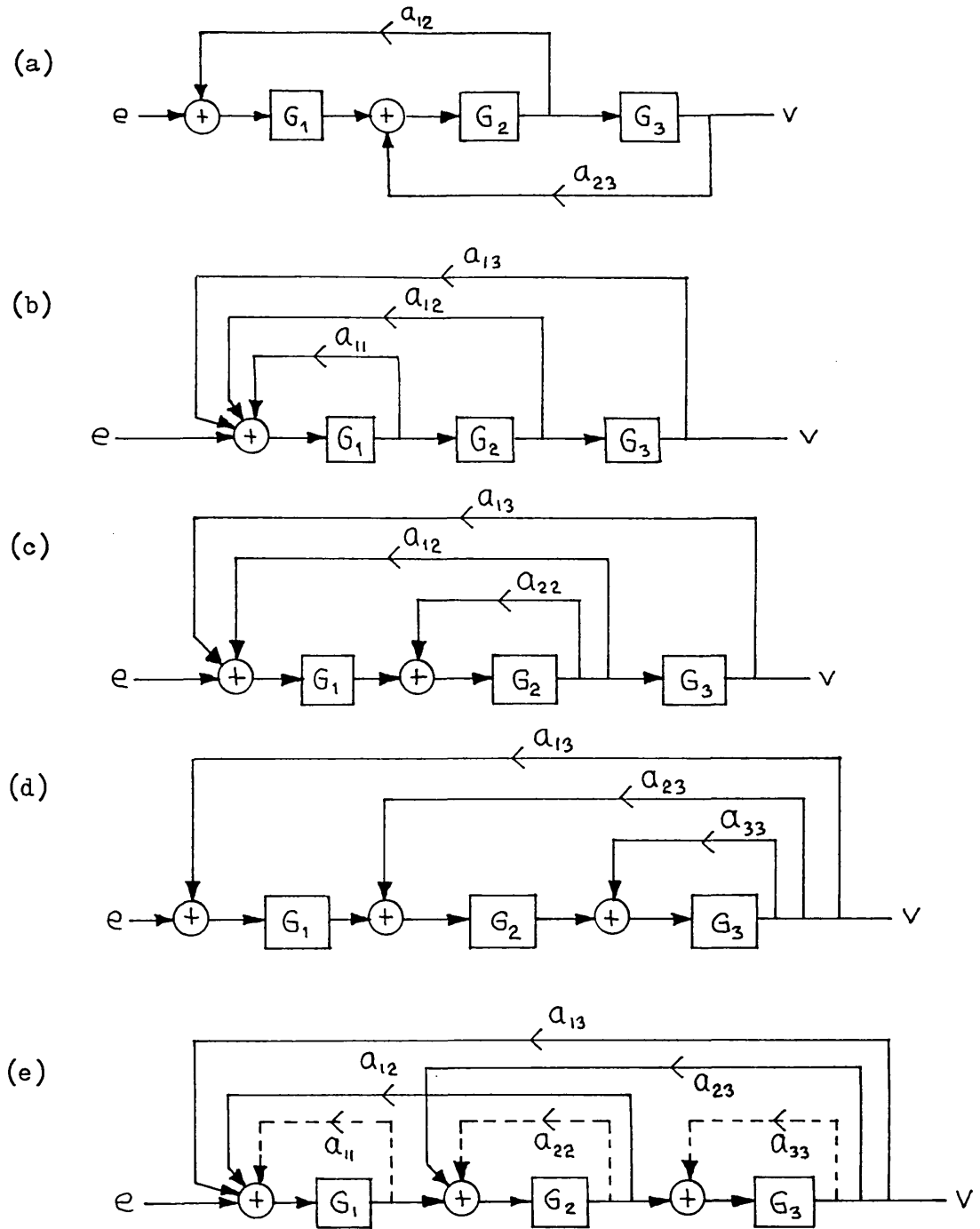


Fig 4.1 Common arrangements of feedback loops for reducing passband sensitivity

- (a) leapfrog feedback [17]
- (b) follow the leader feedback [27]
- (c) example of an intermediate structure [77]
- (d) transpose or FGR follow the leader feedback [84]
- (e) all feedback paths [115]

output multiple feedback filter. We will show that despite the fact that it has all feedback paths, these do not lead to a low sensitivity in the passband. For that reason, the Crab's Eye filter appears in the first column of Table 4.1. It is mentioned here because it is the only example of a published structure which uses all feedback paths in conjunction with parallel forward paths. When the multiple feedback Crab's Eye filter uses more than two blocks, then there exists more than one forward path which passes through all the blocks. A constant multiplier path may appear to be a feedback path with one sequence of block numbering, but may become part of the main forward path with another sequence of numbering.

As indicated in the following matrix, the common feedback structures illustrated in Fig 4.1 are special cases of the structure having all feedback paths.

$$\mathcal{A} = \begin{matrix} & \begin{matrix} a_{11} & a_{12} & a_{13} & a_{14} & a_{15} \end{matrix} \\ \begin{matrix} 1 \\ 0 \\ 0 \\ 0 \end{matrix} & \begin{matrix} a_{22} & a_{23} & a_{24} & a_{25} \\ 1 & a_{33} & a_{34} & a_{35} \\ 0 & 0 & 1 & a_{44} & a_{45} \\ 0 & 0 & 0 & 1 & a_{55} \end{matrix} \end{matrix} \tag{4.2.1}$$

Follow the leader feedback

Leapfrog feedback

Transpose follow the leader feedback

Components on the main diagonal of  $\mathcal{A}$  correspond to feedback paths around single blocks. These are usually, but not necessarily, included in the structure having all feedback paths (Fig 4.1(e)). It is commonly stated that such paths effectively change the Q-factor of the blocks around which they occur, but not the resonance frequency  $\omega_0$ . This is true if the block has a 2nd-degree bandpass, symmetrical notch, or allpass transfer function. It is not true for 2nd-degree lowpass, highpass, or unsymmetrical notch functions, as may be seen by using the equivalent transfer function given in Fig 1.10.

The last column in Table 4.1 is for structures which do not fit

into any of the previous categories. They may use some combination of the previous structures or they may use some other subset of the feedback paths occurring in the general case (4.2.1). In this class there is increasing interest in structures which are essentially like the cascade structure, but which have feedback around pairs of blocks implementing those poles of the transfer function which have the highest Q-factor [38,39,120,133,147,149,161].



### 4.3 Method of producing transmission zeros

We now consider the second aspect of the classification, namely the method of producing transmission zeros. These are listed vertically in Table 4.1.

The multiple feedback structures described in the previous section, and illustrated in Fig 4.1, are suitable for the realization of polynomial filters, that is filters having transmission zeros all either at the origin of the  $s$ -plane or at infinity. This is achieved by using lowpass, highpass or bandpass polynomial sections as appropriate. Design methods for such filters are indicated in the first row of Table 4.1.

For the realization of transmission zeros at finite non-zero frequencies, as used in Cauer filters, there are three possible methods, as described in Chapter 1. The three methods have been referred to as series notch sections, parallel forward paths, and complex feedback. These are listed vertically in Table 4.1. The bottom row in Table 4.1 is for structures which use some combination of the three basic methods.

The three methods of producing finite transmission zeros are illustrated most clearly by three structures which may be called canonic by virtue of the fact that their design methods are adumbrative of the canonic expansions of LC 1-port immittances. They are shown in Fig 4.2. The factored or cascade structure [90] shown in Fig 4.2(a) is designed by expressing the required transfer function as a product of biquadratic factors, and identifying each factor with one of the blocks in the block diagram. Transmission zeros are realized in the cascade structure by the use of series notch sections. The partial fraction structure [93] shown in Fig 4.2(b) is designed by expressing the required transfer function as a sum of quadratic partial fractions, and identifying each partial fraction with one of the blocks in the block diagram. Transmission zeros are realized in the partial fraction structure by means of parallel forward paths. The continued fraction structure [84] shown in Fig 4.2(c) is designed by expressing a lowpass prototype transfer function as a continued fraction, then identifying each partial remainder with one of the blocks in the block diagram, and finally applying a lowpass to bandpass transformation to the block diagram. Transmission zeros are realized in the continued fraction structure by means of complex feedback, as was fully described in section 1.4. These three 'canonical' structures do not use feedback loops for the purpose of

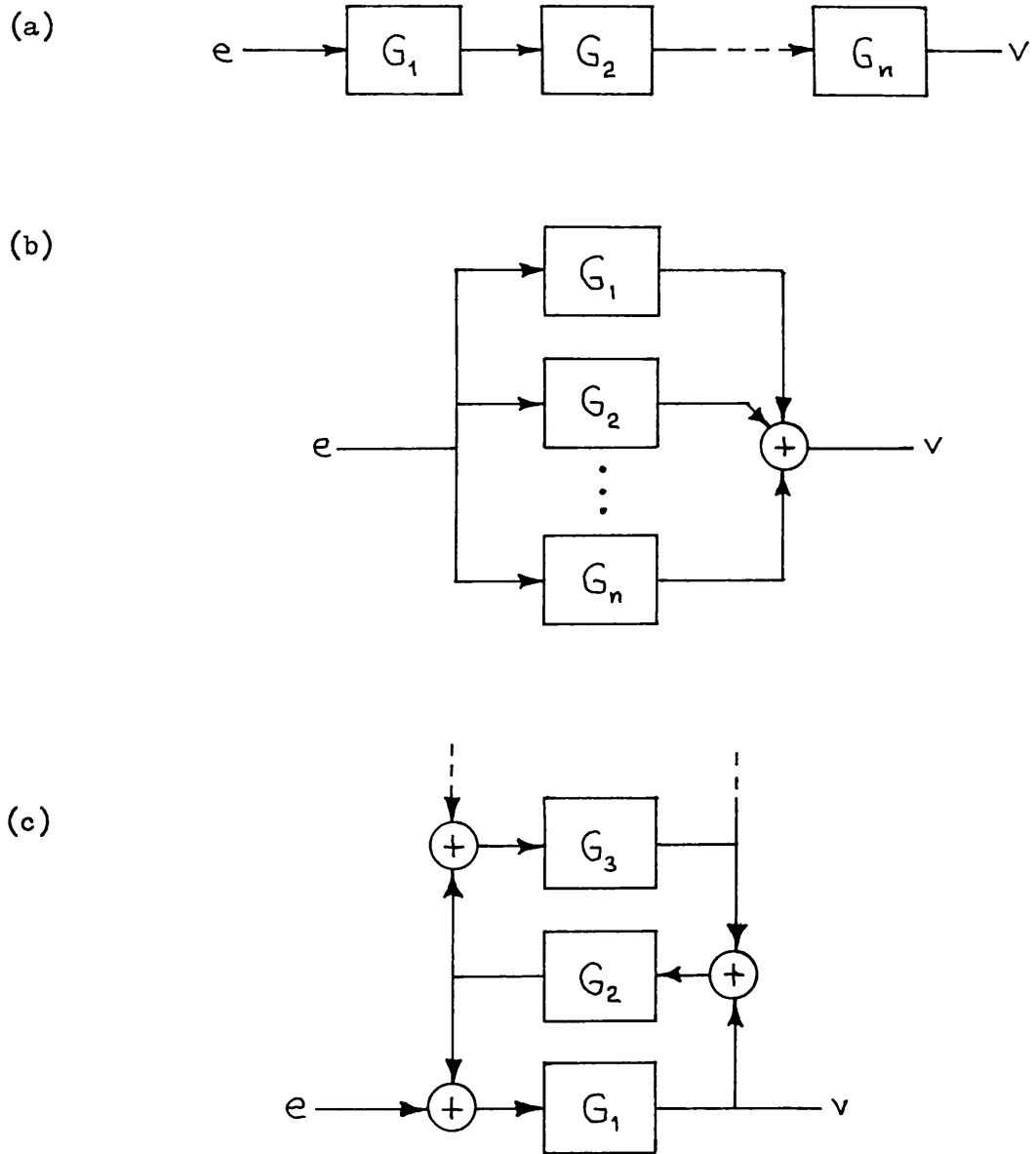


Fig 4.2 The three 'canonical' expansions of a transfer function

- (a) Cascade or factored structure [90]
- (b) Partial fraction structure [93]
- (c) Continued fraction structure [84]

reducing passband sensitivity, and therefore they occur in the first column of Table 4.1.

The three methods of producing finite transmission zeros may also be used in structures which have feedback loops for the reduction of passband sensitivity. Consider for example the leapfrog feedback structures which occur in the second column of Table 4.1, and which are illustrated for the case of 6-th degree filters in Fig 4.3. Series notch sections may be used in the basic leapfrog feedback structure shown in Fig 4.3(a), as described in Chapter 1. This was first proposed by Szentirmai [33]. Parallel forward paths may be introduced in several ways, and Figures 4.3(b) and (c) show the structures proposed by Tow & Kuo [49], referred to respectively as feedforward to the output and feedforward from the input. There are other methods of applying parallel forward paths to the leapfrog feedback structure, and one example is shown in Fig 4.3(d). This has the structure of Ford's lowpass network which was discussed in Section 3.1, and for which the blocks represent integrators. In Ref [84] the writer proposed using the lowpass to bandpass transformation to obtain a bandpass filter for which the blocks  $G_1$ ,  $G_2$  and  $G_4$  represent bandpass quadratic sections. The constant multiplier  $G_3$  together with its associated adder represents a summing amplifier section (see Fig 2.5) which is also required for this structure. Leapfrog feedback may also be used in conjunction with complex feedback as illustrated in Fig 4.3(e). This is one of several structures which may be constructed by SFG simulation of an LCR filter<sup>\*</sup>, using the procedure given by Brackett & Sedra [57]<sup>†</sup>. In this simulation the two leapfrog feedback loops  $\{G_1, G_2, a_{12}\}$  and  $\{G_2, G_3, a_{23}\}$  reduce the sensitivity at passband frequencies, and the two complex feedback loops  $\{G_4, G_5\}$  and  $\{G_2, G_4\}$  realize the finite transmission zeros by complex feedback.

Although the structures shown in Fig 4.3 are for 6-th degree filters, the design methods quoted are applicable to filters of any complexity. The corresponding extension of the structures shown in Fig 4.3 is fairly obvious, except perhaps for Ford's structure in

---

\* The LCR filter used was that shown in Fig 3.2(a), transformed by the usual lowpass to bandpass transformation.

† It will be noted that most of the structures shown in Fig 4.3 use three quadratic sections and possibly one summing amplifier section, whereas the SFG simulation in Fig 4.3(e) uses four quadratic sections and a reciprocator  $G_2$ . This excessive use of sections is characteristic of the simulation method described in Ref [57].

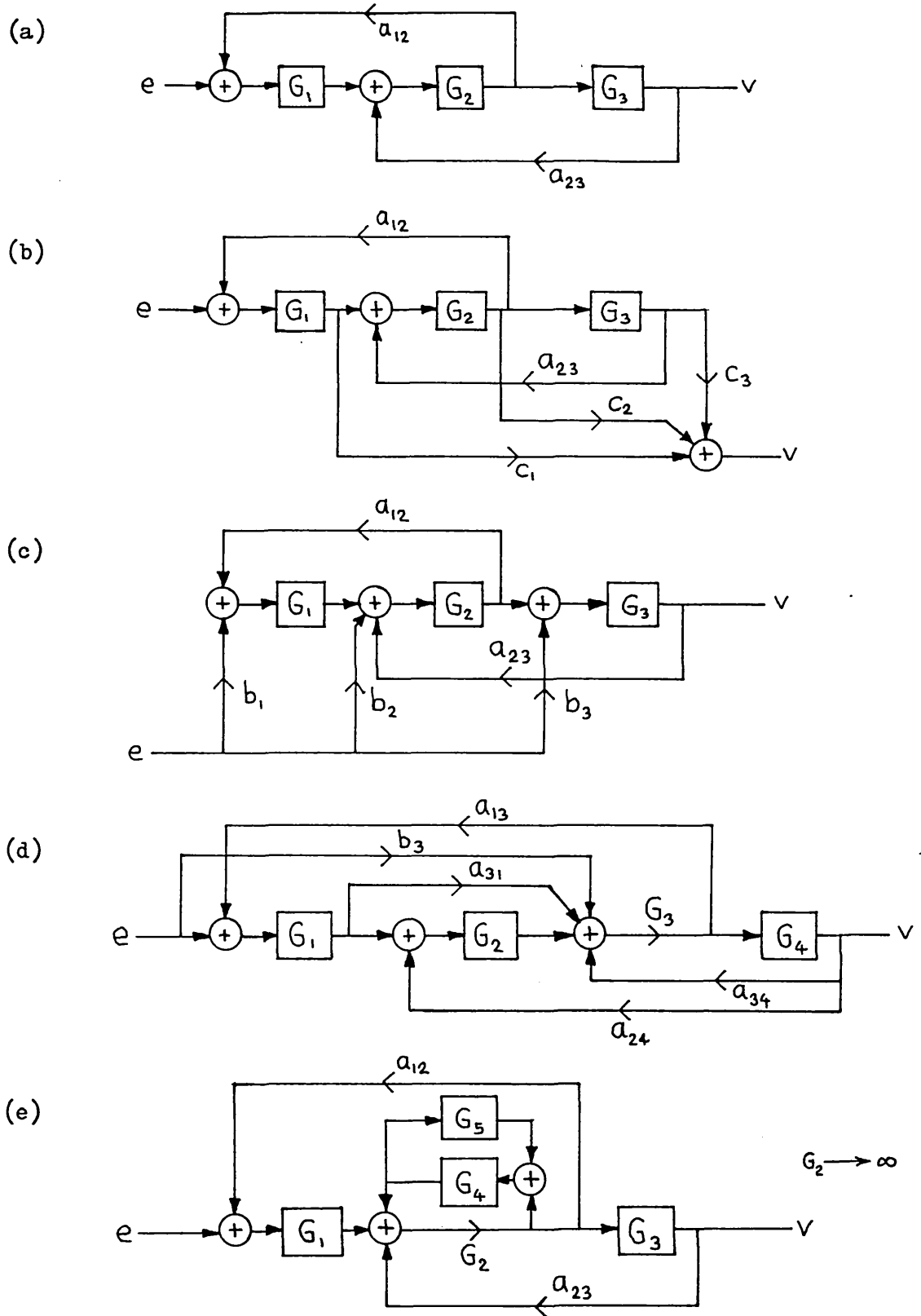


Fig 4.3 Realizing transmission zeros with structures using leapfrog feedback

- (a) Series notch section [33]
- (b) Parallel forward paths: Feedforward to the output [49]
- (c) Parallel forward paths: Feedforward from the input [49]
- (d) Parallel forward paths: Ford's structure [84]
- (e) Complex feedback [57]

Fig 4.3(d). In the Ford simulation the paths  $a_{31}$  and  $a_{34}$  occur as a consequence of the terminating resistances in the LC ladder filter being simulated. In general, the central zero-producing branches of the LC ladder give rise to feedforward paths around pairs of blocks (such as  $b_3$  in Fig 4.3(d)), and to feedback paths which encompass a pair of quadratic blocks and two summing amplifier sections. Müller [53] has extended Ford's original idea to a general and systematic passive ladder simulation method.

We have considered in some detail the first two columns of Table 4.1. Other columns show where the three methods of realizing finite transmission zeros have been applied to the remaining feedback structures. Two examples have been encountered in previous Chapters. In Section 1.4 a design procedure was given for a structure which combines transpose follow the leader feedback with parallel forward paths which are fed forward from the input. This is the entry [45] in Table 4.1. In Section 3.3 an example was given of a structure which combines intermediate nested feedback with parallel forward paths fed forward to the output. This corresponds to the entry D in Table 4.1. The use of series notch sections together with follow the leader feedback was briefly mentioned in Section 1.4.

#### 4.4 New structures indicated by the classification

When references to all existing design methods are entered in the Table, then blank spaces indicate new structures, which may be used to realize filters provided that some design method can be found. We will now describe simple design methods for structures A,B,C & D.

Consider the possibility of reducing passband sensitivity by the use of transpose follow the leader feedback, and simultaneously realizing transmission zeros by feedforward to the output. This is the structure indicated by the letter 'A' in Table 4.1. We have stated in section 3.2 that, for polynomial filters, the follow the leader feedback structure [27] is related to the transpose follow the leader feedback structure [84] by flow graph reversal. The process of FGR also relates the structure 'A' to the follow the leader feedback structure with feedforward from the input [47], as can be seen in Fig 4.4. Hence any design procedure for the latter structure is immediately applicable to the new structure 'A'.

We have shown in Section 3.2 how interchange of cascade subnetworks leads to the intermediate forms of nested feedback. The example given in Section 3.2 was a polynomial filter, but the transformation also applies to filters with series notch sections. Interchange of cascade subnetworks thus allows us to design filters having the intermediate structures 'B' by a trivial extension of the techniques described in references [36] to [42].

Several structures in Table 4.1 are similar to arrangements used to simulate transfer functions on analogue computers. This fact is useful for realizing those bandpass transfer functions which are obtained from lowpass prototype transfer functions by the lowpass to bandpass transformation  $s \longrightarrow q(s + 1/s)$ . It is usually a simple matter to realize a lowpass prototype transfer function as an analogue computer network comprising an interconnection of integrators having the transfer function  $1/s$ . When this network is subjected to the lowpass to bandpass transformation, the integrators become bandpass quadratic sections having the transfer function  $s/[q(s^2+1)]$ . These sections have an infinite Q-factor, but it is possible to arrive at a network having finite-Q sections by pre-distorting the lowpass prototype transfer function. This was described in detail in Chapter 1, in respect of the structure [45] having transpose follow the leader feedback and feedforward from the input. This simple design procedure can utilize any suitable analogue computer circuit, and of particular interest here are the circuits described in section 4.2 of

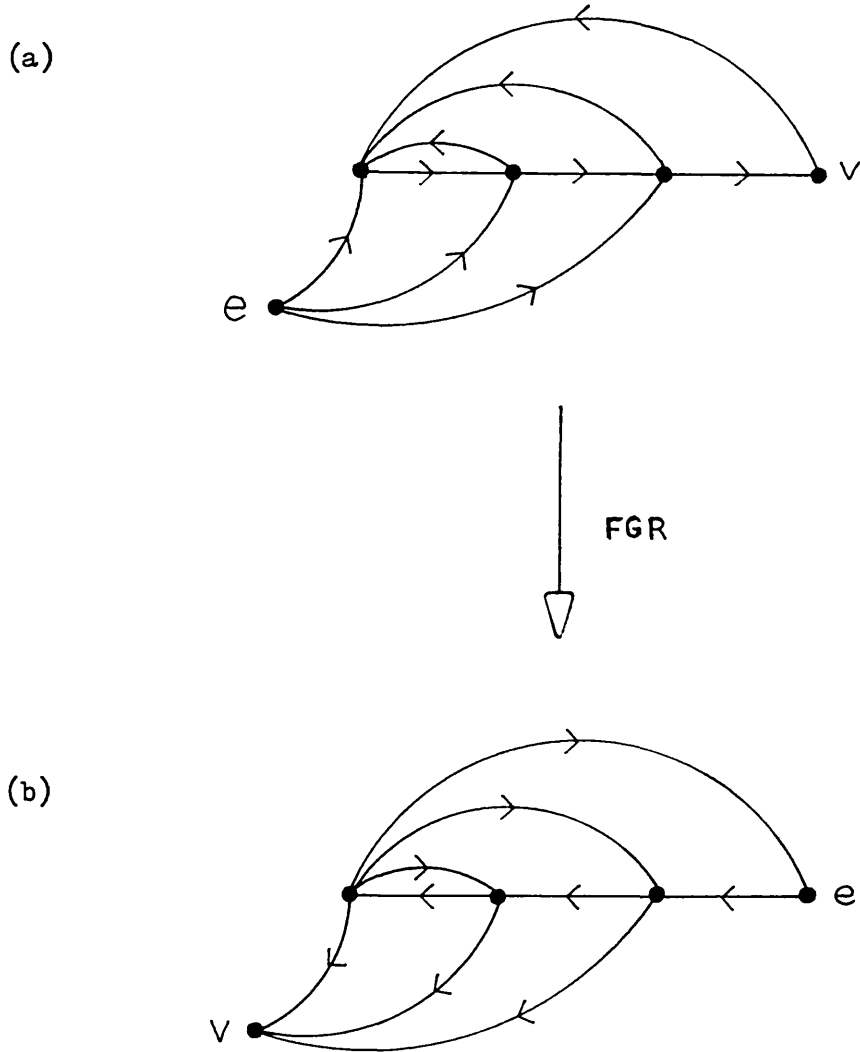


Fig 4.4 Deriving the new structure 'A' by FGR

- (a) Tow's structure [47] using follow the leader feedback and feedforward from the input
- (b) New structure 'A' using transpose follow the leader feedback and feedforward to the output

Ref [46], which have an intermediate form of nested feedback combined with feedforward from the input. The method thus provides a way of designing filters to have some of the intermediate structures marked 'C' in Table 4.1. The use of FGR on these filters would yield D-structures.

There are other intermediate structures which do not correspond to established analogue computer networks, for example the structure shown in Fig 3.5(b). In these cases it is a simple matter to arrive at a suitable analogue computer network by analysing the structure with all of the block transfer functions  $G_j$  set equal to  $1/s$ .

The remaining blank spaces in Table 4.1 indicate the possibility of other structures, but as yet no design procedure has been proposed for them. It is conceivable however that they may arise from known structures as a result of using an optimization programme which alters structure. The existence of such programmes was mentioned in section 3.5 in the context of the similarity transformation.



#### 4.5 Low sensitivity structures

Having classified multiple feedback filters in terms of their structure, it is interesting to examine their structures in order to identify any property of structure which may be common to all low sensitivity multiple feedback filters. Low sensitivity filters are represented in the second and subsequent columns of Table 4.1.

The feature which is common to the majority of published low sensitivity multiple feedback filters is that there exists one, and only one, forward path which passes through all of the blocks in the block diagram<sup>\*</sup>. The only exceptions to this are the few structures which use complex feedback [57,58,59,60] for which there can be no forward path passing through all of the blocks. However in these cases where a forward path cannot pass through blocks because they are in the feedback part of a complex feedback loop, then the forward path will pass through the reciprocator which is associated with those blocks. Our observation is therefore that, for low sensitivity multiple feedback filters, there exists one and only one forward path which passes through each block (or possibly its associated reciprocator) in the block diagram.

In Chapter 5 it will be shown that this is by no means a sufficient condition for low sensitivity. Whether or not it can be regarded as a necessary condition is not yet known.

---

\* The structure may of course have in addition other forward paths which do not pass through all of the blocks.

#### 4.6 Summary

In this chapter we have classified the existing multiple feedback filters composed of biquadratic sections, firstly in respect of the pattern of feedback loops used to reduce passband sensitivity, and secondly in respect of the method by which transmission zeros are realized. Presentation of the classification in the form of a table has indicated new structures. Some of these may be derived from existing structures by the transformations of FGR and interchange of cascade subnetworks. Others may be designed by association with analogue computer networks. There are other possible structures for which specific design procedures have yet to be proposed.

The classification of structure described in this chapter is based on a classification set out by the writer in Ref [84]. This has been extended here, not only by the inclusion of references to subsequent publications, but also by the inclusion of complex feedback as a method of producing transmission zeros. Complex feedback was described by the writer in Ref [88].

The classification has drawn attention to the fact that all published low sensitivity multiple feedback filters have one, and only one, forward path which passes through each block (or possibly its associated reciprocator) in the block diagram, and also to the fact that the common feedback arrangements for reducing passband sensitivity are special cases of the structure having all feedback paths.

This classification provides a framework for the computational study that will be undertaken in the next chapter.

---

COMPUTATIONAL STUDY OF MULTIPLE FEEDBACK FILTERS

---

Multiple feedback filters were initially created to provide filters having a lower sensitivity than that of the simple cascade filter. Having proposed a number of new multiple feedback filters it is therefore necessary for us to study their sensitivity performance and to compare it with the sensitivity of known filters. There are various ways of doing this and we must choose a method which suits our overall objective of obtaining insight into network behaviour. We could follow the example of some authors and compare different filters on the basis of a single scalar measure of sensitivity, such as would be used by a computer optimization programme. However whilst this may be possible in the context of a specific engineering application for which detailed performance requirements are known and for which constraints imposed by the method of fabrication are also known, a scalar measure of sensitivity does not reveal why one filter is better than another, and is therefore an inappropriate tool for our purposes. At the other extreme, listing the algebraic expressions of sensitivity would be equally uninformative. In the approach adopted here, a specific transfer function is synthesized using each of the various structures in turn. For each structure the nominal, sinusoidal steady state, magnitude response is computed and plotted as a function of frequency. Superimposed on this is a family of computed plots showing how the magnitude response is affected by finite changes in the block diagram constants  $a_{jk}$ ,  $b_j$ ,  $c_j$  etc, and by finite changes in the intermediate parameters of the blocks  $\omega_0$ ,  $Q$ ,  $K$  etc. The results will therefore be independent of the particular sections being used, and interpreted with care will allow the various structures to be compared. This approach undoubtedly has its limitations, as it seems does any comparison of sensitivity [138],  
but it will allow some comparison to be made, it will verify some <sup>pp 161-165</sup> theoretical results of earlier chapters, and hopefully it will increase our understanding of network sensitivity.

### 5.1 Details of the sensitivity computation

The transfer function that has been chosen is not intended for any particular application, but it has a bandpass characteristic and it also has transmission zeros at finite non-zero frequencies in view of our interest in such features. The bandpass response is obtained by transformation of a prototype lowpass response. This is the third-order elliptic-function characteristic which is sketched in Fig 5(a). From Tables of poles and zeros [139] we obtain the lowpass prototype transfer function:

$$F_{LP}(s) = \frac{1}{C} \frac{s^2 + \Omega_{\omega_1}^2}{(s - a_0)(s^2 - 2a_1s + a_1^2 + b_1^2)} \quad (5.1.1)$$

where:

$$\begin{aligned} C &= 15.658010 \\ \Omega_{\omega_1} &= 2.6998758817 \\ -a_0 &= 0.4806933238 \\ -a_1 &= 0.2084141239 \\ \pm b_1 &= 0.9617829016 \end{aligned}$$

The bandpass function is obtained by applying the lowpass to bandpass transformation:

$$s \longmapsto q \left( s + \frac{1}{s} \right) \quad \text{where } q = 10 \quad (5.1.2)$$

( $q$  is the required ratio of geometric centre frequency to bandwidth) in turn to each singular point  $s_L$  of the lowpass transfer function to obtain two singular points  $s_B$  of the bandpass transfer function as follows [140]:

$$s_B = \frac{s_L \pm \sqrt{\left(\frac{s_L}{2q}\right)^2 - 1}}{2q} \quad (5.1.3)$$

The bandpass response is scaled to have a centre frequency of 100 rad/s by applying the mapping:

$$s \longmapsto s/a, \quad a = 100 \quad (5.1.4)$$

whence the required bandpass transfer function:

$$F(s) = \frac{K s (s^2 + \omega_{n1}^2)(s^2 + \omega_{n2}^2)}{\left(s^2 + \frac{\omega_{o1}}{Q_1} s + \omega_{o1}^2\right) \left(s^2 + \frac{\omega_{o2}}{Q_2} s + \omega_{o2}^2\right) \left(s^2 + \frac{\omega_{o3}}{Q_3} s + \omega_{o3}^2\right)} \quad (5.1.5)$$

where

$$\begin{aligned} K &= 0.638650761 & \omega_{o1} &= 95.306399 & Q_1 &= 48.036847 \\ \omega_{n1} &= 87.40767309 & \omega_{o2} &= 100.0 & Q_2 &= 20.80328458 \\ \omega_{n2} &= 114.4064319 & \omega_{o3} &= 104.924749 & Q_3 &= 48.036847 \end{aligned}$$

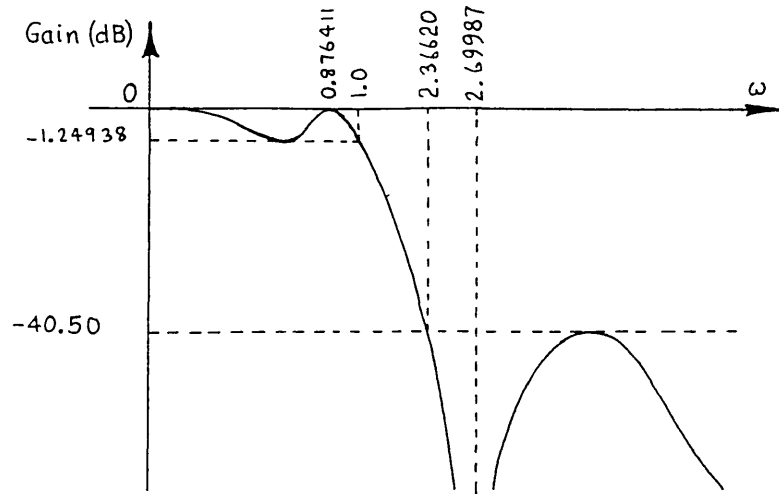


Fig 5(a) Prototype lowpass response

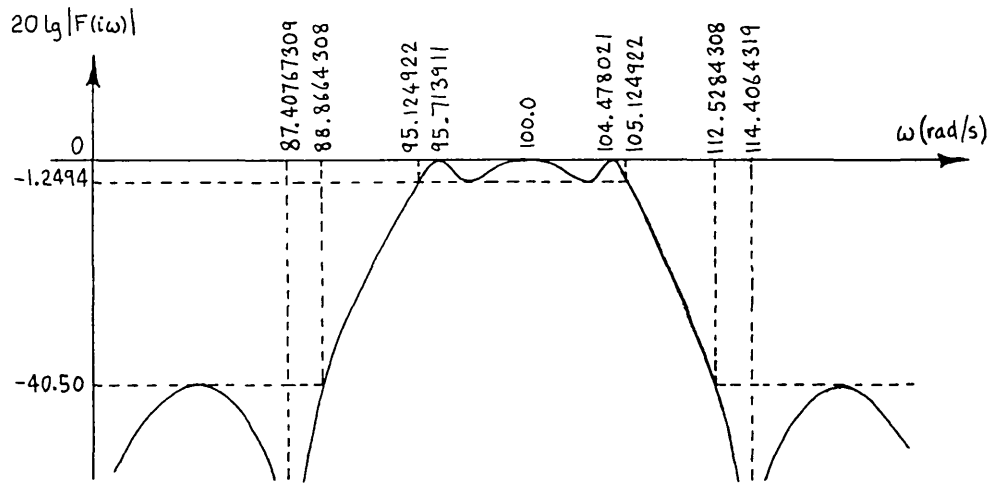


Fig 5(b) Bandpass response

the magnitude response of which is sketched in Fig 5(b).

This 6-th degree transfer function was chosen to have the minimum complexity that was necessary to distinguish between the multifarious structures, without at the same time making the examples unduly complicated. The parameters of the frequency response are limited by this low order of complexity and are somewhat arbitrary, but it may be said that the high value of passband ripple is typical of the crude filters used to separate signalling tones in a telecommunications system. This transfer function has been used in the previous examples shown in Fig 1.9, Fig 1.12 and Fig 3.5.

For the sensitivity analysis in this Chapter, each structure will be realized by an active CR network, for three reasons. Firstly it shows that it is possible for the structure to be realized by an active CR network, although no attempt has been made to select the most appropriate types of quadratic section. Secondly, since the adders will be realized as part of the quadratic sections [22] (see Fig 2.1(b)), it will allow us to determine the minimum number of operational amplifiers needed by each structure (for the particular transfer function being considered). Thirdly it allows us to use a readily available network analysis programme. It would of course have been possible to write a special purpose programme to analyse multiple feedback filters represented in block diagram form, and it would have been relatively easy to obtain the sensitivity graphs from such a programme. However the emphasis in this work is not on writing computer programmes, and the required changes in the block diagram parameters were obtained by altering the values of the appropriate resistances and capacitances of the active CR network.

The characteristics of major interest are the effects, on the magnitude response, of changes in the resonance frequencies  $\omega_0$  of the individual blocks. Since  $\omega_0$  has the dimension of inverse time, it will in theory be proportional to the reciprocal of a CR time constant. Hence  $\omega_0$  has an irreducible variation of at least as much as the product of capacitance and resistance variations. For a thick film construction using ceramic capacitors this might typically have a worst case value of  $\pm 0.013\%/deg\ C$  for temperature variations and  $\pm 3\%$  for selection tolerance.

On the other hand the quality factor  $Q$  is dimensionless and could in theory be made to depend only on the ratios of resistances, and the ratios of capacitances. These can often be controlled more accurately than the CR time constant, depending on the fabrication method used.

However the value of  $Q$  also depends on the gain-bandwidth products of the operational amplifiers, which are less easily controlled.

For bandpass sections in general, the gain constant  $K$  as defined by (2.1.1) will vary in the same manner as  $\omega_0$ , but it will be seen in this Chapter that it has a relatively minor effect on the frequency response. The remaining block diagram parameters  $a_{jk}$ ,  $b_j$ ,  $c_j$  are all determined by ratios of resistances, and are not usually affected by variations in the gain-bandwidth product of operational amplifiers.

For each representative design studied in subsequent sections, we will plot the effect on the magnitude response of changing each of the resonance frequencies  $\omega_0$  by 3%, and of changing each of the remaining parameters  $Q$ ,  $K$ ,  $a_{jk}$ ,  $b_j$ ,  $c_j$  etc by 10%. The resulting collection of graphs will give a good visual impression of the sensitivity performance of each design, and will form the basis for a comparison of structures.

## 5.2 The three canonic expansions of a transfer function

Following the sequence adopted in Chapter 4, we start by describing the performance of the three 'canonical' structures, which occur in the first column of Table 4.1, and which were shown in block diagram form in Fig 4.2. These structures do not employ feedback loops for the purpose of reducing sensitivity, and we shall see that the sensitivity is relatively large.

### 5.2.1 Cascade or factored structure

First the cascade or factored structure [90]. The numerator and denominator factors of the transfer function (5.1.5) have been paired in accordance with Lee's method of pairing poles and zeros for minimum sensitivity [141], and these pairs form the transfer functions of the blocks as shown in the block diagram in Fig 5.1(a). Poles and zeros of the blocks are identically poles and zeros of the transfer function, and transmission zeros are hence produced by series notch sections. The circuit diagram of one possible realization of the block diagram is shown in Fig 5.1(b), and the frequency responses of this circuit are plotted in Fig 5.1(c). Obviously there is scope for scaling the signal levels to improve the dynamic range, and indeed the pairing of poles and zeros could have been chosen to maximize dynamic range [142] instead of minimizing sensitivity, but it is sensitivity that is of immediate concern here.

Consider first the effect of changes in resonance frequency. Since for most biquadratic sections a change in the value of a component is likely to change both  $\omega_0$  and  $\omega_n$  together, we show in Fig 5.2(a) the effect of increasing both  $\omega_{01}$  and  $\omega_{n1}$  of the first section by 3%. Similarly Fig 5.2(b) shows the effect of increasing  $\omega_{02}$  and  $\omega_{n2}$  by 3%. Figure 5.2(c) shows both the effect of an increase and a decrease in  $\omega_{03}$  of the third section. Evidently these changes in resonance frequencies cause a gross error in the magnitude response. Notwithstanding this high sensitivity, the cascade structure is quite adequate for non-critical filter applications, particularly if some form of adjustment is performed since the post-adjustment variation of resonance frequencies may be very much less than 3%.

Changes in the Q-factor of the sections have much less effect on the frequency response of the filter, as can be seen in Fig 5.3. The relatively small effect of Q variations was found also by Bruton [150],



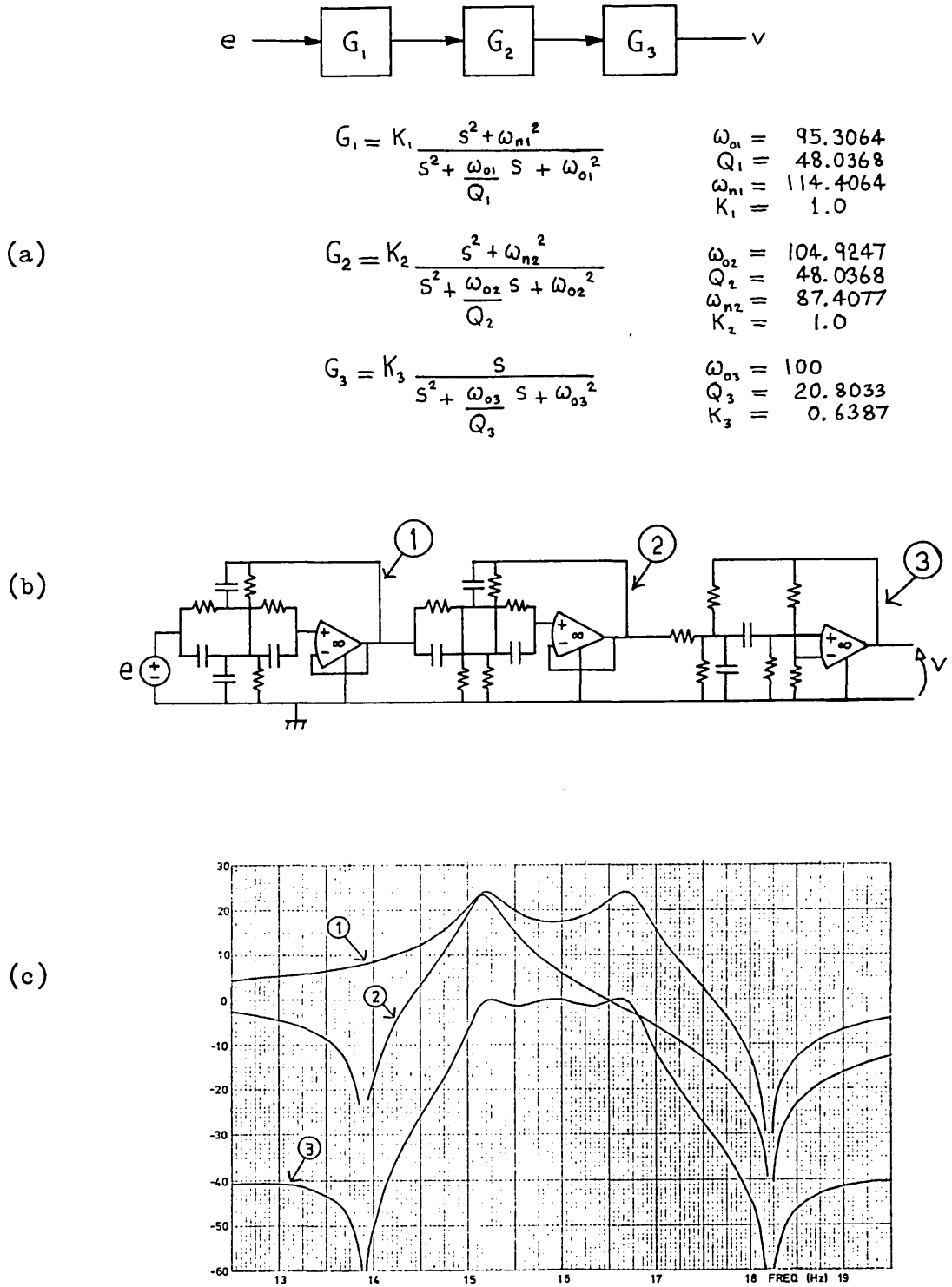


Fig 5.1 Cascade or factored structure [90]

- (a) Block diagram
- (b) Active CR realization of the block diagram
- (c) Computed frequency responses

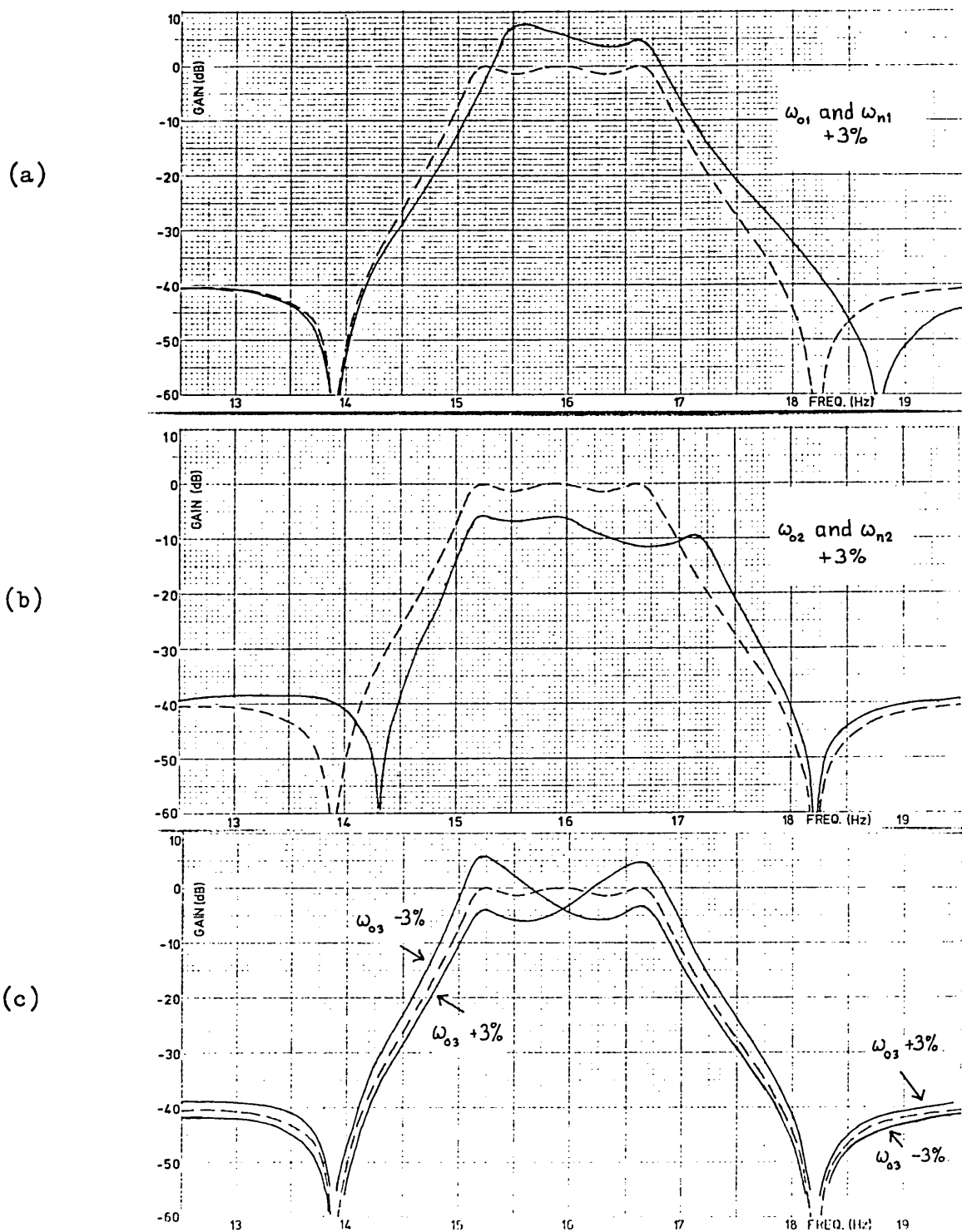


Fig 5.2 Cascade structure sensitivity to changes in resonance frequency

- (a)  $\omega_{o1}$  increased by 3% from 95.3 to 98.2, and  $\omega_{n1}$  increased by 3% from 114.4 to 117.8
- (b)  $\omega_{o2}$  increased by 3% from 104.9 to 108.1, and  $\omega_{n2}$  increased by 3% from 87.4 to 90.0
- (c)  $\omega_{o3}$  increased by 3% from 100 to 103 and  $\omega_{n3}$  reduced by 3% from 100 to 97

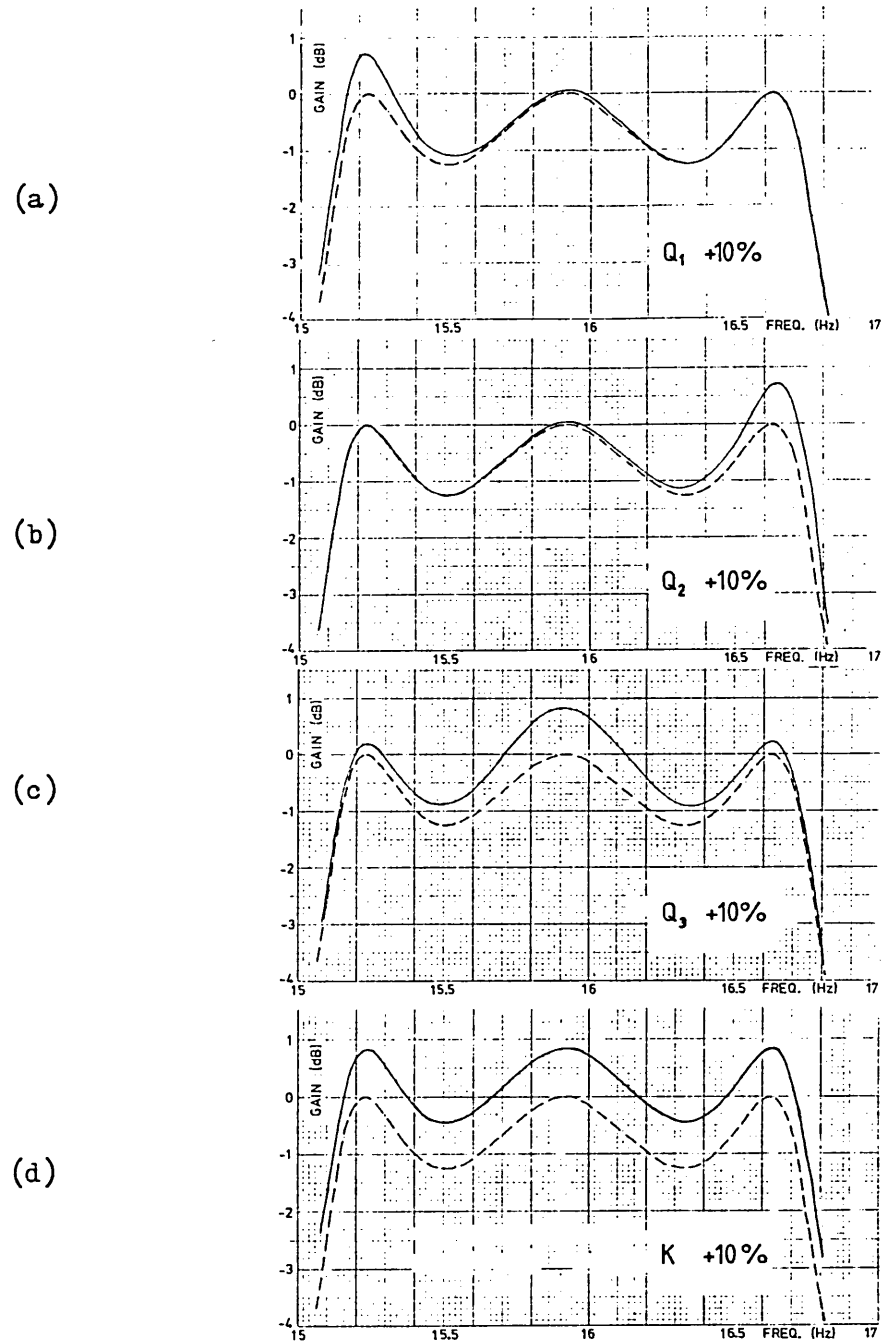


Fig 5.3 Cascade structure sensitivity to changes in  $Q$  and  $K$

- (a)  $Q_1$  increased by 10% from 48.04 to 52.84
- (b)  $Q_2$  increased by 10% from 48.04 to 52.84
- (c)  $Q_3$  increased by 10% from 20.8 to 22.88
- (d)  $K_1$  or  $K_2$  or  $K_3$  increased by 10%

who investigated first-order differential sensitivity of the cascade filter. This does not imply of course that  $Q$ -variations are unimportant since in some sections it is possible for  $Q$  to change much more than  $\omega_0$  (e.g.  $S_A^{\omega_0} \approx 0$ ,  $S_A^Q \propto Q$ ).

The sensitivity of the cascade structure is easily understood since the transfer function  $F$  is simply the product of the block transfer functions:

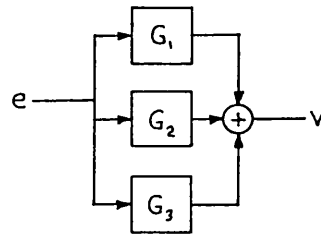
$$F \triangleq \frac{v}{e} = G_1 G_2 G_3 \quad (5.2.1)$$

On a logarithmic scale, the magnitude response is the sum of the magnitude responses of the three sections, and any change in the magnitude response of one of the sections is reflected directly in the overall response. Because of its common usage and simplicity of construction, the sensitivity performance of the cascade structure is often taken as a reference against which the performance of other structures are assessed.

### 5.2.2 Partial fraction structure

The second canonical structure to be considered is the partial fraction structure shown in Fig 5.4. Using the method described by Russell and Chan in Ref. 93, the bandpass transfer function (5.1.5) has been expanded into quadratic partial fractions, and each partial fraction has been identified with a block in the block diagram Fig 5.4(a). As in the cascade structure, the poles of the transfer function  $F = v/e$  are identically the poles of the three blocks. The zeros of the transfer function however are produced by parallel forward paths.

When the resonance frequency  $\omega_{o1}$  is increased by 3%, it can be seen from Fig 5.5(a) that the stopbands become distorted. The upper transfer function zero increases in frequency by about 3%, and the lower zero increases in frequency by 10%, moving to a frequency at the edge of the passband and thereby causing severe distortion of the passband response. Both zeros move away from the imaginary axis, as seen by the reduced depth of the notches. Changes in  $\omega_{o2}$  and  $\omega_{o3}$  also severely distort the stopband as shown in Fig 5.5(b) and (c). Changes in the  $Q$ -factors cause deviations which are almost identical to the corresponding deviations for the cascade structure, and they are not shown explicitly. The very poor stopband sensitivity performance of the partial fraction structure probably accounts for the fact that it has not been widely used.



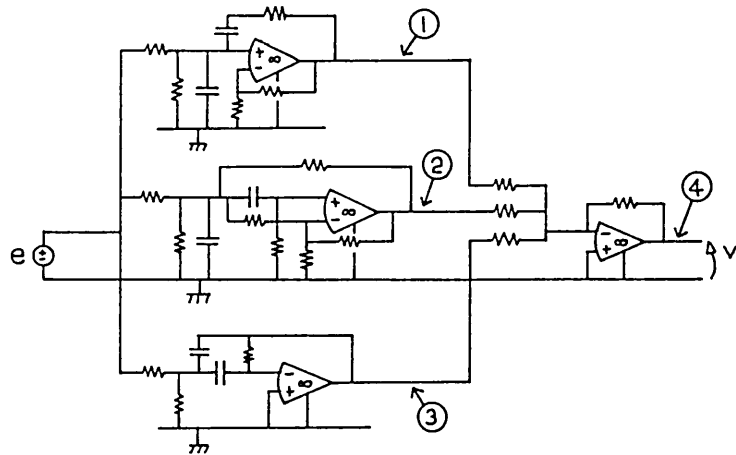
(a)

$$G_1 = K_1 \frac{s + \alpha_1}{s^2 + \frac{\omega_{o1}}{Q_1} s + \omega_{o1}^2} \quad \begin{array}{l} \omega_{o1} = 95.3064 \\ Q_1 = 48.0368 \\ \alpha_1 = 20.5574 \\ K_1 = -1.9887 \end{array}$$

$$G_2 = K_2 \frac{s + \alpha_2}{s^2 + \frac{\omega_{o2}}{Q_2} s + \omega_{o2}^2} \quad \begin{array}{l} \omega_{o2} = 104.9247 \\ Q_2 = 48.0368 \\ \alpha_2 = -22.7342 \\ K_2 = -2.17957 \end{array}$$

$$G_3 = K_3 \frac{s}{s^2 + \frac{\omega_{o3}}{Q_3} s + \omega_{o3}^2} \quad \begin{array}{l} \omega_{o3} = 100 \\ Q_3 = 20.8033 \\ K_3 = 4.80693 \end{array}$$

(b)



(c)

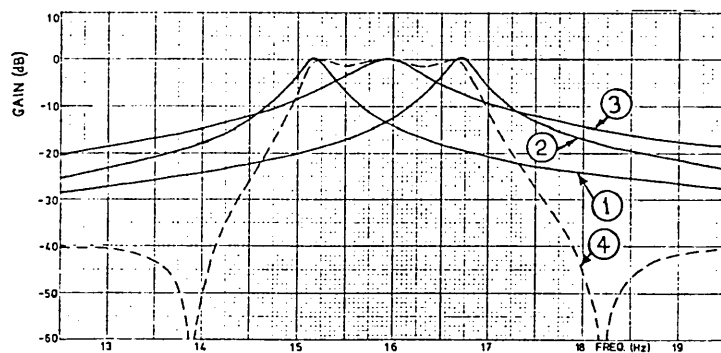


Fig 5.4 Partial fraction structure [93]

- (a) Block diagram
- (b) Active CR realization
- (c) Computed frequency responses

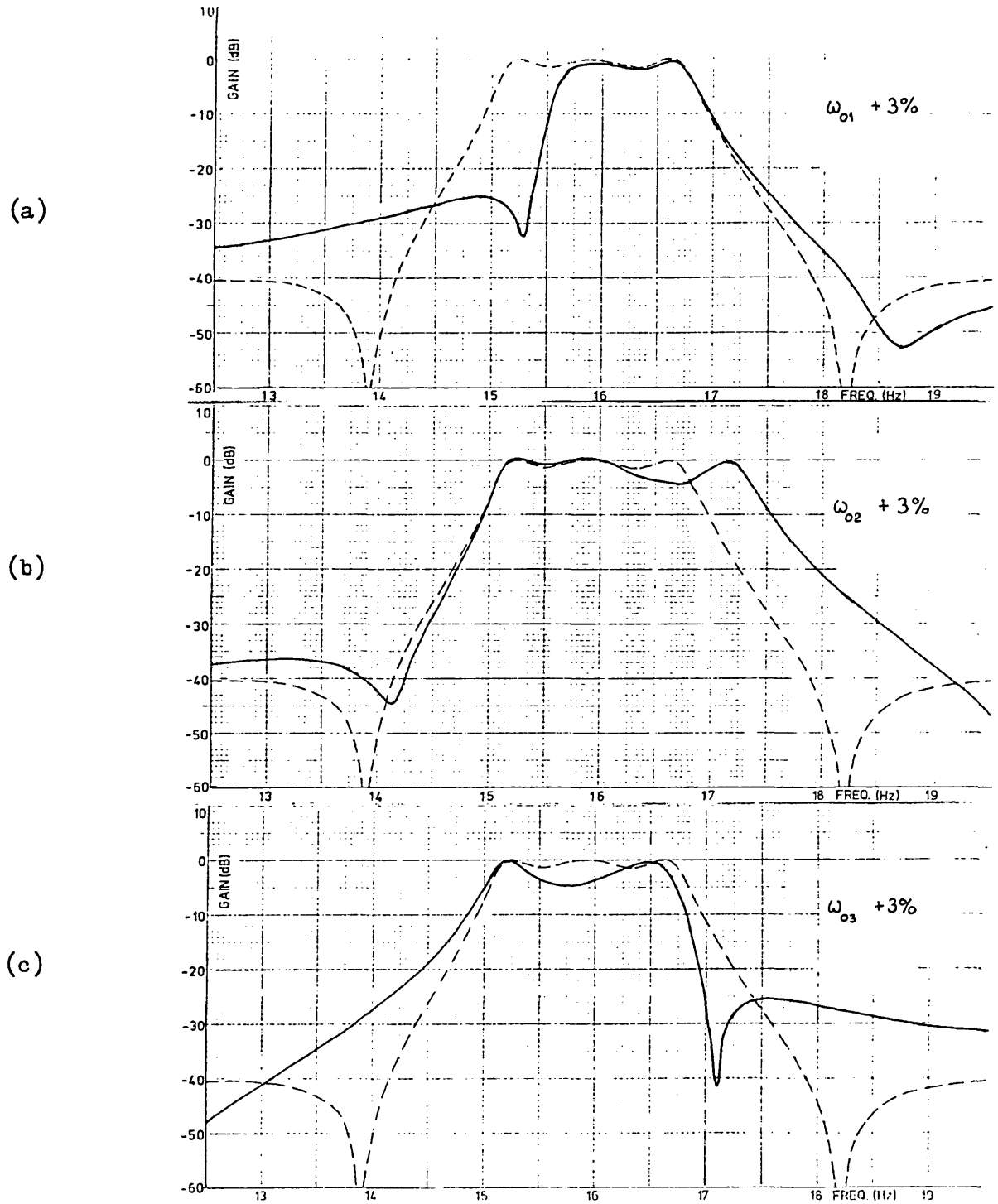


Fig 5.5 Partial fraction structure sensitivity to changes in resonance frequency

- (a)  $\omega_{o1}$  increased by 3% from 95.3064 to 98.1659
- (b)  $\omega_{o2}$  increased by 3% from 104.9247 to 108.0725
- (c)  $\omega_{o3}$  increased by 3% from 100 to 103

### 5.2.3 Continued fraction structure

The third canonical structure to be considered is the continued fraction structure [84], which was introduced in Chapter 1 as an illustration of transmission zeros produced by complex feedback. As was described in Section 1.4, the lowpass transfer function (5.1.1) & (1.4.10) is expanded into a continued fraction, and the three partial remainders (1.4.15) are identified with the denominators of the three blocks in the block diagram Fig 5.6(a). Lowpass to bandpass transformation (5.1.2) and frequency scaling (5.1.4) then yield the required parameters. Use of the scaling transformation (Section 3.4) is also necessary if the single-amplifier sections shown in Fig 5.6(b) are to be used. The transformation increases the signal level at the output of block-1 and the output of block-3. This re-distributes the gain and makes all three blocks realizable by single amplifier sections as shown. The resulting frequency responses are shown in Fig 5.6(c). For uniformity of presentation, however, the frequency responses in Fig 5.7 and 5.8 have all been scaled by a factor which makes the nominal mid-band gain equal to 0dB.

Sensitivity performance of the continued fraction structure has nothitherto been studied. It is found to be very poor in the passband. A change of 3% in  $\omega_0$  can cause as much as 20dB error over the entire passband as can be seen in Fig 5.7. In the stopband however, a change of 3% in  $\omega_0$  causes less than 3% shift in the notch frequencies which is better than the cascade structure. Changes in the Q-factors again cause relatively large errors in the passband response as can be seen in Fig 5.8.

### 5.2.4 Sensitivity relations

If the summed sensitivity invariant (2.2.57) is applied to a cut containing all three blocks of the factored structure described in Section 5.2.1, then the following relationship is obtained:

$$\sum_{G_1} |F| - \sum_{G_2} |F| + \sum_{G_3} |F| = 1 \quad (5.2.2)$$

which is consistent with the fact that:

$$\sum_{G_j} |F| = 1, \quad \forall j \quad (5.2.3)$$

For the partial fraction structure the corresponding expressions are:

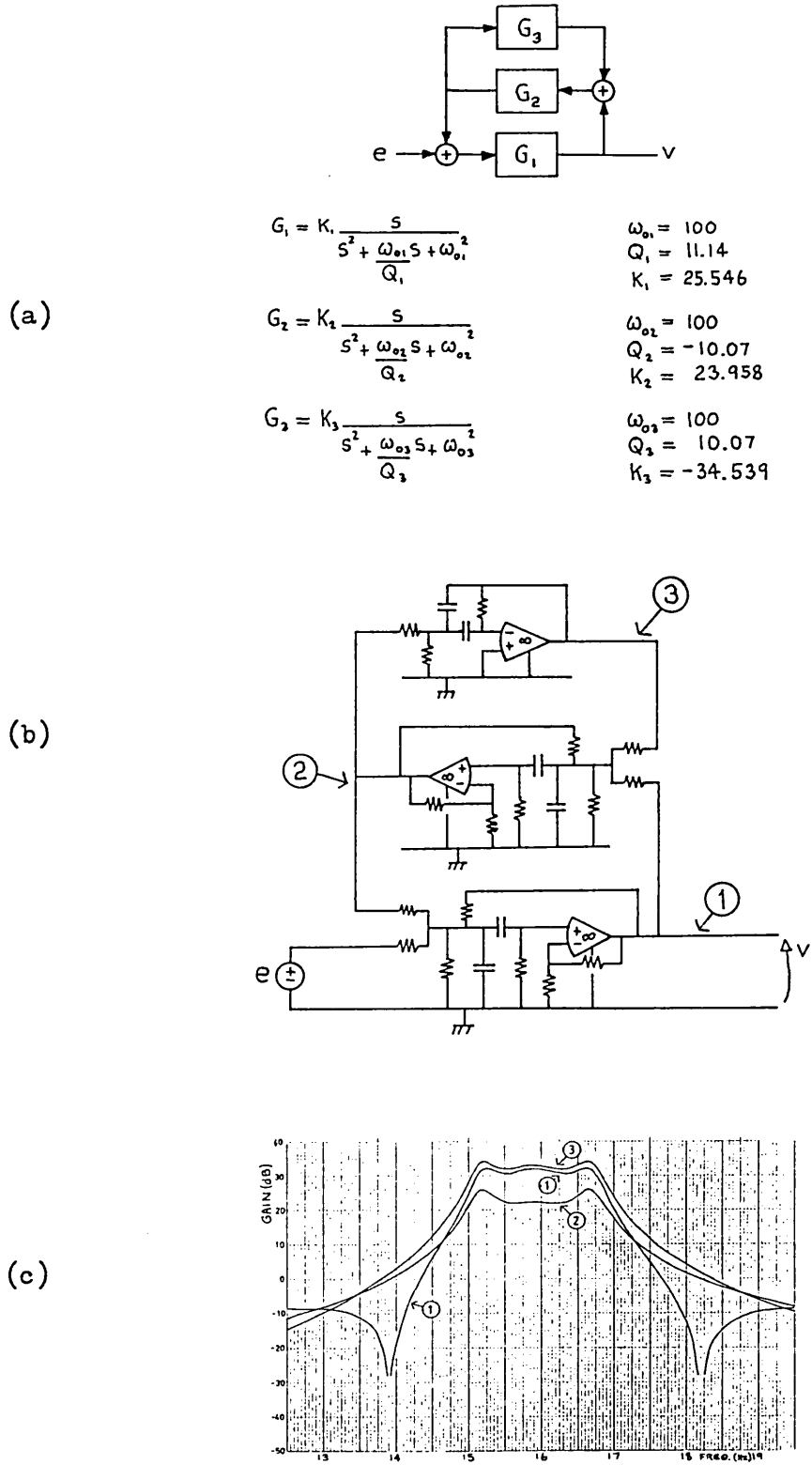


Fig 5.6 Continued fraction structure [84]

- (a) Block diagram
- (b) Active CR realization of the block diagram
- (c) Computed frequency responses



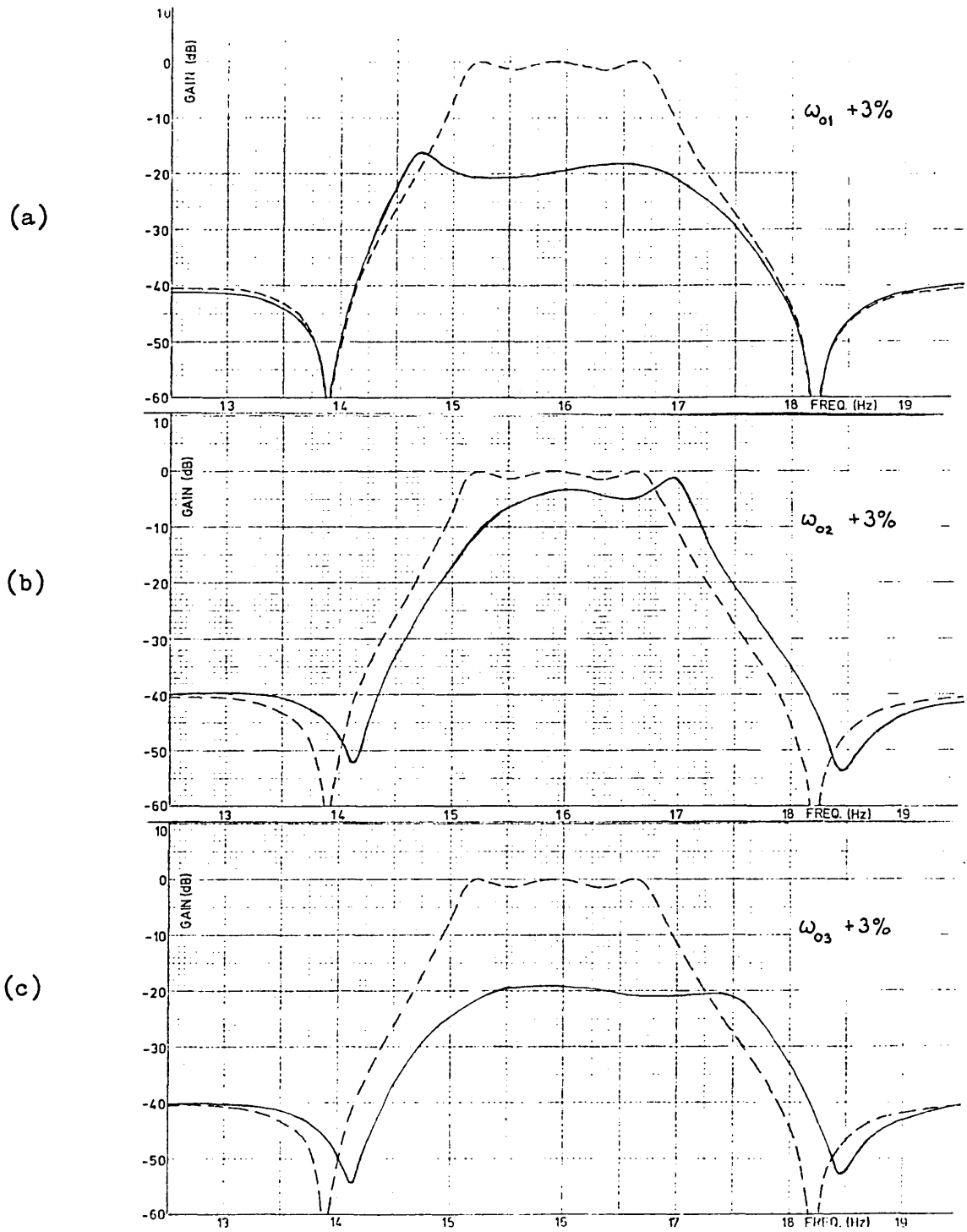


Fig 5.7 Continued fraction structure sensitivity to changes in resonance frequency

- (a)  $\omega_{01}$  increased by 3% from 100 to 103
- (b)  $\omega_{02}$  increased by 3% from 100 to 103
- (c)  $\omega_{03}$  increased by 3% from 100 to 103

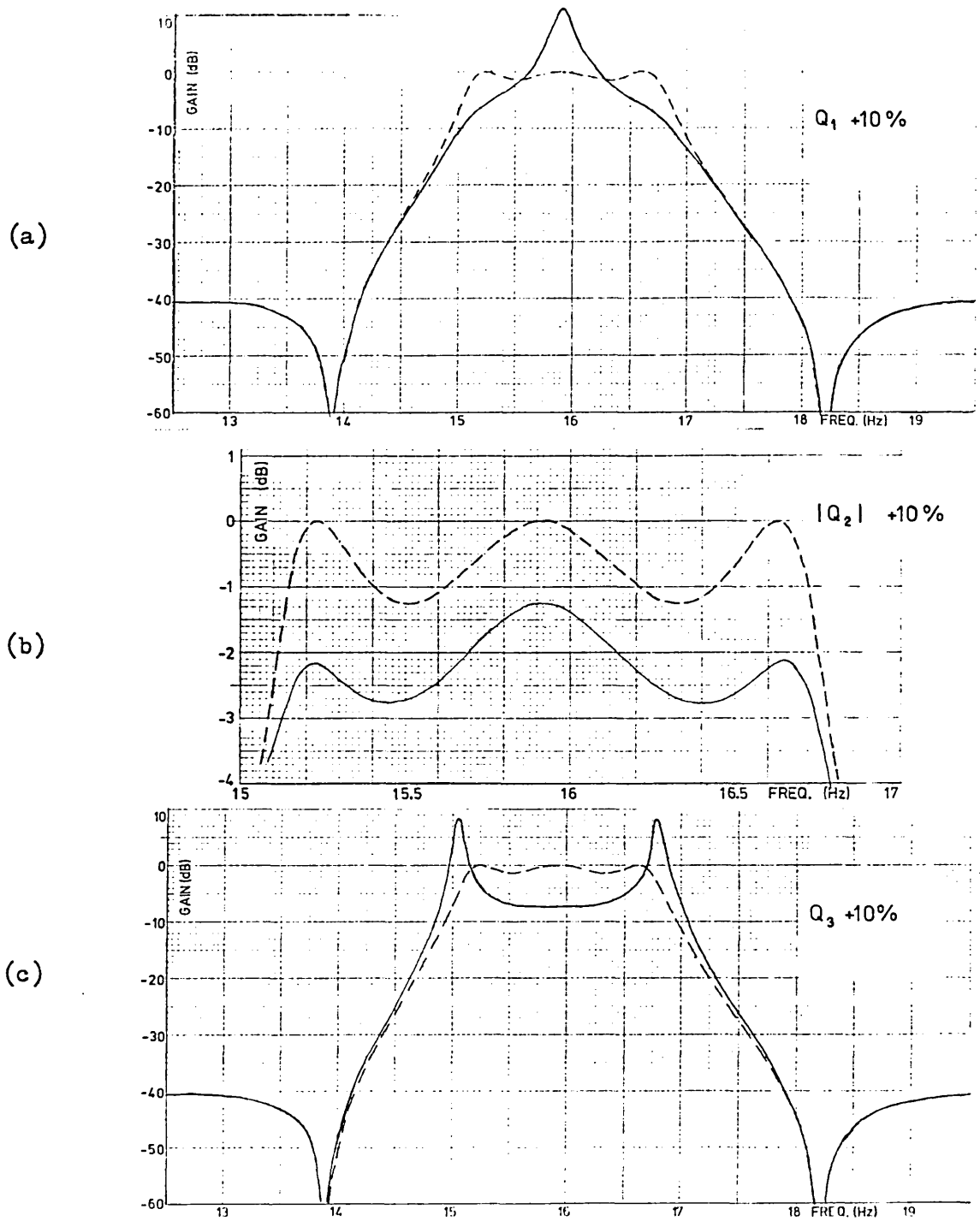


Fig 5.8 Continued fraction structure sensitivity to changes in Q-factor

- (a)  $Q_1$  increased by 10% from 11.14 to 12.256
- (b)  $|Q_2|$  increased by 10% from 10.07 to 11.079
- (c)  $Q_3$  increased by 10% from 10.07 to 11.079

$$S_{G_1}^{|F|} + S_{G_2}^{|F|} + S_{G_3}^{|F|} = 1 \quad (5.2.4)$$

$$S_{G_j}^{|F|} = \operatorname{Re} \frac{G_j}{F}, \quad \forall j \quad (5.2.5)$$

Noting that  $G_1$  and  $G_2$  are inverting quadratic blocks and  $G_3$  is non-inverting, it can be seen that the sensitivities in (5.2.4) are not necessarily all of the same sign, so that individually the sensitivities may be greater than those in (5.2.3) for the factored structure. Conversely, since:

$$-\frac{|G_j|}{|F|} \leq \operatorname{Re} \frac{G_j}{F} \leq \frac{|G_j|}{|F|} \quad (5.2.6)$$

the differential sensitivities (5.2.5) are less than those of the factored structure at frequencies for which  $|G_j| < |F|$ . In the example studied, this applies over the passband, except at the frequencies  $\omega_{0j}$ , as can be seen from Fig 5.4(c). Comparison of Fig 5.5(a) with Fig 5.2(a) shows that there are frequencies in the passband at which the deviation in the response of the partial fraction structure is greater than the corresponding deviation in the factored structure. This may be due to higher order derivatives being significant in this case, or it may be due to the fact that a 3% change of the intermediate variable  $\omega_{01}$  may not produce the same change in  $G_1$  for the two structures, on account of the fact that different types of quadratic blocks are used in the two structures. For the continued fraction structure the invariant (5.2.2) obtains, but expressions for the individual sensitivities are more complex.

Of the three canonic structures, only the cascade is in common use. The partial fraction structure has a greater sensitivity in the stopbands, and the continued fraction structure has a greater sensitivity in the passband. The partial fraction structure has been proposed for use as an all-pass group-delay equalizer [122], which of course does not have a stopband and therefore might not have a greater sensitivity than the corresponding cascade structure. However the partial fraction structure does have the disadvantage of requiring a summing amplifier section

### 5.3 Structures with leapfrog feedback

Continuing the sequence used in Chapter 4, we now present the sensitivity performance of structures which use leapfrog feedback to reduce sensitivity in the passband. These occur in the second column of Table 4.1, and are illustrated in Fig 4.3. Structures in this section will illustrate how the three methods of producing transmission zeros may be applied to low sensitivity filters.

#### 5.3.1 Node-voltage simulation

Firstly we consider the leapfrog feedback structures which incorporate transmission zeros by means of series notch sections. Several synthesis procedures are referred to in Table 4.1, but the method which is most easily applied to the present case is 'node voltage simulation', introduced by Yoshihiro, Nishihara and Yanagisawa in Ref.63. It uses the principles of ladder network simulation described fully in Section 1.1, except that only the node-to-datum voltages are simulated, as indicated in Fig 5.9. Starting with an LCR realization of the bandpass transfer function (5.1.5), shown in Fig 5.10(a), a leapfrog feedback structure is produced by node-voltage simulation and the resulting block diagram is shown in Fig 5.10(b). It will be seen that three sections are used, two of them having multiple inputs (in the sense of Fig 2.2) as indicated by the broken line around the first section. The three sections have different resonance frequencies, but the spread of frequencies is not as great as in the cascade structure (Fig 5.1), or the partial fraction structure (Fig 5.4). One possible realization of the block diagram is shown in Fig 5.10(c), and the frequency responses are shown in Fig 5.10(d). The active CR realization has a mid-band gain of  $-6.02\text{dB}$ , simulating the mid-band gain of the LCR filter. Evidently the scaling transformation (Section 3.4) may be used to improve dynamic range. For uniformity of presentation, the frequency responses in Figures 5.11 to 5.14 have all been scaled by a factor which makes the nominal mid-band gain equal to  $0\text{dB}$ .

The effects of increasing the resonance frequencies associated with each of the three sections in turn are shown in Fig 5.11, from which it can be seen that, as anticipated, the node-voltage simulation has a reduced passband sensitivity compared with the cascade structure. For both structures there tends to be a large error at the edges of the passband, due to the proximity of the steep slope in the transition

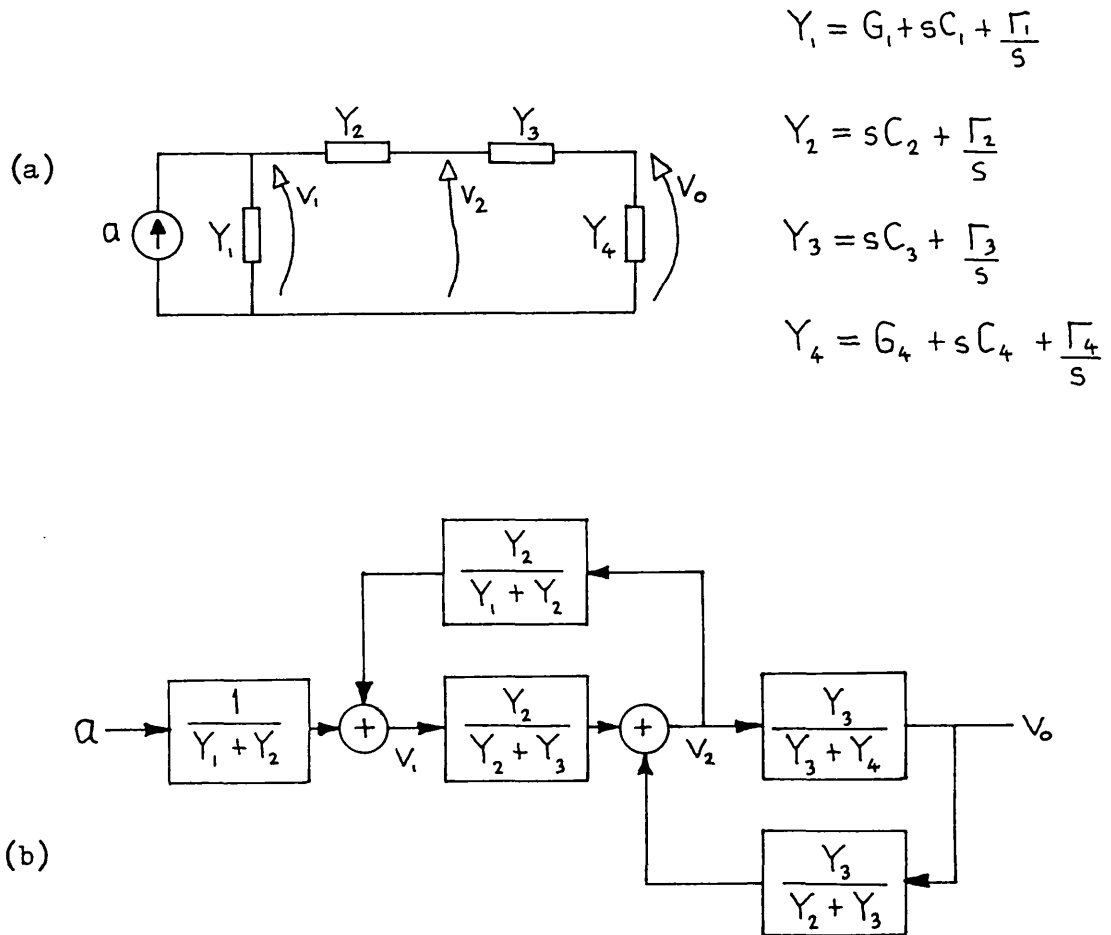


Fig 5.9 Node-voltage simulation [63]

- (a) LCR ladder network  
 (b) Structure produced by node-to-datum voltage simulation



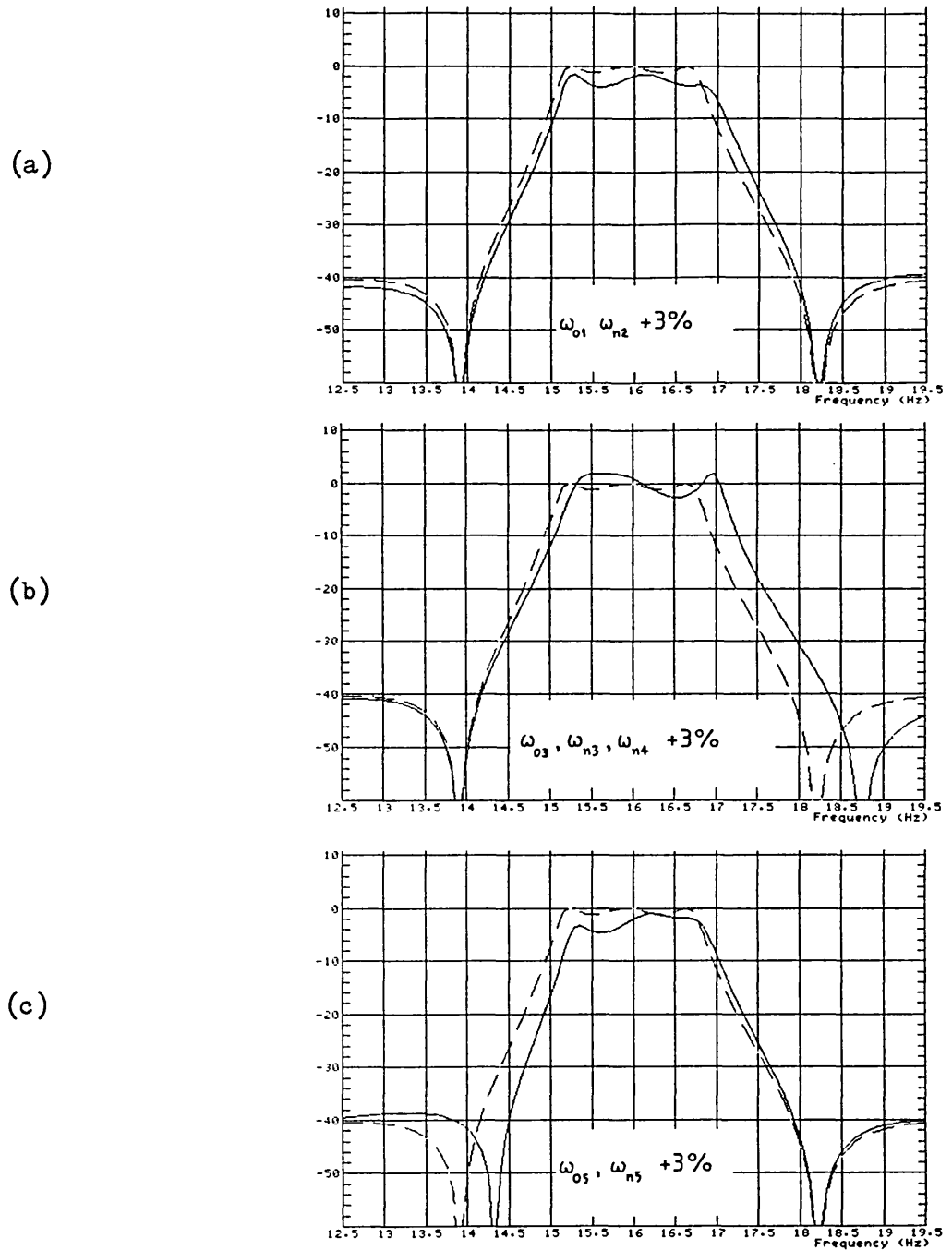
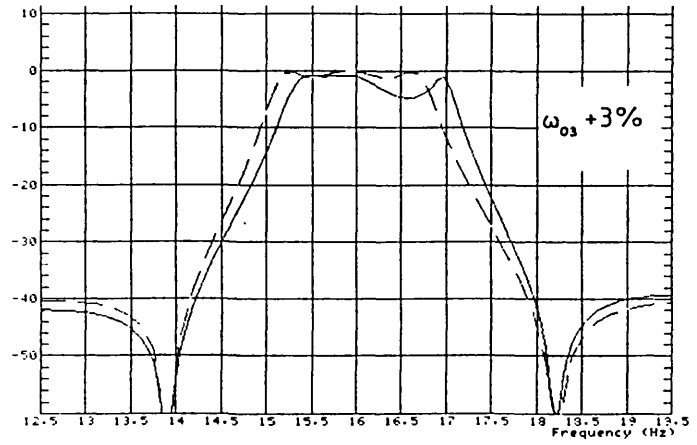


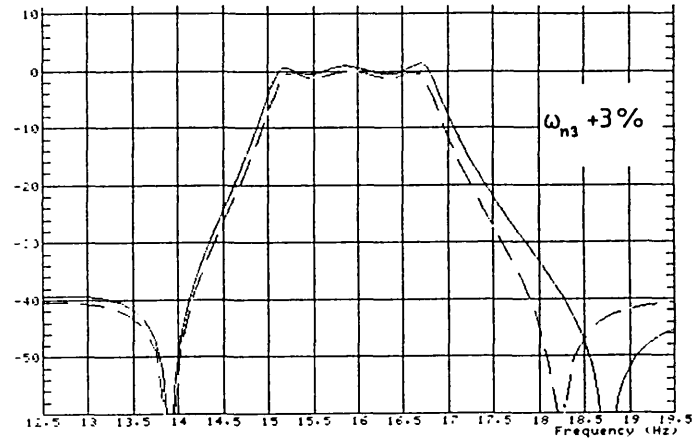
Fig 5.11 Node-voltage simulation sensitivity to changes in resonance frequency

- (a)  $\omega_{01}$  increased by 3% from 101.822 to 104.877 and  
 $\omega_{n2}$  increased by 3% from 114.406 to 117.838
- (b)  $\omega_{02}$  increased by 3% from 100 to 103,  
 $\omega_{n3}$  increased by 3% from 114.406 to 117.838 and  
 $\omega_{n4}$  increased by 3% from 87.407 to 90.03
- (c)  $\omega_{05}$  increased by 3% from 98.21 to 101.156 and  
 $\omega_{n5}$  increased by 3% from 87.407 to 90.03

(a)



(b)



(c)

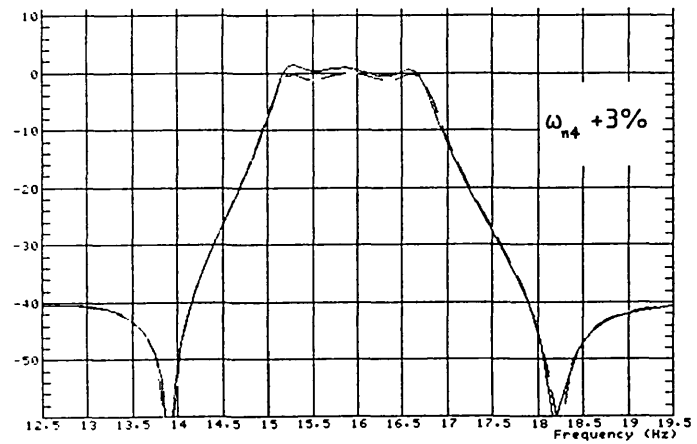


Fig 5.12 Sensitivity to 2nd-section resonance frequencies

- (a)  $\omega_{03}$  increased by 3%
- (b)  $\omega_{n3}$  increased by 3%
- (c)  $\omega_{n4}$  increased by 3%



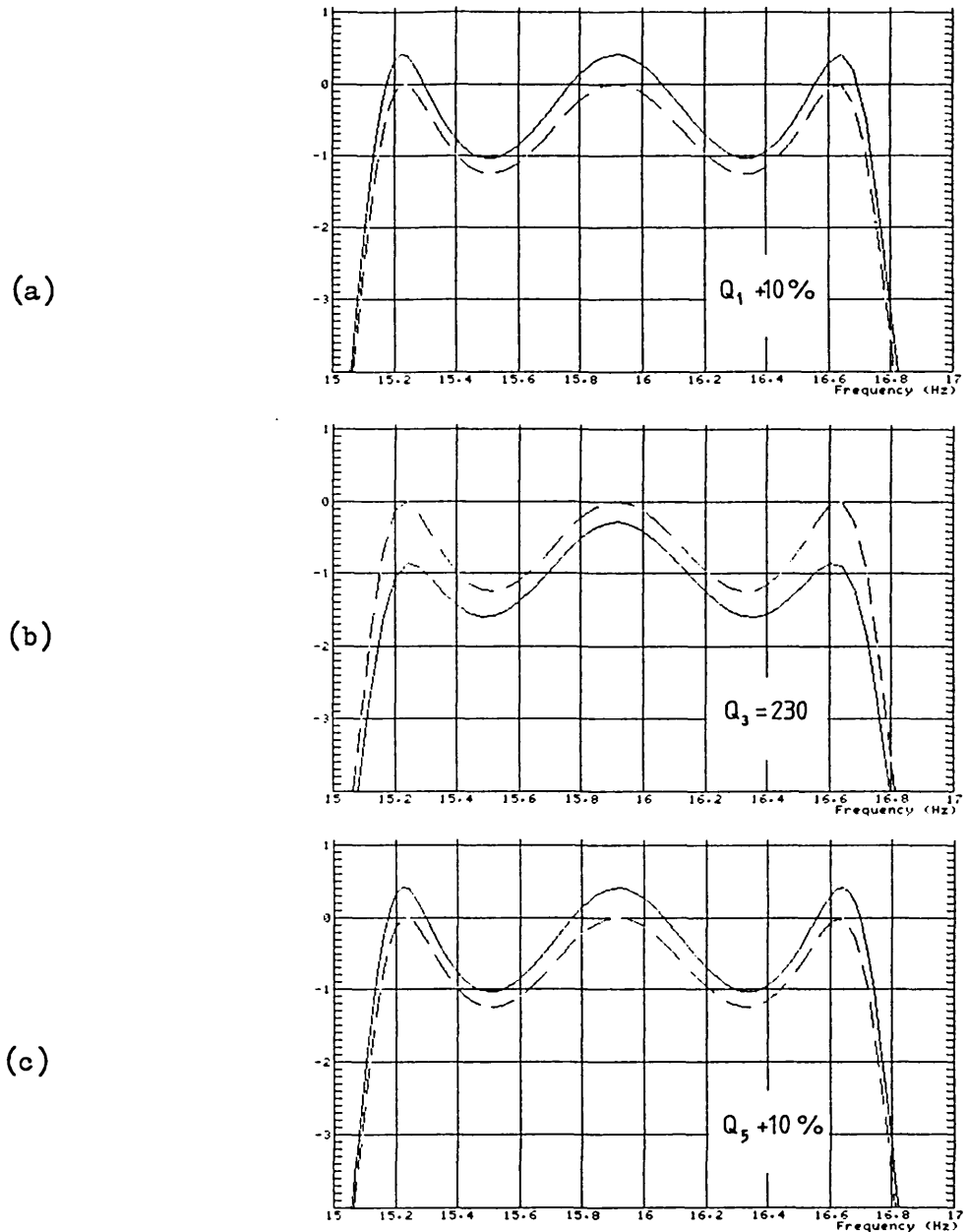


Fig 5.13 Node-voltage simulation sensitivity to changes in Q-factor

- (a)  $Q_1$  increased by 10% from 24.045 to 26.449
- (b)  $Q_3$  reduced from an infinite value to 230
- (c)  $Q_5$  increased by 10% from 24.045 to 26.449

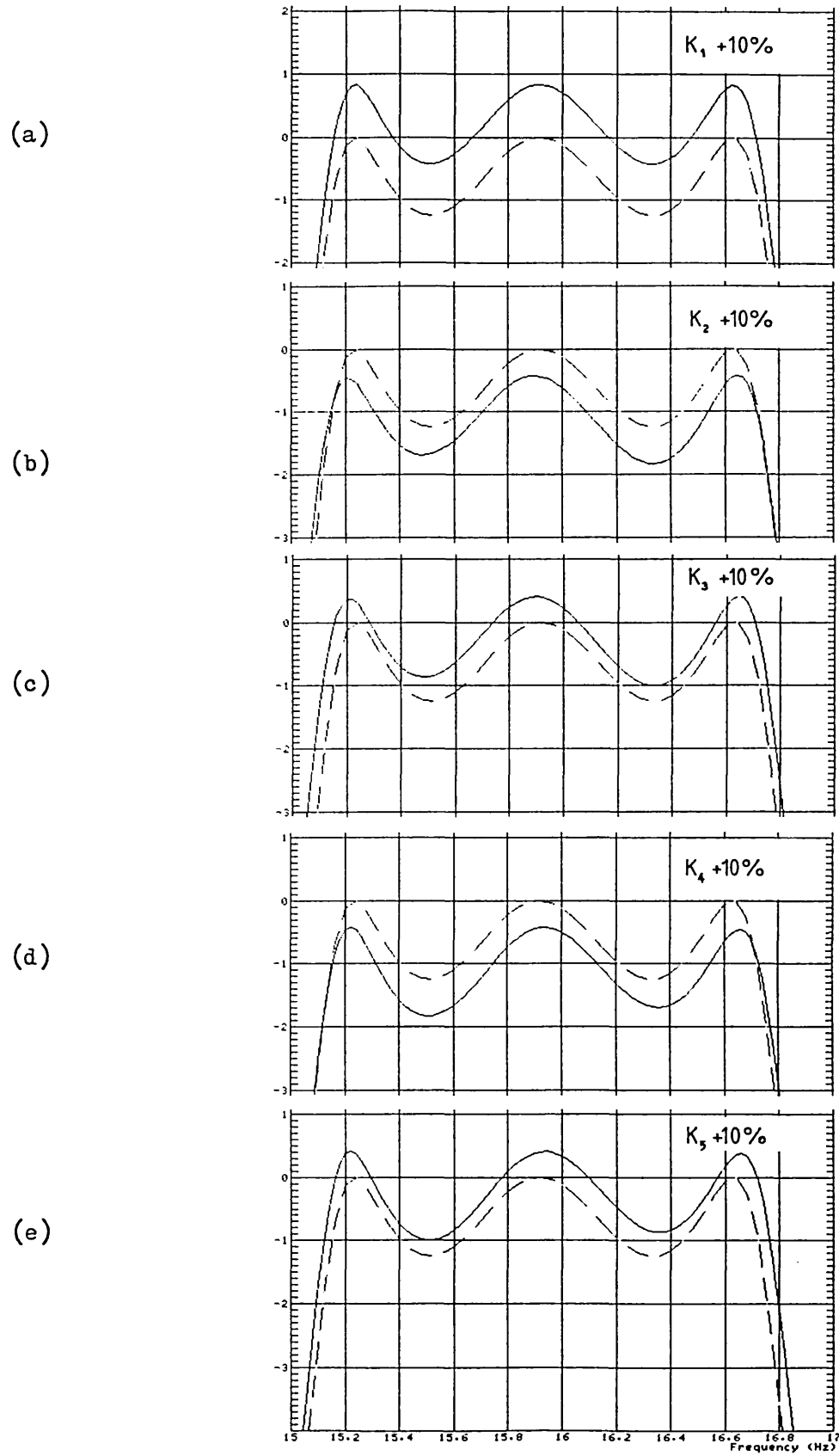


Fig 5.14 Node-voltage simulation sensitivity to changes in gain constants

bands, but over the remainder of the passband the cascade structure exhibits a larger level shift and a greater slope distortion. The stopband sensitivity of the two structures is substantially the same, which is not surprising since in both cases the transmission zeros are produced by series notch sections. As in the case of the cascade structure, all resonance frequencies associated with a particular section have been changed simultaneously to produce the results shown in Fig 5.11. So for example in Section-2 the three frequencies  $\omega_{o3}$ ,  $\omega_{n3}$  and  $\omega_{n4}$  have been increased together by 3% to produce the perturbed response shown in Fig 5.11(b). This response is approximately the additive composition of the three responses shown in Fig 5.12, which are the result of separate changes to the three frequencies.

Changes in the Q-factors of sections 1 and 3 again cause less distortion of the passband response than do corresponding changes in the cascade structure. As can be seen from Fig 5.13(a) and (c), the effect is mainly a slight shift of signal level, which is usually of less importance than a distortion of the passband shape. The second section has a nominally infinite Q-factor which cannot be changed in the same manner. In order to illustrate the sensitivity of the passband response to changes in the value of this Q-factor, the perturbed response in Fig 5.13(b) shows the effect of reducing  $Q_3$  from an infinite value to a somewhat arbitrarily chosen value of 230. The resulting distortion is comparable to that observed in the cascade structure.

A 10% increase in the value of each of the gain constants  $K_1$  to  $K_5$  causes a slight shift of level and a very small distortion of the passband shape, as shown in Fig 5.14. The response shown in Fig 5.14(a) is the same as that obtained for a 10% increase in a gain constant of the cascade structure. All the other perturbations shown in Fig 5.14 are smaller.

The structure produced by node-voltage simulation is easily derived from the appropriate LCR ladder filter. Comparison of the active CR realization in Fig 5.10(c) with the realization of the cascade structure in Fig 5.1(b) shows that the improved block-diagram sensitivities at passband frequencies are achieved at the cost of very few extra components.

### 5.3.2 Coupled-biquad structure

Now we move on to consider the leapfrog feedback structures which

incorporate transmission zeros by means of parallel forward paths. Referring to Fig 4.3, it can be seen that the two cases of feedforward to the output (Fig 4.3(b)) and feedforward from the input (Fig 4.3(c)) can be taken together because they are related by FGR, and we have pointed out in Section 3.3 that block diagram sensitivities are invariant under the transformation of FGR. Noting that feedforward to the output requires the use of an extra summing amplifier section, we choose to study feedforward from the input.

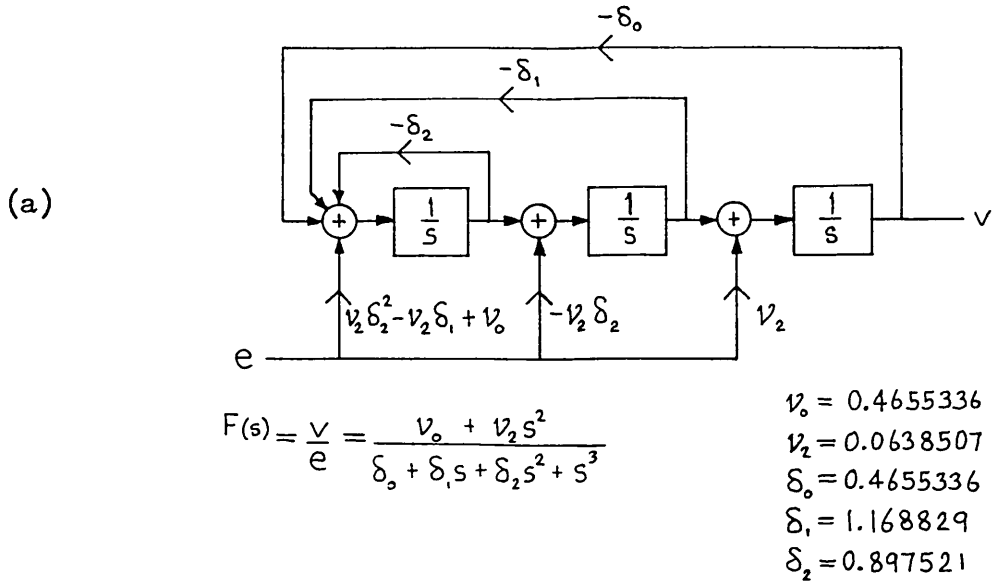
Following the procedure given by Tow & Kuo in Ref. 49, we start with a 'follow the leader feedback' representation of the lowpass transfer function (5.1.1) shown in Fig 5.15(a) (this representation is known from work on analogue computing [46]), and apply the similarity transformation (3.5.1) described in Section 3.5\*. By constructing a transformation matrix  $\mathcal{U}$  such that the matrix  $\mathcal{U}^{-1}\mathcal{A}\mathcal{U}$  is tri-diagonal, the transformed structure has leapfrog feedback as shown in Fig 5.15(b). Although general methods are available [151,152, 153], in this simple example the transformation matrix  $\mathcal{U}$  is produced by the coefficient matching technique described by Tow & Kuo [49]. Taking the structure shown in Fig 5.15(b), we incorporate the path  $a_{11}$  into its associated block so that the transfer function of that block becomes  $1/(s - a_{11})$ , and similarly with the path  $a_{33}$ . Then lowpass to bandpass transformation (5.1.2) and frequency scaling (5.1.4) produce the required bandpass structure. Use is made of the scaling transformation to reduce the number of inverting amplifiers required, and the resulting block diagram is shown in Fig 5.16(a). This is called a Coupled Biquad Configuration by Tow & Kuo. One possible realization of the block diagram is shown in Fig 5.16(b) and the frequency responses are shown in Fig 5.16(c).

The design method is such that the end blocks have a finite Q-factor and the centre block has an infinite Q-factor, as would be the case for a simulation of a doubly terminated LC ladder. Other methods of tri-diagonalization can produce structures which have finite Q-factors for all blocks [51]. Unlike the structure produced by

---

\* Tow & Kuo present their method in terms of state variable equations rather than the matrix representation used in Section 3.5. The difference however is in this case entirely one of presentation; the similarity transformation is identical. Referring to the general structure in Section 2.2.1, if all the blocks are integrators  $g(s) = 1/s U$ , then the state-variable equations (with zero initial conditions) are:  $\frac{d}{dt} \tilde{x}(t) = \mathcal{A} \tilde{x}(t) + b e(t)$

$$v(t) = c_t \tilde{x}(t) + d e(t)$$



$$y = \begin{bmatrix} 1 & a_{33} & a_{33}^2 + a_{12} \\ 0 & 1 & a_{33} \\ 0 & 0 & 1 \end{bmatrix}$$

$\delta_0 = a_{12} (a_{11} + a_{33})$
$\delta_1 = a_{11} a_{33} - 2 a_{12}$
$\delta_2 = -(a_{11} + a_{33})$

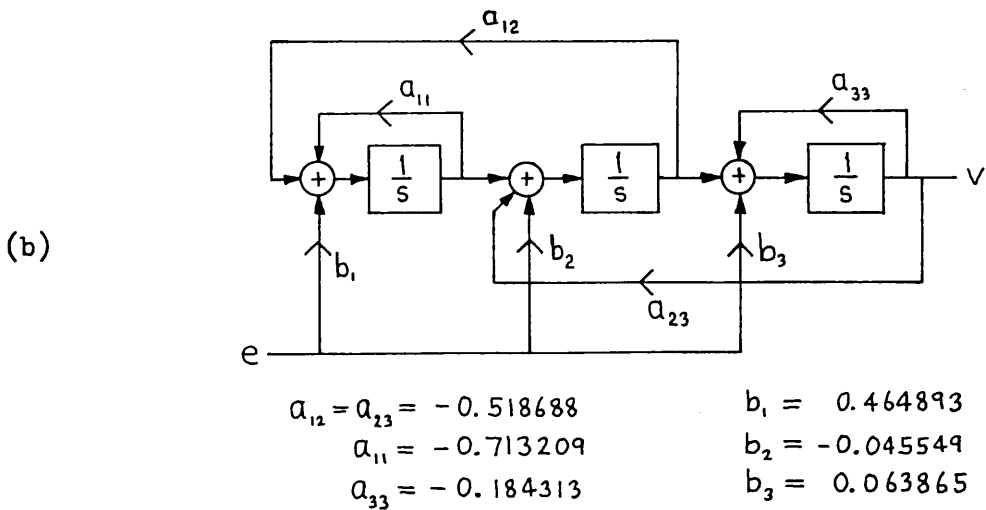


Fig 5.15 Design of Coupled-Biquad structure [49]

- (a) Follow the leader feedback representation of lowpass transfer function [46]
- (b) Structure obtained by use of similarity transformation (3.5.1)

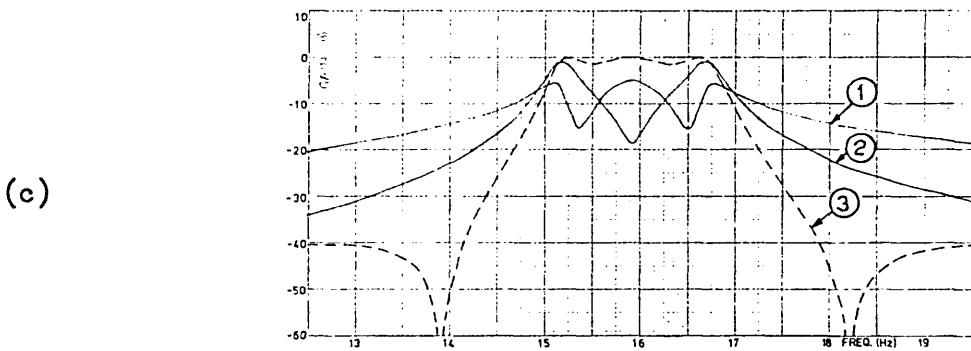
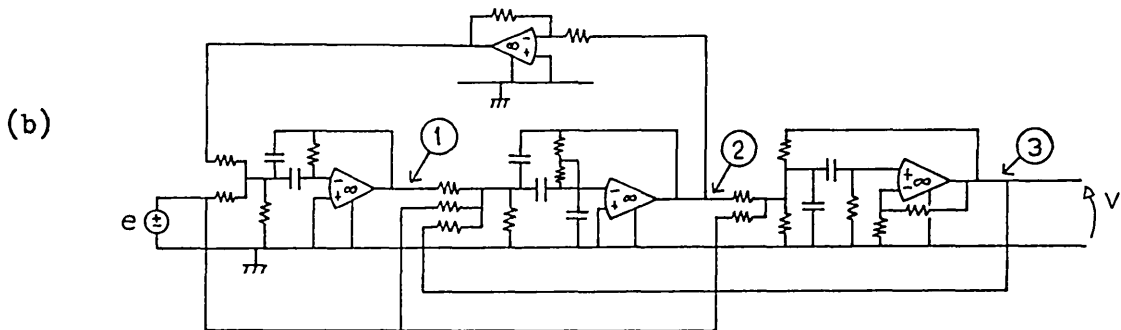
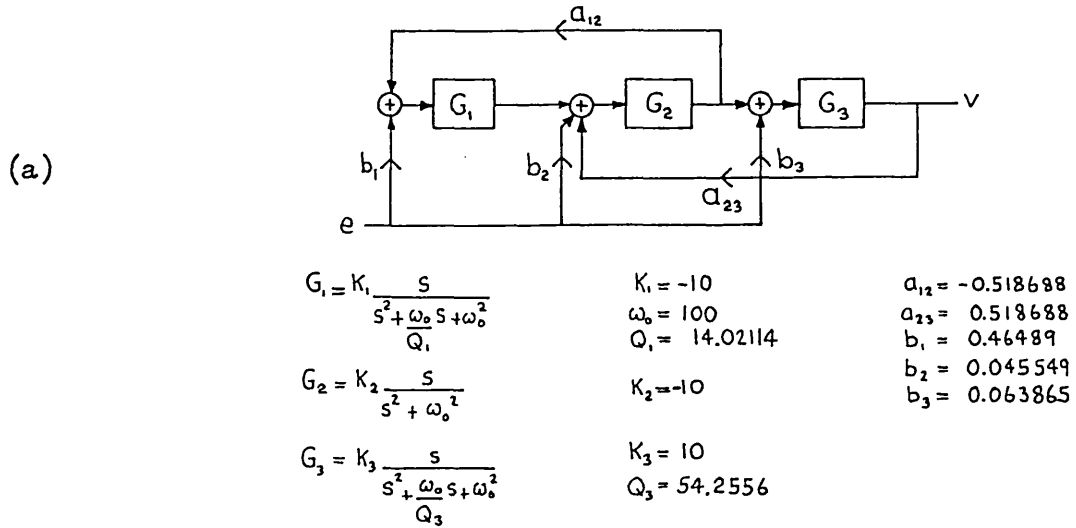


Fig 5.16 Coupled Biquad structure [49]

- (a) Block diagram
- (b) Active CR realization
- (c) Computed frequency responses

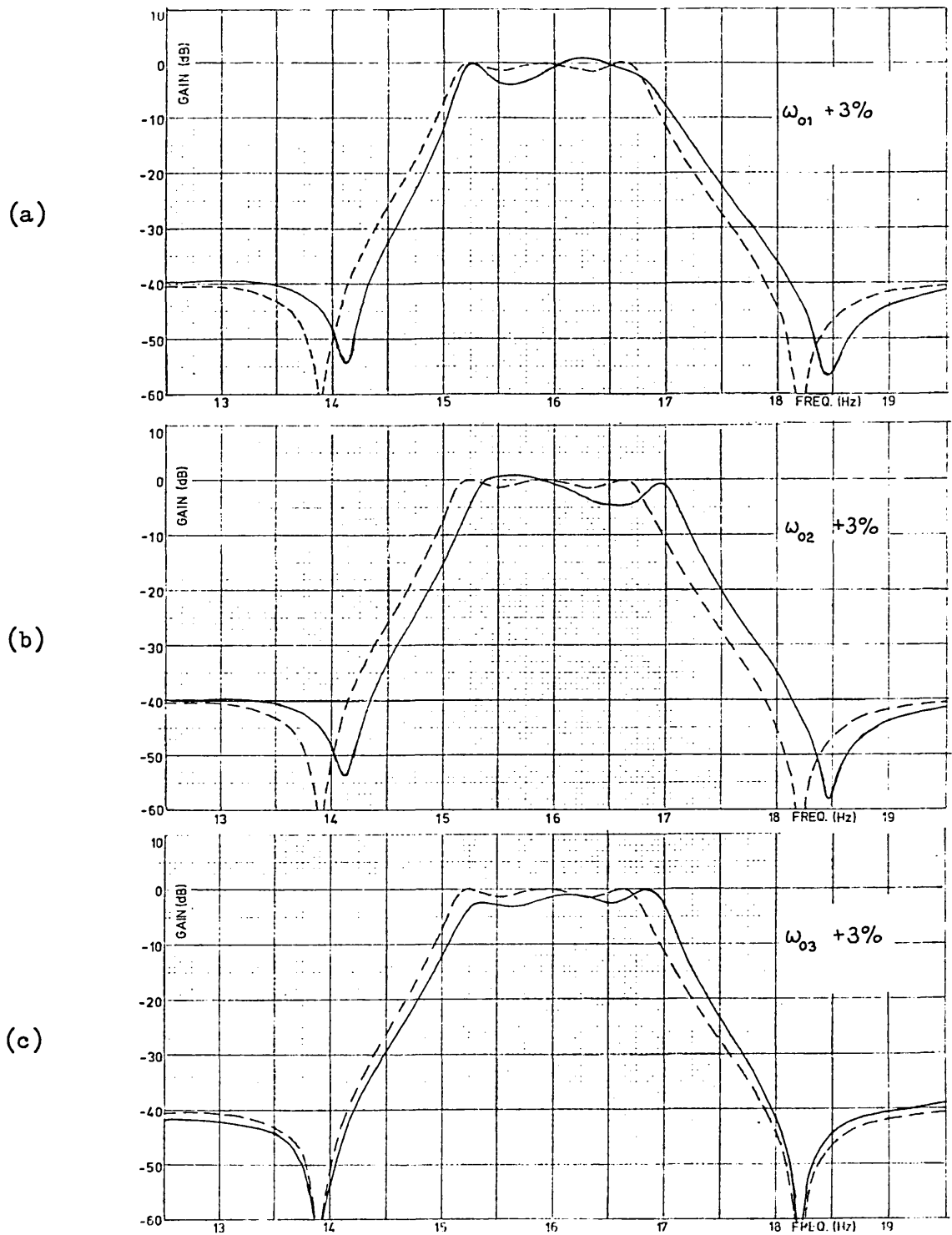


Fig 5.17 Coupled Biquad structure sensitivity to changes in resonance frequency

- (a)  $\omega_{01}$  increased by 3% from 100 to 103
- (b)  $\omega_{02}$  increased by 3% from 100 to 103
- (c)  $\omega_{03}$  increased by 3% from 100 to 103

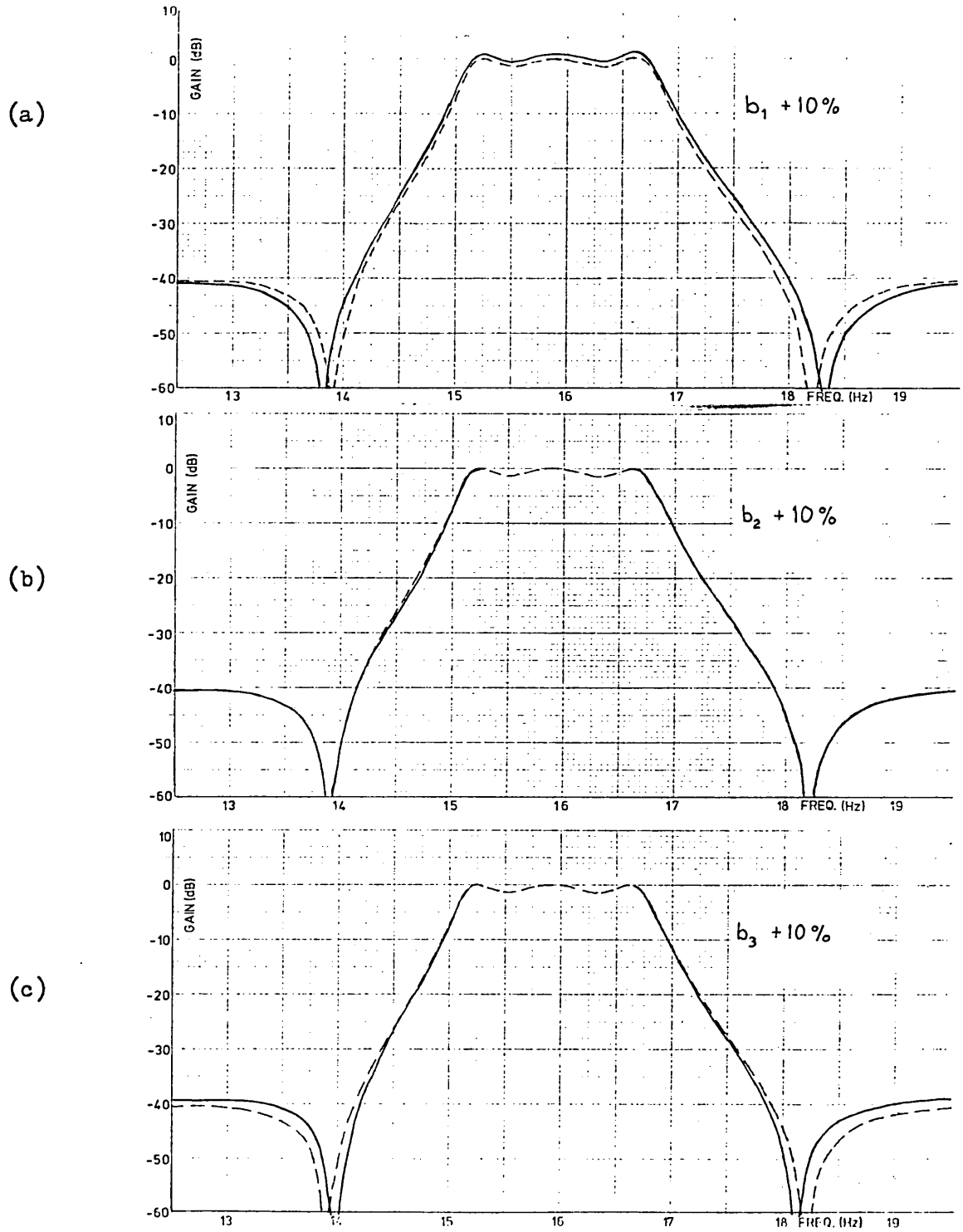


Fig 5.18 Coupled Biquad structure sensitivity to changes in feedforward constants

- (a)  $b_1$  increased by 10% from 0.46489 to 0.511383
- (b)  $b_2$  increased by 10% from 0.045549 to 0.050104
- (c)  $b_3$  increased by 10% from 0.063865 to 0.0702516



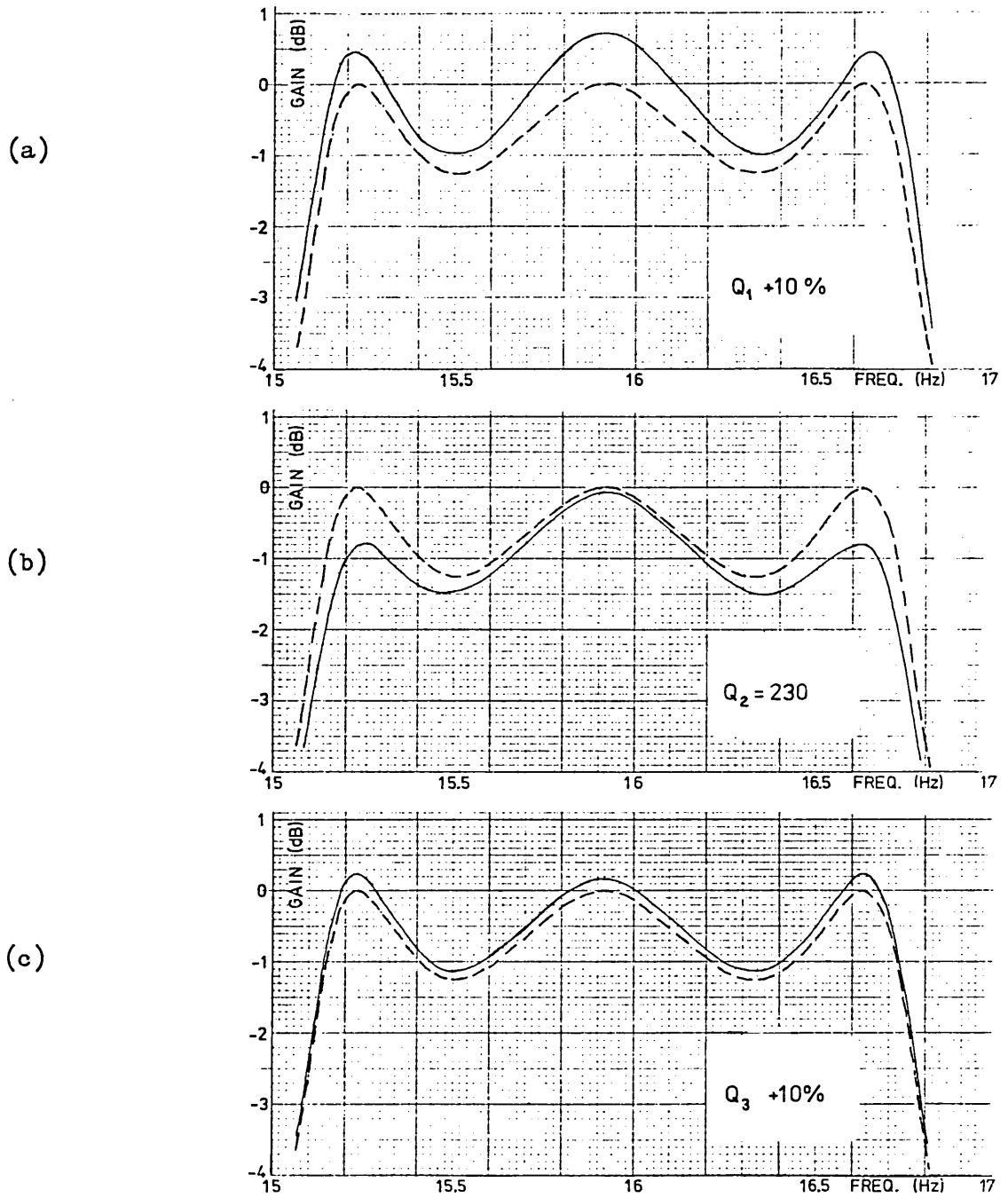


Fig 5.19 Coupled Biquad structure sensitivity to changes in  $Q$ -factor

- (a)  $Q_1$  increased by 10% from 14.021 to 15.423
- (b)  $Q_2$  reduced from an infinite value to 230
- (c)  $Q_3$  increased by 10% from 54.256 to 59.681

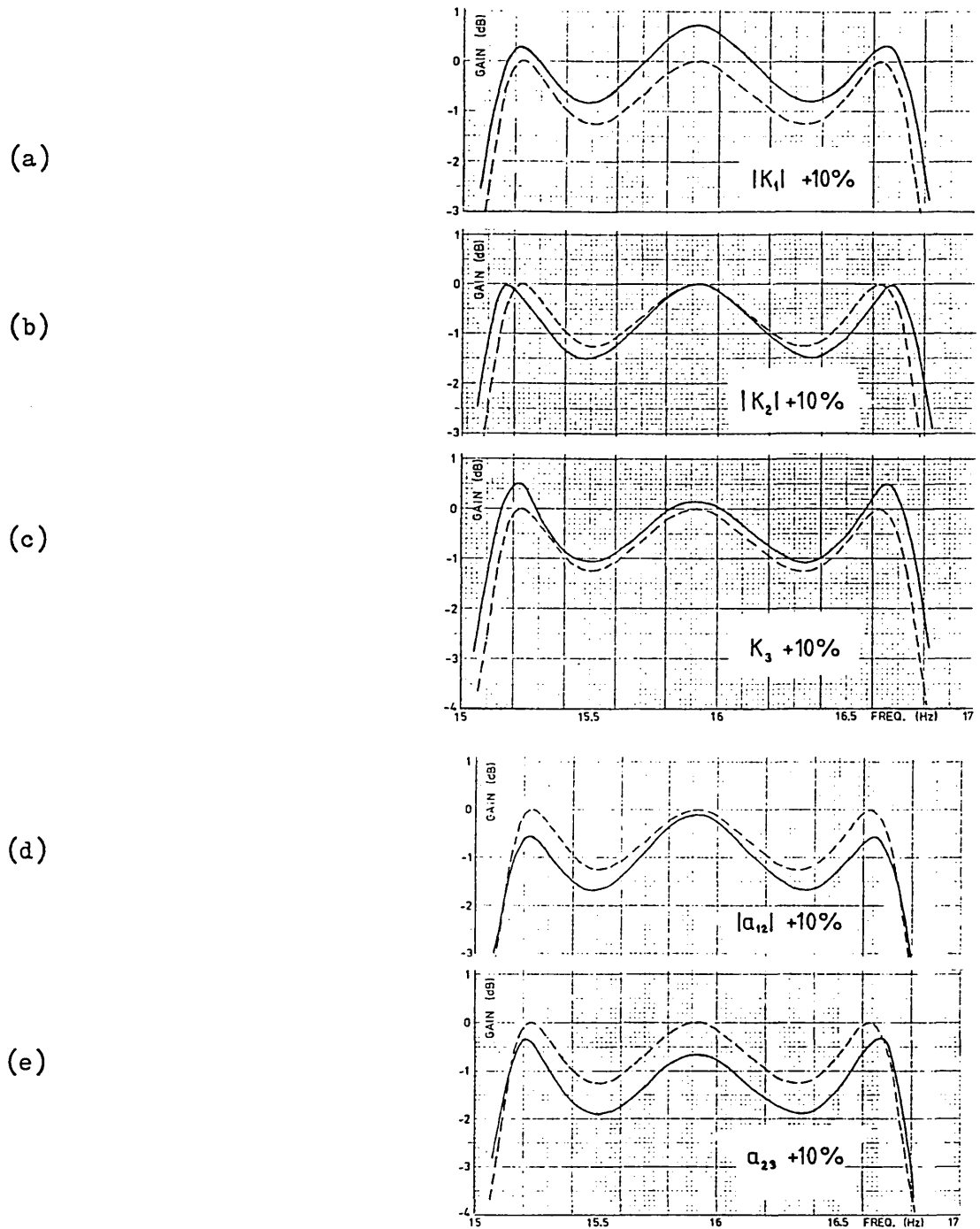


Fig 5.20 Coupled Biquad structure sensitivity to changes in gain constants and feedback factors

- (a)  $|K_1|$  increased by 10% from 10 to 11
- (b)  $|K_2|$  increased by 10% from 10 to 11
- (c)  $K_3$  increased by 10% from 10 to 11
- (d)  $|a_{12}|$  increased by 10% from 0.518688 to 0.570556
- (e)  $a_{23}$  increased by 10% from 0.518688 to 0.570556

node-voltage simulation, all blocks of the Coupled Biquad structure have the same resonance frequency.

The effect of increasing the resonance frequencies of each of the three blocks by 3% is shown in Fig 5.17. Although the Coupled Biquad structure is not a simulation of an LCR ladder, the resulting deviations in the passband are comparable to those observed in the node-voltage simulation. In the stopbands however, there are differences arising from the different method of producing transmission zeros. Section-1 and section-2 both affect the two transmission zeros, and a 3% increase in the resonance frequency  $\omega_0$  of either section produces slightly less than  $1\frac{1}{2}\%$  increase in the frequency of the notches. If changes in the two resonance frequencies are uncorrelated then there is some possibility for cancellation, and a statistical measure of block diagram sensitivity may indicate that there is a reduction of stopband sensitivity compared with any structure using series notch sections [125]. This improvement is somewhat illusory because if both  $\omega_{01}$  and  $\omega_{02}$  are increased by 3% simultaneously, then the notch frequencies will also increase by an average of 3%. Indeed the worst case is slightly inferior to that for series notch sections, because, given that the changes in  $\omega_0$  for the coupled biquad structure are the same as the change in  $\omega_n$  for a structure using series notch sections, there is in the Coupled Biquad structure an additional dependence on the values of the forward path constants  $b_1$  and  $b_3$  as shown in Fig 5.18, and on the values of  $K_1$  and  $K_2$  (not illustrated). It was found for example that, whilst the average deviation of the two notch frequencies did not exceed  $3\frac{1}{4}\%$ , a 10% variation in these constants in addition to the 3% variation of resonance frequencies could, in the worst case, cause the lower transmission zero to deviate by  $6\frac{1}{2}\%$ . It should also be noted from Fig 5.17(a) and (b) that a change in resonance frequency reduces the depth of the notches. The extent to which the notch depth is reduced by a series notch section depends on the nature of the section used.

Since deviations in the frequencies of the transmission zeros have a dominant effect on the stopband response, it is to be expected on the basis of the foregoing results that the Coupled Biquad structure has a higher worst case stopband sensitivity than a leapfrog feedback structure having series notch sections. Conversely, for the same two structures, it is possible for a statistical measure of stopband sensitivity to indicate that the Coupled Biquad structure has a lower variance. Statistical analyses therefore need to be interpreted with

caution. Comparison of the foregoing results with the responses shown in Fig 5.5 however, indicates that the embodiment of parallel forward paths in the Coupled Biquad structure leads to a much lower stopband sensitivity than the arrangement of parallel forward paths in the partial fraction structure.

Changes in the Q-factors of the sections produce the responses shown in Fig 5.19, and changes in the gain constants and feedback factors are shown in Fig 5.20. These are all of a similar nature to the corresponding responses of the node-voltage simulation.

### 5.3.3 Ford's structure

We now consider leapfrog feedback used together with a different arrangement of parallel forward paths. Starting with the LCR realization of the lowpass transfer function (5.1.1) shown in Fig 5.21(a), a leapfrog feedback structure is produced by simulation and subsequent use of SFG equivalents as was illustrated in Fig 3.2. A lowpass filter having the structure shown in Fig 3.2(h) was attributed to Ford in Ref 17. Use of the lowpass to bandpass transformation (5.1.2), and frequency scaling (5.1.4) leads to an interconnection of three bandpass quadratic sections and one summing amplifier section, shown as a block diagram in Fig 5.21(b), and as an active CR realization in Fig 5.21(c). As in the Coupled Biquad structure, all three quadratic blocks have the same resonance frequency  $\omega_0$ , and the centre block  $G_2$  has an infinite Q-factor.

Since SFG equivalents have been used to change the structure from the basic simulation, it is of interest to see how this affects the sensitivity performance. We note that in the LC ladder filter (Fig 5.21(a)) the finite transmission zero is introduced by the inclusion of a modifying capacitor  $C_2$ . If we put  $C_2 = 0$  then in the block diagram (Fig 5.21(b)) the paths  $b_3$ ,  $a_{31}$ ,  $a_{34}$  are eliminated, and  $G_3$  becomes equal to  $-1$  (this is evident from Fig 3.2(h)). The structure then reduces to the basic leapfrog feedback simulation shown in Fig 1.5, the sensitivity of which has been studied by several authors e.g. Adams [19]. By analogy with the LC filter we expect that putting  $b_3 = a_{31} = a_{34} = 0$  and  $G_3 = -1$  will have little effect on the response at passband frequencies, and this is confirmed in Fig 5.22. It follows that in this example, the low passband sensitivity expected of a leapfrog feedback simulation will not be degraded by the manipulations that have been performed on the

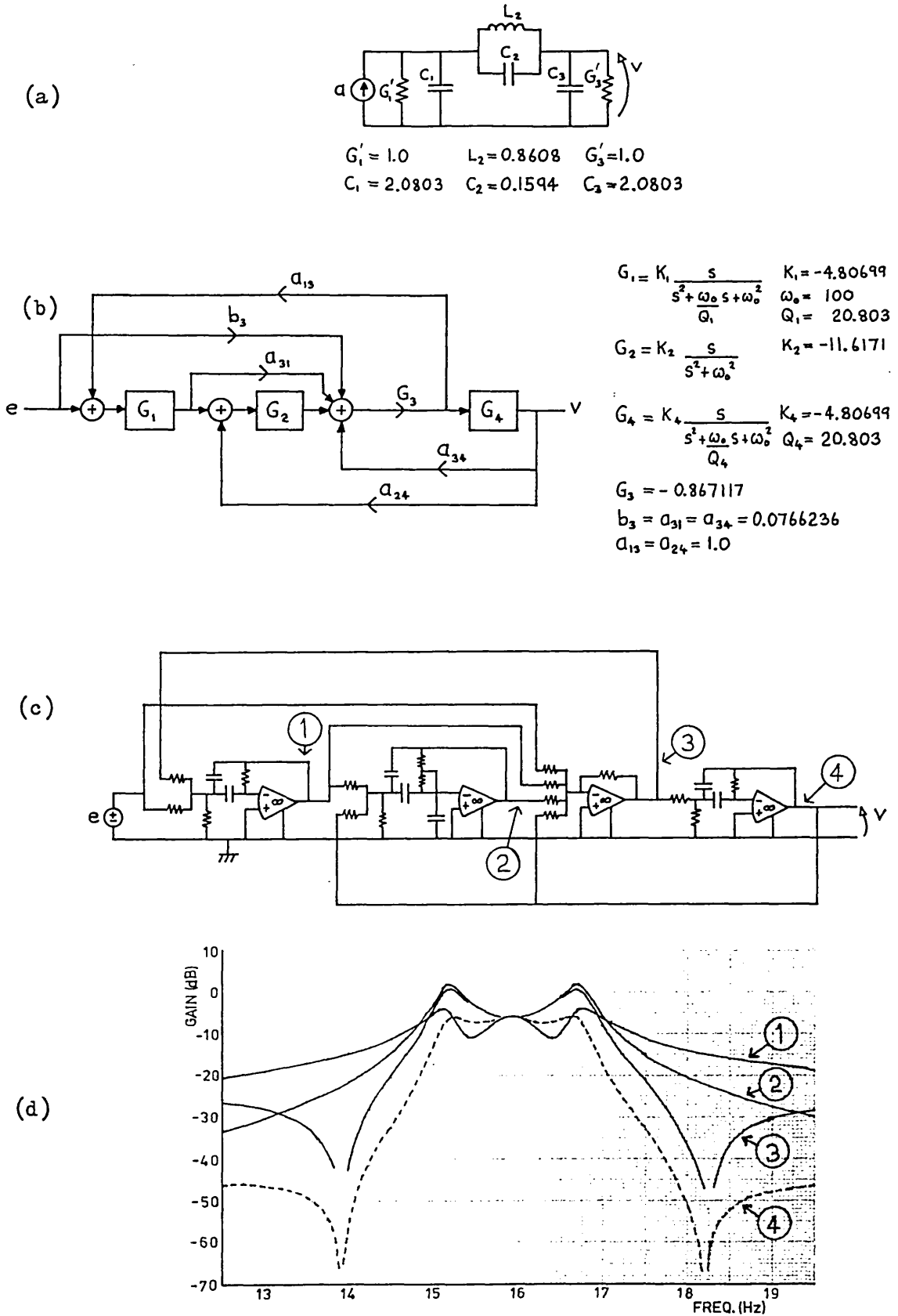


Fig 5.21 Ford's structure [17,84]

- (a) LCR filter
- (b) Block diagram
- (c) Active CR realization
- (d) Computed frequency responses

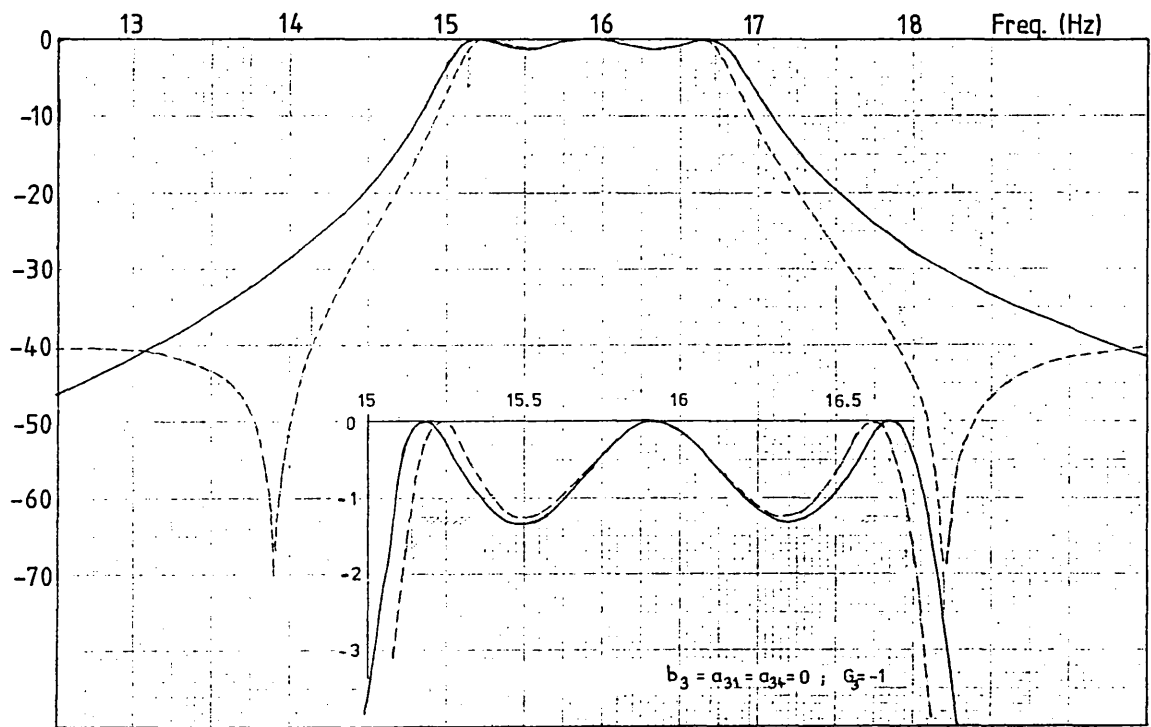


Fig 5.22 Frequency response of Ford structure with  $b_3 = a_{31} = a_{34} = 0$   
and  $G_3 = -1$

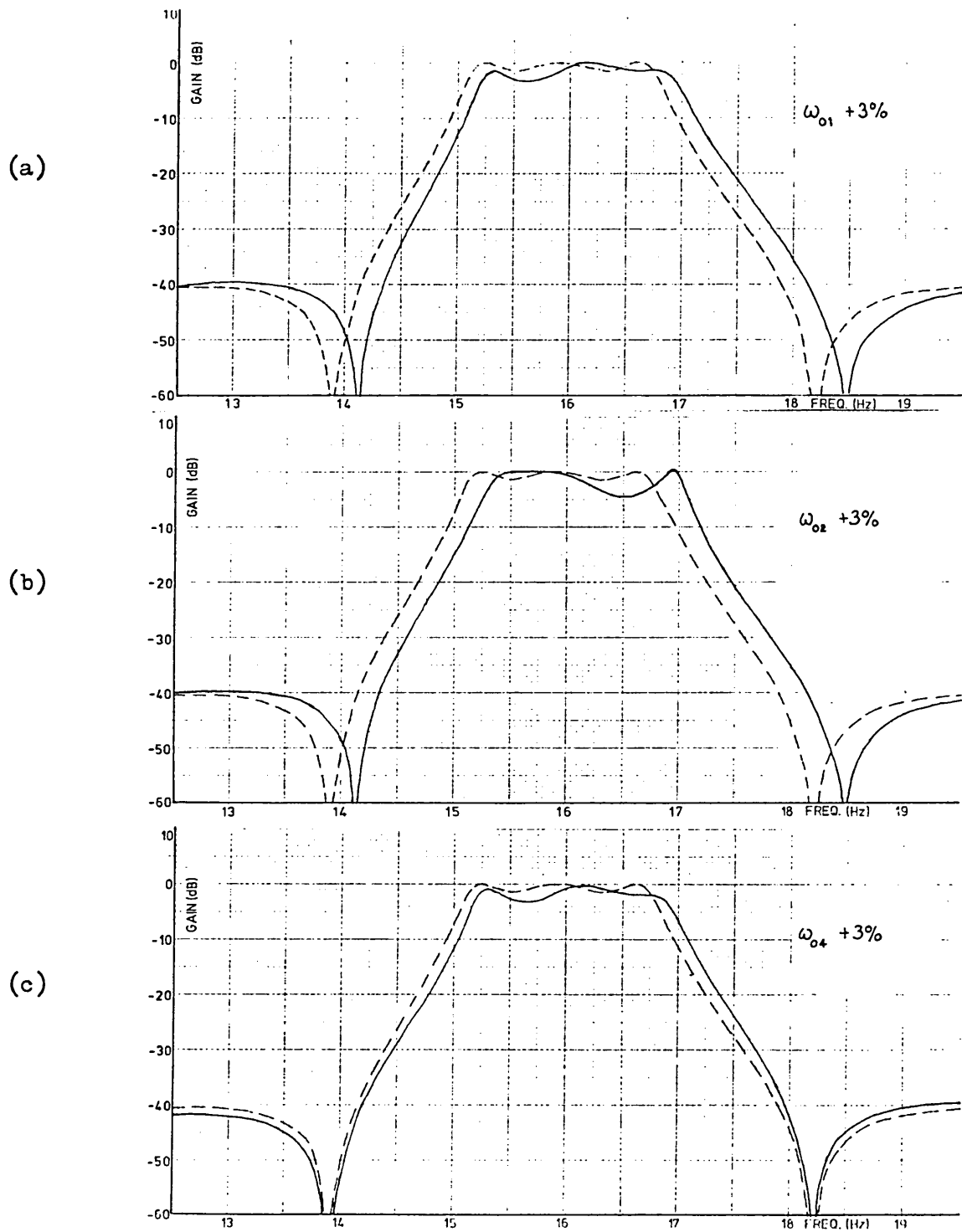


Fig 5.23 Ford structure sensitivity to changes in resonance frequency

- (a)  $\omega_{01}$  increased by 3% from 100 to 103
- (b)  $\omega_{02}$  increased by 3% from 100 to 103
- (c)  $\omega_{04}$  increased by 3% from 100 to 103

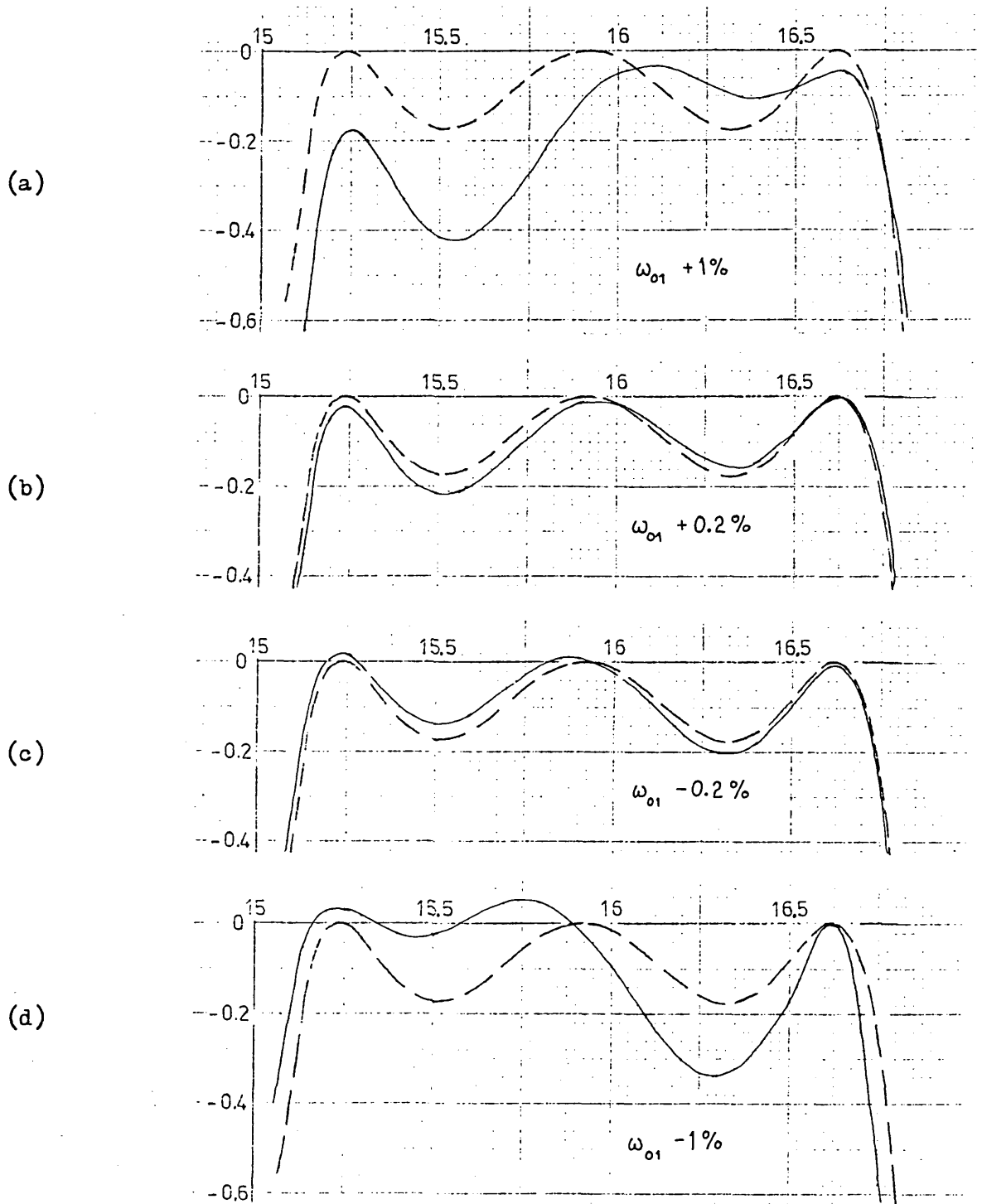


Fig 5.24 Ford structure with 0.2dB nominal passband ripple

- (a)  $\omega_{o1}$  increased by 1%
- (b)  $\omega_{o1}$  increased by 0.2%
- (c)  $\omega_{o1}$  reduced by 0.2%
- (d)  $\omega_{o1}$  reduced by 1%



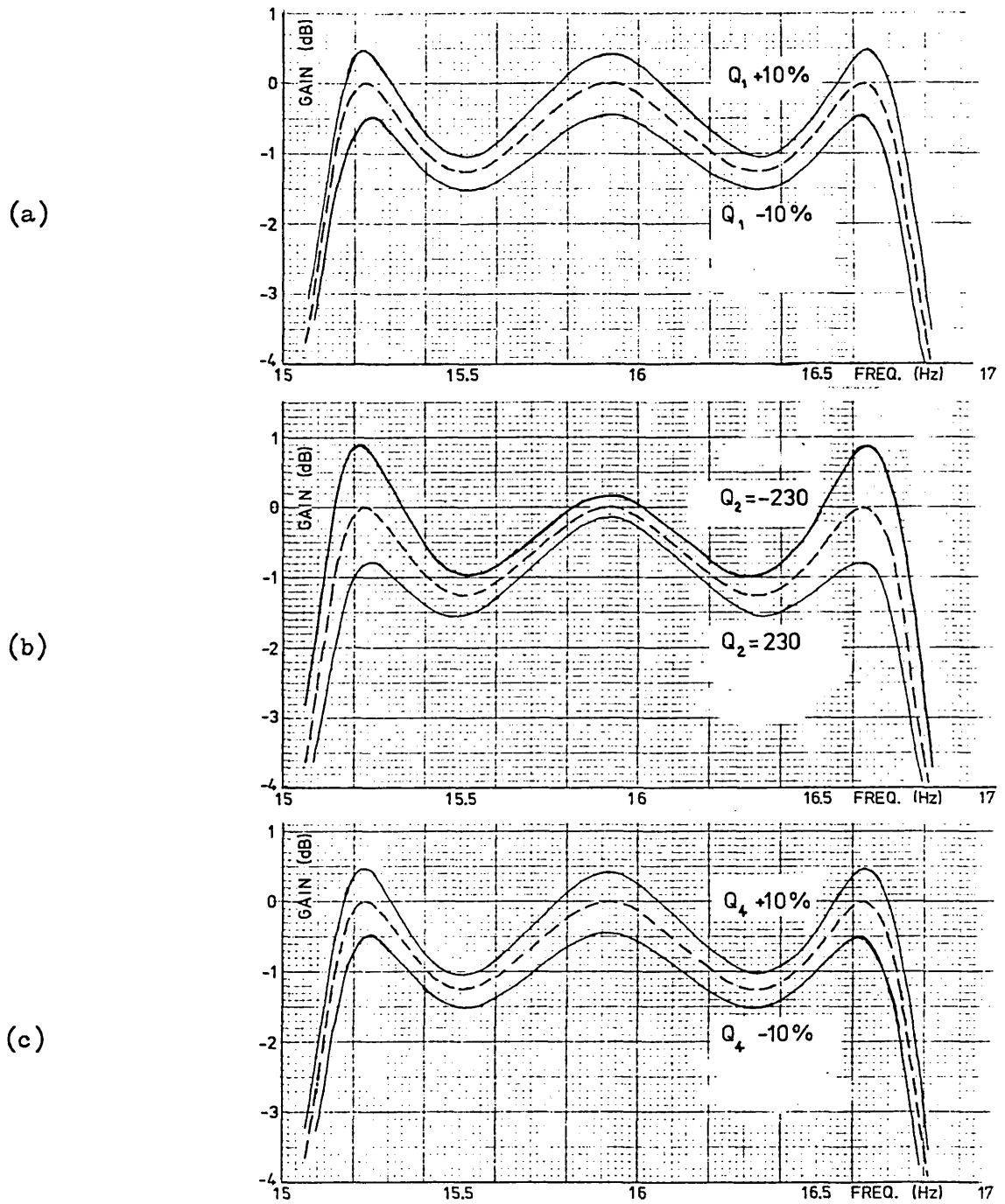


Fig 5.25 Ford structure sensitivity to changes in  $Q$ -factor

- (a)  $Q_1$  increased by 10% from 20.803 to 22.883
- (b)  $Q_2$  changed from an infinite value to a value of 230, and also a value of -230
- (c)  $Q_4$  increased by 10% from 20.803 to 22.883

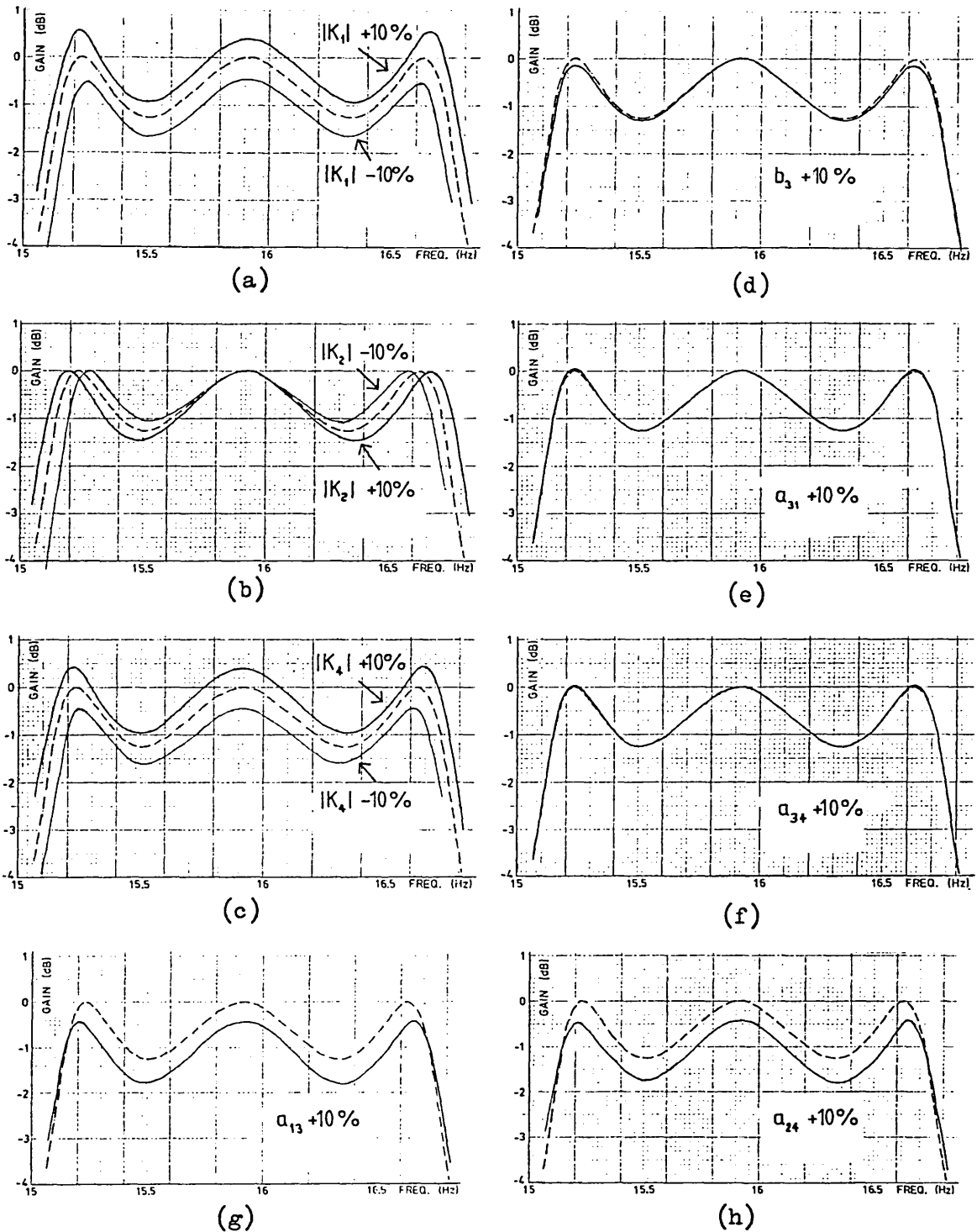


Fig 5.26 Ford structure sensitivity to changes in gain constants

- (a)  $|K_1|$  increased by 10% from 4.8069 to 5.2877
- (b)  $|K_2|$  increased by 10% from 11.617 to 12.778
- (c)  $|K_4|$  increased by 10% from 4.8069 to 5.2877
- (d)  $b_3$  increased by 10% from 0.0766 to 0.08428
- (e)  $a_{31}$  increased by 10% from 0.0766 to 0.08428
- (f)  $a_{34}$  increased by 10% from 0.0766 to 0.08428
- (g)  $a_{13}$  increased by 10% from 1.0 to 1.1
- (h)  $a_{24}$  increased by 10% from 1.0 to 1.1

SFG in order to realize the transmission zeros by means of parallel forward paths. The stopband sensitivity of the Ford structure however cannot be related to that of a passive ladder filter, and furthermore no results have previously been published on the stopband performance of the Ford structure.

The frequency responses of the bandpass Ford structure are shown in Fig 5.21(d). The  $-6.02\text{dB}$  midband gain resulting from the simulation may of course be adjusted by use of the scaling transformation in order to improve dynamic range. All subsequent graphs have been scaled so that the nominal midband gain is  $0\text{dB}$ , for uniformity of presentation.

The effect of increasing the resonance frequency  $\omega_0$  of each of the three quadratic blocks by 3% is shown in Fig 5.23. The resulting deviations at frequencies in the passband are less than those for the node-voltage simulation or the Coupled Biquad structure. In fact the Ford structure has the lowest passband sensitivity of all the structures studied in this Chapter. One noticeable feature, not found in the other structures, is that the perturbed response (Fig 5.23) nowhere exceeds  $0\text{dB}$ . This is also true for the case of  $\omega_0$  being reduced by 3%, although these responses are not shown here. Such behaviour appears to be in accordance with Orchard's theory described in Section 1.1. There is however no reason to expect that changes in  $\omega_0$  alone would conform to the Orchard theory, because such a change does not have a counterpart in the LC ladder filter (see Fig 1.5(a) and (b)). A change in the value of a reactive element of the passive ladder filter would correspond to simultaneous changes in the values of  $\omega_0$ ,  $Q$  and possibly  $K$  in the leapfrog feedback simulation. To investigate this further, the writer has studied a Ford structure implementing a 6-th degree elliptic function bandpass transfer function similar to (5.1.5) but having  $0.2\text{dB}$  nominal passband ripple instead of  $1.25\text{dB}$ . Fig 5.24 shows the effect of various changes to the value of  $\omega_{01}$  for the first section, and from this it can be seen that some responses are slightly in excess of  $0\text{dB}$ . Similar responses were observed by Adams [19] for a leapfrog feedback simulation of the type shown in Fig 1.5. Whilst this detailed examination shows that Orchard's theory does not apply to changes in  $\omega_0$ , it remains true that the resulting distortion of the passband response is relatively small.

Returning to the structure shown in Fig 5.21, and the responses in Fig 5.23, we see that the stopband sensitivity is similar in nature to that of the Coupled-Biquad structure, but rather better than the

Coupled Biquad structure in respect of preserving the depth of the notches. In both structures the transmission zeros are produced by parallel forward paths which span two of the quadratic blocks. It is relevant to note that for higher order filters, the parallel forward paths in the Ford structure will never individually encompass more than two quadratic blocks, whereas in the Coupled Biquad structure, if the response has one zero at the origin and one at infinity, then parallel forward paths will span all but one of the blocks. This has been reported to lead to an unacceptably high stopband sensitivity in the Coupled Biquad structure [125,158]. For high order filters it seems likely therefore that the Ford structure will have a lower stopband sensitivity than the Coupled Biquad structure. The comments made previously, about comparison of the use of parallel forward paths with the use of series notch sections, apply also to the Ford structure. A statistical measure of block diagram sensitivity may indicate that the Ford structure has a lower standard deviation in the stopband, but the worst case shift of the notch frequencies will be lower in a structure such as the node-voltage simulation which uses series notch sections.

Changes in the  $Q$ -factors of the three quadratic sections produce the responses shown in Fig 5.25. They are similar to those of the Coupled Biquad structure and the node-voltage simulation. The effects on the passband response of changing the values of the remaining constants are shown in Fig 5.26. These again are of a similar nature to the preceding leapfrog feedback structures. In addition,  $K_1$ ,  $K_2$  and  $b_3$  affect the frequency of the notches, but curiously  $a_{31}$  and  $a_{34}$  have very little effect at any frequency.

#### 5.3.4 Leapfrog feedback together with complex feedback

It is possible for a leapfrog feedback structure to incorporate transmission zeros by means of complex feedback [57,58,59], however no example of this structure is studied in this Chapter. Although the method is a direct simulation of a passive ladder filter, the excessive number of sections required and the difficulties associated with implementing reciprocators make it less attractive from the practical point of view.

The design method described in Ref. 58 could have been used here in two ways. Either the lowpass LCR ladder network shown in Fig 5.21(a) could have been simulated, followed by lowpass to bandpass transformation and frequency scaling of the resulting structure, or the

bandpass LCR ladder network shown in Fig 5.10(a) could have been simulated directly. The first case produces the structure shown in Fig 4.3(e), which illustrates the fact that four quadratic sections are needed instead of the three quadratic sections required by the node-voltage simulation, Coupled Biquad and Ford structures. Referring to Fig 4.3(e), the two end blocks have transfer functions which are identical to those used in the Ford simulation, and the two centre blocks  $G_4$  and  $G_5$ , used in conjunction with the reciprocator  $G_2 \rightarrow \infty$ , are infinite-Q bandpass sections, producing transmission zeros by complex feedback as described in Section 1.4. The second case referred to above leads to a slightly different structure (see Fig 5.27), but again four quadratic sections are needed. The extra section arises as a consequence of the LCR ladder network being non-canonic in the number of elements. Doblinger [144] has studied the simulation of canonic Brune-sections.

In the commonly used doubly-terminated LC ladder networks the occurrence of cutsets containing capacitors only, and also the occurrence of loopsets containing inductors only, both lead to unobservable and uncontrollable natural frequencies at the origin of the  $s$ -plane. Whilst this is of no consequence for a passive filter, in a direct simulation it leads to operational amplifiers having an uncontrolled d.c. output level. For example the lowpass LCR network shown in Fig 5.21(a) has neither a loopset of inductors nor a cutset of capacitors, and the lowpass simulation in the structure of Fig 4.3(e) is satisfactory at zero frequency. However the bandpass transformation of the network in Fig 5.21(a) has a loopset containing inductors only, and in the bandpass versions of the structures shown in Fig 4.3(e) and Fig 5.27 there is no d.c. feedback around the infinite gain reciprocator  $G_2$ . Amplifier offset voltages are thus unrestrained unless the structure is modified in some way, but this would depart from direct simulation and in some cases could distort the frequency response. Another difficulty is that the phase response associated with a practical implementation of a reciprocator can lead to high-frequency instability. Martin & Sedra have studied the stabilization of reciprocators [59].

Because it is a simulation of a low-sensitivity LC ladder network, the structure illustrated in Fig 5.27 is likely to have a passband sensitivity similar to the other leapfrog structures studied in this section. Stopband sensitivity however has not been studied, and is likely to depend on the specific structure used. For example

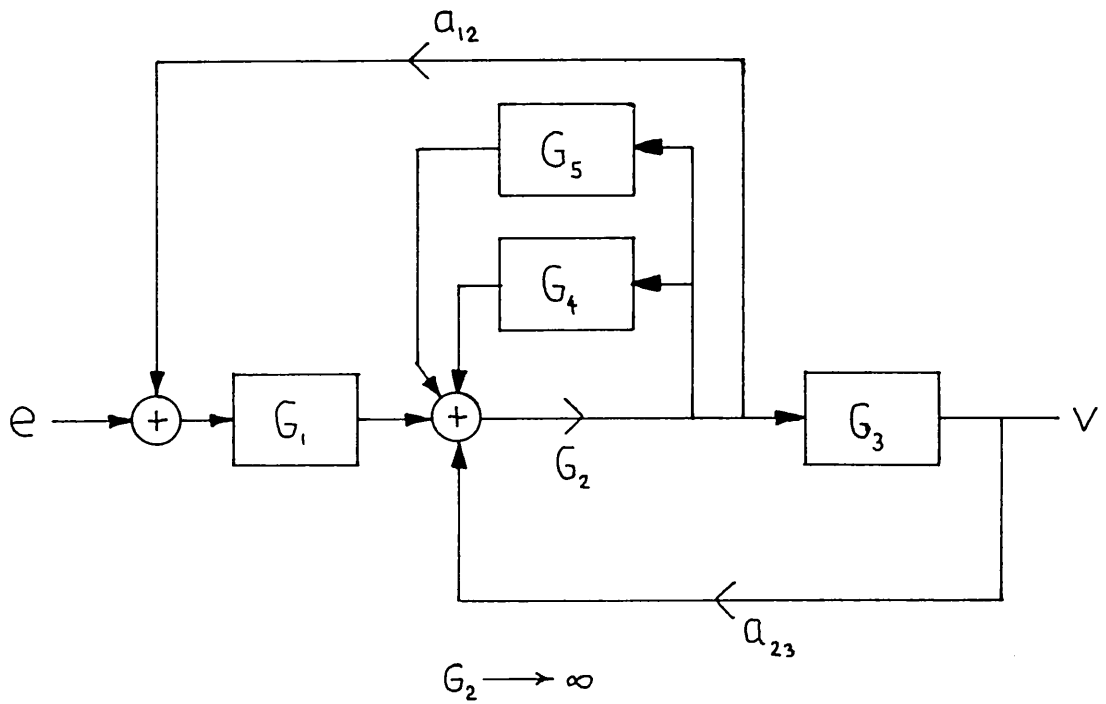


Fig 5.27 Leapfrog feedback together with complex feedback [57]

in Fig 4.3 (e) the part of the structure most affecting the stopbands is associated with the reciprocator. It is similar in form to the continued fraction structure studied in Section 5.2.3. and might therefore have similar sensitivity properties at stopband frequencies. The alternative structure shown in Fig 5.27 will have a stopband sensitivity performance more like that of series notch sections.

## 5.4 Structures having nested feedback loops

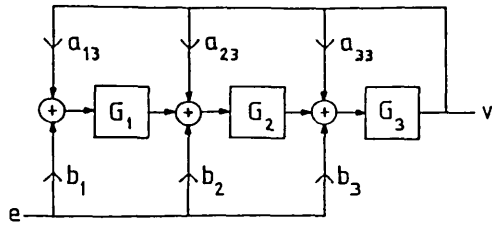
This section presents the sensitivity performance of structures in the third, fourth, and fifth columns of Table 4.1. They all have feedback loops which are nested one inside the other. Results presented here will illustrate the fact that finite difference sensitivity is invariant under the transformation of FGR. Further results will show that there is a common pattern to the sensitivity of structures having nested feedback. It will also be shown that for the simple design procedure described in Section 1.4, the pre-distortion constant  $\alpha_1$  may be chosen for minimum sensitivity.

### 5.4.1 Follow the Leader feedback and its transpose

We start by comparing two structures which are related by the transformation of FGR, without at this stage making any attempt to minimise their sensitivity. The first structure was presented in Section 1.4 as an example of a multiple feedback filter in which the transmission zeros are produced by parallel forward paths. The simple design method described in Section 1.4 has been used to implement the bandpass transfer function (5.1.5), with the pre-distortion constant  $\alpha_1$  chosen to give quadratic blocks having a Q-factor equal to 20. The resulting structure is shown in Fig 5.28. Alongside this, in Fig 5.29, is shown the structure related to it by FGR. It has Follow the Leader feedback and parallel paths fed forward to the output. In both structures the scaling transformation has been used to eliminate the need for inverting amplifiers. This has been achieved by the use of both inverting and non-inverting quadratic sections. Flow graph reversal relates the block diagram parameters of the two structures in accordance with the identities shown in Table 5.1. Note that in both structures the blocks are numbered in sequence from the input to the output, so that for example the first block  $G_1$  of the transpose structure transforms into the last block  $G_3$  of the follow the leader feedback structure.

The effect of increasing the resonance frequencies of each of the three blocks by 3% is shown in Fig 5.30 for the transpose follow the leader feedback structure, and in Fig 5.31 for the follow-the-leader feedback structure. It can be seen that the sensitivities are related by the identities listed in Table 5.1. For example, increasing the resonance frequency  $\omega_{01}$  of the first block  $G_1$  of the transpose structure by 3% produces a perturbed response which is identical to



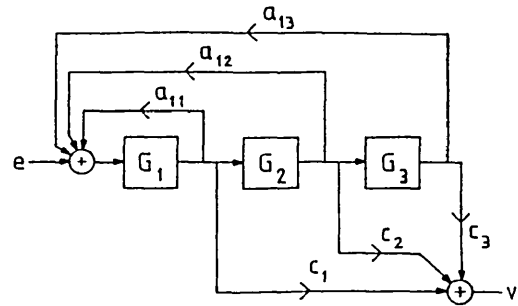


$$\begin{aligned} a_{13} &= 0.019501 & b_1 &= 0.481499 \\ a_{23} &= 1.021308 & b_2 &= 0.063865 \\ a_{33} &= 0.602478 & b_3 &= 0.063865 \end{aligned}$$

$$G_j = K_j \frac{s}{s^2 + \frac{\omega_o}{Q} s + \omega_o^2} \quad j = 1, 2, 3$$

$$\begin{aligned} \omega_o &= 100 & K_1 &= K_2 = -10 \\ Q &= 20 & K_3 &= 10 \end{aligned}$$

(a)

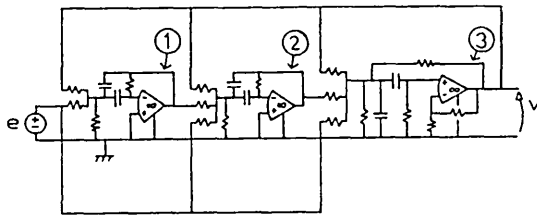


$$\begin{aligned} a_{11} &= 0.602478 & c_1 &= 0.063865 \\ a_{12} &= 1.021308 & c_2 &= 0.063865 \\ a_{13} &= 0.019501 & c_3 &= 0.481499 \end{aligned}$$

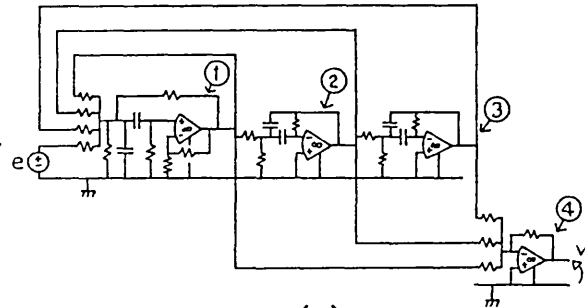
$$G_j = K_j \frac{s}{s^2 + \frac{\omega_o}{Q} s + \omega_o^2} \quad j = 1, 2, 3$$

$$\begin{aligned} \omega_o &= 100 & K_1 &= 10 \\ Q &= 20 & K_2 &= K_3 = -10 \end{aligned}$$

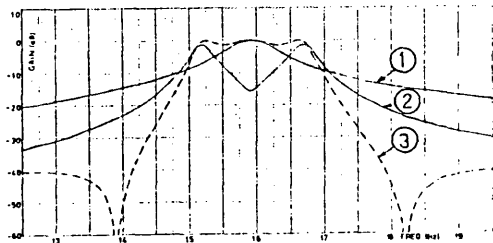
(a)



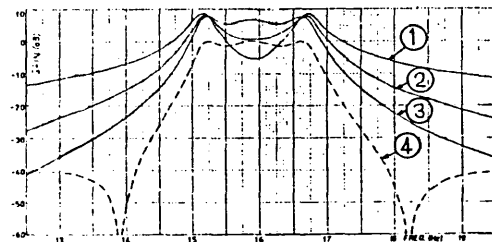
(b)



(b)



(c)



(c)

Fig 5.28 Transpose follow the leader feedback [45]

Fig 5.29 Follow the leader feedback [28]

- (a) Block diagram
- (b) Active CR realization
- (c) Frequency responses

- (a) Block diagram
- (b) Active CR realization
- (c) Frequency responses

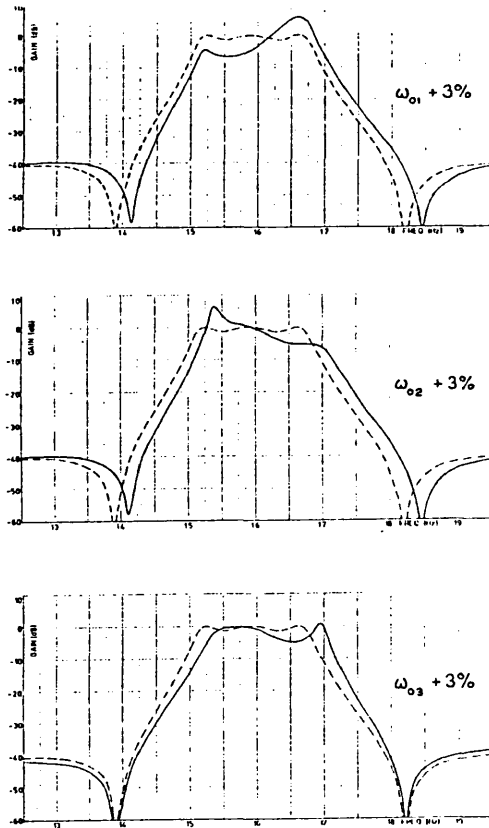


Fig 5.30 Transpose follow the leader feedback sensitivity to changes in resonance frequencies

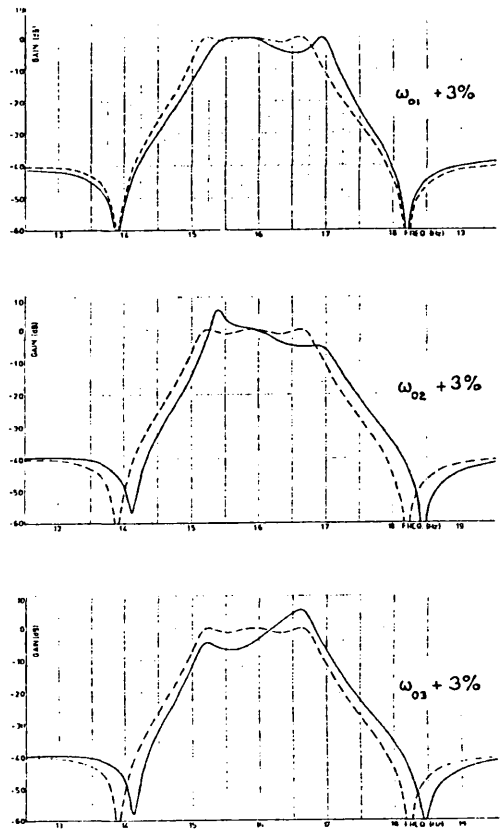


Fig 5.31 Follow the leader feedback sensitivity to changes in resonance frequencies

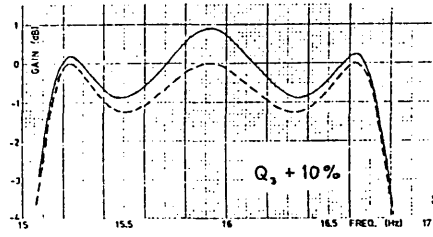
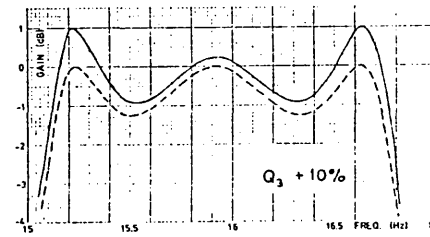
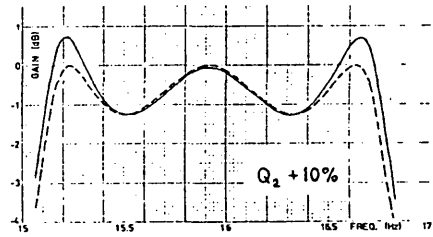
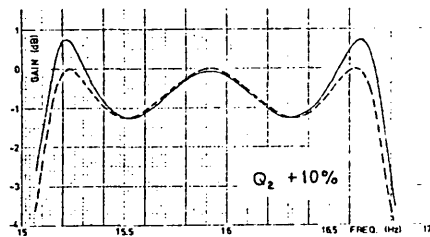
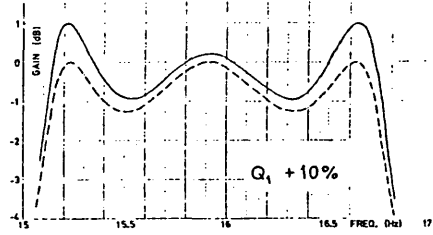
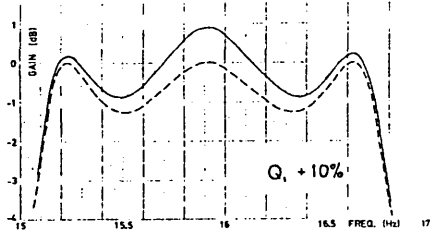


Fig 5.32 Transpose FLF sensitivity to changes in Q-factors

Fig 5.33 FLF sensitivity to changes in Q-factors

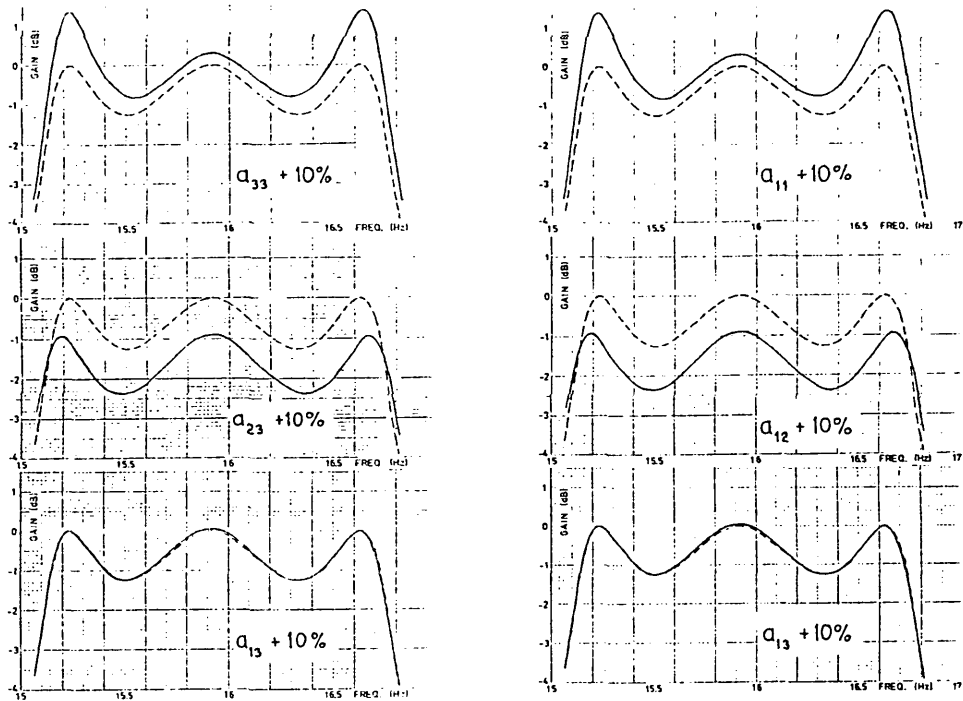


Fig 5.34 Transpose FLF sensitivity to changes in constant multipliers

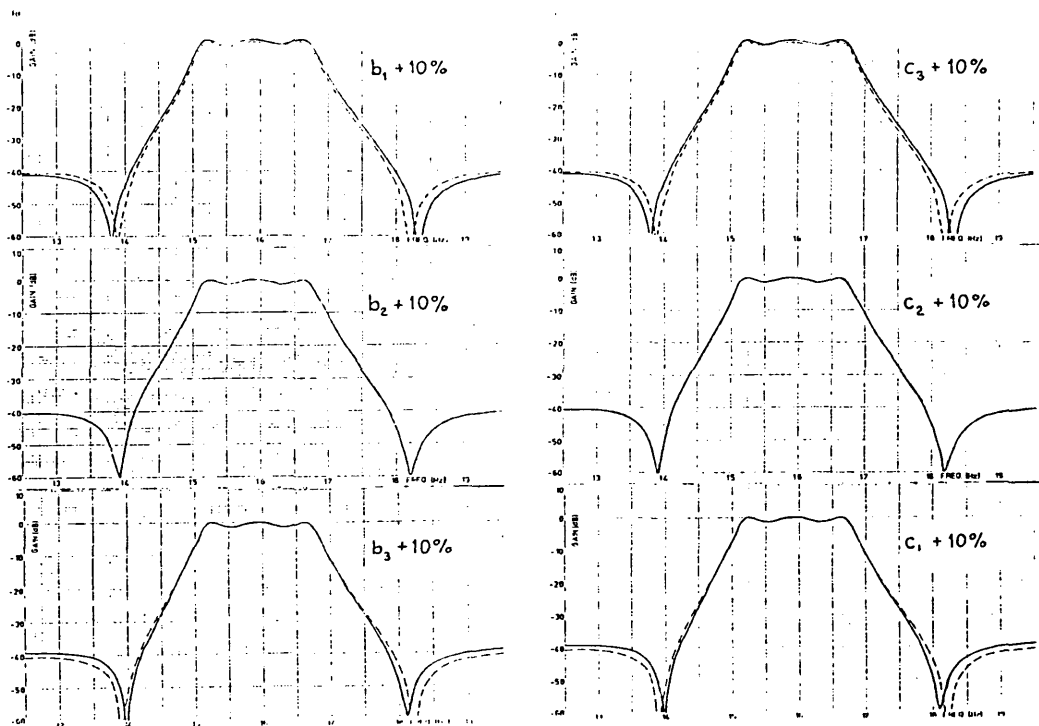


Fig 5.35 FLF sensitivity to changes in constant multipliers

that produced by a 3% increase in the resonance frequency  $\omega_{o_3}$  of the last block  $G_3$  of the follow the leader feedback structure. The responses due to an increase of 10% in the Q-factors of the blocks, shown in Figs 5.32 and 5.33, are related in the same way. These results illustrate the fact that finite difference sensitivities are invariant under the transformation of FGR. Although they are not shown here, responses caused by changes in the values of the remaining block diagram parameters have been computed, and it is again found that parameters related by the identities listed in Table 5.1 have identical finite difference sensitivities.

TABLE 5.1 Flow graph reversal identities

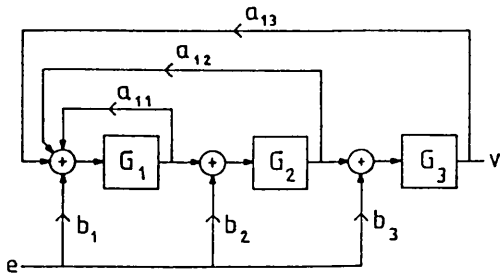
Transpose follow the leader feedback Fig 5.28	← FGR →	Follow the leader feedback Fig 5.29
$G_3$		$G_1$
$G_2$		$G_2$
$G_1$		$G_3$
$a_{33}$		$a_{11}$
$a_{23}$		$a_{12}$
$a_{13}$		$a_{13}$
$b_3$		$c_1$
$b_2$		$c_2$
$b_1$		$c_3$

### 5.4.2 Shifted companion form and intermediate structures

We now consider two more nested feedback structures, both designed by an adaptation of the method described in Section 1.4. The first is Tow's 'shifted companion form' structure [47], and the second is an intermediate structure of Type-C in Table 4.1, first proposed by the writer in Ref 84. For both structures, the block diagram is analysed with the block transfer functions  $G_j$  replaced by  $1/s$  in order to obtain expressions for the path constants in terms of the transfer function coefficients. These expressions are used to implement the required lowpass prototype transfer function (5.1.1), pre-distorted by the constant  $\alpha_1$ . Pre-distortion is removed by replacing  $1/s$  with  $1/(s + \alpha_1)$ , and then lowpass to bandpass transformation and frequency scaling produce the block diagrams shown in Figs 5.36 and 5.37.

Plots of the frequency responses resulting from changes in the values of the block diagram parameters reveal that the sensitivities of the different nested feedback structures are related in a way which encompasses the identities described in the previous section. In cases where FGR does not apply, the relationship is not precise and it is necessary to consider the passband and the stopbands separately.

Take for example the response due to a 3% increase in the value of the resonance frequency  $\omega_{o_3}$  of the third section  $G_3$  in the Shifted Companion Form (Fig 5.38(c)), and compare this with the response due to a 3% increase in the value of the resonance frequency  $\omega_{o_1}$  of the first section  $G_1$  of the intermediate structure (Fig 5.39(a)). At frequencies in the passband the two responses are almost identical, and furthermore they are similar to the responses caused by a 3% increase in  $\omega_{o_1}$  of the transpose follow the leader feedback structure (Fig 5.30(a)), and by a 3% increase in  $\omega_{o_3}$  of the follow the leader feedback structure (Fig 5.31(c)). It is possible to identify a characteristic of the structure which applies to each of these four responses; that is they all relate to a block which is a member of just one feedback loop. Further similarities can easily be found, and they are set out in Table 5.2. This table has been compiled from a study of all the relevant frequency response graphs, not all of which have been reproduced here, for brevity. From the Table, it seems reasonable to conclude that the similarities in the sensitivities are a consequence of the corresponding similarities in the structure, and that the Table may be extended to include other nested feedback structures. The invariance of passband sensitivity indicated by

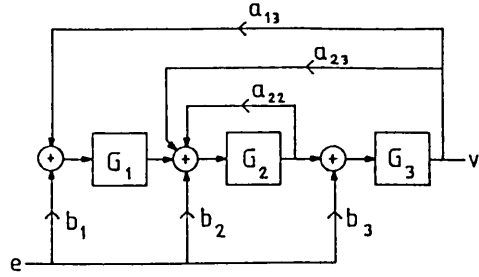


$$\begin{aligned} a_{11} &= 0.602478 & b_1 &= 0.400978 \\ a_{12} &= 1.021308 & b_2 &= -0.025388 \\ a_{13} &= 0.019501 & b_3 &= -0.063865 \end{aligned}$$

$$G_j = K_j \frac{s}{s^2 + \frac{\omega_0}{Q}s + \omega_0^2} \quad j = 1, 2, 3$$

$$\begin{aligned} \omega_0 &= 100 & K_1 &= 10 \\ Q &= 20 & K_2 = K_3 &= -10 \end{aligned}$$

(a)

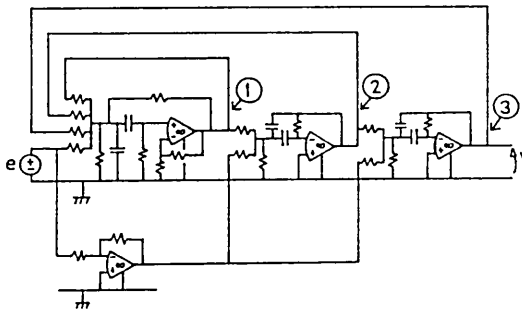


$$\begin{aligned} a_{13} &= 0.019501 & b_1 &= 0.481499 \\ a_{22} &= 0.602478 & b_2 &= 0.025388 \\ a_{23} &= 1.021308 & b_3 &= -0.063865 \end{aligned}$$

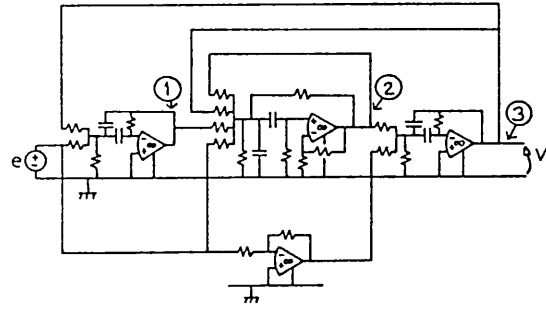
$$G_j = K_j \frac{s}{s^2 + \frac{\omega_0}{Q}s + \omega_0^2} \quad j = 1, 2, 3$$

$$\begin{aligned} \omega_0 &= 100 & K_1 = K_3 &= -10 \\ Q &= 20 & K_2 &= 10 \end{aligned}$$

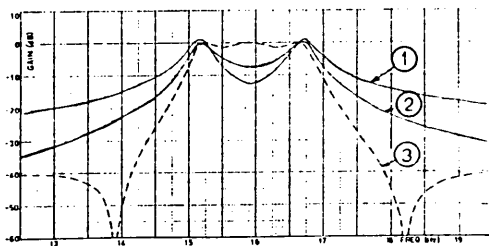
(a)



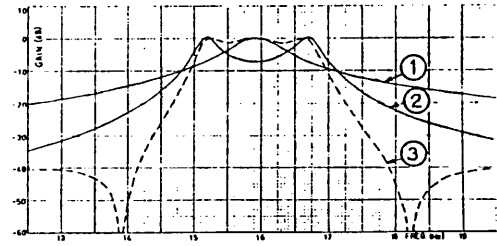
(b)



(b)



(c)



(c)

Fig 5.36 Shifted Companion Form [47]

Fig 5.37 Intermediate structure [84]

- (a) Block diagram
- (b) Active CR realization
- (c) Frequency responses

- (a) Block diagram
- (b) Active CR realization
- (c) Frequency responses

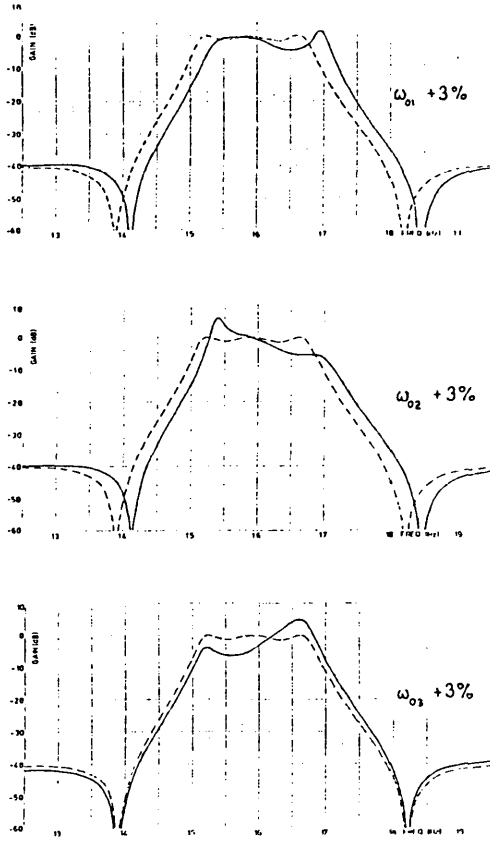


Fig 5.38 Shifted Companion Form sensitivity to changes in resonance frequencies

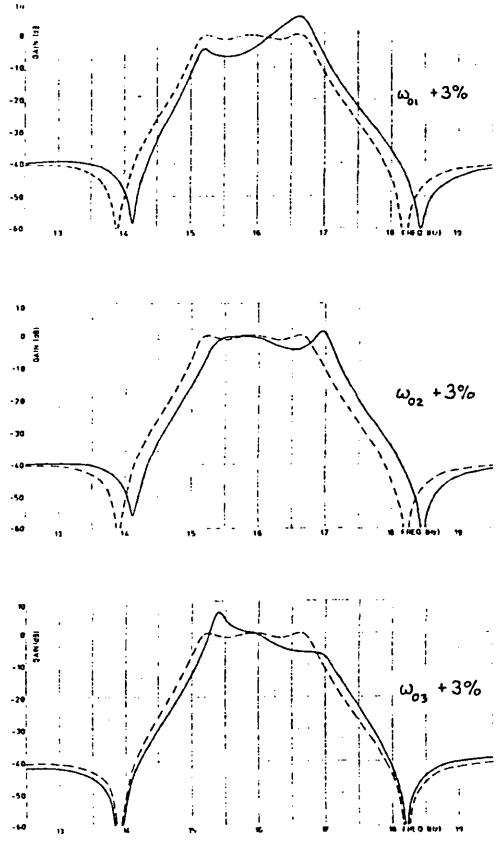


Fig 5.39 Intermediate structure sensitivity to changes in resonance frequencies



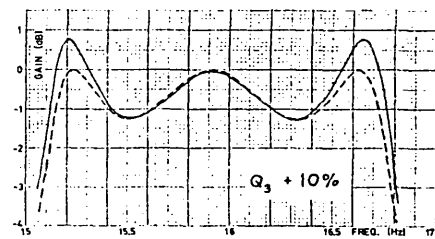
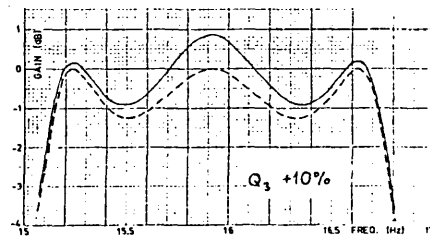
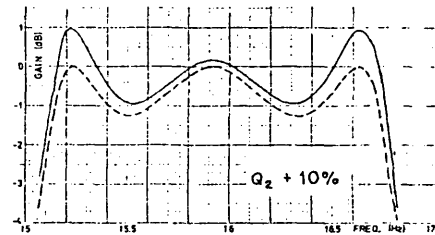
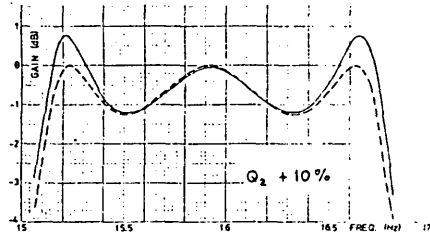
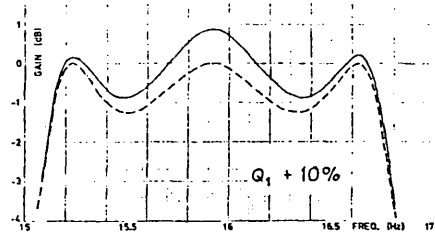
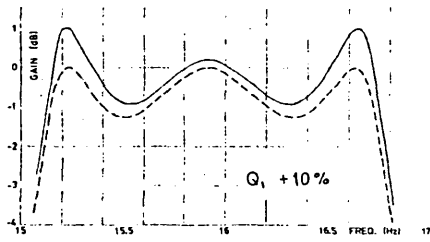


Fig 5.40 Shifted Companion Form sensitivity to changes in Q-factors

Fig 5.41 Intermediate structure sensitivity to changes in Q-factors

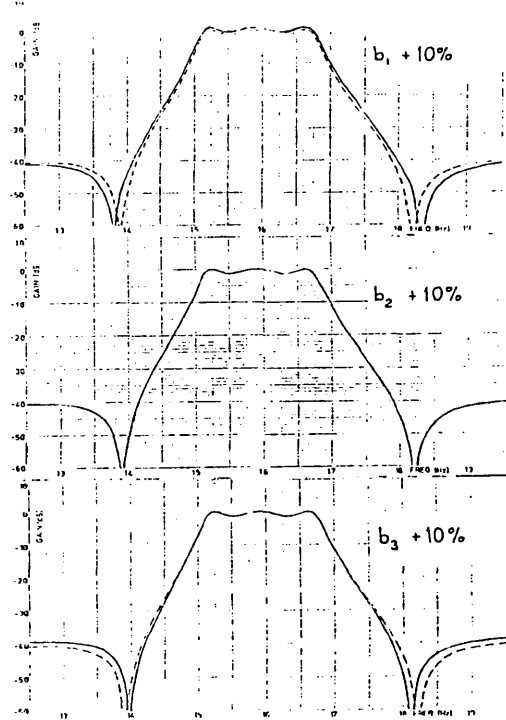
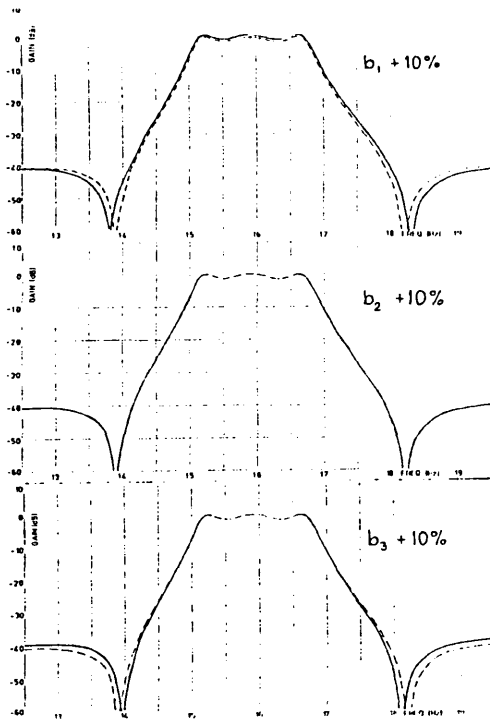
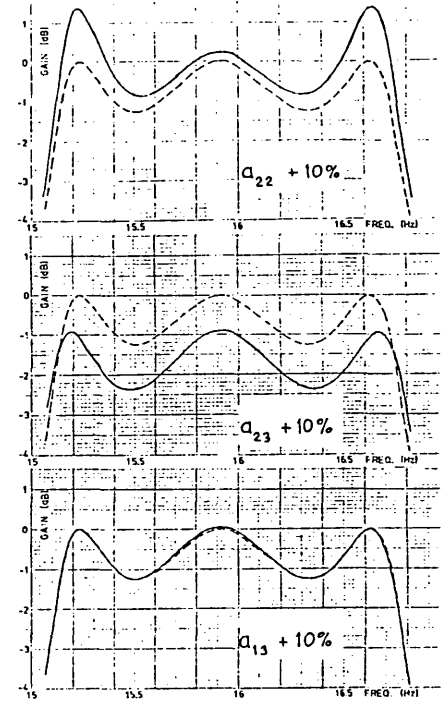
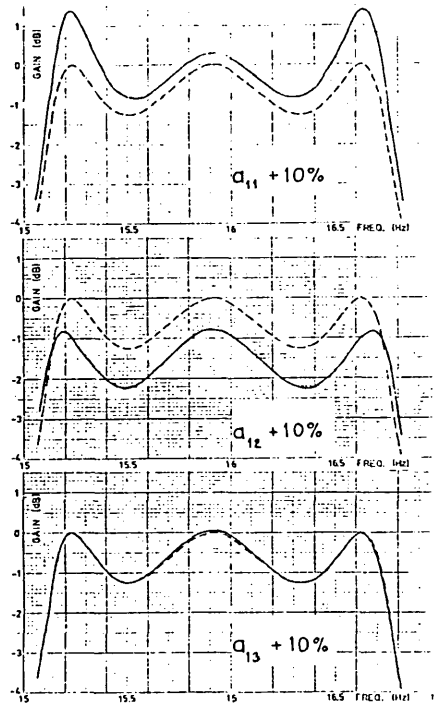


Fig 5.42 Shifted Companion Form sensitivity to changes in constant multipliers

Fig 5.43 Intermediate structure sensitivity to changes in constant multipliers

Table 5.2 is similar to the invariance of sensitivity exhibited by the transformation shown in Fig 3.4. In that transformation, cascaded subnetworks may be interchanged to obtain new structures without affecting the sensitivity performance.

TABLE 5.2 Similar passband sensitivities

Transpose follow the leader feedback Fig 5.28	Follow the leader feedback Fig 5.29	Shifted Companion Form Fig 5.36	Intermediate Structure Fig 5.37	
$G_3$	$G_1$	$G_1$	$G_2$	In three feedback loops
$G_2$	$G_2$	$G_2$	$G_3$	In two feedback loops
$G_1$	$G_3$	$G_3$	$G_1$	In one feedback loop
$a_{33}$	$a_{11}$	$a_{11}$	$a_{22}$	Loop around one block
$a_{23}$	$a_{12}$	$a_{12}$	$a_{23}$	Loop around two blocks
$a_{13}$	$a_{13}$	$a_{13}$	$a_{13}$	Loop around three blocks
$b_3$	$c_1$	$b_3$	$b_3$	Forward path through one block
$b_2$	$c_2$	$b_2$	$b_2$	Forward path through two blocks
$b_1$	$c_3$	$b_1$	$b_1$	Forward path through three blocks

At stopband frequencies there is a slightly different pattern of similarities, and these are set out in Table 5.3. In the stopbands, the response is not affected by the feedback path constants  $a_{jk}$ , and the similarities in the sensitivities relate to the forward paths, as opposed to the feedback loops which have a dominant effect on the passband response. There are in the stopbands some minor variations in respect of the depth of the notches.

On the basis of Table 5.2 and Table 5.3 it can be said that all of the nested feedback structures studied here have almost identical sensitivities, and it is likely that this can be extended to include

other arrangements of nested feedback loops. The choice between these structures, at least for design methods which produce identical blocks, may therefore be made using some other criterion, such as the number of amplifiers used. For a given structure and a given transfer function, the number of amplifiers will depend on the choice of the pre-distortion constant  $\alpha_1$ , and this is studied in the next Section.

TABLE 5.3 Similar stopband sensitivities

	Transpose FLF Fig 5.28	FLF Fig 5.29	SCF Fig 5.36	Intermediate structure Fig 5.37
Block with no parallel paths	$G_3$	$G_1$	$G_3$	$G_3$
Blocks with parallel forward paths	$G_2, G_1$	$G_2, G_3$	$G_2, G_1$	$G_2, G_1$
Forward path through one block	$b_3$	$c_1$	$b_3$	$b_3$
Forward path through two blocks	$b_2$	$c_2$	$b_2$	$b_2$
Forward path through three blocks	$b_1$	$c_3$	$b_1$	$b_1$

### 5.4.3 Choice of pre-distortion constant

For the simple design procedure described in Section 1.4, the selection of a value for the pre-distortion constant  $\alpha_1$  is equivalent to choosing a Q-factor for the quadratic blocks, because the Q-factor of the blocks Q is given by the Q-factor of the required response q, divided by  $\alpha_1$ :  $Q = q/\alpha_1$ . In all previous examples of structures having nested feedback loops, the value of the pre-distortion constant  $\alpha_1$  has been chosen somewhat arbitrarily to give block transfer functions having a Q-factor equal to 20. In this section we discuss how  $\alpha_1$  may be chosen more advantageously.

In Hurtig's Primary Resonator Block filter [27] (a follow the leader feedback structure for polynomial filters), the Q-factors of the blocks are such that the innermost feedback loop is eliminated. The corresponding condition may be found for the nested feedback structure described in Section 1.4. With reference to Fig 1.8, the innermost feedback loop is eliminated when  $Q_{n-1} = 0$ , which, from (1.4.7) with  $k = n-1$ , gives the required condition in terms of the coefficients of the lowpass prototype transfer function as:

$$\alpha_1 = \frac{\delta_{n-1}}{n \delta_n} \quad (5.4.1)$$

Tow [28] reports that the Primary Resonator block filter has near optimum sensitivity.

Johnson, Hilburn and Irons [154] suggested, in respect of a follow the leader feedback polynomial filter, that in some cases it may be possible to choose  $\alpha_1$  to be such that all the feedback path constants  $Q_{jk}$  become non-negative, thus avoiding the need for inverting amplifiers. This depends on the values of the coefficients in the denominator of the transfer function, and it may not always be possible to eliminate amplifiers in this way.

Hrubý and Novotný [108] used a structure having follow the leader feedback and feedforward to the output, in order to realize very narrow band filters. They chose  $\alpha_1$  to suit the high Q-factor of the piezo-electric resonator sections which they used.

In connection with the Shifted Companion Form structure, Tow suggested that  $\alpha_1$  may be selected for optimal sensitivity [28]. He considered standard deviation, as a function of frequency, derived from a 'Monte Carlo' analysis of specific active CR realizations. His observation was that there existed a broad range of  $\alpha_1$  for which the standard deviation was relatively low, and that this range included Hurtig's design. More recently, Schubert [159] arrived at a similar

conclusion from a study of multi-parameter coefficient sensitivity.

In this section we will take the intermediate structure shown in Fig 5.37, and will present the block diagram sensitivities for various values of the pre-distortion constant  $\alpha_1$ . If the lowpass prototype transfer function (5.1.1) is written as

$$F_{LP}(s) = \frac{\nu_0 + \nu_2 s^2}{\delta_0 + \delta_1 s + \delta_2 s^2 + \delta_3 s^3}, \quad \delta_3 = 1 \quad (5.4.2)$$

then the design method gives the following expressions for the block diagram parameters:

$$\begin{aligned} a_{22} &= -\delta_2 + 3\alpha_1 \\ a_{23} &= -\delta_1 + 2\delta_2\alpha_1 - 3\alpha_1^2 \\ a_{13} &= -\delta_0 + \delta_1\alpha_1 - \delta_2\alpha_1^2 + \alpha_1^3 \\ b_3 &= \nu_2 \\ b_2 &= \nu_2(\alpha_1 - \delta_2) \\ b_1 &= \nu_0 + \nu_2\alpha_1^2 \end{aligned} \quad (5.4.3)$$

Approximate values of these parameters are tabulated below to illustrate their dependence on  $\alpha_1$ .

TABLE 5.4 Intermediate structure parameters

$\alpha_1$	-0.5	0	0.01	0.1	0.2	0.33'	0.5	1.0	10
$Q = 10/\alpha_1$	-20	$\infty$	1000	100	50	30	20	10	1
$a_{13}$	-1.40	-0.46	-0.45	-0.35	-0.26	-0.14	0.02	0.81	921
$a_{23}$	-2.82	-1.17	-1.15	-1.02	-0.93	-0.90	-1.02	-2.37	-283
$a_{22}$	-2.40	-0.90	-0.87	-0.60	-0.30	0.10	0.60	2.10	29.1
$b_1$	0.48	0.47	0.47	0.47	0.47	0.47	0.48	0.53	6.85
$b_2$	-0.09	-0.06	-0.06	-0.05	-0.04	-0.04	-0.03	0.006	0.58
$b_3$	0.06	0.06	0.06	0.06	0.06	0.06	0.06	0.06	0.06

Active CR realizations corresponding to each of these values of  $\alpha_1$  have been investigated, and it will be seen that the sensitivities to the different block diagram parameters do not have the same dependence on the value of  $\alpha_1$ .

Consider first the effect of a 3% increase in the resonance frequencies  $\omega_{o1}$ ,  $\omega_{o2}$  and  $\omega_{o3}$  shown respectively in Fig 5.44, Fig 5.45, and Fig 5.46. The stopbands are mostly unaffected by the value of  $\alpha_1$  but the passband is affected, and, depending on the feature of interest, the sensitivity reaches a minimum somewhere between  $\alpha_1 = 0.2$  and  $\alpha_1 = 0.5$ . It is of interest to note that for

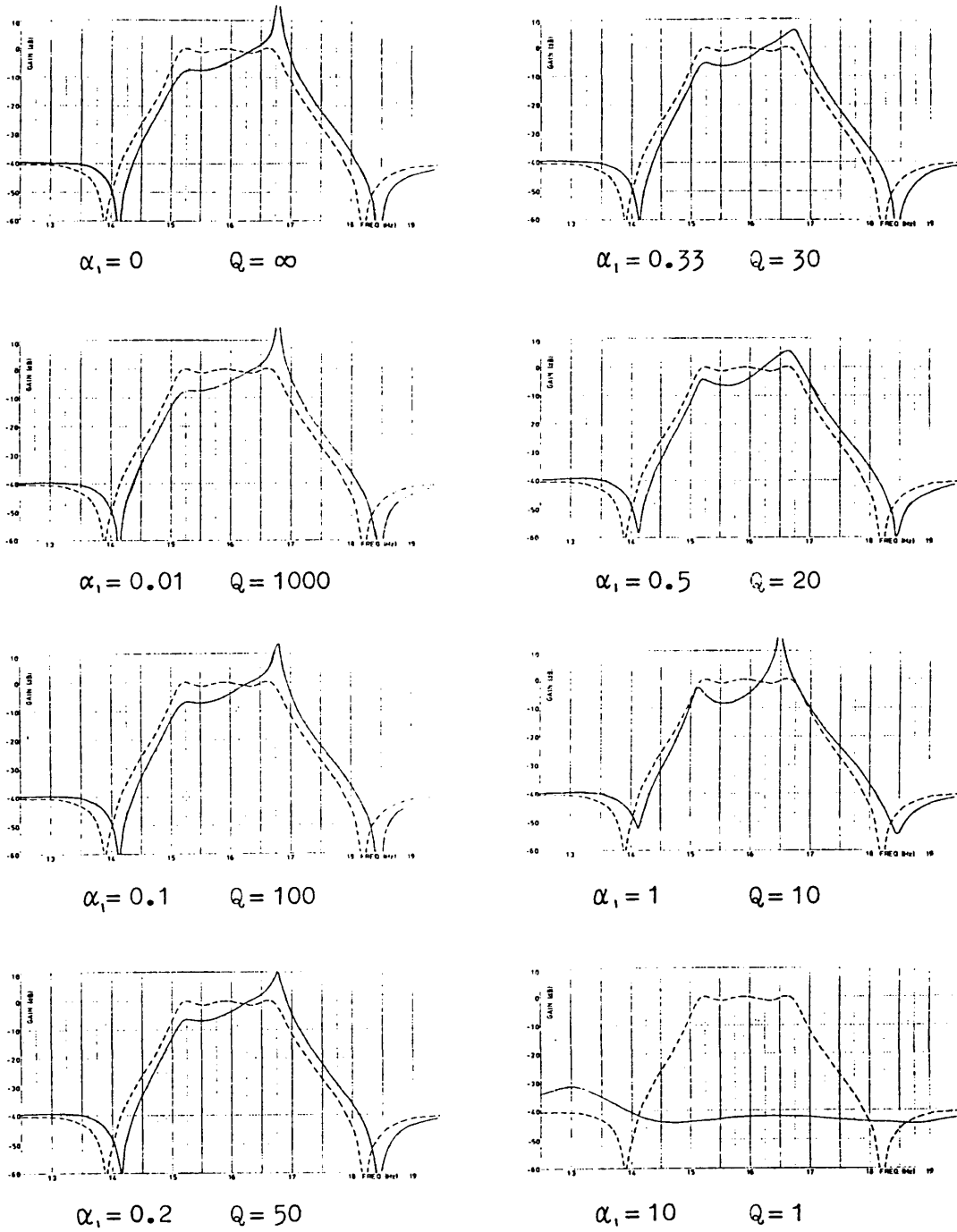


Fig 5.44 Sensitivity to an increase of 3% in the value of  $\omega_{01}$  for different values of  $\alpha_1$

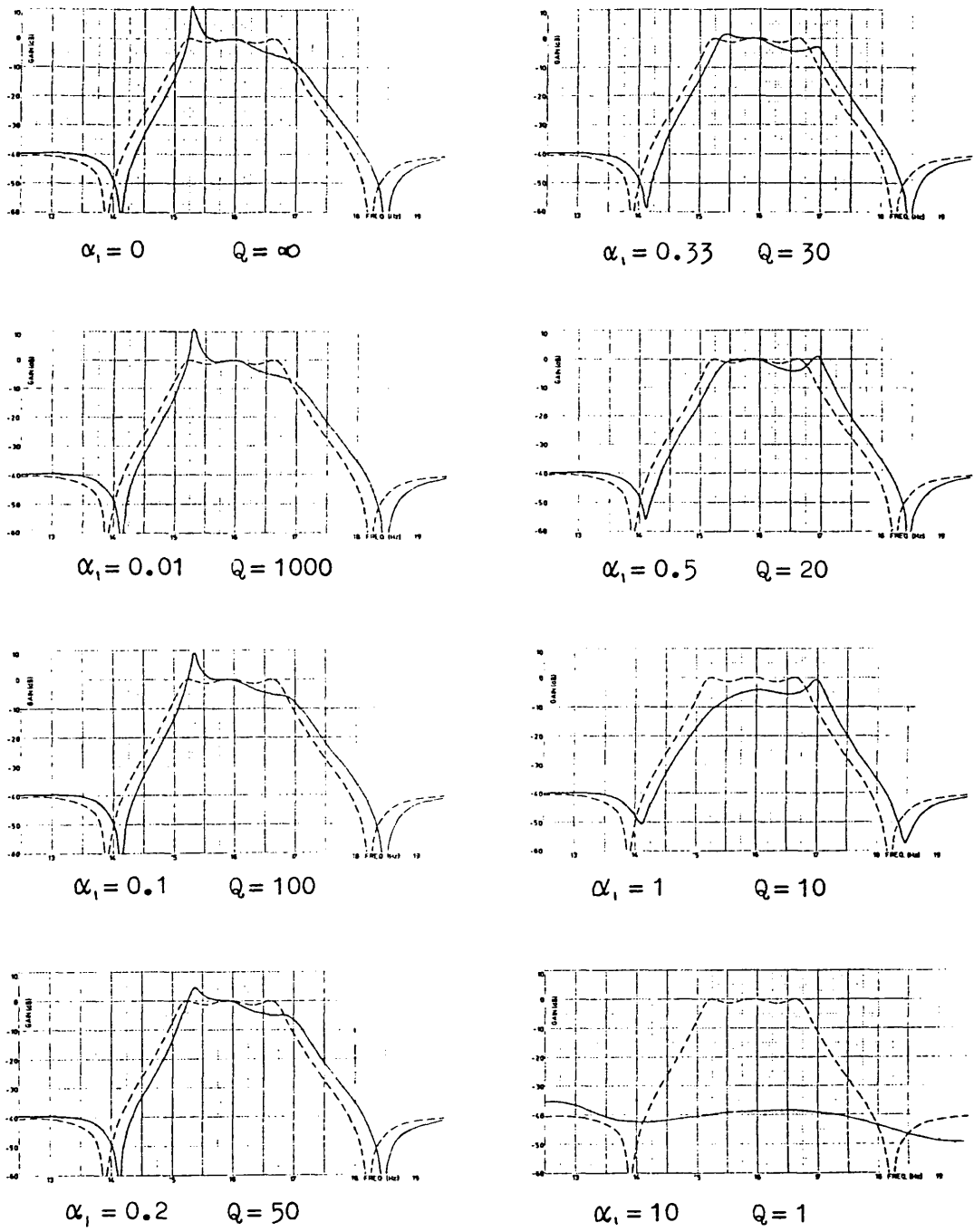


Fig 5.45 Sensitivity to an increase of 3% in the value of  $\omega_{02}$  for different values of  $\alpha_1$



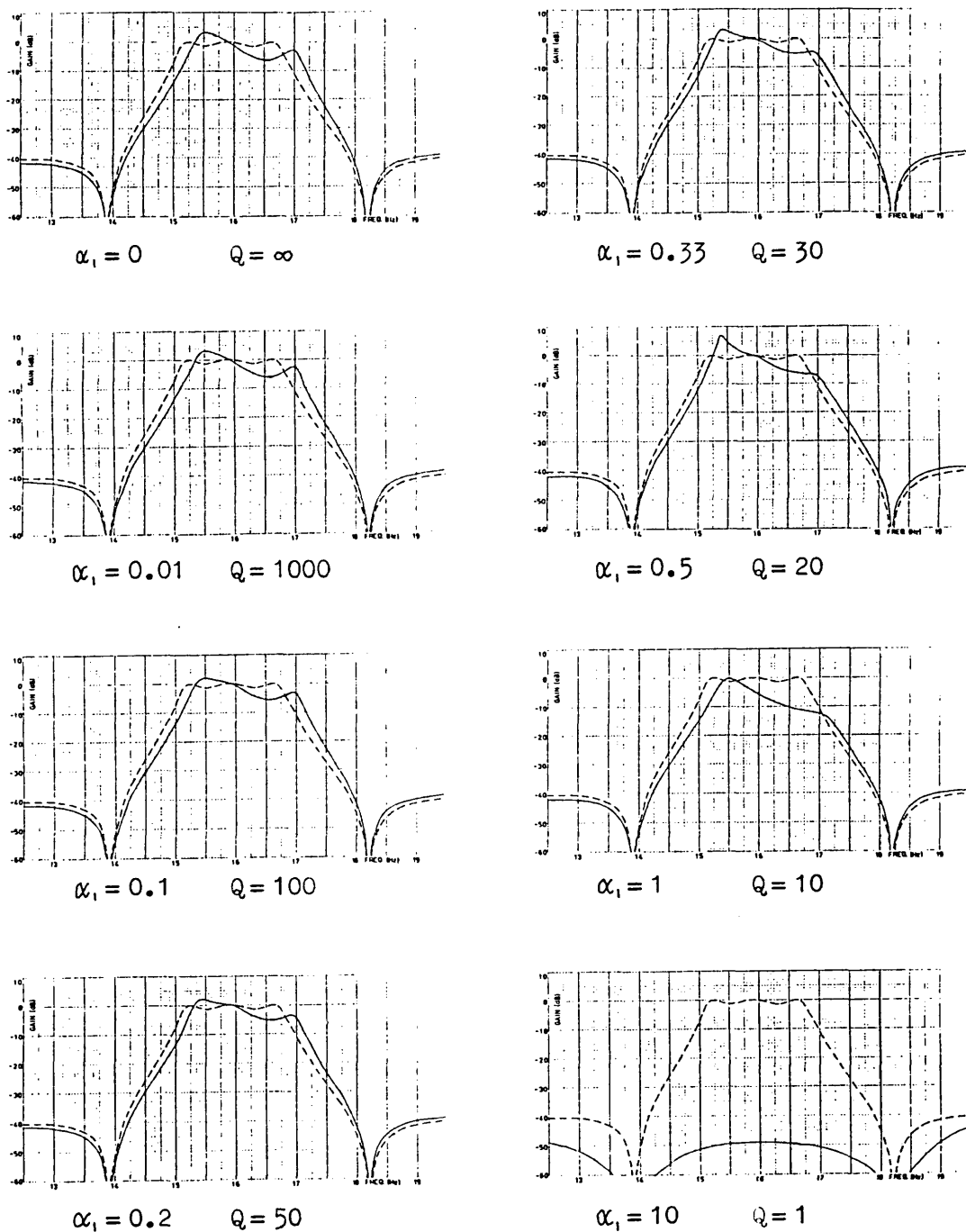


Fig 5.46 Sensitivity to an increase of 3% in the value of  $\omega_{03}$  for various values of  $\alpha_1$

this example the Hurtig condition (i.e. the elimination of the innermost feedback loop) corresponds to:

$$\alpha_1 = \frac{\delta_2}{3\delta_3} = 0.299 \quad (5.4.4)$$

hence the results are in agreement with Tow's empirical observation that the Hurtig condition is near to the optimum. In the region of minimum sensitivity, the performance is not as good as that of the leapfrog feedback structures studied in previous Sections, but it is better than the cascade. At extreme values of  $\alpha_1$ , the sensitivity becomes quite poor. For  $\alpha_1 = 0$  the sensitivity is worse than that of the cascade structure, and when  $\alpha_1 = 10$  the sensitivity is so large that the design is impracticable. At an optimum value of  $\alpha_1$ , the first block has the greatest sensitivity, and it is interesting to note that the first block is in one feedback loop only. The other two blocks are members of two feedback loops ( $\alpha_{22}$  being approximately zero at optimum values of  $\alpha_1$ ), and these blocks have sensitivities which are similar to each other but lower than the sensitivity of the first block. This observation is consistent with the analysis of the differential sensitivities of a leapfrog feedback structure given in Section 1.2, where it was shown that the centre block - a member of two feedback loops - has a lower sensitivity than the two outer blocks, each of which is a member of only one feedback loop. This suggests that the key to obtaining low sensitivity in multiple feedback filters is to include as many feedback loops as possible. Some success has been reported with this approach (Column 6 in Table 4.1), but the only design methods for which confirmatory sensitivity results are available are those which involve a search for minimum sensitivity by means of a computer optimisation routine, as described in Section 3.5.

The sensitivities to changes in the Q-factors of the blocks do not depend on the value of  $\alpha_1$  in the same way. From Fig 5.47 it can be seen that the sensitivity to  $Q_1$  is proportional to  $\alpha_1$  over the range  $\alpha_1 = 0$  to  $\alpha_1 = 0.5$ . The sensitivities to changes in  $Q_2$  and  $Q_3$  are also proportional to  $\alpha_1$ . Since  $\alpha_1 = q_1/Q$ , this balances the tendency for the variability of quadratic sections to increase in proportion to Q-factor.<sup>[138]</sup> For  $\alpha_1 = 1/3$ , the perturbed responses are comparable to those computed for the leapfrog feedback structures, as are the responses caused by changes to the other block diagram parameters.

It will be seen from Table 5.4 that it is possible to use a negative value of  $\alpha_1$ , corresponding to a negative Q-factor for the

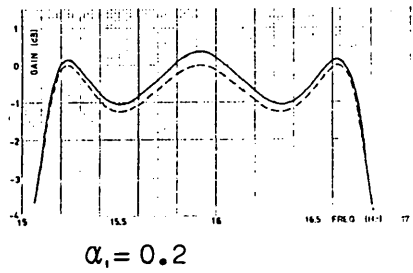
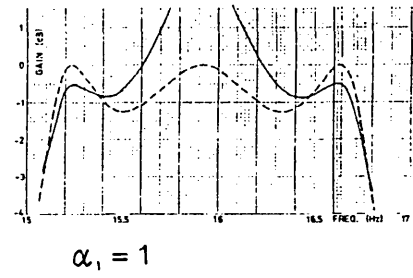
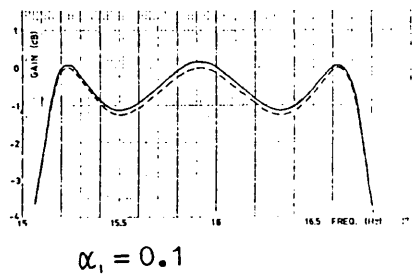
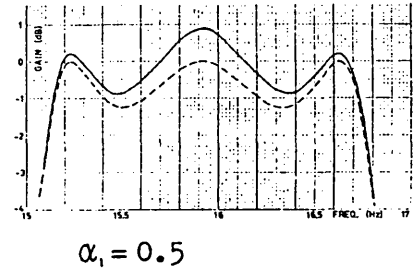
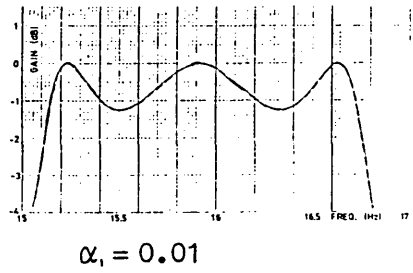
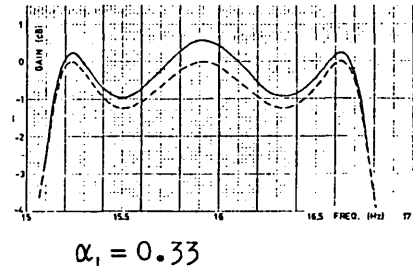
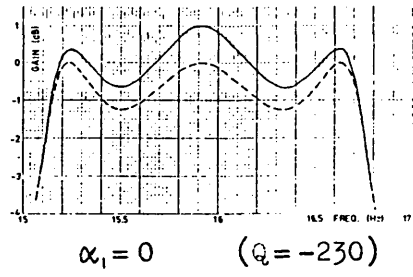


Fig 5.47 Sensitivity to an increase of 10% in the value of Q, for various values of  $\alpha_1$

blocks. Such a design can be realized if the Q-enhancement type of quadratic section is used. There is however no practical advantage in doing so, indeed it was found that with  $\alpha_1 = -0.5$  the passband sensitivity was appreciably greater than with  $\alpha_1 = +0.5$ .

Whilst even for the optimum value of  $\alpha_1$  the passband sensitivity is not as low as that of the leapfrog feedback structures, the nested feedback structures described in this Chapter have a sensitivity lower than that of the cascade structure; they have a simple design procedure, and may be constructed from identical sections having a low Q-factor.

## 5.5 Structures having all feedback loops

The results presented in Section 5.4.3 suggest that the lowest passband sensitivity may be obtainable by including as many feedback loops as possible. Several authors have proposed methods for designing such structures, and these are indicated in Column-6 of Table 4.1. In most of them the added flexibility has been utilized to obtain a minimum measure of sensitivity, for specific examples, by means of a computer optimization programme [70,86,116,136]. Only one design method has been applied to bandpass filters incorporating finite transmission zeros by means of series notch sections [117], and there is a difficulty with that method, not explored by the author of Ref.117, in that early stages of the design procedure require a knowledge of the final result. Sensitivity minimization, by use of the similarity transformation, is not directly applicable to existing structures having series notch sections because these do not have all blocks identical to each other (see discussion in Section 3.5). The similarity transformation has however been applied successfully to structures having parallel forward paths [86], in order to minimize sensitivity. There is as yet no practical method of incorporating finite transmission zeros into a low sensitivity structure having all feedback paths, without invoking a computer optimization routine. The next example will show that the presence of all feedback loops is in itself not sufficient to guarantee low sensitivity.

### 5.5.1 An adaptation of the Crab's Eye filter

Hills' Crab's Eye filter [118] is a bank of band separation filters having the structure illustrated in Fig 5.48(a) for the case of three channels. There is one block for each channel, and each block has a bandpass characteristic centred around its associated channel frequency. Also each block  $G_j(s)$  is arranged to have a transfer function equal to -1 at its centre frequency:  $G_j(i\omega_{oj}) = -1$ . At this frequency the coupling is arranged to cause a cancellation of the signal at the input to the other blocks. Thus at the centre frequency of each channel, all other channels have a transmission zero. By this means the Crab's Eye filter can provide an efficient means of separating tones [119].

The Crab's Eye filter may be adapted for use as a single channel filter, realizing the bandpass transfer function (5.1.5). The structure is re-drawn as a single channel filter in Fig 5.48(b), from which it

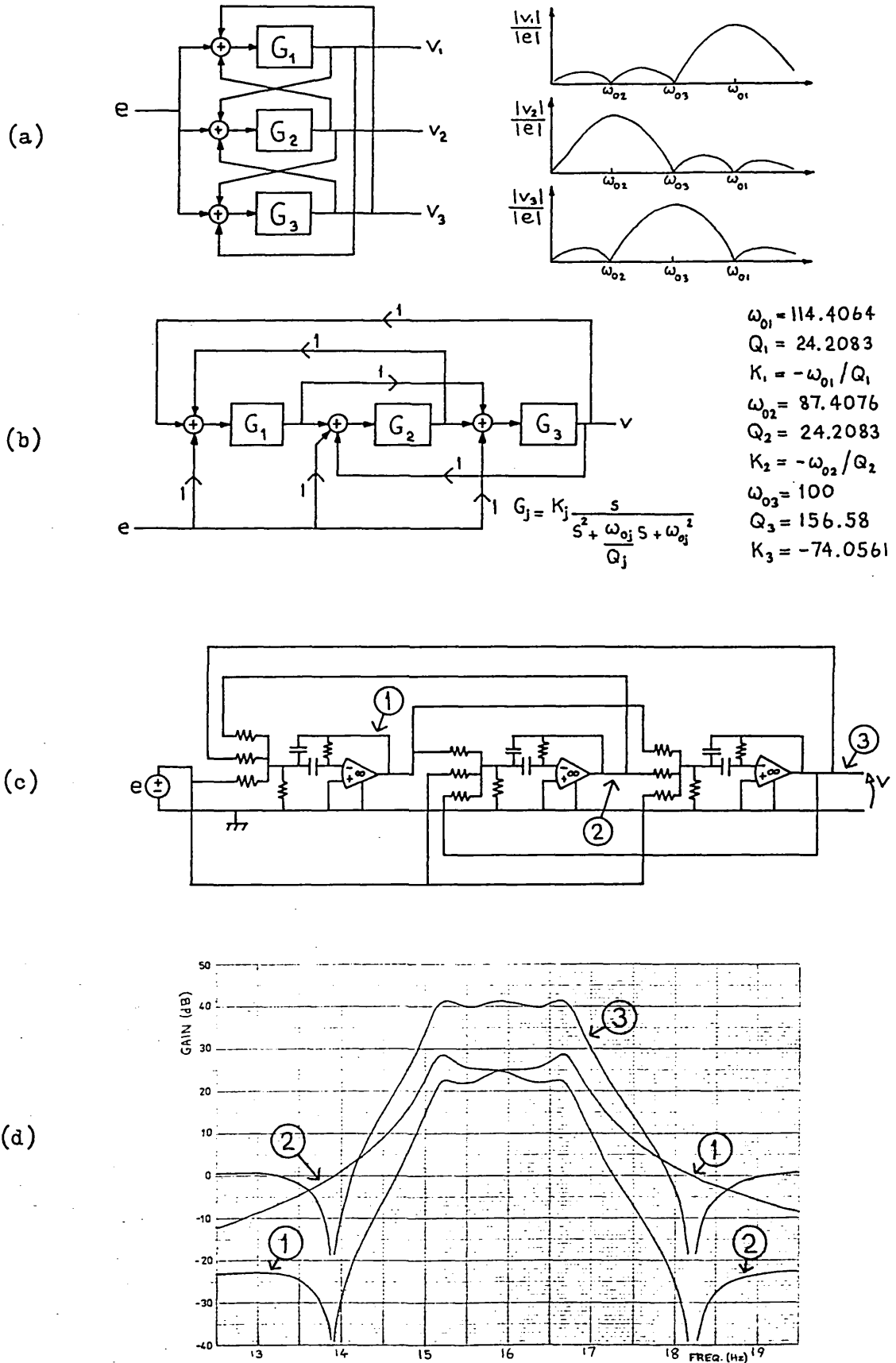


Fig 5.48 Crab's Eye derived structure [118]

- (a) Hills' band splitting Crab's Eye filter
- (b) Crab's Eye derived structure for a single channel
- (c) Active CR realization
- (d) Computed frequency responses

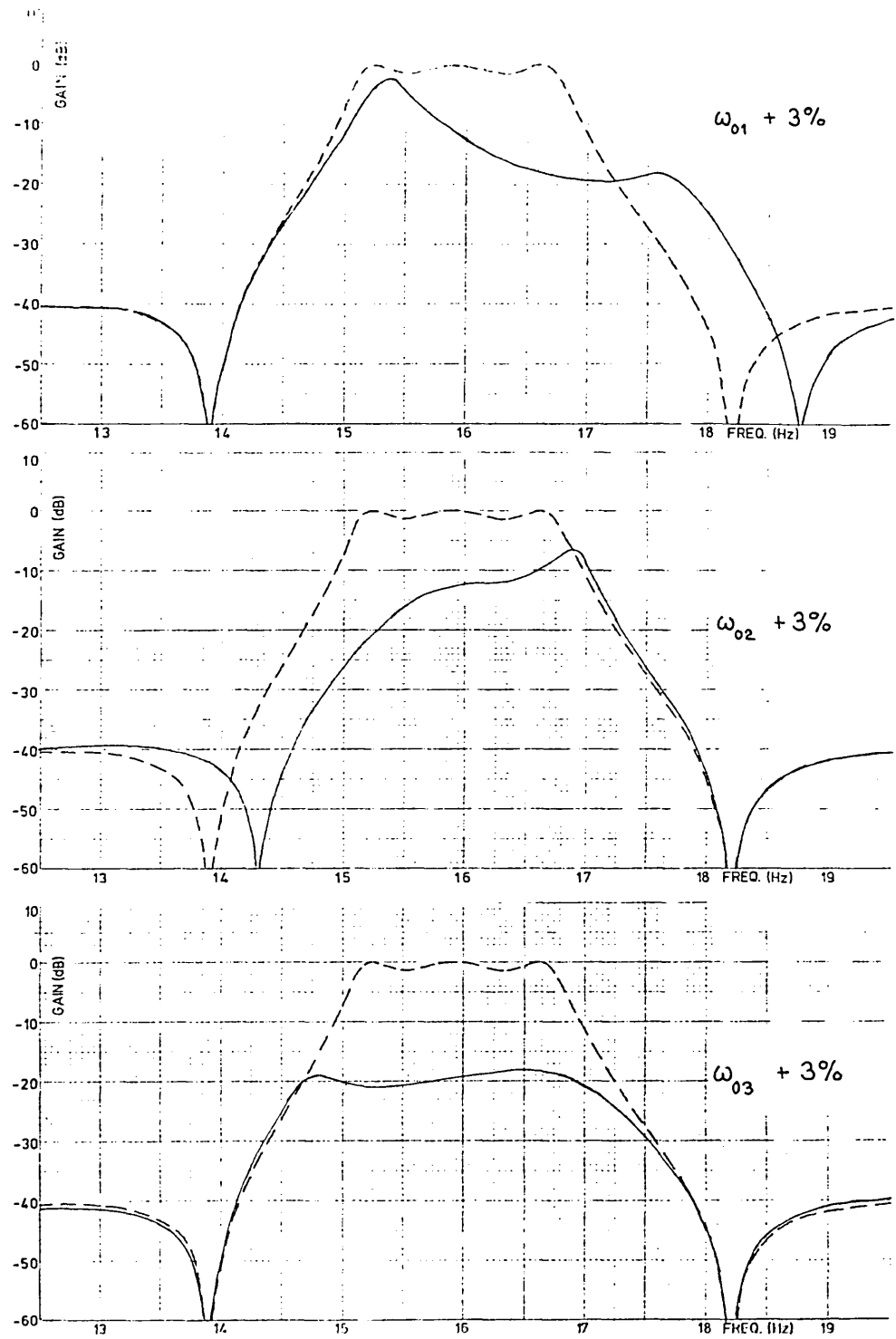


Fig 5.49 Crab's Eye derived structure sensitivity to changes in resonance frequencies

can be seen that all feedback paths are present and that transmission zeros are produced by parallel forward paths. Each block has a bandpass quadratic transfer function, and, in order to realize transmission zeros by the Crab's Eye method,  $\omega_{o1}$  is set equal to the frequency of the upper transmission zero and  $\omega_{o2}$  equal to the frequency of the lower transmission zero. Additionally  $a_{jk} = 1 \quad \forall j, k$ ;  $b_j = 1 \quad \forall j$ ; and  $G_j(i\omega_{oj}) = -1 \quad j=1,2$ . When the structure in Fig 5.48(b) is analysed with these constraints, the remaining free parameters ( $Q_1, Q_2, Q_3, K_3, \omega_{o3}$ ) may be chosen by matching the coefficients of the various powers of  $s$  in the denominator of the resulting transfer function with the coefficients of the corresponding powers of  $s$  in the required transfer function (5.1.5). The resulting structure realizes the required transfer function to within a constant multiplier, as shown in Fig 5.48(d). If required, the scaling transformation (see Section 3.4) may be used to alter the gain, and to improve the dynamic range. The Crab's Eye approach has not previously been applied to a single channel filter, and its sensitivity has been studied only in the context of channel bank filtering.

Increasing the resonance frequencies of each of the three blocks by 3% results in the responses shown in Fig 5.49, from which it can be seen that there is a large sensitivity at passband frequencies, despite the presence of all feedback loops. The feedback loops originate from the Crab's Eye method of producing transmission zeros and are not introduced as a means of reducing sensitivity. In this adaptation to a single channel filter however, the paths  $Q_{13}$  and  $Q_{23}$  do not contribute to the formation of transmission zeros, but the computed results indicate that their presence does not lead to low passband sensitivity. It is of interest to note that the spread in the resonance frequencies of the three blocks is greater than is the case for the cascade structure.

In the stopbands, the sensitivity is similar to that of the cascade structure in that a 3% increase in the resonance frequency of either of the first two blocks causes a 3% increase in the frequency of the associated transmission zero. The depth of the notches is dependent on the value of the gain constant  $K$  of the associated block.



## 5.6 Summary

Whilst it is not usually possible to draw general conclusions from particular examples, the computational analysis undertaken in this Chapter has contributed to our understanding of multiple feedback filters, and it has clarified relationships between the sensitivities of different structures. For some of the structures considered, sensitivity results have not previously been published, and for other structures the sensitivity has not been studied by the method adopted here. The different structures have been considered in four categories.

Structures in the first group are designed by a canonic expansion of the transfer function. They do not have feedback loops for the reduction of sensitivity, and the computed results confirm that the sensitivity is relatively large. Because of its common usage and simplicity of construction, the cascade or factored structure is often taken as a reference against which other structures are compared. The partial fraction structure has a greater sensitivity in the stopbands and the continued fraction structure has a greater sensitivity in the passband. The sensitivity of the continued fraction structure has not previously been studied.

In the second group are structures having leapfrog feedback for the reduction of passband sensitivity. The computed results show these to have the lowest passband sensitivity of all the structures studied. Node-voltage simulation of an LCR ladder filter leads to the use of series notch sections, and it has a low stopband sensitivity similar to that of the cascade structure. A sensitivity analysis of the node-voltage simulation has not previously been published. The Coupled Biquad structure realizes transmission zeros by the use of parallel forward paths, and this enables all the blocks to have the same resonance frequency. Computation shows that in the worst case the transmission zero frequencies can move further away from the nominal than is the case for series notch sections. It was pointed out that a statistical analysis could give misleading results. The Ford structure uses a different arrangement of parallel forward paths and has a slightly better performance than the Coupled Biquad structure in both passband and stopbands. The passband sensitivity of the Ford structure has been related to that of a simple simulation. Sensitivity performance of the Ford structure has not previously been published. Although it is possible for a leapfrog feedback structure to incorporate transmission zeros by means of complex feedback, such

structures have not been analysed in this Chapter, because the excessive number of sections required and the difficulties associated with implementing reciprocators make it less attractive from the practical point of view.

Structures in the third group have feedback loops nested one inside the other. Computed results have illustrated the fact that finite difference sensitivity is invariant under the transformation of FGR. Further results have revealed that there is a common pattern to the sensitivity of structures having nested feedback. The method of plotting finite changes shows clearly that particular structural features produce the same perturbed response in the different nested feedback structures. For the simple design method described in Section 1.4, the pre-distortion constant  $\alpha_1$  may be chosen for minimum sensitivity. A value of  $\alpha_1$  chosen to satisfy Hurtig's condition is close to this optimum value. The computed results show that whilst there is a definite minimum in the sensitivity to changes in  $\omega_0$ , the sensitivity to Q-factors is proportional to the pre-distortion constant  $\alpha_1$ .

Of all the structures studied in this chapter, those having leapfrog feedback exhibit the lowest passband sensitivity. The work of some authors indicates that a further reduction of sensitivity is possible, especially by including all possible feedback paths, but as yet the only means of achieving such an improvement is by recourse to computer optimization routines. The mere presence of extra feedback paths is not sufficient, as shown by the novel adaptation of the Crab's Eye filter.

---

## CONCLUSIONS

---

This thesis has made various contributions to the study of multiple feedback filters. Some of the results are of a theoretical nature, such as the summed sensitivity invariant, whilst others, such as the computational study of sensitivity, address more directly the problem of designing the most appropriate multiple feedback filter for a given application. This requires a balancing of the requirements for minimum sensitivity, maximum dynamic range, fewest component parts, ease of adjustment, standardization of sub-assemblies, ease of design, and so on. The objective in this thesis is to aid the process of design, by acquiring greater insight into the performance of multiple feedback filters.

A wide variety of circuits is encompassed by defining a multiple feedback filter to be an interconnection of single output, multiple input, active CR sections, which form a structure having at least one forward path through the filter, and a multiplicity of feedback loops. Such structures may be represented by a block diagram or by a signal flow graph, and these may be analysed either by a matrix method or by Mason's Topological method. Analysis yields expressions for both the differential and the finite difference sensitivities of the transfer function with respect to the block diagram parameters. Dynamic range may be determined from the noise and limiting properties of the sections, by using the noise transfer functions and the intermediate transfer functions.

The writer has presented a new summed sensitivity invariant. This interrelates the sensitivities of any set of branches which forms a cut of the signal flow graph. Two proofs of this result are available; one based on matrix analysis and the other based on the scaling transformation together with Euler's relation for homogeneous functions.

A multiple feedback filter may be transformed in several different

ways, in order to change its structure or to obtain some improvement in performance. Rudimentary equivalent signal flow graphs may be used to change the structure of a filter into a form suitable for a particular method of implementation. For example SFG equivalents have been used to derive Ford's structure. The structure of a multiple feedback filter may also be changed by the use of a matrix similarity transformation. When this is incorporated into a computer optimization programme, it enables the programme to search for new structures which are in some sense optimum.

The writer has pointed out that some transformations do not affect the differential sensitivities or the finite difference sensitivities of the transfer function with respect to the block diagram parameters. Any pair of subnetworks which are connected in cascade may be interchanged without affecting the sensitivities. Also the signal flow graph of a multiple feedback filter may be reversed without affecting the sensitivities. One effect of flow graph reversal is to interchange the noise transfer functions and the intermediate transfer functions. In view of Schaumann's empirical results on dynamic range [78,80], it is conjectured that it may be possible to construct some expression of dynamic range which is symmetrical with respect to the noise transfer functions and the intermediate transfer functions, thus remaining invariant under the transformation of FGR.

Another transformation is that of scaling. The writer has shown that the signal levels in a multiple feedback filter may be scaled, systematically and with complete generality, by performing the described transformation on the branches of a cut of the SFG. A complex scale factor can sometimes be used to change the nature of the transfer functions required of the sections; a negative scale factor can be used to eliminate unnecessary inverting amplifiers; and a real positive constant scale factor can be used to alter the gain of the filter and to maximise its dynamic range. The writer has proved that neither the differential sensitivities nor the finite difference sensitivities are altered by this transformation.

The writer has classified the existing multiple feedback filters, firstly in respect of the pattern of feedback loops which are introduced specifically for the purpose of reducing passband sensitivity, and secondly in respect of the method used to produce transmission zeros. The three existing techniques for producing transmission zeros are series notch sections, parallel forward paths, and complex feedback. It is thought probable that these are the only possible methods of producing transmission zeros, but this has yet

to be proved. The concept of complex feedback was introduced by the writer and was embodied in the continued fraction structure. This concept has enhanced our understanding of some existing structures.

Presentation of the classification in the form of a Table has shown relationships between existing structures, and has revealed some new structures. Some of these may be derived from existing structures by the transformations of FGR and interchange of cascade subnetworks. Others may be designed by using an analysis of the corresponding integrator network. It has been observed that all known low sensitivity multiple feedback filters, have just one forward path which passes through each block (or possibly its associated reciprocator). It is not known whether this is a necessary condition.

Considerable information on the sensitivity performance of a filter can be obtained by plotting the frequency responses resulting from finite changes to the various block diagram parameters. This has been done for a variety of structures, and for several of these the sensitivity performance has not previously been published. The sensitivity of the cascade structure is taken as a reference against which the performance of other structures are assessed.

The three canonic structures do not use feedback loops for sensitivity reduction, and their sensitivity is relatively high. Compared with the cascade structure, the partial fraction structure has a greater sensitivity in the stopbands, and the continued fraction structure has a greater sensitivity in the passband.

Of all the structures studied, those embodying leapfrog feedback were found to have the lowest passband sensitivity. Any of the three methods of producing transmission zeros can be used together with leapfrog feedback, but it appears that at frequencies in the stopbands, the lowest worst case sensitivity is achieved by the use of series notch sections.

Four structures having nested feedback loops were studied, and they were found to have almost identical sensitivity performance. Similar perturbed responses in the different structures were related to specific structural features. The choice between these structures may therefore be made using some other criterion such as the number of amplifiers used. For the simple design method used here, the value of the pre-distortion constant  $\alpha_1$  may be chosen for a minimum  $\omega_0$ -sensitivity, resulting in a value of  $\alpha_1$  close to that given by Hurtig's condition. The Q-sensitivity did not have a corresponding minimum, but was proportional to  $\alpha_1$ .

The nested feedback structure proposed by the writer [45], and described in Section 1.4, has aroused considerable interest in the literature. It has for example provided the inspiration for Wilson's easily adjustable biquadratic section [163], and it was a stimulus to Schaumann's work on dynamic range [78,80].

The results of the computational study suggest that the key to obtaining further reduction of passband sensitivity is to include as many feedback paths as possible, although this is by no means a sufficient condition. At present the only practical methods available for designing such structures are those which use computer programmes for optimization. There would be some utility in developing suitable design methods which do not require the use of optimization.

---

**REFERENCES**

---

- 1 Orchard H J: Inductorless filters. *Electronics Letters*, vol 2, no 6, June 1966, pp 224-225
- 2 Sheahan D F, Orchard H J: Bandpass filter realization using gyrators. *Electronics Letters*, vol 3, no 1, Jan 1967, pp 40-42
- 3 Neiryneck J: Survey of a filter sensitivity problem. *Proc. 1976 European Conf. on Circuit Theory & Design, Genova, Italy, 7-10 Sept 1976*, pp 658-662
- 4 Bruton L T: Multiple-amplifier RC-active filter design with emphasis on GIC realizations. *IEEE Trans. on Circuits & Systems* vol CAS-25, no 10, Oct 1978, pp 830-845
- 5 Orchard H J: Loss sensitivity in singly and doubly terminated filters. *IEEE Trans. on Circuits & Systems*, vol CAS-26, no 5, May 1979, pp 293-297
- 6 Antoniou A: Realization of gyrators using operational amplifiers, and their use in RC-active-network synthesis. *Proc. IEE*, vol 116, no 11, Nov 1969, pp 1838-1850
- 7 Rollett J M: Improvements in or relating to electrical networks. UK Patent 1238059, 7 July 1971
- 8 Holt A G J, Taylor J: Method of replacing ungrounded inductors by grounded gyrators. *Electronics Letters*, vol 1, no 4, June 1965, p 105
- 9 Silva M, Saraga W: On the classification of active RC circuits simulating floating inductors. *Proc. 3rd Int. Symp. on Network Theory, Split, Yugoslavia, 1-5 Sept 1975*
- 10 Gorski-Popiel J: RC-active synthesis using positive-immittance converters. *Electronics Letters*, vol 3, no 8, Aug 1967, pp 381-382
- 11 Bruton L T: Network transfer functions using the concept of frequency-dependent negative resistance. *IEEE Trans. on Circuit Theory*, vol CT-16, no 3, Aug 1969, pp 406-408
- 12 Saraga W, Haigh D, Barker R G: A design philosophy for microelectronic active-RC filters. *Proc. IEEE*, vol 67, no 1 Jan 1979, pp 24-33

- 13 Saraga W: Minimum inductor or capacitor filters. *Wireless Engineer*, vol 30, no 7, July 1953, pp 163-175
- 14 Larrowe V L: Direct simulation. *Control Engineering*, vol 1, Nov 1954, pp 25-31
- 15 Girling F E J, Good E F: The leapfrog feedback filter. RRE memorandum no 1176, Sept 1955
- 16 Girling F E J, Good E F: Active Filters 12-The leapfrog or active-ladder synthesis. *Wireless World*, vol 76, no 1417, July 1970, pp 341-345
- 17 Girling F E J, Good E F: Active Filters 13-Applications of the active-ladder synthesis. *Wireless World*, vol 76, no 1419, Sept 1970, pp 445-450
- 18 Girling F E J, Good E F: Active Filters 14-Bandpass types. *Wireless World*, vol 76, no 1420, Oct 1970, pp 505-510
- 19 Adams R L: On reduced sensitivity active filters. Proc. 14th Midwest Symp. on Circuit Theory, Denver, Colorado, 6-7 May 1971, pp 14.3.1-14.3.8
- 20 Fliege N: A new class of second-order RC-active filters with two operational amplifiers. *NTZ*, vol 26, no 6, June 1973, pp 279-282
- 21 Haigh D G: Some network transformations by terminal interchange. Proc. IEEE Int. Symp. on Circuits & Systems, New York, 17-19 May 1978, pp 416-421
- 22 Perry D J: Reply to comment on new multiple feedback active RC network. *Electronics Letters*, vol 12, no 2, 22 Jan 1976 p 41
- 23 Turpin R W, Saraga W: Sensitivity comparison of three types of active RC circuits. *IEEE Proc. of the Int. Symp. on Circuits & Systems*, Munich, 27-29 April 1976, pp 114-117
- 24 Blostein M L: Sensitivity analysis of parasitic effects in resistance terminated LC two-ports. *IEEE Trans. on Circuit Theory*, vol CT-14, no 1, Mar 1967, pp 21-25
- 25 Hilberman D: An approach to the sensitivity and statistical variability of biquadratic filters. *IEEE Trans. on Circuit Theory*, vol CT-20, no 4, July 1973, pp 382-390
- 26 Beck C: A method for solving problems on the REAC by the use of transfer functions without passive networks. Project Cyclone Symp. I. On REAC techniques, Reeves Instrument Corp, Garden City, NY. 15-16 March 1951, pp 131-136
- 27 Hurtig III G: Filter networks having negative feedback loops. United States Patent, no 3720 881, 13 Mar 1973
- 28 Tow J: Design and evaluation of shifted-companion form active filters. *The Bell System Technical Journal*, vol 54, no 3 Mar 1975, pp 545-568



- 29 Laker K R, Ghausi M S: A low sensitivity multiloop feedback active RC filter. Proc. 1973 Int. Symp. on Circuit Theory, Toronto, 9-11 Apr 1973, pp 126-129
- 30 Laker K R, Ghausi M S: Computer-aided analysis and design of follow-the-leader feedback active-RC networks. Int. Jour. of Circuit Theory & Applications, vol 4, no 2, Apr 1976 pp 177-184
- 31 Laker K R, Ghausi M S: A comparison of active multiple-loop feedback techniques for realizing high-order bandpass filters. IEEE Trans. on Circuits & Systems, vol CAS-21, no 6, Nov 1974, pp 774-783
- 32 Schaumann R, Kinghorn W A, Laker K R: Minimising signal distortion in FLF active filters. Electronics Letters, vol 12, no 9, 29 April 1976, pp 211-213
- 33 Szentirmai G: Synthesis of multiple-feedback active filters. The Bell System Tech. Jour, Vol 52, no 4, April 1973, pp 527-555
- 34 Dubois D, Neiryneck J: Synthesis of bandpass LF-filters between generalized resistive terminations. Proc. 1977 IEEE Int. Symp. on Circuits & Systems, Phoenix, Arizona, 25-27 April 1977, pp 348-350
- 35 Müller E G: Optimization of leapfrog structure active RC filters. Arch Elektron & Übertragungstech, vol 33, no 11, Nov 1979, pp 432-437 (In German)
- 36 Biernacki R, Mulawka J: Synthesis of active filters in the basic FLF configuration. Proc. 3rd Int Symp. on Network Theory, Split, Yugoslavia, 1-5 Sept 1975, pp 459-466
- 37 Dubois D, Neiryneck J: General synthesis method for FLF active filters. Proc. 1976 European Conf. on Circuit Theory & Design, Genova, Italy, 7-10 Sept 1976, pp 565-570
- 38 Tow J: Some results on generalized follow-the-leader-feedback active filters. Proc. 1977 IEEE Int. Symp. on Circuits & Systems, Phoenix, Arizona, 25-27 April 1977, pp 462-465
- 39 Tow J: Some results on two-section generalized FLF active filters. IEEE Trans. on Circuits & Systems, vol CAS-25, no 4, April 1978, pp 181-184
- 40 Gensel J: Entwurf von RC-aktiven FLF-filtern. Nachrichtentechnik Elektronik, vol 27, no 5, June 1977, pp 200-202
- 41 Gensel J: On the design of RC-active follow-the-leader feedback filters. Int. Jour. of Circuit Theory & Applications, vol 5, no 4, Oct 1977, pp 361-365
- 42 Padukone P R, Mulawka J, Ghausi M S: Sensitivity minimization in generalized follow the leader feedback active filters. Proc. IEEE Int. Symp. on Circuits & Systems, Houston, 28-30 April 1980, pp 801-806
- 43 Johnson CL: Analog computer techniques. McGraw-Hill, 1956 pp 82-83

- 44 Schüssler W: Zur allgemeinen theorie der verzweigungsnetzwerke. Archiv der Elektrischen Übertragung, vol 22, no 8, Aug 1968, pp 361-367
- 45 Perry D J: New multiple feedback active RC network. Electronics Letters, vol 11, no 16, 7 Aug 1975, pp 364-365
- 46 Matyáš J: Programování lineárních diferenciálních rovnic s konstantními koeficienty na analogových diferenciálních analyzátorech. Slaboproudý Obzor, vol 21, no 1, Jan 1960, pp24-29
- 47 Tow J: Design and evaluation of shifted companion form (follow the leader feedback) active filters. Proc. 1974 IEEE Int. Symp. on Circuits and Systems, San Francisco, 22-25 April 1974, pp 656-660
- 48 Laker K R, Ghausi M S: Synthesis of a low-sensitivity multiloop feedback active RC filter. IEEE Trans. on Circuits & Systems, vol CAS-21, no 2, March 1974, pp 252-259 (also corrections in Nov 1974)
- 49 Tow J, Kuo Y L: Coupled-biquad active filters. IEEE Proc. Int. Symp. on Circuit Theory, North Hollywood, California, 18-21 April 1972, pp 164-168
- 50 Wetenkamp S F, Van Valkenberg M E: Another approach to multiloop feedback. Proc. IEEE Int. Symp. on Circuits & Systems, Newton, Mass, 21-23 April 1975, pp 258-260
- 51 Krüger K E: Design of analogue multiple-feedback active RC networks. Nachrichtentechnik Elektronik, vol 27, no 5, June 1977, pp 197-199
- 52 Jacobs G M, Allstot D J, Brodersen R W, Gray P R: Design techniques for MOS switched capacitor ladder filters. IEEE Trans. on Circuits & Systems, vol CAS-25, no 12, Dec 1978, pp 1014-1021
- 53 Müller E G: Design of canonical signal-flow graph active RC filters. Proc. 1979 Int. Symp. on Circuits & Systems, Tokyo, 17-19 July 1979, pp 30-33
- 54 Gorski-Popiel J, Drew A J: RC active ladder networks. Proc. IEE, vol 112, no 12, Dec 1965, pp 2213-2219
- 55 Constantinides A G: Realization structures for digital filters. IEE Colloquium on Digital & Distributed Filters, March 1973, IEE Colloquium Digest no 1973/6, pp 4/1-4/2
- 56 Scott H H: A new type of selective circuit and some applications Proc. IRE, vol 26, no 2, Feb 1938, pp 226-235
- 57 Brackett P O, Sedra A S: Application of signal flow graphs to the synthesis of linear systems - Part I A general theory of network simulation - Part II Design of active ladder filters. Proc. 1975 IEEE Int. Symp. on Circuits & Systems, Newton, Mass, 21-23 April 1975, pp 242-249

- 58 Brackett P O, Sedra A S: Direct SFG simulation of LC ladder networks with applications to active filter design. *IEEE Trans. on Circuits & Systems*, vol CAS-23, no 2, Feb 1976, pp 61-67
- 59 Martin K, Sedra A S: Design of signal-flow graph (SFG) active filters. *IEEE Trans. on Circuits & Systems*, vol CAS-25, no 4, Apr 1978, pp 185-195
- 60 Adams R L: Coupled band-elimination active filters. *Proc. IEEE Int. Symp. on Circuits & Systems*, New York, 17-19 May 1978, pp 845-849
- 61 Deliyannis T: High Q factor circuit with reduced sensitivity. *Electronics Letters*, vol 4, no 26, 27 Dec 1968, pp 577-579
- 62 Bach Jr R E: Selecting RC values for active filters. *Electronics* vol 33, no 20, 13 May 1960, pp 82-85
- 63 Yoshihiro M, Nishihara A, Yanagisawa T: Low sensitivity active and digital filters based on the node-voltage simulation of LC ladder structures. *Proc. IEEE Int. Symp. on Circuits & Systems*, Phoenix, Arizona, 25-27 April 1977, pp 446-449
- 64 Okine M: Active RC synthesis of transfer functions for LC filters. *Electronics & Communications in Japan*, vol 59-A, no 10, Oct 1976, pp 1-9
- 65 Mason S J: Feedback Theory - some properties of signal flow graphs. *Proc. IRE*, vol 41, no 9, Sept 1953, pp 1144-1156
- 66 Mason S J: Feedback Theory - further properties of signal flow graphs. *Proc. IRE*, vol 44, no 7, July 1956, pp 920-926
- 67 Mason S J, Zimmermann H J: *Electronic circuits signals and systems*. John Wiley, 1960
- 68 Sandberg I W: On the theory of linear multi-loop feedback systems. *The Bell System Tech. Jour*, vol 42, no 2, Mar 1963 pp 355-382
- 69 Biswas R N, Kuh E S: Optimum synthesis of a class of multiple-loop feedback systems. *IEEE Trans. on Circuit Theory*, vol CT-18, no 6, Nov 1971, pp 582-587
- 70 Styblińska B: Sensitivity minimization in multiloop-feedback active filters with modification of the frequency response. *Proc. 5th Summer Symp. on Circuit Theory*, Prague, Sept 1977, pp 290-294
- 71 Constantinides A G: Some sensitivity aspects concerning digital filters. *IEE Colloquium on Sensitivity Theory and Tolerance Design of Circuits*, London, 29 Jan 1973, *IEE Colloquium Digest* no 1973/3 p2/1 (Full text available from the author)
- 72 Neiryneck J, Van Bastelaer P: Tables on sensitivity invariants and bounds for lossless two-ports. *Int. Jour. of Circuit Theory & Applications*, vol 3, no 3, Sept 1975, pp 285-291

- 73 Biswas R N, Kuh E S: A multiparameter sensitivity measure for linear systems. IEEE Trans. on Circuit Theory, vol CT-18, no 6, Nov 1971, pp 718-719
- 74 Reed M R: The seg - a new class of subgraphs. IRE Trans. on Circuit Theory, vol CT-8, no 1, March 1961, pp 17-22
- 75 Forsén A, Kristianson L: The jump phenomenon in active RC networks. Proc. European Conf. on Circuit Theory & Design, London, 23-26 July 1974, pp 331-335 (IEE Conf. publication no 116)
- 76 Schaumann R, Chalstrom R E, Laker K R: Optimisation of sensitivity and dynamic range of IFLF active filters. Electronics Letters, vol 13, no 12, 9 June 1977, pp 367-368
- 77 Perry D J: Improvement of dynamic range and reduction of limiting effects in multiple feedback filters. IEE Colloquium on Electronic Filters, 20 June 1978, pp 36-40, IEE Conf. publication no 167
- 78 Schaumann R, Chalstrom R E: The dynamic range properties of high-order active bandpass filters. Proc. IEEE Int. Symp. on Circuits & Systems, New York, 17-19 May 1978, pp 146-150
- 79 Chiou C-F, Schaumann R: Comparison of dynamic range properties of high order active bandpass filters. Proc. IEEE Int. Symp. on Circuits & Systems, Houston, 28-30 April 1980, pp 816-819
- 80 Chiou C-F, Schaumann R: Comparison of dynamic range properties of high-order active bandpass filters. IEE Proc. pt G, vol 127, no 3, June 1980, pp 101-108
- 81 Smith L, Sheingold D H: Noise and operational amplifier circuits. Analog Dialogue, vol 3, no 1, March 1969, Analog Devices Inc, Cambridge, Massachusetts 02142
- 82 Guggenbühl W, Bächler H: Active filter design for minimal noise and gain sensitivity. Proc. IEEE Int. Symp. on Circuits & Systems, Phoenix, Arizona, 25-27 April 1977, pp 328-331
- 83 Cooper G R, McGillen C D: Probabilistic methods of signal and system analysis. Holt Rinehart and Winston, 1971
- 84 Perry D J: Multifarious multifeedback filters. IEE Colloquium on Electronic Filters, London, 7 May 1976, IEE Colloquium Digest no 1976/33
- 85 Wetenkamp S F, Van Valkenburg M E: Improved sensitivity through generalized multiloop feedback. Proc. 3rd Int. Symp. on Network Theory, Split, Yugoslavia, 1-5 Sept 1975, pp 213-223
- 86 Mackay R, Sedra A S: Generation of low-sensitivity state-space active filters. IEEE Trans. on Circuits & Systems, vol CAS-27, no 10, Oct 1980, pp 863-870
- 87 Courant R: Differential and Integral Calculus, Vol II. Blackie & Son 1936
- 88 Perry D J: Scaling transformation of multiple feedback filters. Proc. IEE, vol 128 pt G, no 4, Aug 1981, pp 176-179

- 89 Sallen R P, Key E L: A practical method of designing RC active filters. IRE Trans. on Circuit Theory, vol CT-2, no 1, March 1955, pp 74-85
- 90 Kerwin W J, Huelsman L P: The design of high performance active RC bandpass filters. IEEE International Convention Record, vol 14 pt 10, 21-25 Mar 1966, pp 74-80
- 91 Pearl J: Optimum synthesis of inductorless bandpass filters using a combination of identical RC coupled amplifiers. IEEE Trans. on Circuit Theory, vol CT-11, no 4, Dec 1964, pp 457-461
- 92 Calahan D A: Comments on "Inductorless Filters". IEEE Trans. on Circuit Theory, vol CT-12, no 3, Sept 1965, p 435
- 93 Russell H T, Chan S-P: Generation of n-th order active filter transfer functions using canonic quadratic networks. IEEE Int. Symp. on Circuits & Systems, San Francisco, 22-25 April 1974, pp 672-676
- 94 Moran P L: A low-cost parallel implementation for active filters. Electronic Circuits & Systems, vol 2, no 1, Jan 1978, pp 21-25
- 95 Urbas A: Multiloop feedback synthesis method of BP active filters. Acta Polytechnica-Series III, no 7, (III,1,1977), pp 7-15
- 96 Bruton L T: Topological equivalence of inductorless ladder structures using integrators. IEEE Trans. on Circuit Theory, vol CT-20, no 4, July 1973, pp 434-437
- 97 Bruton L T, Salama A I A: Frequency limitations of coupled biquadratic active ladder structures. IEEE Jour. of Solid State Circuits, vol SC-9, no 2, April 1974, pp 70-72
- 98 Laker K R, Ghausi M S, Kelly J J: Minimum sensitivity leapfrog active RC filters. IEEE Int. Symp. on Circuits & Systems, San Francisco, 22-25 April 1974, pp 201-204
- 99 Laker K R, Ghausi M S, Kelly J J: Minimum sensitivity active (leapfrog) and passive ladder bandpass filters. IEEE Trans. on Circuits & Systems, vol CAS-22, no 8, Aug 1975, pp 670-677
- 100 Constantinides A G, Papadakis J A: Biquad multiple feedback structures based on linear transformations. IEEE Int. Symp. on Circuits & Systems, Houston, 28-30 April 1980, pp 101-104
- 101 Haigh D G: Some novel bandpass and bandstop active-RC filter circuits of multifeedback type. European Conf. on Circuit Theory & Design, Warsaw, 2-5 Sept 1980, pp 376-381
- 102 Szentirmai G: On multiple-feedback active filter structures. 7-th Asilomar Conf. on Circuits Systems & Computers, 27-29 Nov 1973, pp 368-377
- 103 Tuttle D F Jr: A common basis for the Darlington and Szentirmai network synthesis. Proc. IEEE, vol 62, no 10, Oct 1974, pp 1389-1390

- 104 Dubois D, Neiryneck J: Synthesis of a leapfrog configuration equivalent to an LC-ladder filter between generalized terminations. *IEEE Trans. on Circuits & Systems*, vol CAS-24, no 11, Nov 1977, pp 590-597
- 105 Laker K R, Schaumann R, Brand J R: Multiple-loop feedback active R filters. *IEEE Int. Symp. on Circuits & Systems*, Munich, 27-29 April 1976, pp 279-282
- 106 Schaumann R, Brand J R, Laker K R: Effects of excess phase in multiple-feedback active filters. *IEEE Trans. on Circuits & Systems*, vol CAS-27, no 10, Oct 1980, pp 967-970
- 107 Laker K R, Ghausi M S: Computer-aided analysis and design of multiple-loop feedback active RC networks. *Proc. 8th Annual Princeton Conf. on Information Sciences and Systems*, 28-29 March 1974, pp 408-412
- 108 Hrubý J, Novotný V: FLF synthesis of active RC and active electromechanical filters. *European Conf. on Circuit Theory & Design*, Warsaw, 2-5 Sept 1980, pp 571-576
- 109 Biernacki R, Styblińska B: Synthesis of multiloop active filters with identical biquadratic blocks. *Acta Polytechnica-Series III*, no 7, (III,1,1977), pp 45-55
- 110 Biernacki R M, Styblińska B: Properties of transfer functions of the multiloop feedback active filters with identical biquadratic sections. *IEEE Int. Symp. on Circuits & Systems*, New York, 17-19 May 1978, pp 871-875
- 111 Biernacki R M, Styblińska B: General synthesis of active filters with identical biquadratic sections. *European Conf. on Circuit Theory & Design*, Lausanne, 4-8 Sept 1978, pp 63-67
- 112 Biernacki R M, Styblińska B: Properties of transfer functions of multiloop feedback active filters with identical biquadratic sections. *IEEE Trans. on Circuits & Systems*, vol CAS-27, no 5, May 1980, pp 350-357
- 113 Spudil I: "Find the friend feedback" structure for the synthesis of the active RC networks. *Proc. 5th Summer Symp. on Circuit Theory*, Prague, Sept 1977, pp 286-289
- 114 Hurtig G III: Voltage tunable multipole bandpass active filters. *IEEE Int. Symp. on Circuits & Systems*, San Francisco, 22-25 April 1974, pp 569-572
- 115 Gorski-Popiel J: An active synthesis procedure using multiple feedback paths. *7-th Asilomar Conf. on Circuits Systems & Computers*, Pacific Grove, California, 27-29 Nov 1973, pp 85-90
- 116 Laker K R, Ghausi M S: Minimum sensitivity multiple loop feedback bandpass active filters. *IEEE Int. Symp. on Circuits & Systems*, Phoenix, Arizona, 25-27 April 1977, pp 458-461
- 117 Gönüleren A N: Analysis and design of generalized multiloop feedback (GMF) active networks. *23rd Midwest Symp. on Circuits & Systems*, Toledo, Ohio, 4-5 Aug 1980, pp 206-210

- 118 Hills M T: Crab's eye filter. Proc. IEE, vol 119, no 6, June 1972, pp 641-648
- 119 Gadenz R N: Some considerations on the crab's eye approach to channel filter design. IEEE Int. Symp. on Circuits & Systems, New York, 17-19 May 1978, pp 124-128
- 120 Biey M, Premoli A: The use of MCPER functions in the design of two-section generalized FLF active filters. IEEE Int. Symp. on Circuits & Systems, Houston, 28-30 April 1980, pp 91-94
- 121 Plotkin E: Notch filter based on identical building blocks with arbitrary transfer functions. Int. Jour. of Circuit Theory & Applications, vol 8, no 1, Jan 1980, pp 31-37
- 122 Lüder E: Design and RC active realization of an equalizer with parallel structure. European Conf. on Circuit Theory & Design, London, 23-26 July 1974, pp 446-451
- 123 Takasaki Y, Kita T, Maeda N, Nakagawa J, Ishizuka K: Inductorless variable equalizers using feedback and feedforward. IEEE Trans. on Circuits & Systems, vol CAS-23, no 6, June 1976, pp 389-394
- 124 Gadenz R N: On low-sensitivity realizations of band-elimination active filters. IEEE Int. Symp. on Circuits & Systems, Munich, 27-29 April 1976, pp 78-81
- 125 Gadenz R N: On low-sensitivity realizations of band-elimination active filters. IEEE Trans. on Circuits & Systems, vol CAS-24, no 4, April 1977, pp 175-183
- 126 Takasaki Y, Kita Y, Nakagawa J, Ishizuka K: High precision inductorless variable equalizers with wide variable range. IEEE Trans. on Circuits & Systems, vol CAS-24, no 12, Dec 1977, pp 704-708
- 127 Schaumann R, Brand J R: Integrable analogue active filters for implementation in MOS technology. IEE Proc. vol 128, pt G, no 1, Feb 1981, pp 19-24
- 128 Greenwood Q E: Feedback amplifier. US Patent, no 2281238, 28 April 1942
- 129 Graham R E: Linear Servo Theory. The Bell System Technical Journal, vol 25, no 4, Oct 1946, pp 616-651
- 130 Roszkiewicz J, Wojtyna R: Feedback models of VCO controlled by one variable network element. European Conf. on Circuit Theory & Design, Lausanne, 4-8 Sept 1978, pp 538-542
- 131 Haine J: New active quadrature phase-shift network. Electronics Letters, vol 13, no 7, 31 Mar 1977, pp 216-218
- 132 Deliyannis T, Fotopoulos S: Noise in the cascade of biquartic section filter. IEE Proc. vol 128, pt G, no 4, Aug 1981, pp 192-194
- 133 Deliyannis T, Fotopoulos S: High-order realization by cascading biquartic sections. European Conf. on Circuit Theory & Design, The Hague, 25-28 Aug 1981, pp 962-966

- 134 Snelgrove W M, Sedra A S: A novel synthesis method for state-space active networks. 23rd Midwest Symp. on Circuits & Systems, Toledo, Ohio, 4-5 Aug 1980, pp 196-200
- 135 Zurada J M, Bialko M: Digitally tunable active-RC filters. European Conf. on Circuit Theory & Design, The Hague, 25-28 Aug 1981, pp 280-291
- 136 Laker K R, Ghausi M S: Design of minimum sensitivity multiple loop feedback bandpass active filters. Journal of the Franklin Institute, vol 310, no 1, July 1980, pp 51-64
- 137 Acar C: Determination of dependent and independent sensitivity functions in signal-flow graphs. European Conf. on Circuit Theory & Design, The Hague, 25-28 Aug 1981, pp 1039-1042
- 138 Heinlein W H, Holmes W E: Active filters for integrated circuits. Prentice Hall 1974
- 139 Christian E, Eisenmann E: Filter design tables and graphs. Wiley 1966
- 140 Geffe P: Bandpass filter shapes up from a low-pass network. Electronics, vol 43, no 14, 6 July 1970, pp 80-84
- 141 Lee S C: Sensitivity minimization in active RC integrated circuit design. 4-th Annual Allerton Conf. on Circuit & System Theory, Monticello, Illinois, 5-7 Oct 1966, pp 269-281
- 142 Lueder E: A decomposition of a transfer function minimizing distortion and inband loss. The Bell System Technical Journal, vol 49, no 3, March 1970, pp 455-469
- 143 Davis A M: Synthesis of active ladder filters with continuants. Proc. 1981 Int. Symp. on Circuits & Systems, Chicago, 27-29 April 1981, pp 492-495
- 144 Doblinger G: High-order elliptic analog low-pass and band-pass filters with current controlled frequency response. Proc. 1982 Int. Symp. on Circuits & Systems, Rome, 10-12 May 1982, pp 350-353
- 145 El-Masry E I: Strays-insensitive state-space switched-capacitor filters. IEEE Trans. on Circuits & Systems, vol CAS-30, no 7, July 1983, pp 474-488
- 146 Fliege N: GIC-derived filter sections for multiple-feedback techniques. Proc. 1981 IEEE Int. Symp. on Circuits & Systems, Chicago, 27-29 April 1981, pp 509-512
- 147 Gonuleren A N: Multiloop feedback unsymmetrical active filters using quads. Int. Jour. of Circuit Theory & Applications, vol 10, no 1, Jan 1982, pp 1-18
- 148 Krüger K E: Entwurf von MLF-schaltungen mit hilfe der matrixerweiterung. Nachrichtentechnik Elektronik, vol 32, no 2, 1982, pp 63-64, p 69
- 149 Biey M: Design of lowpass two-section generalized FLF active filters. Electronics Letters, vol 19, no 16, 4 Aug 1983, pp 639-640



- 150 Bruton L T: Sensitivity of narrowband cascade bandpass filters. *The Radio and Electronic Engineer*, vol 43, no 5, May 1973, pp 325-328
- 151 Navot I: The synthesis of certain subclasses of tridiagonal matrices with prescribed eigenvalues. *SIAM Journal on Applied Mathematics*, vol 15, no 2, March 1967, pp 241-251
- 152 Marshall T G: Synthesis of RLC ladder networks by matrix tridiagonalization. *IEEE Transactions on Circuit Theory*, vol CT-16, no 1, Feb 1969, pp 39-46
- 153 Holbrook J G: The recurrent-continuant method of transfer function synthesis. *The Radio & Electronic Engineer*, vol 38, no 2, Aug 1969, pp 73-79
- 154 Johnson D E, Hilburn J L, Irons F H: Multiple feedback higher-order active filters. *IEEE Southeastcon Proceedings (Region 3 Conf.)*, April 1974, pp 132-137
- 155 Constantinides A G, Dimopoulos H G: Active RC filters derivable from LC ladder filters via linear transformations. *Electronic Circuits and Systems*, vol 1, no 1, Sept 1976, pp 17-21
- 156 Martin K, Sedra A S: Exact design of switched capacitor bandpass filters using coupled biquad structures. *IEEE Trans. on Circuits & Systems*, vol CAS-27, no 6, June 1980, pp 469-475
- 157 Fliege N: Tolerance reduction in active filters. *Proc. 1980 Int. Symp. on Circuits & Systems*, Houston, 28-30 April 1980, pp 780-783
- 158 Laker K R, Schaumann R, Ghausi M S: Multiple-loop feedback topologies for the design of low-sensitivity active filters. *IEEE Trans. on Circuits & Systems*, vol CAS-26, no 1, Jan 1979, pp 1-21
- 159 Schubert E: Entwurf eines mehrfach rückgekoppelten Bandpasses bei mittleren Frequenzen. *Nachrichtentechnik Elektronik*, vol 32, no 2, 1982, pp 72-76
- 160 Takagi S, Fujü N: A synthesis of active RC elliptic bandpass filters using identical biquad sections. *Electronics and Communications in Japan*, vol 67-A, no 3, Mar 1984, pp 1-7
- 161 Fotopoulos S, Deliyannis T: Active RC realization of high-order bandpass filter functions by cascading biquartic sections. *Int. Jour. of Circuit Theory & Applications*, vol 12, no 3, July 1984, pp 223-238
- 162 Mijat T, Moschytz G S: Multiple-critical-pole coupled active filters. *Int. Jour. of Circuit Theory & Applications*, vol 12, no 3, July 1984, pp 249-268
- 163 Wilson G: Lossy-integrator biquadratic RC-active filters. *IEEE Trans. on Circuits & Systems*, vol CAS-24, no 8, Aug 1977 pp 455-459